Tectonics of dyke swarms: Insights from case studies and analogue modelling

Ana Isabel Martínez Poza

UAB
Universitat Autònoma de Barcelona

3.3. INDEPENDENCE DYKE SWARM: DYKE EMPLACEMENT AND FABRIC DEVELOPMENT AT MID-CRUSTAL BRITTLE-DUCTILE CONDITIONS. STRAIN LOCALIZATION AROUND DYKES.

3.3.1. Introduction

We present a research case in the Independence Dyke Swarm, an area that has been widely studied previously by classic geology authors (Moore and Hopson 1961; Smith, 1962; Chen and Moore, 1979; James, 1989). However, we are going to apply different methods not used in this dyke swarm until now. All of them are intended to obtain a detailed structural analysis of the intrusion. The Independence Dyke Swarm has been a widely studied dyke swarm because its implication in the geological history of the eastern California.

The Independence Dyke Swarm (IDS from now on) has been classically interpreted as a mafic/lamprophyre dyke swarm which based on the literature (Hutton 1988; Petford *et al.* 2000), usually represents intraplate extensional events. However, other studies relate the presence of this dyke swarm with a transpressive setting (Glazner *et al*., 1999; Carl, 2000).

We will focus our study only in the Jurassic suv-vertical dykes of a small area of the IDS (South Fork Big Pine Creek) (Fig. 3. 25). This portion will let us discover the dyke-pluton relations, as well as, the different dyke generations. Moreover, we are going to try to constrain a better age for the dyke families and increase the compositional dataset build for IDS during years of research (Moore and Hopson, 1961; Coleman *et al*., 1995; Coleman and Glazner, 1997; Carl, 2000; Coleman *et al*., 2000, 2005, Glazner *et al*., 2008). Another important part of the study will be the stress analysis of the dyke intrusions and its relation with the deformation features present in the rocks (dykes and host rock). The proposed final model will try to clarify the processes occurred during and after the IDS emplacement.

3.3.2. Geological setting

We are focusing our project in the IDS part near Big Pine (California, USA), in an area called South Fork Big Pine Creek, where we were able to find really well exposed outcrops due to the effect of the last glacial age. The outcrops have a drumlin morphology which gives us a 3-D vision of the intruded bodies (Figs. 3. 26b. and 28a). This geomorphological feature is really useful for the structural study of the dykes.

The extension of the dyke swarm is around 600 km long (N-S). The first mapping works in the 60s found similar dykes exposures in different areas of California (Moore and Hopson 1961; Smith, 1962), from the area nearby Independence to the south, in the Mojave Desert. The intrusion of Cretaceous plutons and later deformation processes caused difficulties in the determination of the IDS extension and the limits of the Jurassic batholiths (Glazner, 1999).

However, the extension of the dyke swarm were established in later works (Chen and Moore, 1979; James, 1989) with the presence of dykes from the northern Sierra Nevada and White Mountains (Mt. Morrison quadrangle and Blanco Mountain quadrangle, Rinehart and Ross, 1964 and Nelson 1966; Ernst 1997, respectively) to the south of California (possibly even Baja California) in the Mojave Desert (Chuckwalla Mountains) (James 1989; Davis, 1994).

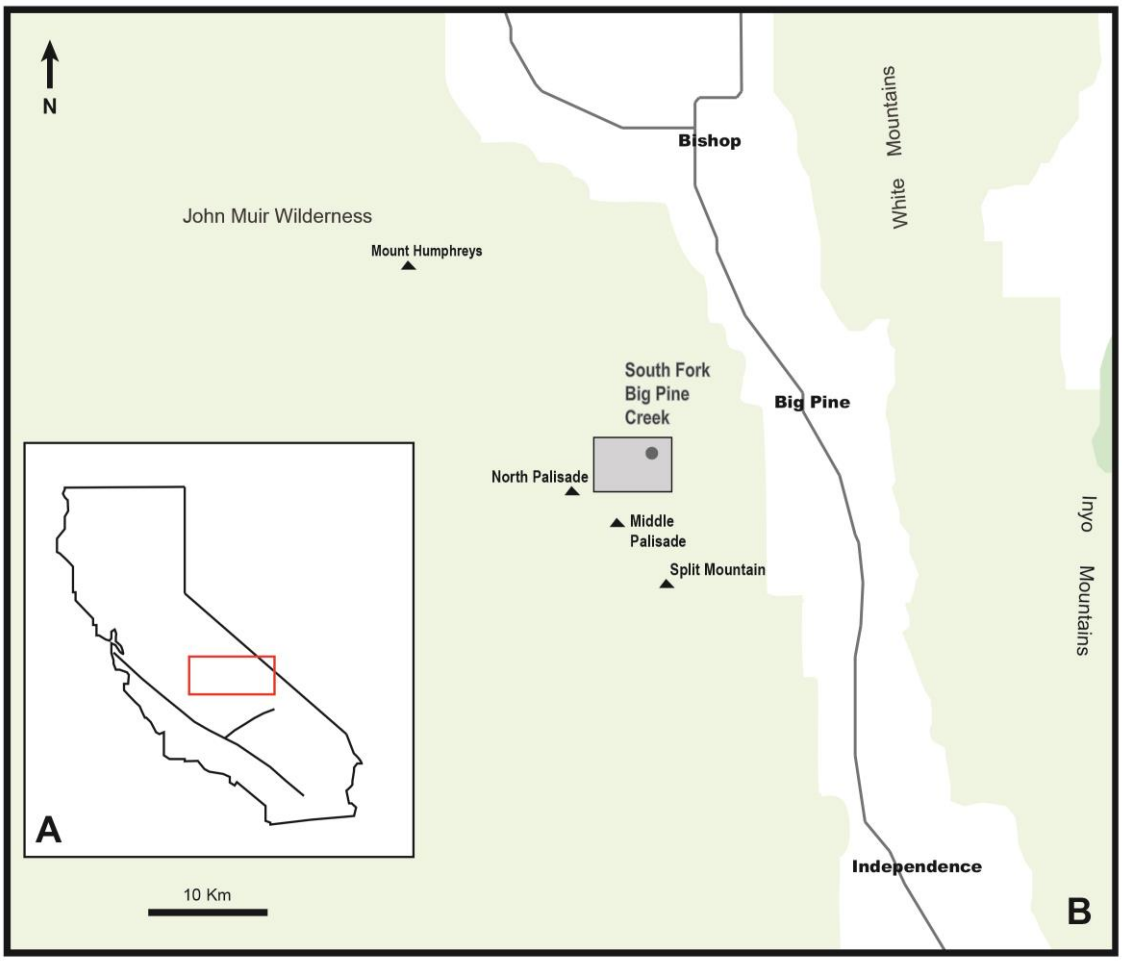

Fig. 3. 25. A) Location of the outcrop area in the California (USA) map. B) Location of the South Fork Big Pine Creek outcrop in the Sierra Nevada area.

In the outcrop area (Fig. 3. 25 and 3. 26), dykes are intruded into Jurassic granodioritic plutons with leucogranitic parts (~100m thick, subvertical and west striking) (Bateman, 1965). These plutons form an igneous belt throughout the eastern part of California with an orientation ~320º (Bateman, 1992). In general, the U-Pb zircon age of the plutons of the eastern Sierra Nevada range between 180-165 Ma or 96-88 Ma (Stern, 1981; Chen and Moore, 1982; Saleeby, 1990; Coleman, 1995; Coleman and Glazner, 1997). In the Cretaceous plutons, there can be found a great number of basaltic and dioritic rocks (Moore 1963; Frost and Mahood, 1987; Coleman *et al*., 1995; Sisson, 1996). The Jurassic plutons can be recognized because they are crosscut by the 148 Ma IDS dykes. Although, some of the IDS dykes in the Sierras have a Cretaceous age (Coleman *et al*., 2000).

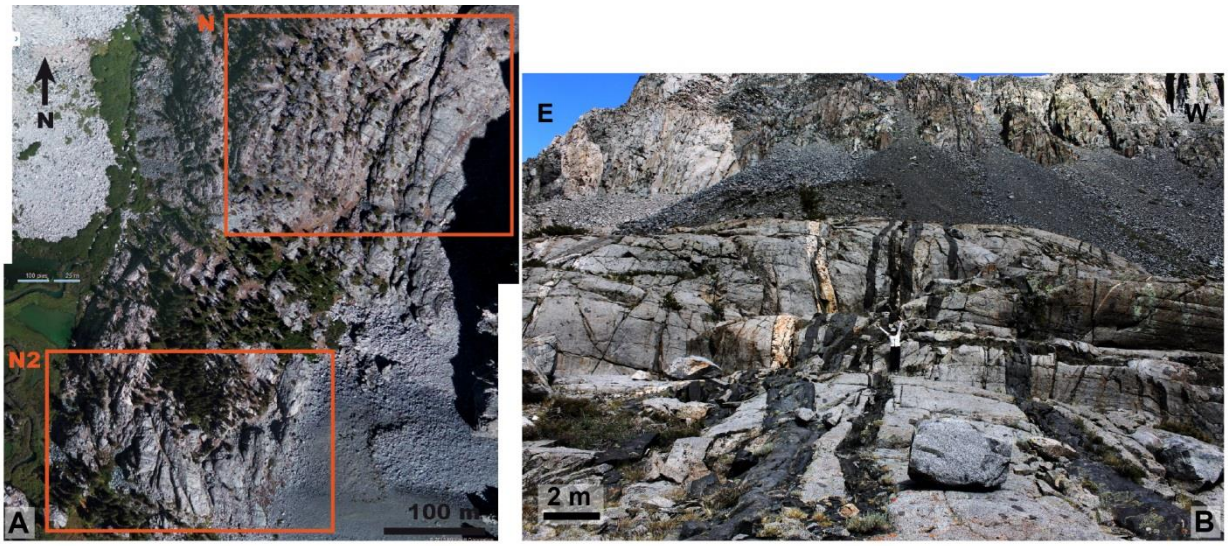

Fig. 3. 26. A) Aerial photograph of the outcrops in the South Fork Big Pine Creek area. The area was divided in two zones, *N* zone in the north and *N2* zone in the south. B) Phothograph of the outcrop *N2* view with the drumlin morphology.

The Tinemaha granodiorite, where IDS dykes are intruded in the SFBPC area, is composed by hornblende graniodorite with 1cm K- feldesper phenocryst. It is also rich in enclaves (Wiebe and Collins, 1998). The origin of these enclaves must have been some comingling process of mafic injections together with the granodiorite intruded deeper in the granodiorite (Coleman *et al*., 2005). No evidences of stopped blocks of the pluton floor indicate an irrelevant stopping process. The pluton age is estimated in 165 Ma (Chen and Moore, 1982). It contains numerous shear zones and the IDS mafic dykes. In some cases, mafic-felsic commingling is a predominant mechanism found in the plutons of the Sierra (Coleman *et al*., 2005).

The majority of the IDS dykes are Jurassic (~148 Ma), with a NW mean trend and a minor NE trend (Carl, 2000). The first dyke age estimations proposed (Moore and Hopson, 1961) a distinction of two different plutonism ages in the Mt.Pinchot quadrangles. The authors differentiated the areas depending the presence of the IDS dykes or not. The estimated Pb-alpha and K-Ar ages of dykes and host rocks as Cretaceous. Later geochronological work (Chen and Moore, 1979) obtained a Jurassic age of 148 Ma for the silicic dykes of the Mojave Desert and eastern Transverse Ranges. More recent studies (Coleman, 1994) established a more complicated story for the IDS emplacement. The U-Pb ages of the mafic dykes resulted to be not as narrow as thought before. However, several ages turned out to be Late Cretaceous (90-94 Ma). In the Mt. Pinchot quadrangle (Moore, 1963), there are IDS dykes crosscutting Cretaceous dykes (Carl et al., 1996; Coleman et al., 2000). More dykes in Pine Creek Canyon are also Late Cretaceous (Coleman et al., 1994, 2000). After these new ages, the possibility of the IDS to be Cretaceous was open, although the 148 Ma U-Pb ages (Coleman et al., 1994, 2000; Whitmarsh, 2000) contradict this hypothesis.

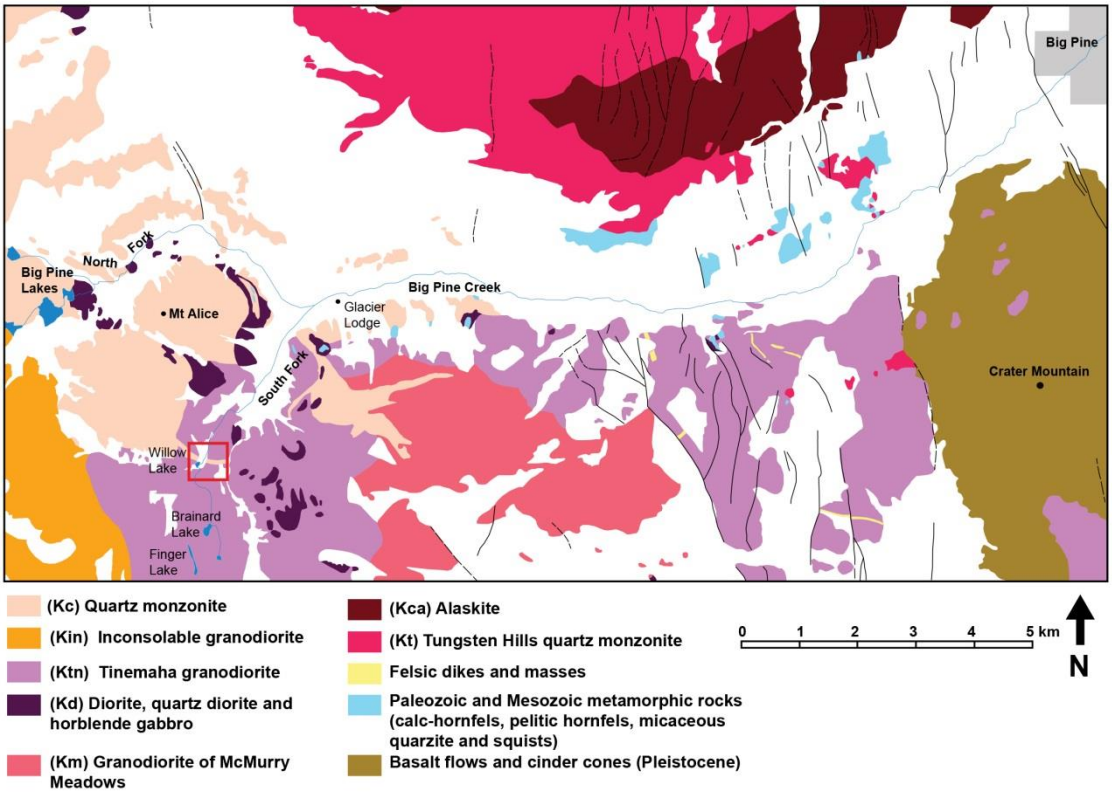

Fig. 3. 27. Geological map of Sierra Nevada in the Big Pine Creek area. Red rectangle marks the location of the outcrop in South Fork Pig Pine Creek. Modified from Bateman, P. (1964) Geological map of Big Pine 15' quadrangle. U.S. Geological Survey.

Carl (2000) proposed an alternative method to distinguish between the Jurassic dykes and the Cretaceous ones. This was to look in detail the internal fabric of the dykes. In general, all the Jurassic dykes clearly show a sinistral fabric. In general, the Cretaceous dykes strike towards the Late Cretaceous plutons and some of them also contain a dextral linear fabric (Carl, 2000). The Cretaceous ones are just located in the Pine Creek area. In this case, it would be interesting to check if other localities have the same age or if this is an isolated event during the later IDS intrusion.

The short time expanse and the great extension of the dykes that crosses different geological settings is very useful as a marker for the regional tectonic events in the eastern Sierra Nevada and White Mountains (Lahren 1990; Schweickert and Lahren, 1990; Walker 1990; Walker and Martin 1991; Dunne and Walker 1993; Stephens 1993; Dunne 1994; Davis 1994). Consequently, the dyke swarm has been used as reference indicator for stratigraphic and age control markers of geological relations of the region (Smith, 1962; Karish, 1987; Glazner, 1989, Dunne and Walker, 1993; Schermer, 1993; Martin, 1993; Dunne, 1994; Schermer and Busby, 1994; Ron and Nur, 1996).

A characteristic of dykes from southern locations in the desert is that normally dykes do not present deformation features and they also display cataclasys. However, dykes in the glaciar polished outcrops (in Sierra Nevada) display deformation fabrics (Glazner *et al*., 1999) as seen in the field. These differences in features from both locations presumably respond to a variation in the emplacement depth, being shallower in the south and eastern outcrops and

deeper in the Sierra outcrops. One explanation for the shallower levels is that it is more likely to develop brittle structures since the temperature is cooler (Carl *et al*., 1998).

The composition of the dykes is quite heterogeneous along the swarm. Hopson (1988) described the dykes as lamprophiric and microdioritic to granophyric. The majority of them are predominantly bimodal (silicic or dioritic to granitic, Moore and Hopson, 1961), but the intermediate ones show this composition too (McManus and Clemens-Knott, 1997). These results propose a short time period for the emplacement phase (Carl, 2000).

The different textures found in the dykes vary from glassy to aphyric, to medium-grained porphyric (> ~30% phenocrysts) (Carl, 2000). In the northern part of the swarm (Inyo Mountains and Sierra Nevada), the IDS dykes are mainly mafic (~90% of the dykes in Mt.Pinchot quadrangle) and they range from diabase to horblende diorite (Glazner *et al*., 2008). Carl (2000) described the composition of the suite as calc-alkaline (SiO_2 ~60% by weight when CaO equals K_2O+Na_2O), while the basaltic dykes are slightly alkali-SiO_2 on the alkali-SiO_2 diagram (Mcdonald and Katsura, 1964). There are other types of dykes with two different types of compositions, they are called *composite dykes* (Carl, 2000) and they represent an important part of the present study. These *dykeletes* are composed of 5-10 pulses with a thickness ~1m and they display chilled margins (Coleman *et al*., 2005). There are also dykes with more than 50% of enclaves (Carl *et al*., 1997; Martinez-Poza *et al*., 2013) and several aplite dykes generations (Glazner *et al*., 1999). The majority of the dykes show segmentation structures as jogs and steps that are very useful as markers of dyke opening and reference points after the emplacement (Glazner *et al*., 1999).

Deformation processes can be described within the dyke walls and fabric (Carl, 2000; Coleman *et al*., 2005; Glazner, 2008). The strain is mainly localized in the NW dykes, on the margins, which gives as a result ductile shear zones. The shear movement is sinistral, it is parallel to the dyke walls and marked by the angle between the oblique foliation (clockwise to the dyke walls) and the dyke wall. The tectonic fabric does not continue inside the dyke or in the host rock (Glazner *et al*., 1999; Coleman *et al*., 2005; Glazner *et al*., 2008; Martinez-Poza *et al*., 2013). Because of the existence of other markers in the host rock, as mafic enclaves, crosscutting relations with older dykes and melted wall screens disconnected sinisterly, this sinistral movement is confirmed. Succeeding dykes strike clockwise to the sheared dykes and form boudins while dykes that strike counterclockwise to the sheared dykes are folded (Coleman *et al*., 2005; Glazner *et al*., 2008). The markers on the dyke walls also let set the opening of the dykes with NS direction (Glazner *et al*., 1999).

Traditionally, the IDS has been interpreted as an extension indicator of the Late Jurassic (Chen and Moor, 1979; James, 1989; Schermer, 1993). During the Late Jurassic, more tectonic events at regional scale occurred apart from the intrusion of the dyke swarm, although relationships between them are not clear. Contrary to what would have been expected, the emplacement of the IDS occurred in a period of non-important plutonic activity (Chen and Moore, 1979),

it happened during the arc related to subduction interval. However, at the same time, more plutonic emplacements were happening in the south (Mojave Desert and Inyo Mountains) (Schermer, 1993; Dunne and Walker, 1993; Glazner 1994). Therefore, some authors relate the IDS emplacement with the Nevadan Orogeny since it was occurring at the same time (Bateman and Clark, 1974; Tobish, 1987; Edelman, 1991). Another interpretation for the dyke swarm is that it could be related to a collisional event (Ingersonll and Scheweickert, 1986; Harper, 1994). In addition, the opening of the Gulf of Mexico could be involved in the IDS for some authors (Davis, 1994; Fackler-Adams, 1997).

The origin of the plutonic arc is genetically linked to the coeval swarm (Hopson, 1988). For example, the Cretaceous mafic dykes in east and central Sierra Nevada are related to coeval mafic plutons, sometimes they are mapped within the same pluton (Coleman *et al*., 2000).

In broad sense, during the Late Jurassic in the western United States, there was an important magmatic and tectonic change. It was a time when the magmatic activity decreased until a hiatus that lasted up to the middle Cretaceous (Stern *et al*., 1981; Chen and Moore, 1982; Glazner *et al*., 1999). So, after the geochronological data, the IDS probably represent the last magmatic pulse before the hiatus (Glazner, 1991). Central and eastern California was affected by the Nevadan orogeny during the Late Jurassic (Bateman and Clark, 1974; Ingersoll and Schweickert, 1986). It is still not clear the tectonic origin of the Nevadan orogeny, although some authors suggest that it could be related to the collision of an island arc with the North American margin. A reconstruction of hot-spot made by Glazner (1991) proposes a sinistral assemblage in the arc during the Jurassic. Other authors (Wolf and Saleeby, 1995) based on plate reconstructions (Page and Engebretson 1984; Engebretson, 1985) pointed out the time coincidence in the intrusion of the IDS and other NW- striking dyke swarms, that synchronize with the cusp J2 (May and Butler, 1986 and May *et al*. 1989) in the polar wander path for North America. The palaeomagnetic data for the J2 event denotes the increase in the North America velocity up to ~150 km/Ma northward. This increase in the velocity towards the North suggests a possible sinistral shear between the oceanic plate and North American plate (May and Butler, 1986 and May *et al*., 1989). Stratigraphic works discuss that the Coast Range ophiolite involves a dextral oblique subduction during the Late Jurassic (Dickinson *et al*., 1996). However, there are more evidences of sinistral movement during at least the last part of the Late Jurassic (Oldow *et al*., 1984; Wolf and Saleeby, 1995; Glazner et al., 1999).

All the deformation features brings the intrusion of the IDS into a sinistral shear zone of crustal-scale, related to the left-oblique subduction zone during the Late Jurassic magmatic arc in the part of the North American plate (Glazner *et al*., 1999).

3.3.3. Methodology and results

The Independence Dyke Swarm is an area widely studied in the petrological-geochemical-geochronological and structural aspects. However, more in detailed work can be done in order to fully understand the intrusion mechanisms and the multiple dyke relations.

We have combined classical field work with laboratory analysis, and the result gives us a clear understanding of this small area which may be extrapolated to a bigger picture in the regional extension of the IDS.

3.3.3.1. General pattern of dykes and segmentation description

Generally, IDS dykes have a W-NW orientation with a mean trend of N140º-N155º (Moore and Hopson, 1961; Chen and Moore, 1979 and James, 1989). However, individual dykes seem to strike 10º-30º more to the west than the batholith and the mean trend of the dykes in the swarm (Glazner *et al*., 1999). The part of the dyke swarm north to Garlock fault strike ~N135º, counterclockwise to the mean trend ~N150º (Glazner *et al*., 1999). The IDS was probably intruded in a pre-existing network of fractures with this preferent orientation. This joint system due to their oblique orientation is the responsible of the dyke swarm actual arrangement (Glazner *et al*., 1999). Nevertheless, there are some dykes that differ up to 90º in strike from the mean trend. The reason could be the effect of later deformation processes during the intrusion of plutons in the Cretaceous (Moore and Sisson, 1987).

During field work in the area of South Fork Big Pine Creek (SFBPC, Big Pine, California) (Figs. 3. 25, 3. 26 and 3. 27), located at 3000 m altitude, we took measurements of the different sub-vertical dyke walls, aplite veins and mylonite zones (Fig. 3. 26b, and 28) (aplite and mylonite diagrams described in the following section). The resulting rose diagrams show the different orientations of each structure found in this particular area. All the dykes where plotted together in the same diagram (Fig. 3. 28e). The mean direction for the dykes is ~N95º (275º) with a secondary set at ~N175º (Fig. 3. 28e). There is a big variation from this data with respect to the mean value for the whole IDS of more than ~55º, as well as in the secondary set.

After combining the results with the field notes, we could establish four different types of dyke intrusions in our study area (Fig. 3. 28) as follows: The secondary set from the rose diagram corresponds to a group of coarse-grain dykes, probably older than the IDS (Fig. 3. 28a). Another type of dykes found very frequently are the *composite dykes*, which are a combination of several mafic *dykelets* (Fig. 3. 29d). They present greysh fine-grained centers with mafic fine-grained margins. Usually, they have the same orientation as the IDS dykes found in the area (~E-W trend). The more abundant group is formed by mafic fine-grained dykes. They represent the most characteristic IDS intrusion with the mean trend ~E-W in this area (Fig. 3. 28a, b and c).

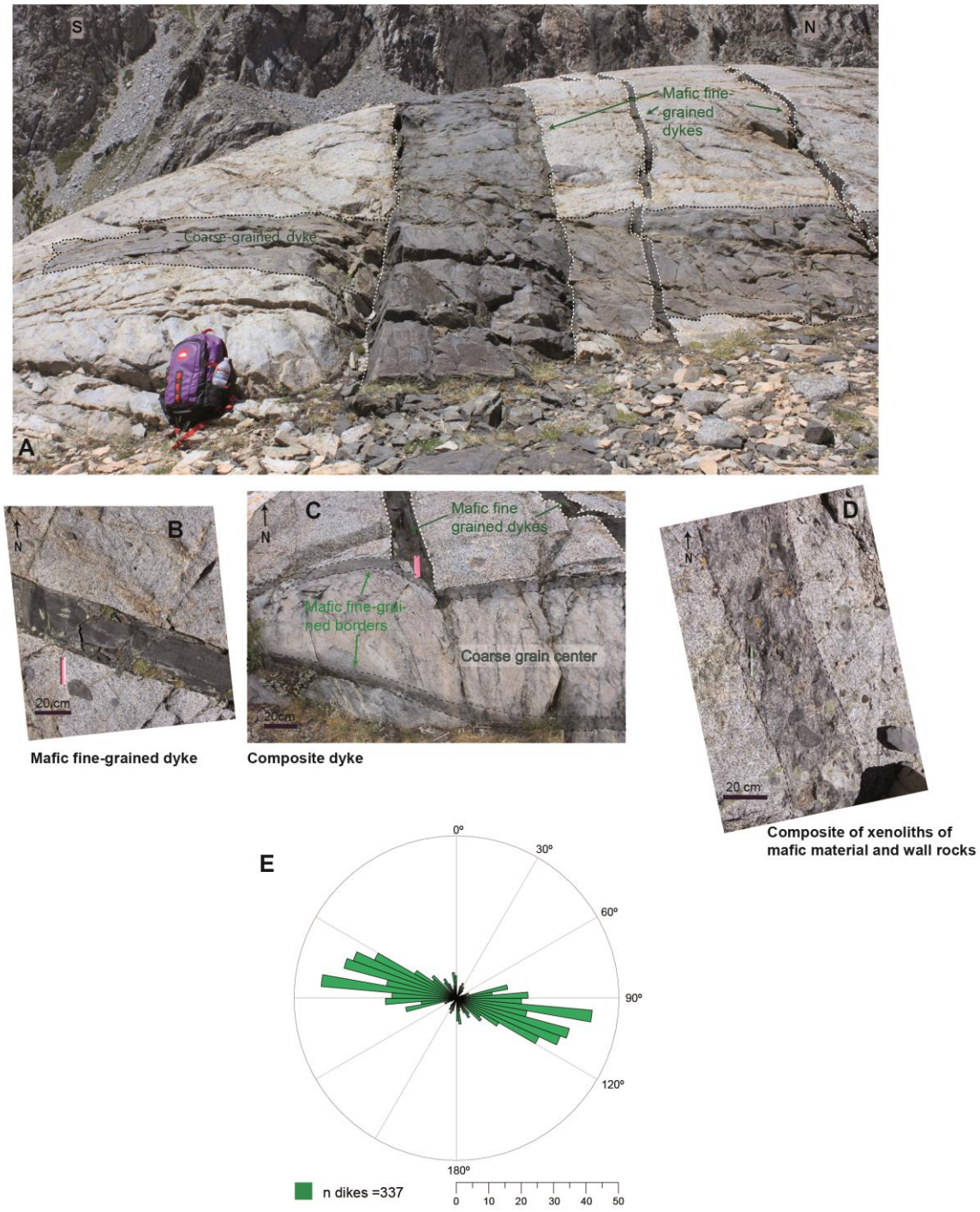

Fig. 3. 28. A) View of a sub-vertical outcrop with drumlin morphology where several dyke families can be recognised: Mafic fine-grained dykes crosscutting other dyke family with coarse grain centers. B) Example of mafic fine dyke. C) Example of crosscutting relations between a coarse grained dyke and a mafic grained dyke. Notice the opposite cutting relation in this case with image A, where occurs the contrary relation. D) Example of composite of mafic xenoliths and wall rock material and E) Rose diagram of dyke orientation measurements taken from aerial images (@Bing).

Finally, we found some dykes composed of xenolith of mafic material and wall rock, similar to the ones described by Glazner *et al*. (2008) in Woods Lake. These dykes have a mean direction of ~NNE-SSW (Fig. 3. 28d).

Crosscutting relations in the field helped us to reveal the chronological order of the intrusions which will try to be supported by geochronological data (later

described). Therefore, the intrusion order would be: N-S coarse-grained dykes (probably pre-IDS) (Fig. 3. 28a). Later, the *composite dykes* (IDS trend), followed by the mafic fine-grained dykes (Fig. 3. 28a, b and c). Ultimately, we found the composed intrusion of xenoliths and wall rock (~NNE-SSW trend), they probably represent the later pulse of the IDS (Fig. 3. 28e). There are also two aplite veins sets that are crosscut and crosscut the different dyke set, which may imply the relation with the last pulses of each mafic intrusion (Fig. 3. 26). We can see shearing evidences with some of these aplites as markers (Fig. 3. 29a). There are also shear related S structures and folds (Fig. 3. 29f).

In this particular area, it was not possible to do a good estimation of the fracture system in the outcrops (as in other similar research e.g. Martinez-Poza *et al*., 2014). The reason is the weathering of the host rocks due to the last glacial age, which widely polished the outcrops. This process facilitated the superficial gashing of the granitoides, so it is very difficult to distinguish between pre-existing joints and relative new fractures (Fig. 3. 26b).

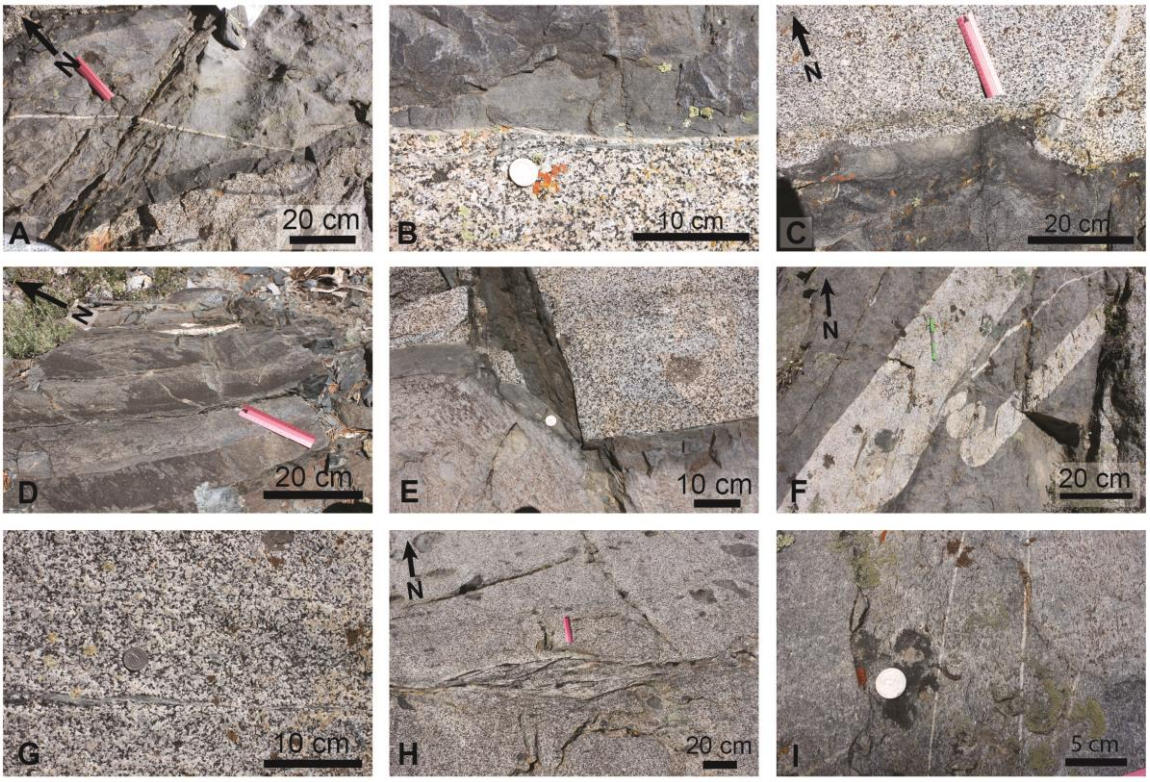

Fig. 3. 29. Catalogue of segmentation structures and dyke walls features in sub-horizontal outcrops. A) Coarse grained dyke with fine grain borders, crosscut by an aplite vein. B) Mylonitic border in a mafic dyke. C) Deformed horn structure. D) Dyke composed of several *dykelets.* E) Folded aplite dyke inside a mafic dyke. G) Mylonite zones in the granitoid host rock. H) Mylonite zones with sigmoidal shapes. I) Interior of a mafic dyke with outstanding mineral lineation and crosscut by several aplite veins.

Using observation and in detail outcrop-scale mapping, we can describe the segmentation structures present in the dyke intrusions. This kind of configurations has been widely studied in the literature as good indicators for dilation, stress analysis and dyke propagation (Delaney and Pollard, 198; Rubin, 1995; Weinberger *et al*., 2000). They can be classified depending on the rock relations that affect host rocks (Hoek, 1991; Baer, 1991; Druguet *et al*.,

2012; Gudmunsson, 2002) or regional and local fluid stress regimes (Olson and Pollard, 1989; Pollard and Aydin, 1984). Segmentation structures found in the area are linear and continuous sections, both in map and outcrop scale. Moreover, they show the same style in sub-horizontal and sub-vertical outcrops (Fig. 3. 26 and 3. 28). The majority of the sub-vertical dykes vary between cms to 1m thick (Fig. 3. 26 and 3. 28.). There are not many dyke offsets or dyke jogs or steps, either on horizontal or vertical surfaces, as dykes present 3-D exposures. This fact can be related to the orientation of the pre-existing joint network. If there is a constant orientation of the fractures, then few possibilities of change in direction could occur during the dyke intrusion, also associated with the stress regime in the area. Segmentation literature explains the cause of the different structures as changes in the injection direction due to the multiple joint sets.

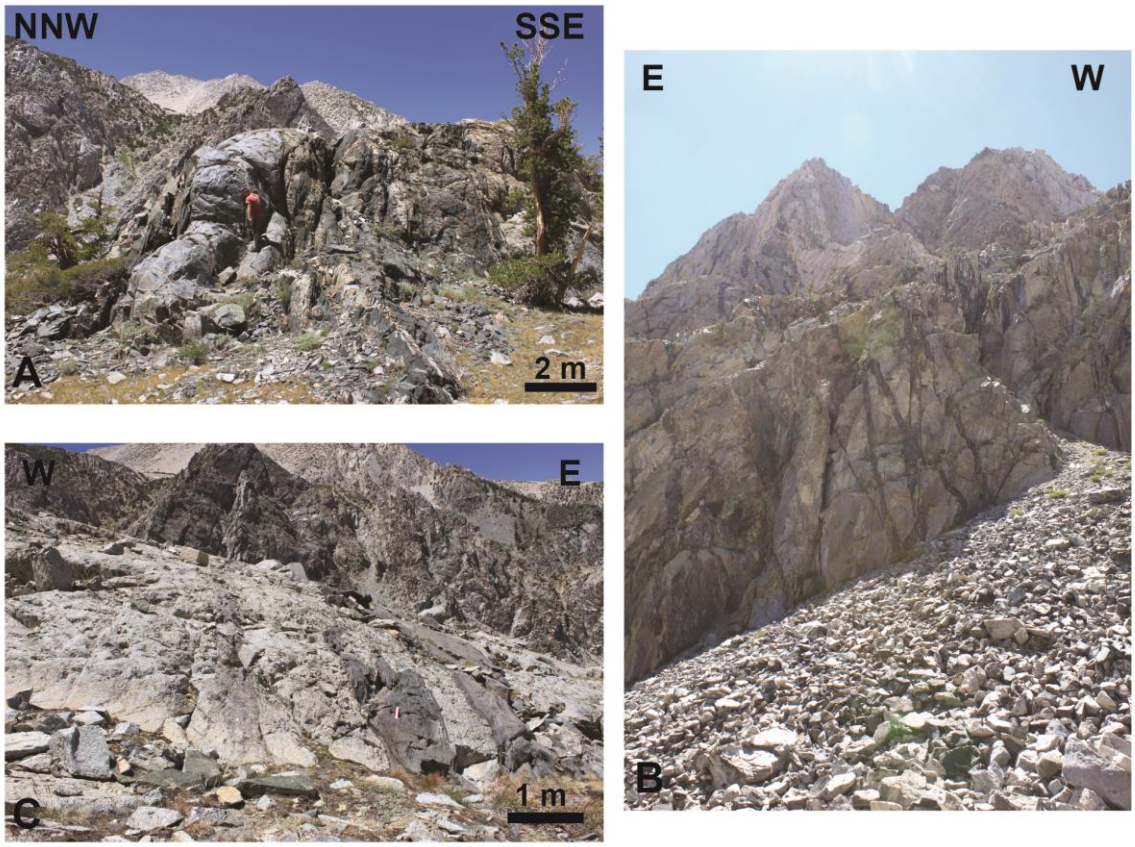

Fig. 3. 30. Examples of sub-vertical dyke segmentation. A) Image of a large intermediate dyke together with other mafic dykes. B) Sub-vertical dykes in a big wall exposure. C) Several sub-vertical dykes (from left to right: composite of xenoliths and granitoid host rock, mafic dyke and coarse grained dyke with mafic borders).

The majority of the dykes show a continue exposure, with long and straight segments (Fig. 3. 26a). During the field work, we were able to distinguish just few evidences of dyke coalescence, since no real steps are observed, but horn structures left after the link of two dyke tips are locally found (Fig. 3. 29c). Other merging structures are rarely observed in a few localities, we could find a raft of host rock between two coalescent dykes (Fig. 3. 34a). Discontinues structures like horns or dyke tips are very rare in this area, as well as zigzags or interaction features between two nearby dykes. The more common features are

related to the crosscutting relations between the different magmatic intrusions and later deformation (Fig. 3. 29e).

3.3.3.2. Mylonites and dyke deformation

Oblique foliation in IDS dykes was first described by Moore and Hopson (1961) in the mafic dykes of the eastern Sierra Nevada. This foliation supposes a sinistral deformation marker in the dyke mass which could be related to a sinistral strike-slip kinematics in the magmatic arc during the Late Jurassic (Wolf and Saleeby, 1995). There are evidences of foliated dykes in other areas, like Coso Range (Whitmarsh *et al*., 1996) and Spangler Hills. Other studies describe similar structures in IDS dykes south of Garlock fault (Karish *et al*., 1987, Powel *et al*., 1984). The origin of this common feature is not clear yet, although it could be related to a local shearing produced by the magma-wall rock interaction (Carl *et al*., 2002).

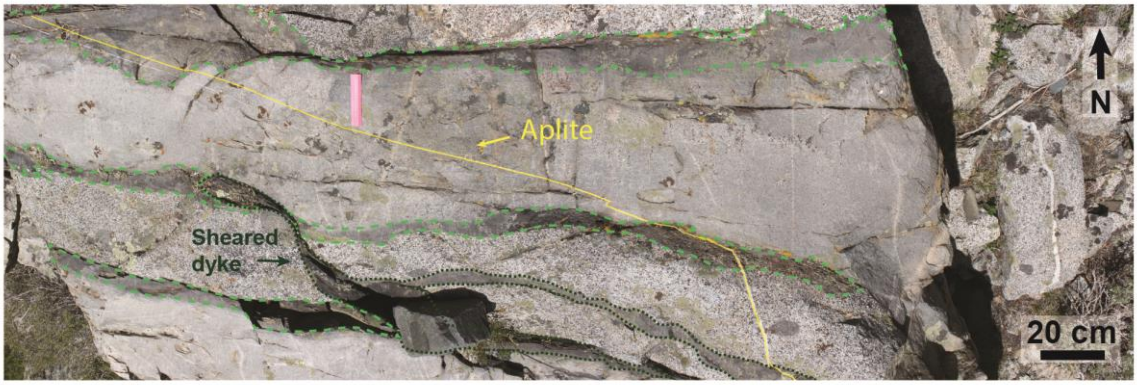

Fig. 3. 31. Example of a sheared mafic dyke intruded between two coarse grained dykes with fine grain borders.

During the data acquisition in the field, we found out that markers in the host rock, like aplite dykes, older dykes, mylonite zones, were displaced from their original positions by a parallel shearing process along the dyke margins (Fig. 3. 31). This process was described as well in Glazner *et al*. (1999) and Carl *et al*. (2002). In addition to this, we observed a tectonic fabric in the dykes, also generated by deformation processes (Fig. 3. 31 and 3. 33a). We took measurements of the markers, so we could generate rose diagrams in order to clarify their main orientations. This could help us to interpret the deformation trend. The rose diagram for the aplites shows a great scatter of orientations (Fig. 3. 32a). A predominant range of aplites between ~N5º to ~N40º (with ~N30º as maximum) (Fig. 3. 32a), probably related to a pre-dyke intrusion setting. The secondary group of aplites range between ~N120º and ~N160º, this orientation fits with the IDS trend and it could represent the later pulse of the IDS material. Even in some localities we can see how the aplite crosscut a dyke and present the S fabric inside the dyke, so the intrusion should have been probably during the deformation phase (Fig. 3. 34a). The mylonite zones are planar structures (Fig. 3.29g and h) which can be measured, so we plotted them in a rose diagram and the results show a range of orientations between ~N85º

and ~N135º (with the maximum at ~N105º) (Fig. 3. 32b). These sets have a similar range to the IDS dykes mean trend. Then, it opens the possibility to be connected to a pre to sin-intrusion shearing event (Martinez-Poza *et al*., 2013).

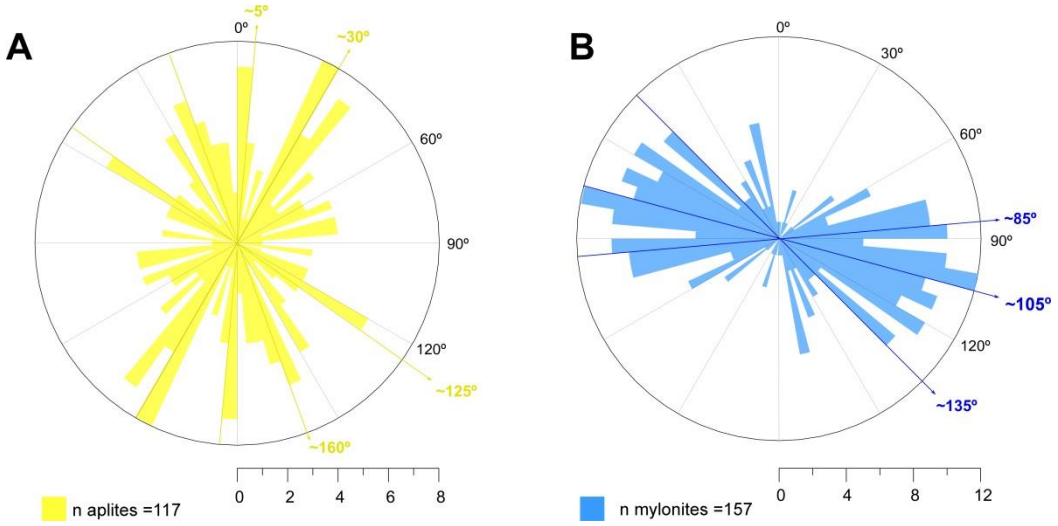

Fig. 3. 32. A) Rose diagram of aplite orientations measured in the field. B) Rose diagram of mylonites measured in the field.

The mylonite zones can be found in the host rock as fine linear structures that affect the whole rock mass (Fig. 3. 29g and h) or in the dyke margins, where the border of the granitoid in contact with the dyke appears affected by the shearing with the presence of tectonic fabric (Fig. 3. 29b). Inside some dykes, foliation is a remarkable feature, with the characteristic S fabric that together with the shear markers describe the sinistral shearing (and dextral shear in some examples too). Some aplites are affected by the shearing as well.

Other noticeable features found in the outcrops are bleaching bands and epidote veins that affects all the area as a later alteration phase. Propably associated younger brittle structures.

3.3.3.3. Apparent dilation analysis

The rose diagrams constructed for the collected measures from aplites, dyke jogs and other dilation markers show a preferential ~NW-SE opening trend (Fig. 3. 33d). A first approach for the opening direction characterization is made by taking pairs of measurements from matching offsets (aplites, dyke jogs and other markers) and the corresponding dyke walls (Fig. 3. 33d). The total number of pairs is 27 and they were registered in sub-horizontal and sub-vertical surfaces thanks to the 3-D outcrops configuration. The value for the apparent dilation strike shows a wide range of orientations, between ~N30º and ~N175º. The apparent mean dilation has a net direction of ~N140º, there are secondary sets as well (Fig. 3. 33d). The range span is similar to the dyke strike range (for

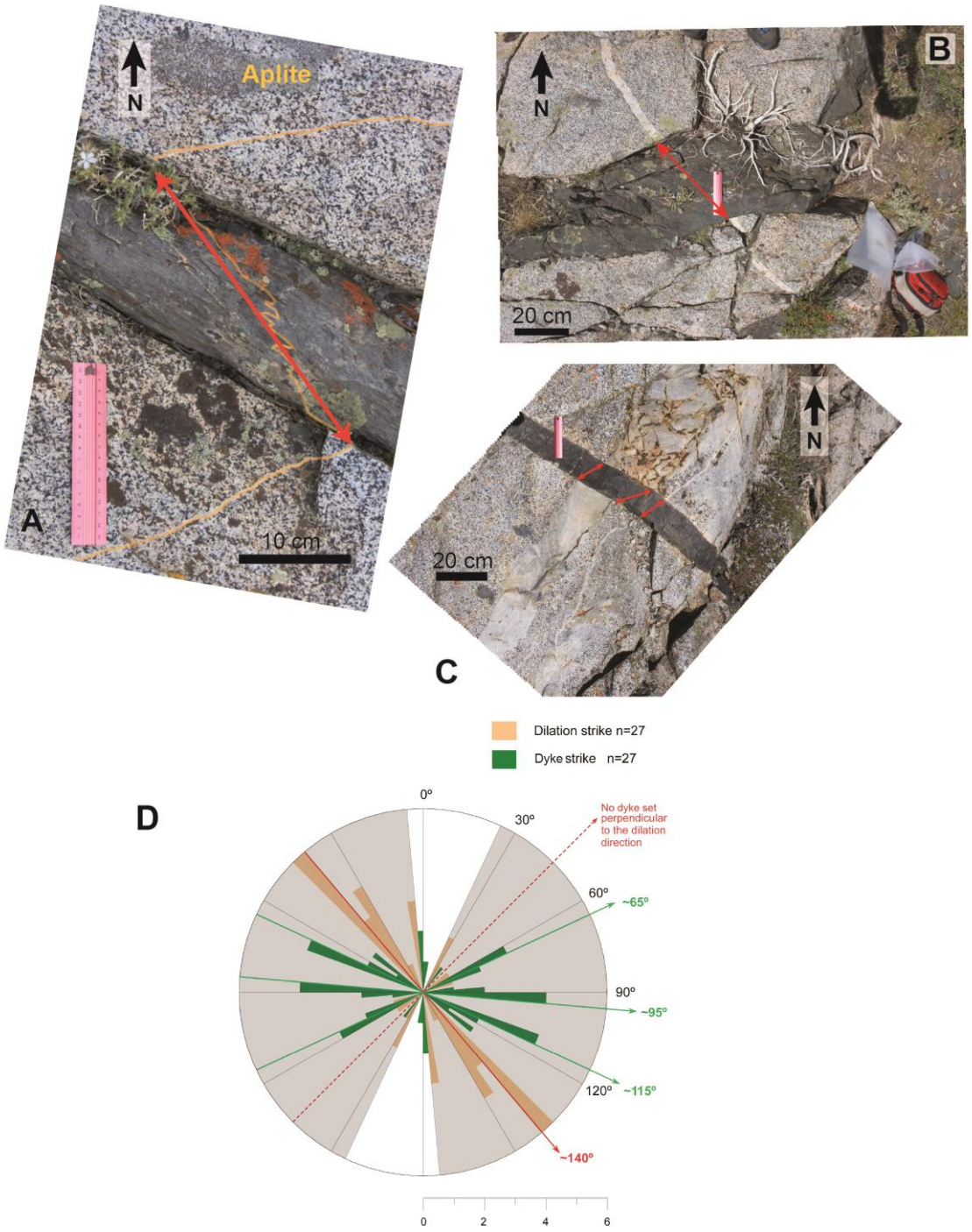

Fig. 3. 33. Examples of apparent dilation markers, all of them are photographs of sub-horizontal outcrops. A) Aplite vein displaced and folded inside the dyke. Dyke shows mineral lineation. B) Aplite dyke crosscut by a mafic dyke. C) Example of several aplite veins and dykes crosscut by a mafic dyke. D) Rose diagram showing frequency of 27 pairs of strikes of dyke segments and their corresponding apparent opening directions (measured from in detail oriented photographs). The gray area corresponds to the range in opening directions, which represents a wide range of dilation orientations. No dyke set is found in a normal orientation to the mean apparent dilation direction.

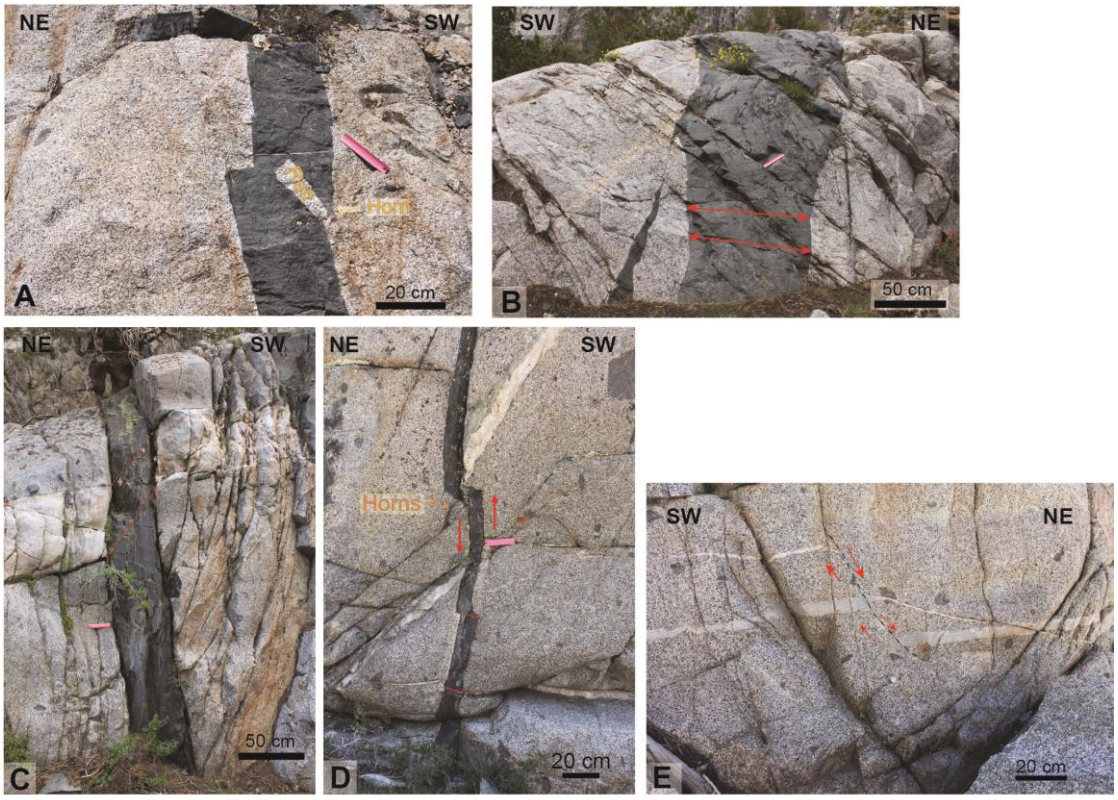

Fig. 3. 34. Examples of displaced markers and dyke segmentation in sub-vertical outcrops. A) Two dyke segments merged with a raft of host rock in between the dyke tips (horn). B) Aplite veins displaced almost perpendicularly to the dyke walls. Also some apophyses are observed. C) Mafic dyke displacing an aplitic dyke. D) Dyke segment where we can describe several left steps probably related to secondary joints and horn structures. In addition, an aplitic dyke is displaced sinistrally. E) Several aplite veins and dykes displaced along a dextral shear zone.

this diagram from ~5º to ~180º). In this case, the mean opening direction obtained does not match with the presupposed perpendicular value to the mean dyke direction. There is no dyke set perpendicular to the dilation direction (Fig. 3. 33d). As we describe later, the measured offset vectors do not agree either with the predicted values from the stress analysis (Martinez-Poza *et al*., 2013). Because of this wide range of opening directions and its difference in the dilation values with the model, the result implies a displacement of the original markers due to a (later) deformation process (shearing) within the dyke walls (later described).

3.3.3.4. Maximum dyke thickness

We measured digitally the dyke thickness using aerial photographs from the outcrop area (©Bing Maps, Microsoft Corp.), in grids of 5x5 m. We based our analysis in the geometrical method proposed by Baer *et al*. (1994) (applied by Le Gall *et al*. 2005) where it was settled that in a dyke segment (step, zigzag vein or dyke), the thickness can be determined if it has a constant net dilation (D) value, applying the following equation: $W = D\cos\alpha$, where α is the angle between the dilation vector and the normal vector to the dyke wall where W is measured. Then, if the segments present $\alpha=0$, they have the maximum possible

thickness, W_{max}=D and it corresponds to a pure extension situation with segments normal to the dilation. Therefore, following this fact, a correlation between strike and thickness of dykes can be significant in the estimation of the dilation direction (Baer *et al*., 1994; Le Gall *et al*., 2005).

During the analysis, we could distinguish a differential dyke orientation in the two areas of study. While in the *N* outcrop the mean trend is ~N120º; in the second outcrop, *N2*, we found out a deviation from the previous trend, ~N95º. The reason of this variation could be related to later block faulting, since evidences of fault planes with mineral growing and striation are found in

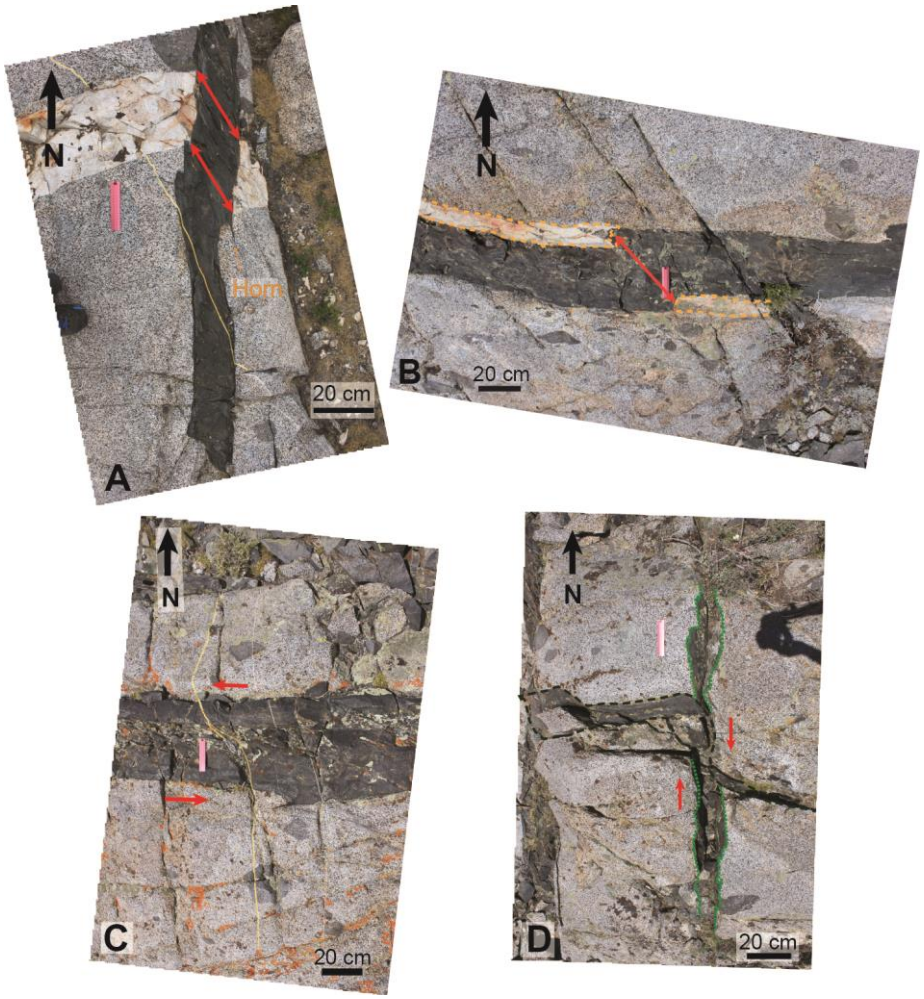

Fig. 3. 35. All the images were taken in sub-horizontal outcrops. A) Example of apparent dilation markers in an aplite crosscut by a mafic dyke. A horn structure and a later aplite veins are noticeable in the photograph. B) Example of an apparent dilation marker in an aplite displaced by the injection of a mafic dyke. C) Example of sinistral shear in an aplite vein intruded through a mafic dyke. D) Example of dextral shear occurred along a later mafic dyke.

the area between outcrops. This value of ~N95º is also de mean trend for the field measurements of the dykes, due to the major quantity of these dykes in the area. The general mean trend for both outcrops is ~N113º and the maximum extension is set at ~N112º, where the maximum dyke thickness is found (3.3

meters) (Fig. 3. 36c), with a range between ~0.4 to 1 m. Therefore, there is a good fit between the data. However, the apparent dilation direction obtained in the previous section (~N140º) (Fig. 3. 33d) does not match with the value of this diagram (~N112º). The divergence in more than 30º can be probably related to a shear event occurred along the dykes.

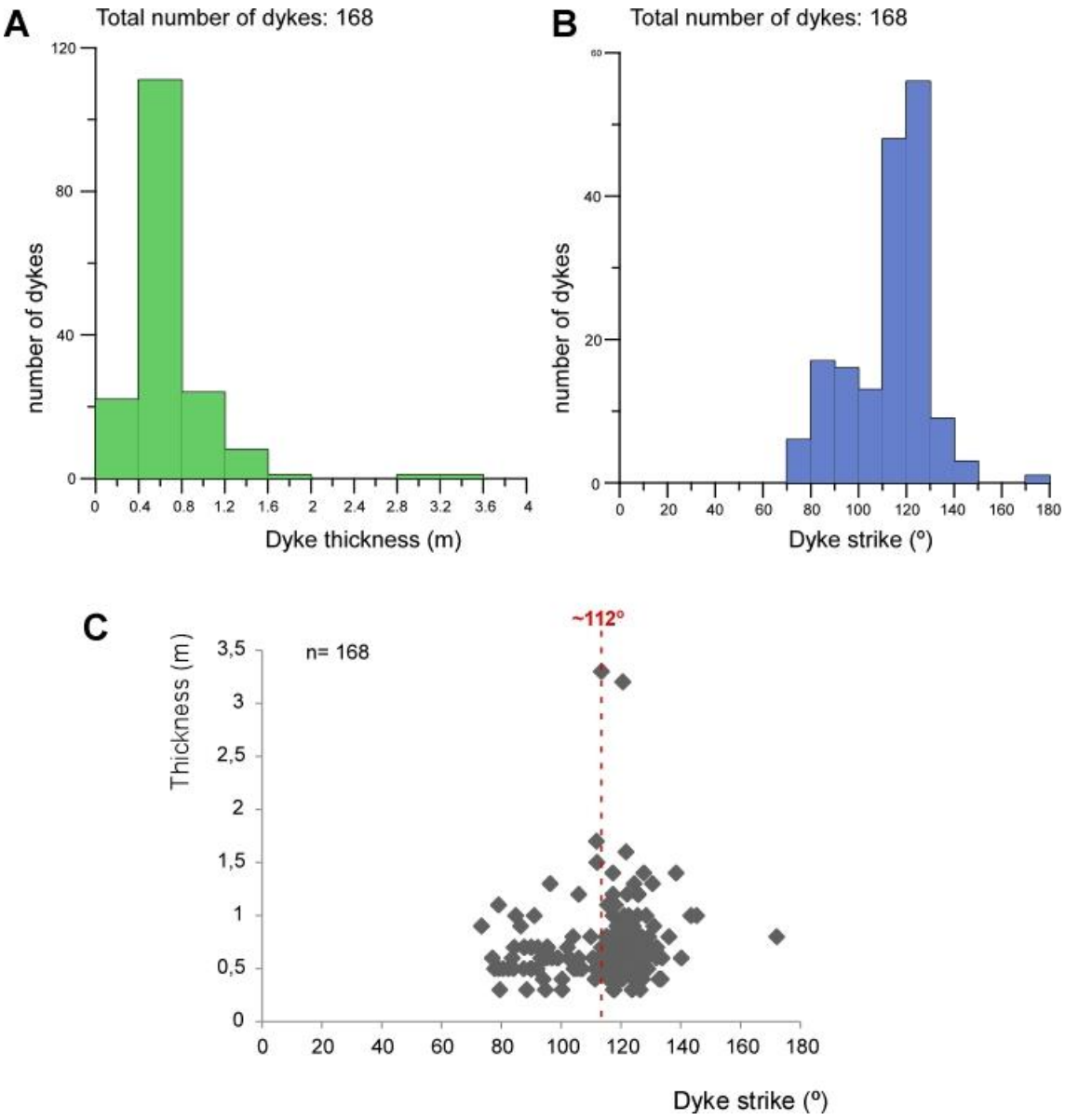

Fig. 3. 36. A) Frequency histogram of dyke thickness distribution. Measures are from aerial photographs of the two study areas. B) Frequency diagram of dyke segments thickness. More than 50% of these dyke s egments have strikes between N70° and N150° with a peak in the N110º-N130º interval. C) Plot of dyke segment strike vs. dyke thickness recorded from aerial photographs of the two sub-horizontal outcrops (*N* and *N2*) investigated in this study. The majority of dykes strikes between ≈N70° and ≈N150° and they reach thicknesses < 2m.

3.3.3.5. 3D paleostress analysis

We assumed that the intrusion took place into a network of preexisting fractures as proposed by Glazner *et al*. (1999). This assumption takes us to the 3-D analysis of the stress state during the swarm emplacement using the approach

firstly applied by Jolly and Sanderson (1997). The method obtains the Mohr circle for the opening of a preexisting fracture system due to the emplacement of mafic material. Previously to our application in the IDS area, many other studied have utilized the same methodology to describe the intrusion of fluids into the crust e.g: André *et al*. (2001), McKeagney *et al*. (2004), Mazzarini and Isola (2007), Yamaji *et al*. (2010), Mazzarini *et al*. (2011), Mondal and Mamtani (2013), Yamaji and Sato (2011), Sato *et al*. (2013) and Martinez-Poza *et al*. (2014).

The parameters related to the state of stress and the magmatic pressure can be deduced as well from the pattern of the pole diagram (fractures and dyke walls measurements). The dyke measures are plotted in a stereographic projection (using Stereonet software by Almendinguer, 2002). This method is based on previous studies by Baer *et al*. (1994), which correspond to a 3-D analysis, and by Delaney *et al*. (1986), that represents a 2-D Mohr construction. Using the 3-D approach by Baer *et al*., (1994) we can calculate the driving pressure ratio (R‘) and stress ratio (Φ) parameters. The driving pressure value (R‘) represents the deviation between the principal stress axes and the fluid pressure, while the stress ratio (Φ) defines the relative magnitude of the principal stress axes, it is also responsible of the shape of the stress ellipsoid (Angelier, 1984; Baer *et al*., 1994).

$$R' = \frac{P_m - \sigma_3}{\sigma_1 - \sigma_3} \quad (15)$$

$$\Phi = \frac{\sigma_2 - \sigma_3}{\sigma_1 - \sigma_3} \quad (16)$$

This shape is determined with the Φ values: Φ= 0, prolate stress ellipsoid; Φ=1, oblate stress ellipsoid and intermediate Φ values, triaxial stress, σ1> σ2> σ3. The driving pressure (R‘) is the parameter that establish the range of fracture opening; when R‘< 0, there is no possible opening; when R‘ > 0, the opening of the fractures depends on the stress ratio (Baer *et al*., 1994). When the dyke wall poles are plotted in a stereogram, their distribution is essential to describe the stress axis disposition (Jolly and Sanderson, 1997). If the disposition of the poles is concentrated around the minimum principal stress (σ_3), then the fluid pressure will be lower than the intermediate stress value (σ_2). In the other hand, when the dyke poles show a girdle organization with an empty zone around the maximum stress axis (σ_1), the fluid pressure will have a higher value than the intermediate stress axis (σ_2). We plotted the dyke wall data using the Stereonet software (Almendinguer, 2002) that includes Bingham statistics (Mardia, 1972), essential for the calculation of the symmetry axes. In addition to this, we need to calculate the angles that describe the Mohr circle. These angles depend on the fluid pressure of the system, if the fluid pressure is lower than the intermediate stress σ_2, the angle θ_1 is obtained from the σ_2-σ_3 plane, and θ_2 is measured in the σ_1-σ_3 plane. The two angles are disposed in a cluster of poles (Fig. 3. 37a). Then, in the case of the fluid pressure higher than the intermediate stress axis, σ_2, the necessary angles to describe the Mohr circle are θ_2 and θ_3, measured in the σ_1-σ_2 plane. Both angles display a girdle of poles.

In order to calculate the values of the stress ratio and the driving pressure we need the angles θ_1, θ_2 and θ_3 (depending on the fluid pressure case) to apply the following equations (Jolly and Sanderson, 1997):

$$\Phi = \frac{\sigma_2-\sigma_3}{\sigma_1-\sigma_3} = \frac{\tau_{max1}}{\tau_{max2}} = \frac{1+cos2\theta_2}{1+cos2\theta_1} \quad (17)$$

$$\Phi = \frac{\sigma_2-\sigma_3}{\sigma_1-\sigma_3} = \frac{\tau_{max1}}{\tau_{max2}} = 1 - \frac{1-cos2\theta_2}{1-cos2\theta_3} \quad (18)$$

$$R' = \frac{P_m-\sigma_3}{\sigma_1-\sigma_3} = \frac{a}{2\tau_{max2}} = \frac{(1+cos2\theta_2)}{2} \quad (19)$$

Our case has a fluid pressure $P_m < \sigma_2$, then we use the equation (18). The plot obtained for the dyke poles is a girdle of data centered in the upper part of the diagram (Fig. 3. 37a), with a subvertical dipping. This girdle disposition is consistent with a situation where the $P_m < \sigma_2$. The principal stress axes are calculated from the symmetry dyke poles using Bingham analysis (Fig. 3. 37a). The result for the maximum stress axis, σ_1, is N181/77, SE-NW and sub-vertically dipping; the intermediate stress axis, σ_2, is sub-horizontal (N286/4) and the minimum stress axis, σ_3, is also sub-horizontal with a NNE orientation (N017/13). The value of the apparent dilation axis from field data (~N140E/9) is not consistent with σ_3 axis after this analysis. This fact brings us to a context where a later shearing process should have occurred so there is a~47º anticlockwise rotation of the initial dilation vector (Martinez-Poza *et al*., 2013). Moreover, we calculated the stress ratio (Φ) and the driving pressure ratio (R‘) with the angles θ_1 (54.7º) and θ_2 (70.8º) applying equations (18) and (19). The

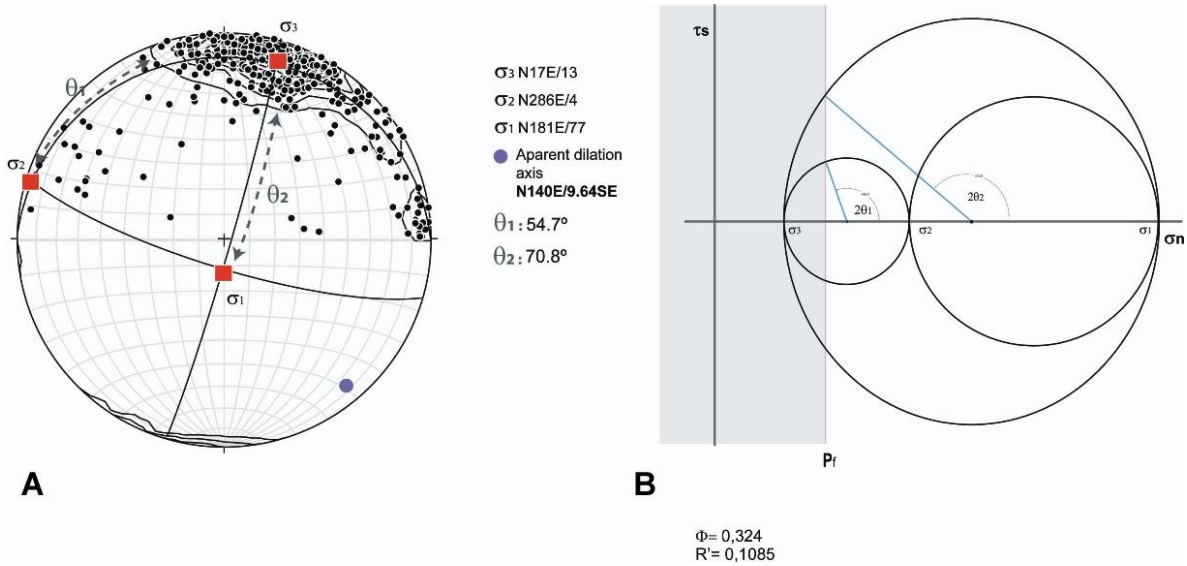

Fig. 3. 37. (A) Equal area, lower hemisphere stereoplot of poles to dyke segment walls fromall measured dykes in the IDS. The contoured area (contours at 1 per 1% area) indicate the orientations of fractures thatwere able to dilate duringmagma intrusion. Orientations of the principal stress axis (σ1, σ2, σ3) are derived from the cluster-like distribution of dyke poles and the angles σ1 and σ2. The apparent dilation direction obtained from field measurements is depicted for comparison. (e) 3-D Mohr circle producing a stress ratio (Φ) of 0.324 and a driving pressure ratio (R′) of 0.1085.

result for the stress ratio is Φ = 0.324 corresponding to a close to prolate stress ellipsoid with σ_1>>σ2>σ3 and R'= 0.108 for the driving pressure, this value is consistent with a magmatic pressure lower than the intermediate stress axis (σ_2). All this data allow us to construct a 3-D Mohr circle (Fig. 3. 37b). We can notice the fact that σ_2 and σ_3 are smaller than σ_1. Therefore, the tectonic regime and the pre-existing fracture network in the host rock took the main role during the emplacement of the mafic material.

3.3.3.6. Estimation of regional extension

We tried to evaluate the magnitude of the regional extension produced by the dyke emplacement. The procedure to obtain the extension value was proposed by Jolly and Sanderson (1995). First, using the same aerial photographs (©Bing Maps, Microsoft Corp) as in the maximum dyke thickness section, we traced scanlines with 5 m of distance between them at an angle of 120º, which corresponds to the general mean value of the IDS dykes for this area (corrected from the 95º obtained in field measurements due to the bias of field data). The parameter obtained in order to quantify the extension was the true extension value (TE), which is quantified using the value of the dyke segments width (t_i) and the spacing between dykes (s_i) by applying the following equation (Jolly and Sanderson, 1995):

$$\mathrm{TE} = \frac{\sum_{i=1}^{n} t_i - \frac{1}{2}(t_1 + t_n)}{\sum_{i=1}^{n-1} s_i} \times 100 \quad (20)$$

The mean TE value is ~15% extension, being the two areas of the outcrop similar in extension percentage (Table 3.1).

	Area (m^2)	Mean % TE
Group *N*	42000	16,17
Group *N2*	30225	14,69
Total	72225	**15,43**

Table 3. 1. TE% values

3.3.3.7. Geochemistry

The geochemical analysis started with the rock collecting during the field work Fig. 3. 38). We tried to choose all types of rock intrusions in order to characterize the geochemical range present in the IDS. In addition, we could complete and compare the new dataset with the previous geochemical studies (e.g. Carl, 2000, Glazner *et al*., 2008). The total number of geochemical samples is 41 (Appendix 1. Table 2). All the sample preparation and the later analysis was carried out in the rock-crushing and geochemistry laboratories of the University of North Carolina at Chapel Hill under the supervision of the Prof. Allen Glazner. First of all, the samples were crushed until they reached a size of 1/16 mm. This powder was first weighted (as well as the cruciable), then dried

in an oven at ~120ºC (~1h) so we could extract the humidity of the sample, then we measured again the sample and we placed the samples in a fumace at 1000ºC during 1h. This last step oxidize Fe^{2+} to Fe^{3+} and erase the presence of the structural bound H_2O^+ so we can analyze the LOI (Loss-on-ignition) (Appendix 1. Table 2) (Equation 21). In these samples, the highest value of LOI is found in the sample PC-3b (3.745% located in Poison Canyon, Ridgecrest), followed by the CC-1 sample (2.341% located in Crooked Creek, White Mountains). The other samples do

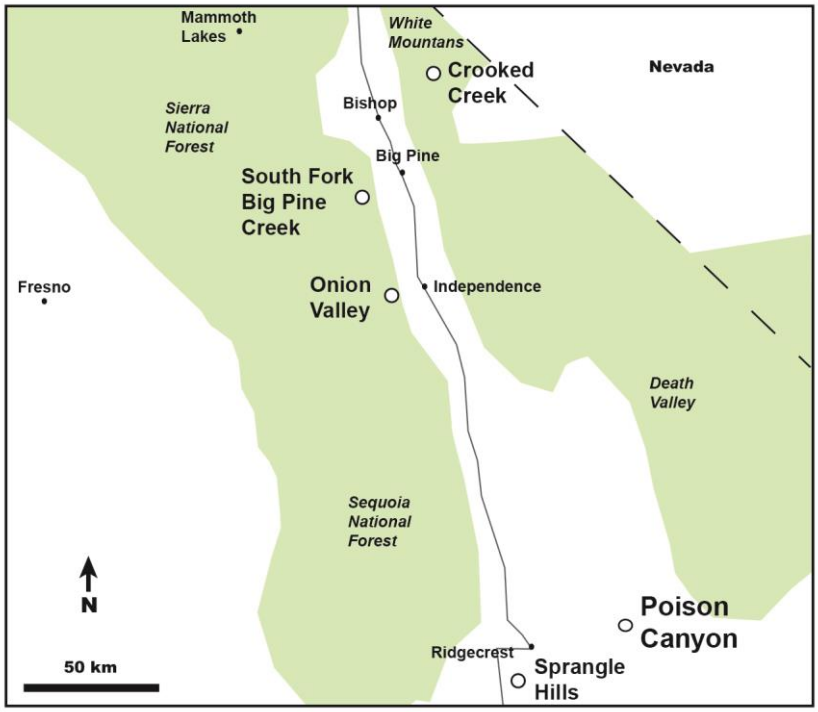

Fig. 3. 38. Map of samples locations. Poison canyona and Sprangle Hills in the south, near Death Valley and Mojave Desert. Onion Valley and South Fork Big Pine Creek in Sierra Nevada area and Crooked Creek in the White Mountains.

not overpass 1% (OV-1a reach the value of 1.826%, Onion Valley, Independence) of loss with an average value of 0.897%.

$$\mathrm{LOI} = \frac{Dried\ mass - ignited\ mass}{Dried\ mass} \times 100 \quad (21)$$

The LOI distribution helps us to distinguish the alteration grade of the sampled rocks and the possible connection with deformation processes that weaken the dykes (weathering, alteration processes, recrystallization, etc). Later on, this powder was treated in the Katanax K1 automatic fluxer in order to create the disks that were measured in the X-Ray Fluorescence spectrometer (Rigaku Supermini wavelength-dispersive XRF spectrometer). Using this technique we measured the major elements of the selected rocks. Appendix 1. Table 2, shows the major elements values for 41 samples.

Many dykes are described in the field as intermediate because of its texture and color characteristics, after the major elements analysis turned out to be basic in composition as seen in the Fig. 3. 39. Out of the total 41 samples, 23 of them

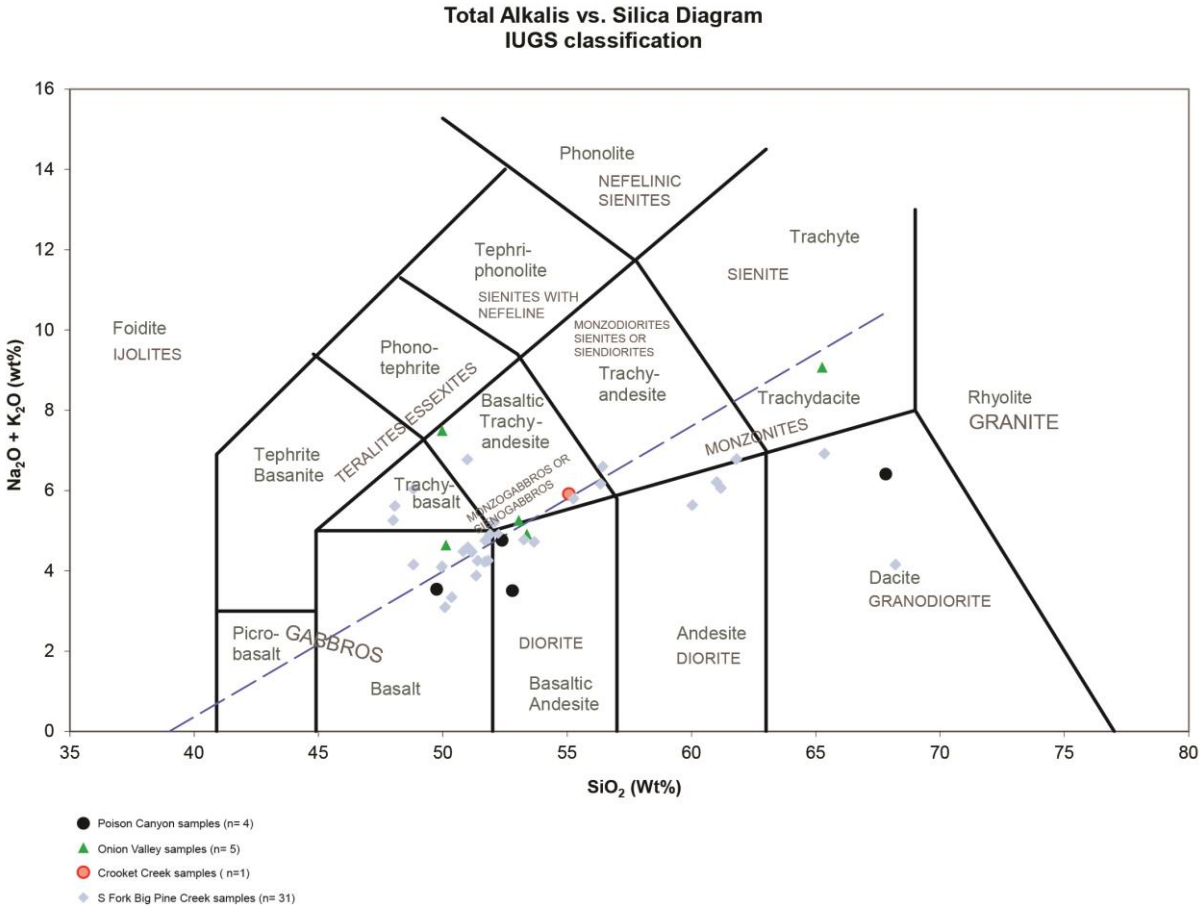

Fig. 3. 39. Total Alkali vs. Silica Diagram. IUSGS classification. Modified from Bartels spreadsheet .

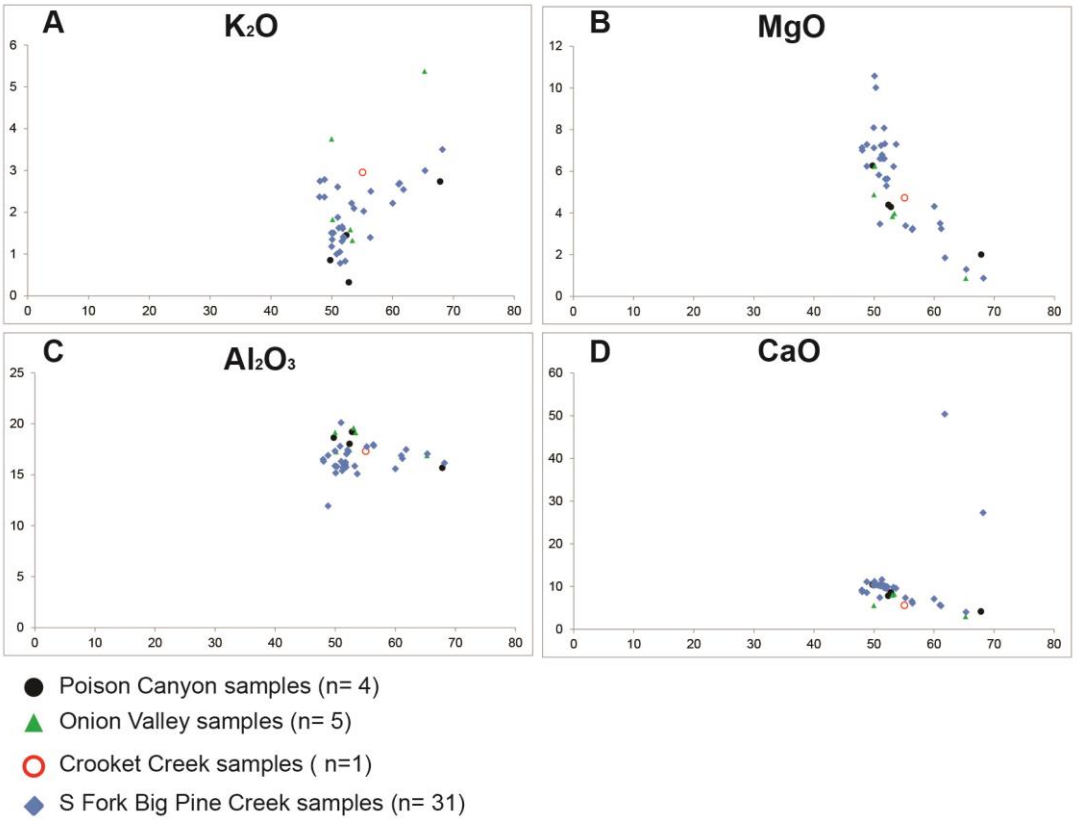

Fig. 3. 40. Diagrams of major elements vs. SiO_2. A) Diagram of K2O vs SiO_2, B) Diagram of MgO vs. SiO_2, C) Diagram of Al_2O_3 vs. SiO_2 and D) Diagram of CaO vs. SiO_2.

(~56%) are dykes with basic composition (45-52% SiO_2), while 16 are intermediate (~39%) (>52%<66% SiO_2) and just 2 of them are felsic (~5%) (<45% SiO_2) (Appendix 1. Table 2). In the IUGS total alkali vs. silica diagram (Fig. 3. 39) (IUGS Diagram), the SFBPC samples lay in a wide range of fields, from mafic to felsic: gabbros (the majority) to diorite and granodiorite; there are also some monzogabbros and monzodiorites. Samples from Sprangler Hills and Poison Valley show gabbro to diorite character with one granodioritic sample, while the samples from Onion Valley have a similar nature but with a more alkali content. The single sample from Crooked Creek (White Mountains) is a monzogabbro and it plots in the medium part of the diagram (Fig. 3. 39).

Several mayor elements vs. SiO_2 diagrams were constructed with the data from the XRF analysis (Fig. 3. 40). We can observe the basic character of the dykes (~56% of the dykes), although there is a high number of intermediate intrusions (~40% of the dykes). Only the MgO/SiO_2 and CaO/SiO_2 diagrams (Fig. 3. 40b and d) show a linear correlation between elements, the others do not really show any correspondence, being the K2O/SiO2 diagram the more divergent. It presents high potassic rocks (Onion Valley sample, Fig. 3. 40a), similar to older data from the same area (Glazner *et al*., 2008; Soresen *et al*., 1998; Sisson *et al*. 1996).

3.3.3.8. Petrographic description

The thin sections from the different dykes were very interesting to look in detail, mostly because we had thin sections of border and interior of the same dykes so we could compare their deformation texture and mineralogy. We used an optic microscope and the scanning-electron microscope (SEM backscattered images) in the UNC lab. The use of the SEM was also helpful for searching zircons, since it is a not very common mineral in mafic rocks and their sizes are small. All the samples show a medium to fine grain size, depending on the part of the dyke they are from. The textural description made with the optical microscope gave us a clear idea of the differences between dykes interiors and deformed borders. These characteristics as well as mineral zoning were supported by the later SEM study.

We have described in detail eight samples (Fig. 3. 41):

OV-4a: (monzogabbro) this thin section corresponds to the contact between a mafic dyke and the granitoid (in Onion Valley). Using the optical microscope, we can observe a very deformed sample in the contact between the granite and the dyke (Fig. 3. 41a). The mineral assemblage in the granite is composed by amphibole, titanite, quartz (with ondulant extinction), plagioclase, K-feldspar, biotite (aggregates). There is a lot of alteration. In the dyke, there is much oriented amphibole. It shows a parallel fabric to the granite contact, with a decrease in the amphibole grain size. The hornblende is small with a predominant fabric, but there are as well bigger crystals without orientation. There are phenocrystals of zoned pyroxene and elongated amphibole (actinolite) with a bigger grain size than the matrix. Titanites show a perfect

euhedral habit. Quartz –is~~h~~” and thin veins have ondulant extinction and same orientation as the hornblende fabric. Muscovite, epidote and zircons are also present. The SEM image (Fig. 3. 41g and h) confirms the texture and we found allanite grains inside apatites and Na-Ca plagioclase (Fig. 3. 41g).
BPN2-2a: (gabbro) this sample corresponds to the margin of an IDS mafic dyke (in South Fork Big Pine Creek). It presents a greenish colour near the contact. It has altered plagioclase (albite), titanite, pyroxene (diopside) as phenocrystals. In the matrix there is present pyroxene, titanite, quartz and plagioclase. In the granite there is pyroxene (exsolutions), quartz, altered plagioclase, titanite, biotite, amphibole (hornblende) and epidote. In the SEM images we can see

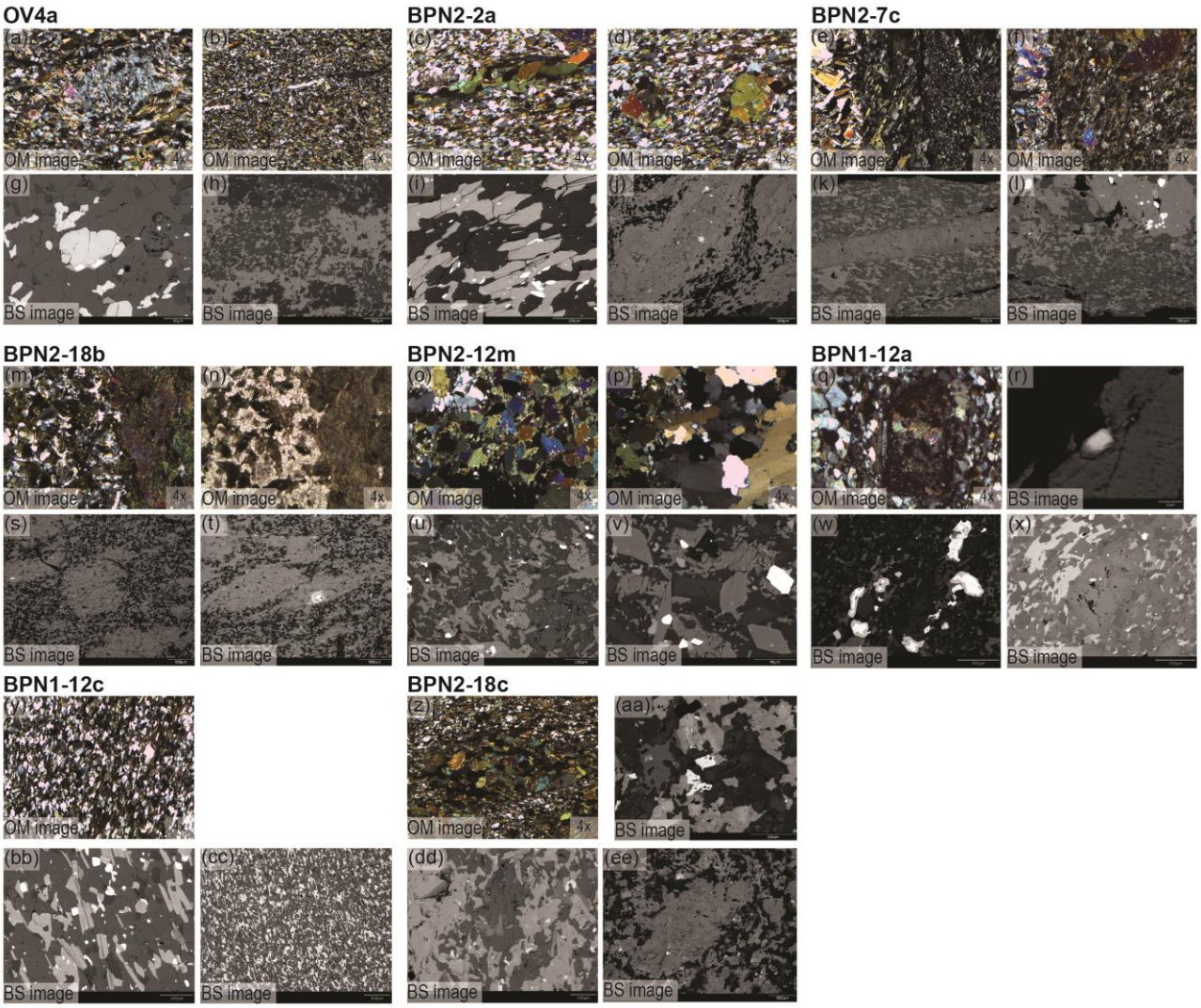

Fig. 3. 41. Thin section images. In each block, the upper images were taken with an optical microscope and the lower images correspond to SEM images.

inter-grow of chromite and titanite and minerals like biotite, chlorite, amphibole, plagioclase and pyroxene inside amphibole crystals (Fig. 3. 41c, d, l and j).
BPN2-18b: (diorite) it is the center of an intermediate IDS dyke. The texture shows agglomerate phenocrystals with a predominant orientation. It presents pervasive alteration. The plagioclase has a bigger grain size and zoning. There are phenocrystals of amphibole and pyroxene. Other minerals are biotite altered

to chlorite, titanite, zircon, epidote and Fe. Oxides. The matrix is composed by plagioclase, pyroxene, quartz, amphibole and titanite. The SEM shows detailed images of foliation around amphibole phenocrystals and some fractured amphiboles (Fig. 3. 41s and t).
BPN2-18c: (gabbro) this sample represents the mafic center of a dyke croscutting the intermediate (BPN2-18b) dyke. In visual observation the thin section has a dark colour. In detail, it shows mineral lineation of the phenocrystals and the matrix with elongate minerals. The mineral association is composed by biotite, pyroxene (diopside) and amphibole (hornblende) phenocrystals, chlorite, altered plagioclase, K-feldspar, muscovite, epidote and titanite (Fig. 3. 41z, aa, ss and ee). Same situation is observed in SEM images.
BPN2-7c: in this case, the sample corresponds to the margin of a basic dyke and the granodiorite contact. In the granodiorite, the plagioclases are totally altered to sericite, the quartz presents ondulant extinction and the amphibole is chrolitized. More minerals present are pyroxene, amphibole (actinolite) titanite and Fe. Oxides. Inside the dyke part, there is much alteration too; the grain size of the matrix minerals is small, it could be denominated as a cryptocrystalline matrix. There are empty fractures and other filled with quartz-muscovite (Fig. 3. 41f and k).
*BPN2-12a: (*granodiorite*)* this sample represents the center of an intermediate IDS dyke. In visual observation is remarkable the mineral lineation marked by dark and clear minerals, both oriented. There are altered phenocrystals of zoned plagioclase, amphibole, pyroxene, biotite, Fe. Oxides, K-feldspars, quartz, titanite, epidote, chlorite, rutile, muscovite, apatite and zircons. In SEM images, we could distinguish pyrite minerals surrounded by rutile (Fig. 3. 41w).
*BPN2-12c: (*monzogabbro*)* this sample is the border of an intermediate IDS dyke (the border corresponds to the dyke in sample BPN2-12a). There is also noticeable mineral lineation in visual observation. It shows a general reduction in the grain size, all the sample can be described as matrix (cryptocrystalline). The minerals distinguishable are quartz, amphibole (actinolite) as phenocrystals with mineral lineation, epidote, plagioclase (albite), elongate biotite, titanite and Fe. Oxides (Fig. 3. 41y, bb and cc).
BPN2-12m: this thin section comes from a mylonite. It presents greenish pyroxene (diopside-hedenbergite) full of inclusions, quartz, with ondulant extinction and partially recrystallized and other type of pyroxene. More minerals are Fe. oxides, euhedral titanites, plagioclase, amphibole, muscovite, zircons and apatite. There are zones of grain size reduction (Fig. 3. 41o, p, u and v).

3.3.3.9. Geocronology analysis

Some of the samples (14-BP-01, 14-BP-02, 14-BP-03 and 14-BP-04) were selected to be dated through zircon and titanite analysis. The separation and picking process was effectuated in the geochronology lab at the UNC. After the crushing step, we conducted the water table separation where we collected just the heavy fraction of material, in which the heavy minerals should be found. However, we had to use the medium fraction as well, since there were a small proportion of zircons in the heavy part. Later on, we continued with the separation of the heavy minerals, in this case, with the heavy liquids separation

procedure. We followed the steps required of mounting and waiting times. The heavy liquid used was methylene iodine (ρ = 3.32 g/cm^3) and our minerals of interest were zircons, with a density of 4.65 g/cm^3 and titanite, ρ = 3.48 g/cm^3, therefore, the heavy liquid used is appropriate for the separation process. Afterwards, the separated part was dried out and finally passed through a Frantz magnetic separator where we collected the zircon, titanite and other minerals depending on their magnetic susceptibility. In our case, we separated the minerals with a current higher than 0.62 amps, which is appropriate to separate titanites; zircons need a higher current to be separated but we did this process manually. The following steps were handpicking of the zircons and titanites. We discovered the tiny size of the zircons, although some of them had a perfect habit. This fact reduced the quality of the measurements with the laser since the spot size (3 nm) is very close to the crystal size. All of them were mounted in epoxy and polished (with 1µm diamond abrasive on a polish-wheel) previous to the analysis. Finally, a map of the minerals was made, in the SEM laboratory of the Geology department at UNC, before sending them to the geochronology lab in the LA-ICP-MS (LASS, laser-ablation split-stream inductively coupled 6 plasma mass spectrometer) facilities of the Department of Earth Science at UCSB. The results were adquired and processed with the Iolite software (version 2.3, Paton *et al*., 2011). The Concordia diagram (Fig. 3. 42) was obtained using Isoplot software (Ludwing, 2008) based on the 206Pb/238U ratios, so the lead contamination of the sample surface is not taken into account. The diagram shows a good fit of the data. Although some points lie in the right side of the concordia.

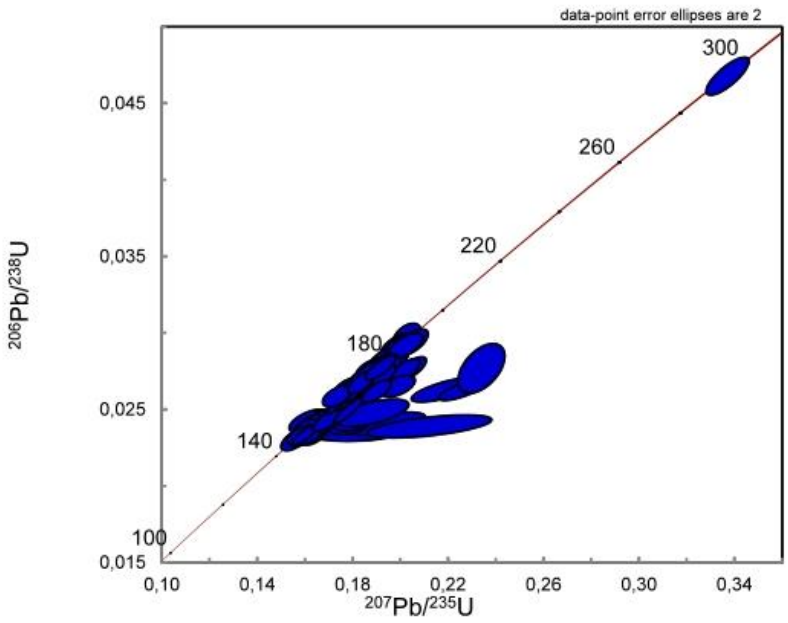

Fig. 3. 42. Concordia diagram for the analysed samples from SFBPC. $^{206}Pb/^{238}U$ vs. $^{207}Pb/^{235}U$, with data point error of 2. The total of data is 91 age points.

The results of the zircon analysis for $^{206}Pb/^{238}U$ ages give us a range of data between 147-190 Ma, and we can distinguish an inherited crystal of 295 Ma (Appendix 1. Table 3). The total number of ages obtained are 90 from the two mounts analysed (Z and Z2). Mount Z has zircons from 14-BP-01 sample (intermediate IDS dyke); 14-BP-02, a mafic IDS composite dyke; 14-BP-03, which corresponds to a basic pre-IDS dyke (in the field it was characterized as intermediate because of the pale green colour) and, finally, 14-BP-04, a very sheared mafic pre-IDS dyke. Mount Z2 only has zircons from samples 14-BP-02 and 14-BP-04 because these samples present the fewer amount of zircons, so a rerun of the separation process was made in order to obtain more and better crystals. The Z mount displays 83 ages, with a range of age between 147 Ma to 190 Ma, over 40 Ma of difference. The Z2 mount only gives 7 age data. The ages vary between 162 to 176 Ma one of them the 295 Ma. This age corresponds, with total security, to the sample 14-BP-04.

Titanites were firstly proposed to be dated as well. However, all the crystals turned out to be metamorphic, so no age analysis could be carried out.

3.3.4. Discussion

3.3.4.1. Dyke pattern

We found out an important variation of the dyke orientation in this particular area. The rose diagram of dyke walls shows a mean trend of ~N95º (Fig. 3. 28e) while the general mean value for the dyke swarm is ~W-NW (~N140º to ~N155º) (Moore and Hopson, 1961; Chen and Moore, 1979 and James, 1989). This mean value is variable in some areas around 10º-30º west (Glazner *et al*., 1999). However, the variation found in this particular outcrop is bigger than the proposed by Glazner *et al*. (1999); in this case there is a bigger shift of ~45º to ~60º anticlockwise in the dyke trend. Other studies (Moore and Sisson, 1987) found out some dykes with a change in orientation ~90º. They proposed an explanation based on the later deformation processes that took place during the Cretaceous. The secondary set present in the rose diagram (Fig. 3. 28e) at ~N175º is more coincident with the overall value. These facts bring us to the hypothesis of a local change in the intrusion direction due to the pre-existing joint network, inside an echelon array of fractures. Or another interpretation based on local anomalies due to later block faulting in the area since we observed some faults and striation in the outcrop.

The typology of dykes is described based on visual characteristics as wall orientation, crosscutting relations and, later supported by the geochemical analysis. Four types of intrusions are distinguished (older to younger): (1) a pre-IDS set of coarse grain dykes (in the field described as intermediate but after XRF analysis characterized as basic). (2) *Composite dykes* (IDS, ~E-W), formed by the injection of several *dykelets.* Usually they present fine-grain mafic margins and intermediate fine-grained centers. Same characteristics as the

ones described by Glazner *et al*. (2008) in Woods Lake and Big Pine area. (3) The more abundant set consist of a group of fine-grained mafic dykes from the IDS main pulse (~E-W to ~NE-SW) and (4) the last dyke set is a composite of felsic material and xenoliths (~NNE-SSW). The dyke sets represent the intrusion history of the area and give us a clue of the different magmatic pulses and the possible changes in tectonic stresses during a short period of time. This is also supported by the presence of several aplite sets that show crosscutting relations with the dykes.

The general hypothesis for the dyke swarm is an intrusion process through pre-existing fractures produced by the transtensional/transpressional setting generated by the oblique subduction (Glazner *et al*., 1999). However, we were not able to measure these linear features in the outcrop. This area is full of joints caused by the glacial polish, meteorization and cooling of the granitoides. Hence the measurement of the joint system was very difficult, even some of these pre-intrusion fractures could be obliterated by later ruptures. A possible solution is trying to look for other areas of the swarm with less glacial effect and describe the joint pattern.

Segmentation as classically described in the literature (Delaney and Pollard, 1981; Pollard and Aydin, 1984; Olson and Pollard, 1989; Hoek, 1991; Baer, 1991; Rubin, 1995; Weinberger *et al*., 2000; Gudmunsson, 2002; Druguet *et al*., 2012 and many more) can be very easily characterized in the area. The majority of the dykes present a linear and continuous sub-vertical disposition with dyke offsets, jogs and steps in some points which are helpful for the analysis of the dilation direction. Also we could describe some merging structures with associated horns. Discontinue segments were rarely observed.

3.3.4.2. Deformation markers

3.3.4.2.1. Mylonites

The most noticeable features in some of the dykes are shearing evidences, as displacements of dykes and aplites markers, mylonite bands in the host rock and in the dyke margins or affecting aplite dykes. A tectonic fabric is also present in some sheared dykes that even fold and displace aplitic veins inside dykes (Figs 3. 29f; 3.31; 3.33; 3.34 and 3.35). Figs 3. 33a and 3. 43 shows how the aplite vein can be folded. The vein is located in the shortening domain inside a pure shear zone. The effect is produced due to the viscosity contrast between the aplite vein and the mafic dyke. Generally, the shear markers show a sinistral sense of motion. The plotted data from mylonitic bands show a very similar range of orientations (~N85º to ~N135º) to the mean IDS trend, so is possible that the shear event occurred in a period closed to the intrusion of the dyke swarm.

Previous work by Carl *et al*. (1998) in Woods Lake pluton described mylonites with a WNW orientation and sinistral shear, while NNE mylonites had dextral shear. Crosscutting relations in the Woods Lake pluton where sinistral to

reverse-sense and the mylonites were cutting the pluton (Chen and Moore, 1982) and they are affected and affecting the IDS. The mean mylonite orientation is NE and dip SE and its size range from <1m to >10m, with probably more than 100s meters of displacement in some points (Carl, 2000). All these evidences suggest that the shearing process occurred simultaneously to the IDS intrusion (Carl *et al*., 1998).

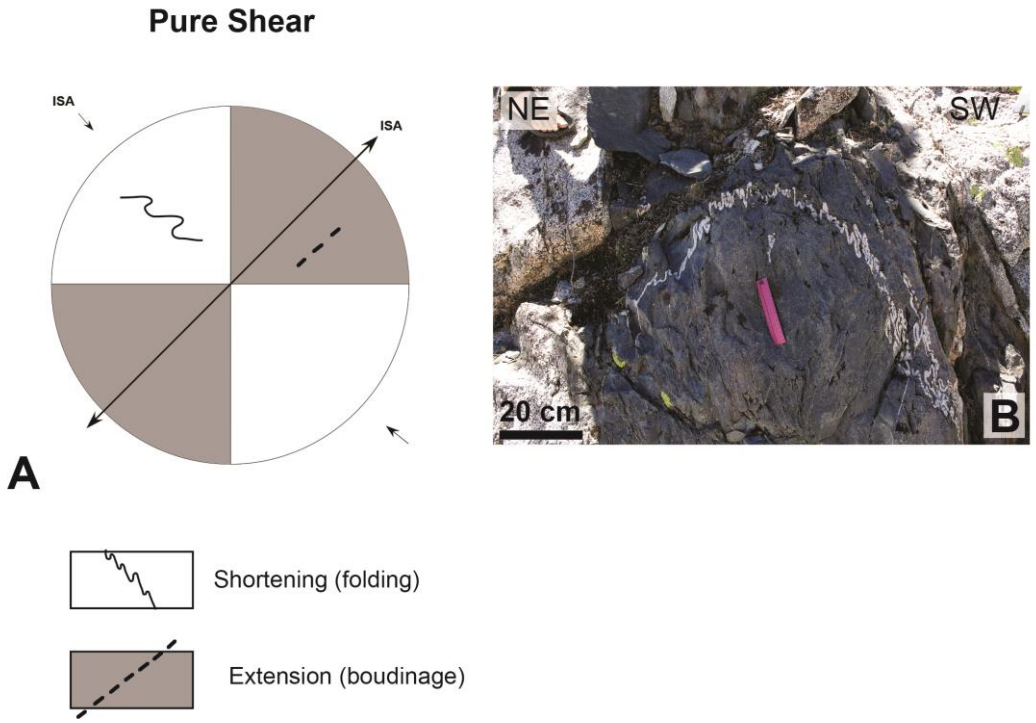

Fig. 3. 43. Example of folded aplite dyke inside a mafic dyke. A) Diagram of theoretical *Pure shear* situation. B) Image of the folded aplite.

This foliation and shear fabric is found in other parts of the dyke swarm, from the eastern Sierra to the south in Coso Range and Spangler Hills, even south of the Garlock fault (Moore and Hopson, 1961; Whitmarsh *et al*., 1996; Karish *et al*., 1987, Powel *et al*., 1984; Glazner *et al*., 1999; Carl, 2000; Carl and Glazner, 2002). As discussed in some of the articles named before, the origin of the deformation structures could be related to the shearing localization in the dyke-host rock margin (Carl and Glazner, 2002).

In the Lake Erisson granodiorite and Mono Lake granite (Sierra Nevada, California), Pennacchioni *et al*. (2013) described the nucleation of mylonites in homogeneous granitoides. They described several deformation structures in the area as bulk foliation, joints, ductile shear zones, epidote-quartz veins and faults with cataclasites and pseudotachylytes. This features formed in different time periods of deformation related to the temperature conditions. The foliation is localized near tips of ductile shear zones, related to C planes, with a dextral shear sense. Ductile shear zones accommodate the deformation via foliation in the two margins of the shear zones. There mylonite bands has ~mm-cm thick with sigmoidal foliation and also affects leucogranitic dykes. Generally, they are right-stepped when it is a sinistral shear zone and left-stepped when dextral. For Pennacchioni *et al*. (2013) this represents a contractional regime between strain and faults. There are also sheared quartz veins and the leucogranites

transformed to mylonites because they have localize the deformation (also described by Christiansen and Pollard, 1997). In general, dykes seem to be weaker than the granitoides and they resulted to be affected by the shear zones.

Pennacchioni and Mancktelow (2007) proposed that the origin of this type of shear zones was planar heterogeneities in granitoides. The orientation of these planes was not related to state stress, so multiple directions can be expected for the shear zones. Therefore, joints, faults, veins, dykes can operate as shear localization areas.

3.3.4.2.2. Apparent dilation direction

We plotted the data from the dilation markers in the dykes (displaced aplites and dyke jogs) and we obtained a ~NW-SE mean trend. The opening range is large (~N30º to ~N175º), so the apparent dilation value is not accurate enough. Theoretically, dyke opening should present a perpendicular orientation to the mean dyke trend which is not noticeable in the diagram (Fig. 3. 33d). There is no dyke set with a perpendicular orientation to the dilation. The explanation we proposed for this shift in the opening trend is related to a displacement of the markers due to a later (or close to the injection) deformation event. We can propose a shift in the apparent dilation strike between ~5º clockwise to ~150º anticlockwise.

Glazner (1999) carried out an in deep research about the oblique deformation found in diverse locations of the IDS. He found evidences of a N-S net opening direction in Woods Lake and Twin Lake areas. The data collection of the pre-dyke markers indicates a sinistral movement in the NW oriented dykes and dextral movements in the NE oriented dykes, in both cases, the opening vectors show a N-S trend, then oblique to the dyke opening direction. The opening vectors seems to have been modified obliquely by the later shear occurred along the dykes and even dykes without ductile fabrics show an oblique dilation direction. The analysis was made basically in sub-horizontal surfaces, so the vertical component when measurable, showed a small number. The 2-D shear sense was ambiguous in previous works (Wheeler, 1987). Aplites can be good indicators since they have an apparent separation coherent with the real shear sense. There are evidences of parallel shearing in the dyke walls, thus the dykes were still molten when the deformation occurred (Philpotts and Asher, 1994). This is known because there are blocks of host rock embedded with dyke material and separated sinistrally from their original locations. This is an unpredictable relation due to the composition of the two rocks, since the mafic dyke is supposed to be stronger than the granodiorite wall rock. Because of that, during the deformation phase, dykes probably were hotter than wall rock, so this shearing should have been coeval or shortly after the intrusion. In this context, dyke intrusion represented a preferential path for the shearing evolution

Based on structural correlations that support a lateral component for the dilation, this deformation should have probably happened during the cooling of the mafic dykes. Consequently, the sequence of intrusion should have been dilation normal to the dyke walls, followed by shear parallel to the dyke walls.

The stress analysis for this situation sets the principal stress axes rotated counter-clockwise to original stress axes during the emplacement. If the sinistral shear occurred simultaneously to the dyke injection, the tectonic setting should have been transtensional. Therefore, at the same time there was occurring sinistral shearing, magma intrusion and horizontal compression.

An important upgrade in the dilation measurement would have been applying Bussell's method (1989), which requires the measurement of the segments of a step in a dyke. These segments represent two planes in which intersection is implied the opening vector. The reason why we could not apply this analysis here was the lack of steps in these dykes, since they show a more linear disposition. Having the estimation of the parallel to dyke walls shearing we could obtain the real opening direction value for the net dilation.

3.3.4.3. Maximum dyke thickness and extension range

The thickness vs. dyke strike diagram obtained for the description of the dyke thickness show a range of values between ~0.4 to 1 m, being the thickest dyke ~3.3 m, at an orientation of ~112º (Fig. 3. 36c). The mean orientation is ~N113º. This value represent a good fit if we take into account the theory of dyke opening, although if we compared the data with the dilation value from the previous section (~N140º) there is a difference of ~28º. The clockwise rotation shown by the relative dilation value is probably related to the shearing event that displaced all the markers and produced the tectonic fabric.

The calculated value of True Extension for the two outcrops is ~15%. Both areas show similar extension percentage. A broader analysis in other IDS locations would help to characterize the general extension range in the dyke swarm. Moreover, the intrusion distribution could be described if the magma source of the swarm, which is supposed to be the area with higher extension, is found. Thus, we could infer the center of the dyke swarm intrusion and the dyke swarm pattern (related to the regional setting).

3.3.4.4. 3-D Paleostress analysis

This analysis can be carried out under the premise of an intrusion of the magmatic material into a pre-existing joint network (Glazner *et al*., 1999). This is necessary to apply the 3-D Jolly and Sanderson (1997) method. We obtained the three principal axes and we constructed the Mohr circle for the emplacement setting. The principal axis (σ_1) has a N181/77 orientation; the intermediate axis (σ_2) is sub-horizontal, N286/4 and the minimum stress axis (σ_3) is N017/13. We compared the σ_3 value (N017/13) with the data for the apparent dilation direction obtained from the dyke markers (~N140E/9); however they are not coincident as they were supposed to be. There are ~47º of anticlockwise rotation, possibly related to the shearing process occurred shortly after (or during) the intrusion of the mafic dykes. This rotation value is even bigger than the amount of rotation obtained in the maximum thickness analysis.

Thus, the total range of anticlockwise axis rotation should lie between ~28º to ~150º and ~5º clockwise. Taking into account the wide range of values from the apparent dilation markers, the rotation obtained from the maximum dyke thickness and the difference between σ_3 and the apparent mean dilation vector.

We calculated other indicators of the stress state, as the stress ratio (Φ) and the driving pressure ratio (R'). The stress ratio (Φ) describe the relative value of the main stress axes, hence it defines the stress ellipsoid. In our analysis we got a value of Φ= 0.324 corresponding to a close to prolate stress ellipsoid, $\sigma_1 >> \sigma_2 > \sigma_3$. The driving pressure parameter describes the fluid pressure which means the divergence between the stress axes, then, R'= 0.108 as the fluid pressure is lower than σ_2. This is consistent with field observations since not much segmentation or damage zones are observed either in sub-vertical or sub-horizontal dispositions. Using this values together with the estimation of the correspondent angles (θ_1= 54.7º and θ_2 =70.8º), we obtained the 3-D Mohr's circle. The analysis of the Mohr diagram gives us the idea of an intrusion controlled by the tectonic setting rather than by the magmatic pressure.

3.3.4.5. Geochemical analysis

The insights provided by the XRF analysis of the dyke samples give us a better understanding of the intrusion. Dykes described in the field as intermediate because its visual characteristics turned out to be mafic. They also have a very similar composition as their darker and fine-grained margins. Generally, dyke margins show systematically a more mafic character than dyke interiors. One explanation could be possibly related to chemical differentiation (Latypov *et al*. 1999) helped by shearing processes, another can be a later pulse of mafic magma intruded trough the same fracture system and forming the dyke margins. The samples taken in other areas of the swarm (Poison Canyon, Spangler Hills, Onion Valley and Crooked Creek) follow the same pattern as previous samples studied over the years. This gives us a good control marker of the analysis, so no contamination process has occurred. The LOI analysis is interesting because we can decipher which sample is more altered and related this value to the deformation process (Appendix 1. Table 1, LOI data). However, in this case, the LOI differences are not so indicatives of the shearing process. The more altered samples are found in desert-like (Poison Canyon) and high mountain (Crooked Creek, White Mts.) outcrops. Moreover, not all the pairs of margin/interior samples show the highest LOI % in the margin sample, then no correlation can be made.

The classification of the samples depending on alkali content and major elements shows a very similar distribution as in the previous compilation of geochemical data (Glazner *et al*., 2008). The majority of the intrusions have a basic character, but intermediate dykes are abundant as well. Previous authors (McManus and Clemens-Knott, 1997) proposed that the variability in composition from mafic to felsic (~47% to ~72% SiO_2) was produced by the fractionation of hornblende or pyroxene and plagioclase from the parental source. Studies by Hopson (1988), described the intrusion as the result of the

exposition of large deep plutonic bodies from the Late Jurassic. Hopson (1988) also noted the more silicic composition of the IDS in comparison to other large rift related swarms, so the origin could be related to other tectonic setting rather than the classical extensional origin.

The petrographic description of the thin sections illustrates the changes suffered by the minerals due to the shearing processes, mainly in dyke margins and deformed dykes. We can recognize grain reduction in dyke borders, quartz grains with ondulant extinction (Fig. 3. 41) which imply plastic deformation. We observed aggregates of pyroxenes and amphiboles with a preferred orientation. In addition, there are pyroxene and amphibole porphyroclasts around which the foliation is concentrated (Fig. 3. 41a and d). In several samples, an aggregate lineation is well developed (Fig. 3. 41y) (Paschier, C.W. and Trouw, R. J. A, 2005). All these characteristics agree with the existence of mylonite zones. Some of them are visible in the granitoides and also they concentrate in the dyke margins and affect dyke interiors as well. The conditions for the growth of this mylonite bands were probable low to medium grade, since they do not display big thickness and the main deformation mechanisms are grain reduction, deformed grains wrapped by foliation, well developed foliation (e.g. inside dykes) and sharp boundaries. Oriented thin sections would have helped us to confirm the sinistral shear sense.

3.3.4.6. Age of dyke emplacement

The intrusion ages give us the general idea of the event/s that produced the magmatic injection. The majority of the ages are around 147 to190 Ma, this supposes a duration of ~40 Ma for the intrusion (Early Jurassic (Pliensbachian) until the end of the Late Jurassic (Tithonian)). This time period matches with the previous hypothesis of the IDS intrusion during the oblique convergence in the Jurassic.
In particular, we can separate the ages of each zircon mount. In the Z mount there are all the samples types from intermediate IDS dyke, to a mafic IDS composite dyke; a basic pre-IDS dyke and a very sheared mafic pre-IDS dyke. However, mount Z2 is more restricted and only has samples from mafic and sheared dykes, so we can delimit the age of this two types. Mafic dykes are delimited around 162 to 176 Ma (Middle Jurassic) (5 data). And the sheared dyke has one age at 295 Ma (inherit crystal) and other age at 176 Ma, in the same range as the other type of dyke. No clear difference in intrusion age can be found in the dated ages, all of them are represented in the same time interval. Therefore, only crosscutting relations can help us to differentiate the different intrusions.

In addition, the age of the Tinemaha granodiorite where the dykes locally intruded is ~165 Ma. This fact supposes a coeval intrusion of both magmatic fluids, since there are dykes with an older age than the pluton. Therefore, there is a good reason to improve the dating ages. Maybe a better in detail analysis of a larger number of zircons from each dyke family will help us to constrain a better intrusion age for dykes and plutons. This is a difficult task since in mafic

dykes there is not much presence of zircons and the found ones usually are tiny fragments, which are difficult to date by geochronology.

3.3.4.7. Proposed model for dyke emplacement

The final proposed model that results from the combination of the evidences observed in the field is formed by two steps process (Fig. 3. X). First, a setting where the dykes families intruded sequentially into an *en echelon* fracture system (Glazner *et al*. 1999): Coarse grain dykes (~N95º), composite IDS dykes, mafic fine grained IDS dykes (~N113º), aplites veins, composed of xenoliths and wall rock and finally a later set of aplites. The aplite veins performs as dilation indicators

Right after, a deformation event occurred and the aplite and other markers are displaced from their original positions. The mylonite bands are developed and the tectonic fabric in the dykes formed together with folding of aplite veins inside dykes. The sense indicators (matching veins and steps) show a sinistral movement (Fig. 3. 44). This deformation phase probably supposes the reason of the rotation of the dilation markers as seen in the stress analysis (Martinez-Poza *et al*., 2013). The tectonic stresses during this time suggest a transpressional setting (Glazner *et al*., 1999)

All the different evidences occurred in a very small area (~72000 m^2) in comparison to the extension of the Independence Dyke Swarm throughout California, so the question is whether this is just a local process or it can be extrapolated to other areas of the dyke swarm

Previous geochronological studies settled a limited time for the intrusion of the dyke swarm generated by a discrete tectonic event (Chen and Moore, 1979; James, 1989) that increment the amount of sinistral shear. Several causes are proposed to explain the modification in the tectonic setting to produce the magma injection. One explanation is a probable collision between and arc and the continental margin, another is the rapid change in plate kinematics during the end of the Jurassic (Glazner *et al*., 1999). The effect of the oblique convergence between arcs and plate borders is observed as fault bands with strike-slip movement, associated with a weakening and thinning of the crust together with an increase in the geothermal flux (Fitch, 1972; Jarrard, 1986). This weakened setting is an easy path for the fluids to intrude. Other works proposed events of increase in plate lateral motion during subduction (McCaffrey, 1992) or the occurrence of an oblique collision that induced the sinistral shear event. Riedel fractures related to the shearing process could be the response to the weakening of the upper crust (Sylvester, 1988), later used by the mafic magma (latest fluids of the arc evolution) to intrude under sinistral shear conditions.

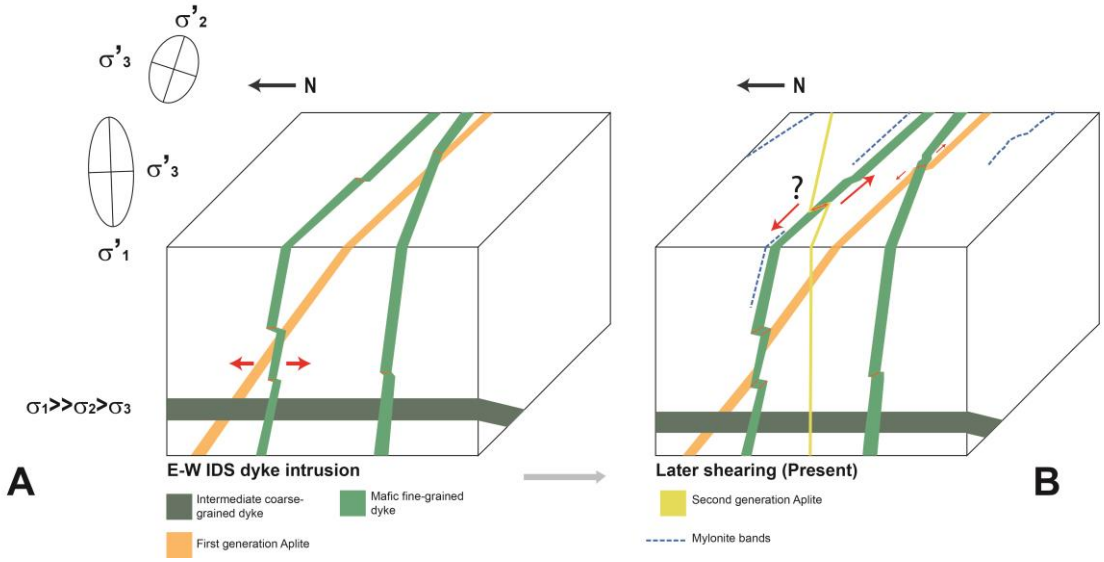

Fig. 3. 44. Model of dyke emplacement for the Independence dyke swarm. A) Situation where all dyke families are already intruded. B) Subsequent deformation phase as inferred from the outcrops.

Consequently, the regional setting should have been a sinistral shear zone along the arc in the upper brittle part over the previously intruded plutons. The shear zone was presumably initiated in the lithospheric area affected by thermal weakening due to the presence of the arc related to subduction. This idea supports the studies that propose the sinistral convergence during the development of the Cordilleran orogeny in the Late Jurassic (Oldow *et al*. 1984).

3.3.5. Conclusions

The Independence Dyke Swarm is characterized by mafic intrusions of sub-vertical dykes, forming single or composite structures with evidences of deformation. Several dyke families are distinguished, being the most prominent ~N95º and a secondary set at ~N175º. The crosscutting relations between the dyke intrusions helped to differentiate the relative timing of intrusion and the diverse mafic to intermediate intrusions. The True Extension analysis gave a mean extension value of ~15% in the area. The paleostress analysis points out a dyke intrusion controlled by the tectonic regime rather than by overpressure, since the value of the magma pressure is lower than σ_2. This is given by the driving pressure ratio, R'= 0.108. The principal stress axis describes a NNE-SSW minimum stress axis, a sub-vertical maximum stress axis (N181/77) and sub-horizontal intermediate axis (N286E/4). The stress ratio, Φ = 0.324, corresponds to a close to prolate stress ellipsoid (σ_1>> σ_2> σ_3). These axes are rotated as noticed by the non coincident value of apparent dilation with σ_3. Therefore, a change in the tectonic regime occurred from an extensional to slightly oblique intrusion (depending on the fracture network orientation) to a sinistral shear sense phase afterwards. Indicators as the mismatching between field markers and σ_3 orientation, together with the localized deformation in mylonite zones through the host rock, dyke margins and internal fabric in dykes and aplites, support this hypothesis.

Finally, the intrusion occurred between ~147 to ~190 Ma., which supposes the entire Jurassic period. As the intrusion age for the Tinemaha pluton is set at ~165 Ma, the intrusion of both materials was coeval. Consequently, the shearing processes took place while the intrusions were not fully solidified and fabric and deformation localization developed. During this time, an oblique arc-continent collision (related to subduction) was taking place in the Cordilleran orogeny; hence it supposed the origin of the shear zone where the Independence Dyke Swarm intruded.

3.4. ANTI-ATLAS: COMPLEX PATTERNS OF INTERNAL FABRICS DUE TO EMPLACEMENT INTO MID-CRUSTAL DUCTILY DEFORMING HETEROGENEOUS HOST ROCKS. STRAIN LOCALIZATION AROUND DYKES.

3.4.1. Introduction.

The general trend of this reseach work continues with the study of different dyke intrusions, in different crustal levels. In this case, the dyke emplacement took place in the middle crust and the dykes has suffered later deformation processes. The context where dykes are intruded in this case is in a deeper crust than in other areas. Moreover, we can distinguish two types of host rock, granitoids and schists which imply differences during the intrusion process.

Numerous authors (Choubert, 1963; Soulaimani, 1998; Soulaimani *et al*., 1997; Soulaimani *et al*., 2001; Thomas *et al*., 2002; Walsh *et al*., 2002; Gasquet *et al*., 2004 and many others) have studied the Anti-Atlas belt in Morocco, so there is a good characterization of the geological events occurred in the area since the craton assemblage up to the present. However, there are still many unkowns in the tectonic evolution that need further work and the combination of several geological approaches, as geochemical, petrological, geochronological and structural analysis.

In this reseach we are going to focus in three areas of the Anti-Atlas. This three areas are characteristics in the regional geology because they are very peculiar structures denominated *boutonnières* in their classic description, they are in fact, are erosive windows or inliers (Fig 3. 46). The outcrops are localized in three of these inliers: the Zenaga inlier, Tagragra d'Akka inlier and finally, the Kerdous inlier. Our work will resume the general geology of the area and we will try to describe the deformation patterns and foliation found in the dykes and in the host rock. As well as the intrusion mechanism that could be inferred from the dyke features.

3.4.2. Geological setting.

The Anti-Atlas fold belt is located in the SW of Morocco (Fig. 3. 45). The later uplift event and subsequent erosion left a great area of preserved outcrops due to the desertic conditions. This chain represents the external part of the Variscan-Appalachian-Ouachita-Mauritanides orogen. It is located in the cratonic part of the orogen, composed by stacks of thick layers of Palaeozoic sediments. In the areas where the Palaeoproterozoic basement is uplifted, it affects thick Palaeozoic cover series with a sucession of folds without duplex structures (Helg *et al*., 2004; Thomas *et al*. 2004). The later studies about the structure of the Anti-Atlas describe it as a succession of cylindrical folds related

to the NNW-SSE collision (Caritg, 2003; Helg *et al*., 2004; Soulaimani *et al*., 1997).

The evolution of the Anti Atlas is a complex story, it began with the union of several terranes to the WAC. The basement of the Anti-Atlas is composed by crystalline, metamorphic and sedimentary rocks. The oldest rocks are granitoids, gneisses and metamorphic rocks series that belong to the West-African Craton (WAC) from the Eburnean orogeny (2000 Ma) (Ait Malek *et al*. 1998; Thomas *et al*. 2002; Walsh *et al*., 2002). The final collision of the African plate took place during the Panafrican orogeny (~700 to 600 Ma) (Hefferan *et al*., 2000). The sequences are related to the orogenic phase (plataform deposits, basic dykes and sills, volcano-sedimentary units, ophiolitic rocks) which are unconformally covered by the volcano-sedimentary rocks of the Ouarzazate Group (Thomas *et al*., 2002). The evidences of the suture can be found in the Bou Azzer ophiolite (Hefferan *et al*., 2002; Leblanc and Lancelot, 1980; Saquaque *et al*., 1989; Thomas *et al*., 2002), an inlier interpreted as an aulacogen in the WAC (Ennih and Liégeois, 2001).

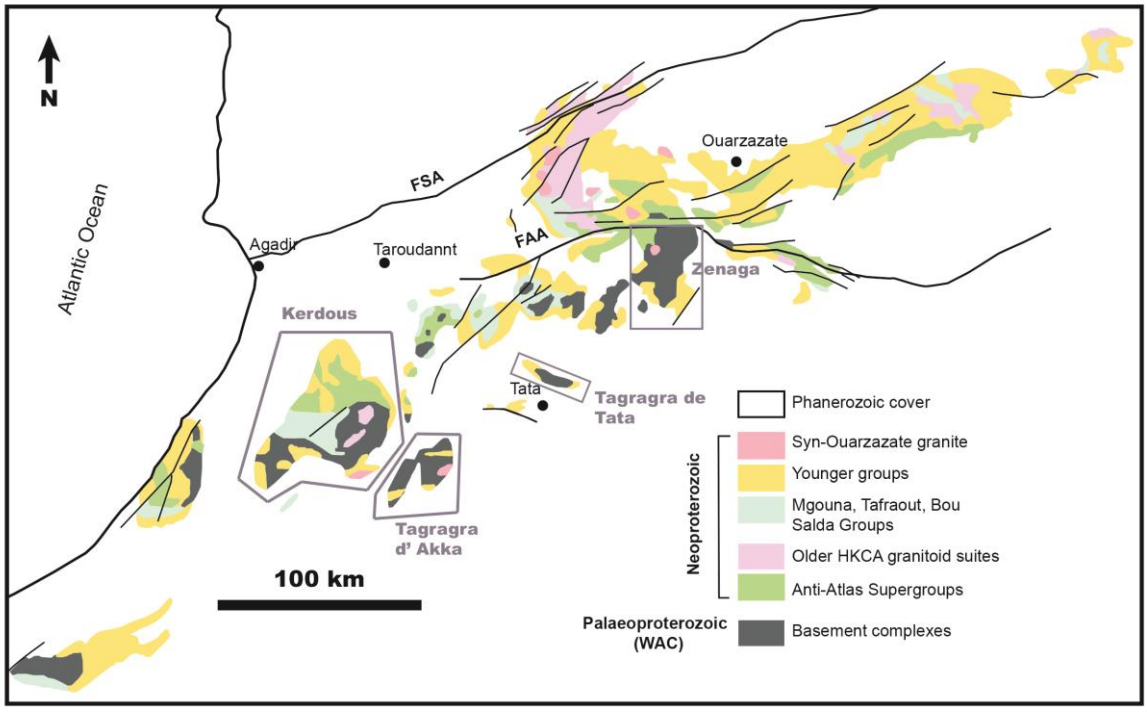

Fig. 3. 45. Geological map off the main parts of the Anti-Atlas (modified from Thomas *et al*., 2004).

In the rest of the Anti-Atlas chain, the Panafrican orogeny produced shear zones and thrusts (Hassenforder, 1987). Later to this event, a continental extension took place in the entire Anti-Atlas region (Piqué *et al*., 1999; Soulaimani *et al*., 2003) as indicated by the synsedimentary tectonics in the clastic series of the Saghro group (PII3) (Soulaimani *et al*., 2001), the Ouarzazate group (PIII) and upward to the Cambrian series. The sucession of events during the Late Neoproterozoic (600-540 Ma) is still not clear since there is not a good geochrology stablished. The range of tectonic settings vary from syn-orogenic (Late Panafrican) deposition in a collisional scenario to post-orogenic extension and collapse wich would led to the formation of blocks and

half grabens (Leblanc and Lancelot, 1980; Soulaimani, 1998; Soulaimani *et al*., 1997). The latest interpretation by Soulaimani (2004) suggests a Neoproterozoic extensional event, based in the volume of volcanic rocks found in the Ouarzazate series. The volcanism would be related to an important melting of the lower curst. They even suggest that the inliers would suppose re-activated core complexes.

In the northwest and west limits, some continental crust broken up during the Palaeozoic. The margin with the Sahara craton in the southwestern part, continued stable during the Palaeozoic. Later, during the Neoproterozoic-Early Cambrian, an extensional phase began, so many basins were filled with clastics deposits that correspond to the PIII phase (Chourbet, 1963). The tholeiitic-alkaline volcanism occurred in this period is consistent with a continental setting. The extension could be related to a southeast subduction zone, so it would produce a wide extensional area similar to the Basin and Range. Another explanation could be the existence of hot spots in Gondwana (Burhard *et al*., 2006). During the Middle Cambrian to Middle Carboniferous, the west Anti-Atlas basin suffered subsidence (Stampfli and Borel, 2002). The breaking up of Avalonia, Armorica and the Hunic terranes from the Gondwana margin in successive phases should have left the Anti-Atlas closer to the Reic and Palaeo-Tethys oceans. After the Silurian, the Anti-Atlas basin turned into the passive margin of the Palaeo-Tethys. However, few of this sediments can be recognized in the Anti-Atlas (Belfoul *et al*., 2002; Michard *et al*., 1982).

The Palaeozoic series have a mean thickness of 10km, increasing to the west and decreasing up to ~6m to the east. The series start in the lower Adounian and finish with the PIII conglomerates of the Ouarzazate series. This PIII/Adounian transition concurs with the Neoproterozoic/Cambric boundary (Buggisch *et al*., 1988; Geyer *et al*., 1995). The cover series are shallow marine sediments in the Lower Cambrian (Boudda *et al*., 1979), from Middle Cambrian to Late Silurian there is a detrital sedimentation from the African craton (Buggisch *et al*., 1988; Destombes, 1976). The Anti-Atlas cover was deposited in a shallow sea from the Lower Cambrian until Lower Carboniferous, with a change from carbonate platforms at the begging up to detrital sediments from the craton, again carbonatic sedimentation mixed with detritic periods in the Devonian until the Lower Carboniferous (Boudda *et al*., 1979; Geyer et al., 1995; Buggisch *et al*., 1988; Destombes, 1976; Hollard, 1981 and Wendt, 1985). The regional thickness of the series increase to the west and northwest, then it is easy to interpret the Anti-Atlas as a far distance basin from the Gondwana margin. Therefore, it would be feasible to have been an intracratonic basin (Burkhard *et al*., 2006). Some tectonic models (Smith *et al*., 1999; Schenk, 1971) propose the Meseta as a small micro-plate (continent), similar to Avalonia or the Hunic terrains (Stampfli and Borel, 2002), that moved away from the northen margin of Gondwana during the Lower Palaeozoic and later accreted to Africa in the Late Carboniferous collisional event (Boulin *et al*., 1988; Feinberg *et al*., 1990). The inexistence of a suture area between the Meseta and the Anti-Atlas is the weak point to this explanation (Burkhard *et al*., 2006). The final Late Carboniferous-Permian orogenic event produced the uplift of the basement and inversion and folding of the cover series. The basement uplifts created the inliers (*boutonnières*) (Burhard *et al*., 2006).

Burkhard *et al*. (2006) proposed the Anti-Atlas as the center of a thermal anomaly dome linked with the development of syn-rift deposits and not a rifting area. Hence, the final consecuence would have been thermal subsidence during the Palaeozoic.

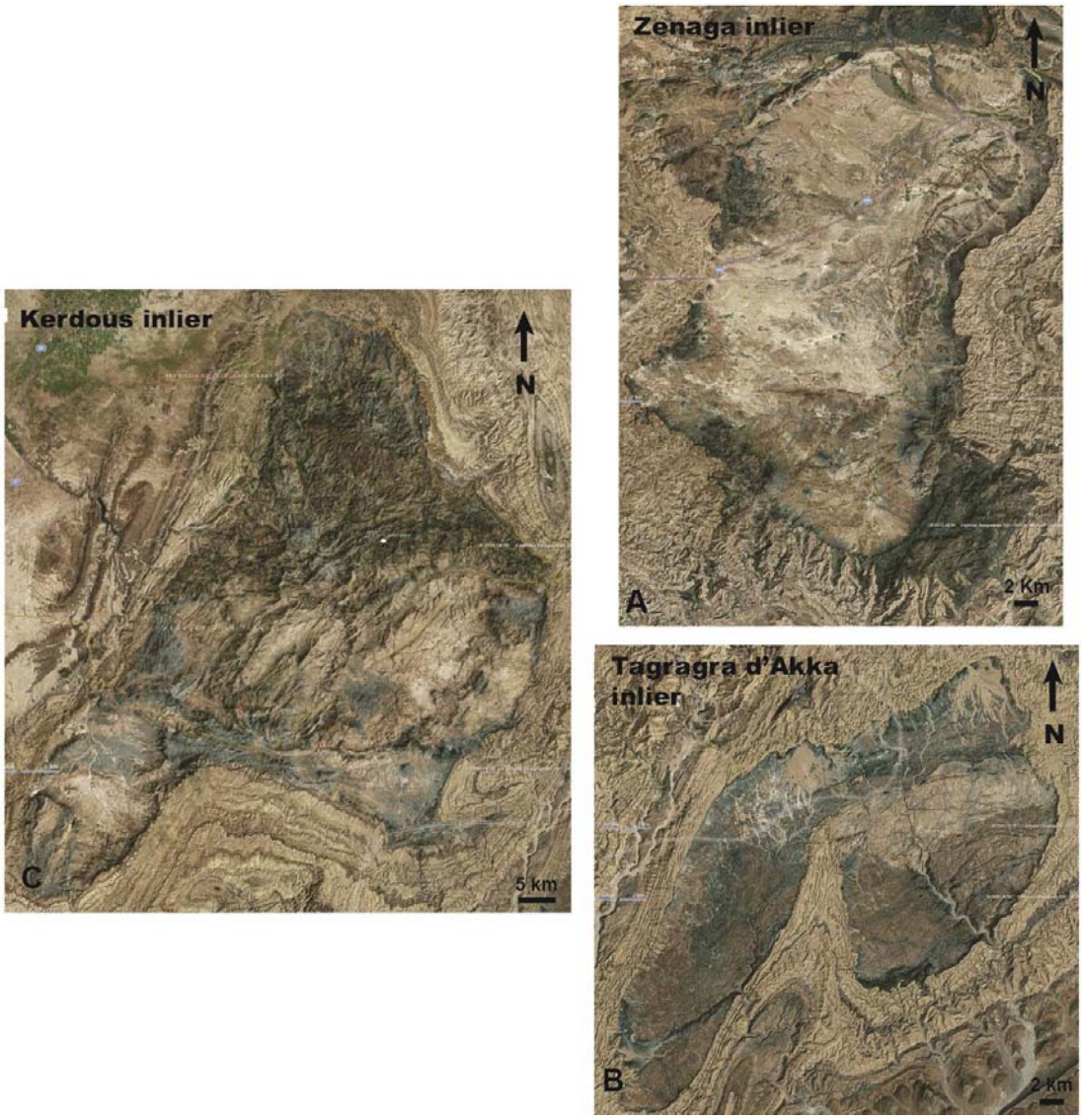

Fig. 3. 46. Aerial images from the inliers of the study. A) Zenaga inlier, B) Tagragra d'Akka inlier and C) Kerdous inlier (images obtained from ®Bing images).

The *boutonnières* are disposed very closed from the south-east front of the south-western Anti-Atlas (Choubert, 1963). They represent the top of the Palaeozoic cover folds. Some authors attribute this structures to be the hinge of crustal scale folds (Choubert, 1963; Choubert *et al*.,1971). For other authors, the balancing and rheology characteristics made this type of folding improbable for this area (Mitra and Mount, 1998), but the uplift of the Palaeoproterozoic basement should have been caused by crustal scale reverse faults (Mitra and Mount, 1998; Rodgers, 1987; Stone, 2002). The Anti-Atlas is considered as an inverted intracratonic basin of thick-skinned style rather than the foreland front of an orogeny or a thin-skinned fold and thrust foreland of the Appalachian-

Variscan orogeny, even though its close position to the Appalachian-Variscan chain (Burkhard *et al*., 2006). The Anti-Atlas share the inverted basin characteristics with other Palaeozoic fold belts in northern Africa (Coward and Ries, 2003; Haddoum *et al*., 2001).

The Anti-Atlas domain is separated in two main areas by the Anti-Atlas major fault, also considered as the northern margin of the WAC (Hefferan *et al*. 2000). Although, Ennih and Liégois (2001) proposed the South Atlas fault as the norther margin of the WAC taking into account rheological and isotopic arguments. The WAC basement in the Anti-Atlas outcrop in the ENE-WSW direction of the Anti-Atlas Major Fault (Choubert, 1963; Gasquet *et al*., 2008; Thomas *et al*., 2004). The inliers within the Anti-Atlas are comprised between two fault zones, the South Atlas Fault and the Anti-Atlas Major Fault (Fig. 3. 45). There are several hypothesis about the nature of the AAMF, either the suture of a Pan-African ocean (Leblanc and Lancelot, 1980; Guiraud *et al*., 2000) or the Neoproterozoic aulacoge limit (Ennih and Liégeois, 2001). The area north-east to the AAMF is composed by Neoproterozoic rocks deformed in the Pan-African orogeny and the south-west are Palaeoproterozoic rocks deformed by several Pan-African events (Gasquet *et al*., 2004). Tagragra d'Akka and Kerdous inliers both are in the south-west area, while Zenaga and Tagragra de Tata are in the Central Anti-Atlas.

The latest geochronology study in the Anti-Atlas *boutonnières* was done in four different dykes and the result is a ~1750 Ma event. The authors (Youbi *et al*., 2013) observed evidences for a LIP event in the WAC. The ages obtained are: ~1758 Ma in Tagragra d'Akka; 1741+10 Ma in Tafeltast-Kerdous; 1746.8+3.7 in Iguerda-Taifast and, finally, 1734+5 in Zenaga. These ages support the magmatic event in 1.75 Ga, related to the intrusion of a mafic dyke and sill swarm and felsic rocks, which is named as the Tagragra d'Akka LIP. The extension is lower than the standars for the LIP designation (Tagragra d'Akka LIP: ~41000 km^2; minimum for the LIP assignment: 100000 km^2), however other indicators as the thickness of >10m of the dykes point out a larger magmatic event with similarities to a LIP (Ernst, 2007). There are others intrusions with the same age in different areas as Laurentia or Siberia, so all of them could have taken part of an extensive LIP related to the beginning of the Supercontinent Columbia (1800 to 1500 Ma) breakup (Youbi *et al*., 2013). This intrusion was preceded by a 2040 Ma event (Walsh *et al*., 2002; Kouyate *et al*., 2013) which was the oldest intrusive phase in the Anti-Atlas basement. Later magmatism occurred in different phases: ~1650 Ma, ~1385-1410 Ma, 890 Ma and 575 Ma, also an ophiolite with an age of 760 Ma.

3.4.2.1. The West African Craton

The West African craton is an ensemble of three Archaean and Palaeoproterozoic shields. The components are: the Man shield, the Reguibat shield and the Anti- Atlas belt (Ennih and Liégois, 2008) (Fig. 3. 47). This basement is composed by the sucession of several orogenyc phases, from the Palaeoarchean-Leonian cycle (3.5-3 Ga) (Potrel *et al*., 1996; Rocci *et al*., 1991), followed by the Liberian cycle (2.95-2.75 Ga) (Auvray *et al*., 1992; Potrel *et al*.,

1998). Then, the WAC was affected by the Eburnian orogeny (2 Ga) (Abouchami *et al*., 1990; Aït Malek *et al*., 1998; Hirdes *et al*., 1992). Later to that, there is no evidence of other WAC rocks. The gap period between 1.7 to 1 Ga was the responsible of the craton formation (Black and Liègois, 1993). In the Neoproterozoic, the WAC was affected by extensional tectonics related to

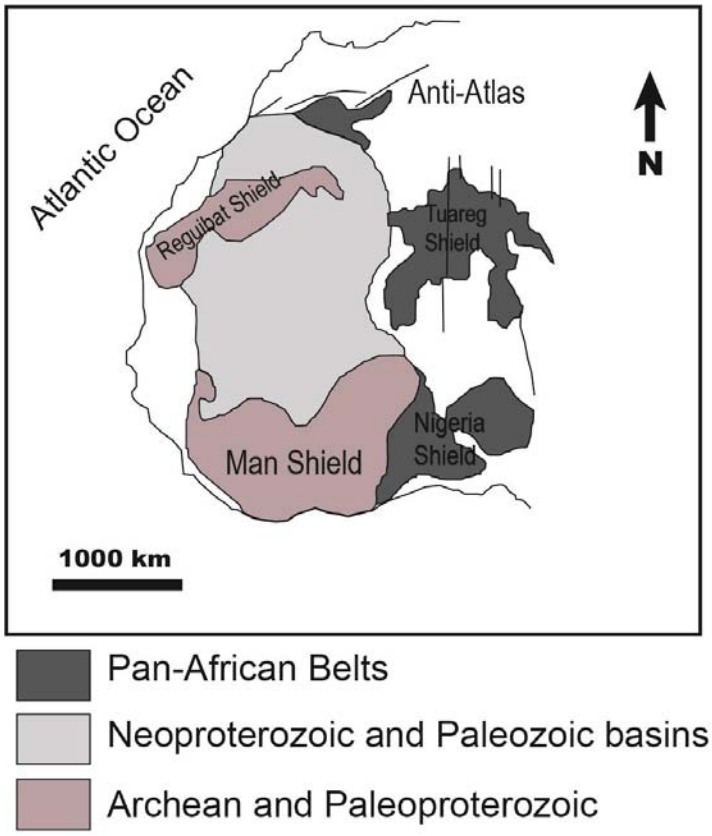

Fig. 3. 47. Tectonic map of the West African craton (modified from Abati *et al*., 2010).

continental breakup (Ennih *et al*., 2008). In the northern margin (Anti-Atlas), it occurred an important sedimentation event (Bouoigri and Saquaque, 2004). In the Neoproterozoic, the WAC suffered the accretion of an island arc (760-660 Ma) in the Anti-Atlas area (Thomas *et al*, 2002; Samson *et al*. 2004; D'Lemos *et al*. 2006). Finally, the WAC suffered convergence in all its borders during the Pan-African orogeny (Hefferan *et al*. 2000; Ennih and Liégeois, 2001; Black *et al*. 1979, 1994; Affaton *et al*. 1991; Villeneuve Gasquet *et al*., 2008; Leblanc and Lancelot, 1980; Samson *et al*., 2004; Thomas *et al*., 2002) and constituted a rigid area in this period. In the area of interest, the lithosphere suffered transpression and transtension mechanisms, intrusion of granitoids and even volcanism (Ouarzazate Supergroup) (Ennih and Liégois, 2008). The occurrence of metamorphism caused movement of fluids that created mineralization in the Anti-Atlas, e.g. gold deposits (Inglis *et al*. 2004). Later, in the early Palaeozoic, the west part of the WAC suffered extensional tectonics with basin production and volcanism and the separation of several Peri-Gondwanic terranes. A thick sedimentary cover was deposited until the Devonian. The Variscan orogeny generated a thick-skin type of tectonics in the basement while it created thin-skin tectonic in the cover (Caritg *et al*. 2004; Burkhard *et al*. 2006). During the Mesozoic, the Atlantic began to open in the west and south margins of the WAC

and a large dolerite intrusion occurred in the Jurassic together with the basaltic Central Atlantic magmatic province (Marzoli *et al*. 1999; Deckart *et al*. 2005; Verati *et al*. 2005). There were riftings to the east and to the north (Anti-Atlas) linked to the opening of the Central Atlantic and Western Mediterranean (Laville *et al*. 2004; Guiraud *et al*. 2005). The final orogenic events affecting the WAC were in the Cenozoic, due to the collision between Africa and Eurasia, with the creation of the High Atlas range, the uplift of the Anti-Atlas (Malusa *et al*., 2007) and volcanism events to the west and the Hoggar (Liégois *et al*., 2005).

3.4.2.2. Inliers of the study

3.4.2.2.1. The Zenaga inlier

It is located south of the Anti-Atlas major fault, in the Central Anti-Atlas. It is a depressed area with an extension between 500 km^2 to 800 km^2, depending on the authors (Kouyate *et al*., 2012). It is maily composed of Palaeoproterozoic gneisses and granitoids (Eburnian age) (PI) (Choubert, 1963), covered by the Ouarzazate Supergroup (Neoproterozoic) and by the Tata Group (Cambrian) (Ennih and Liégeois, 2008) (Fig. 3. 45, 3. 46a and 3. 48). The basement rocks consist on grey gneisses in high-grade amphibolite facies, schists, paragneisses (garnet and sillimanite rich), calc-silicate rocks, migmatites and amphibolites (Ennih and Liégeois, 2008). The gneisses and the migmatitic leucosome present isoclinal ductile folding. Age has been studied by inherit zircons in the granitoids that crosscut the schist, with a result of 2170 Ma for the schist and 2035 Ma for the granitoids (Thomas *et al*., 2002). The Palaeoproterozic plutons are composed by the Azguemerzi granodiorite and the Aït Daouni, Assersa, Tamarouft and Tazenakht granites. There are evidences (metasedimentary/psamitic xenoliths, aluminous minerals, migmatites, etc.) that suggest the Zenaga granitoids origin to be due to partial crust melting. More ages of the granites and the granodiorites have been obtained, 2037+7 Ma, 2037+9 Ma and 2035+5 Ma (Thomas *et al*., 2002). The cover rocks are also passive margin deposits (Taghdout Group) (Thomas *et al*., 2004) and doleritic dykes and sills (pre Pan-African), together with an alkaline ring complex (late Pan-African). The Taghdout group present the effect of faults and folds linked to a thrust event, as well as, well preserved sedimentary signs (Bouougri and Saquaque, 2004) and it is intruded by doleritic dykes (Kouyate *et al*., 2012). It has 2 km thick and it was deposited in an extensional setting. An indirect age obtained from clay with the Rb-Sr method gives a minimum deposition age of 788+9 Ma (Clauer, 1976), also valid for the emplacement of the dolerites. The Ifzwane Group is an ensemble of tholeiitic sills and dykes that crosscut the sedimentary group and the basement, these intrusions are found in other inliers of the Anti-Atlas. They form an extensive swarm with three main sets oriented: NNE, ENE and NW (Thomas *et al*., 2004). The dolerites show enrichment in incompatible elements, so they seem to be related to continental rift setting (tholeiites) (Hafid *et al*., 2001; Thomas *et al*., 2002). Afterwards, the basement was overthrusted by a rhyolitic unit (605+9 Ma, Thomas *et al*., 2002) which are covered as well by the

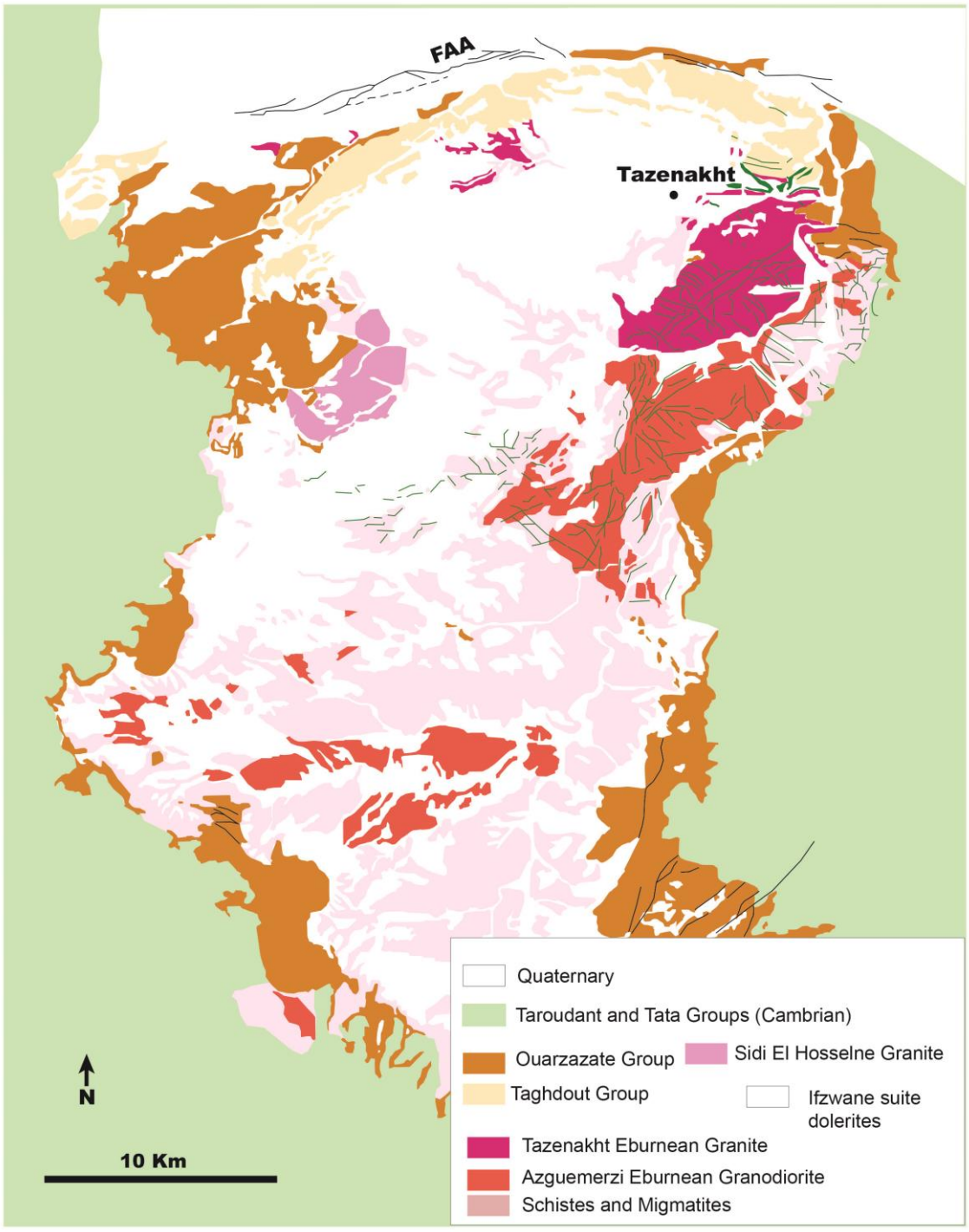

Fig. 3. 48. Geological map from the Zenaga inlier (modified from Kouyaté *et al*., 2012).

Ouarzazate Group (PIII, Choubert, 1963)(581+11 Ma to 543+9 Ma, Thomas *et al*., 2002; Walsh *et al*., 2002; Gasquet *et al*., 2005). The Ouarzazate Group is composed by a volcanosedimentary succession (volcanic conglomerates, ignimbritic rhyolites, trachytes, andesites, basaltic trachyandesires, tuffites and intercalation of stromatolites and fault breccias). This group was presumably deposited during a rifting or in a transtensional event and it does not display any Pan-African deformation (Gasquet *et al*., 2008; Soulaimani *et al*., 2003). The

Ouarzazate magmatism is related to the Central Iapetus Magmatic Province occurred in the Ediacaran period (Doblas *et al*., 2002; Ernst and Bleeker, 2010) and related to an extensional-transtensional tectonics that produced hydrothermal deposits, as present in the Anti-Atlas. The late Precambrian-early Cambrian rocks overlain unconformably the Ouarzazate series. They are the Taroudant and Tata Groups, they suppose transgressive marine successions dated in the Cambrian-Precambrian limit, 542 Ma (stable oxygen isotope, Margaritz *et al*., 1991 and U/Pb Compston *et al*., 1992).

Recent studies connect the granites in the Zenaga basement with the 2.04 Ga dykes named as Tagragra de Tata LIP by Kouyate *et al*. (2012). This was an extensional event associated to melting in the lower crust and to the production of mafic magmatism (Bryan and Ernst, 2008)

The orientation of the Eburnian deformation was stablished as N-S to NE-SW (Ennih *et al*., 2001). The later Pan-African event was oriented NW-SE, located along the Anti-Atlas Major fault under greenschist conditions (Ennih *et al*., 2001). During the Variscan orogeny, the dome structures and the décollements were developed in the Palaeoproterozoic-Neoproterozoic limit. The Variscan folds can be recognized in the Ouarzazate and Tata Groups, also listric faults that reach the basement (Burkhard *et al*., 2006). Moreover, Pan-African faults were reactivated during this period (Soulaimani *et al*., 2004). Later, during the Alpine orogeny, the extensional faults were reactivated and they produced the high altitudes in the Anti-Atlas.

The calc-alkaline granites in the Zenaga inlier (Azguemerzi and Tazenakht) have a dated age of 1856+29 Ma and 1735+11 Ma (Charlot, 1976, 1978). Later work obtained U-Pb ages from the Proterozoic (Malek *et al*., 1998) so the Eburnian orogeny probably took place around 2 Ga with another event at 1800 Ma that opened the system (Ennih *et al*., 2001).

The Zenaga granitoids have a calc-alkaline affinity (Ennih *et al*., 2001). They intruded during the Eburnian Orogeny and later they suffered a north oriented Pan-African deformation (Ennih *et al*., 2001). Some authors described the sedimentary cover of the inlier as autochthonous with cratonic characteristics (Choubert, 1963 and Leblanc et Lancelot, 1980). Ennih *et al*. (2001) performed a structural analysis of the inlier in which he described two main deformation phases (Eburnian and Pan-African), with three deformation phases each one. In the Azguemerzi granite, the magmatic foliation shows NW vergence, produced by the Eburnian orogeny. In the Tazenakht granite, the Eburnian deformation has been almost totally neglected by the events occurred during the Pan-African orogeny. Structural studies in the Tazenakhy granite shows that it was affected by shear zones during the Pan-African (Leblanc, 1981). Therefore, the Anti-Atlas Major Fault is a large shear zone (Ennih *et al*., 1999).

In the Neoproterozoic, the mafic rocks intruded as sills (Hafid *et al*., 2001). The dykes are mainly dolerites with gabbroic centers. If they preserve their original mineralogy, the minerals are plagioclase, clinopyroxene, ilmenite, apatite, hornblende and biotite (Hafid *et al*., 2001). Using rare earth elements, two different groups of dykes have been differentiated. One with a high content of

LREE, which correspond to the N-S to NW-SE and E-W dykes, and the other group with a small amount of LREE correspond to the NE-SW dykes, which intruded afterwards (Hafid *et al*., 2001).

According to Clauer, 1976, the intrusion setting for the dolerite swarm is an extensional phase before the Pan-African folding at an age of 788+8 Ma. Their tholeiitic composition suggest that they were original from an enriched mantle similar to E-MORB basalts (Sun and McDonough, 1989). These dykes could be coetaneous to other dykes found in the western and central Anti-Atlas (Hassenforder, 1987; Naidoo *et al*., 1991; Ikenne *et al*., 1997 and Hafid, 1999), so the northern part of the WAC suffered an extension phase.

The Tikitar granite has been dated (U-Pb,De Beer *et al*., 2000) with an age of 559+6 Ma, this rocks are connected with the volcanic and hypabyssal intrusions of the Ouarzazate group.

All the geochemical and isotopic data obtained from the Zenaga magmatism (Palaeoproterozoic) denotes partial melting of a young crust for the source of the peraluminous magmatism. These plutons were later affected by Pan-African deformations and the resultant fluids (F-rich) are associated with the extrusion of the Ouarzazate material and the intrusion of coeval plutons (~580 Ma) in preferred orientations along shear zones. This was not a major event since the signal imprinted in the rocks were of greenschist facies and the sediments from the passive margin (~800 Ma) and the ophiolite (~750-700 Ma) are well preserved. Therefore, the Anti-Atlas belt represent a classical metacratonic scenario with all the structures preserved and just the faults are the pipes of the fluids movement, that also generated the important mineralizations in the area (Ennih and Liégeois, 2008).

3.4.2.2.2. Tagragra d'Akka

The Tagragra d'Akka inlier is located south-west of the Anti-Atlas Major Fault, at ~60 km south-west to the Tagragra de Tata inlier and ~30 km south-east of the Kerdous inlier. It has an area of ~900km^2 with a double lobulated shape (Fig. 3. 35, 3. 46b and 3. 49). This inlier follows the same rock succession as the other inliers in the Anti-Atlas: a Palaeoproterozoic basement formed with intruded granites (Tafeltast granite), dated 2049+2 Ma and 20146+8.3 Ma, in a metapsamitic and metavolcanic succession (Gasquet *et al*., 2004; Walsh *et al*., 2002). The basement is covered by the Ouarzazate Group (Late Neoproterozoic) or by the Taroudant and Tata Groups (Late Neoproterozoic-Cambrian). The basement displays a dyke swarm of mafic composition (microgranitic, aplitic, pegmatitic and dacitic composition), named as Mechbouk Suite (Gasquet *et al*., 2004; O'Connor, 2010). The dyke orientation is grouped in several sets: N60º-N70º, N90º-N110º, N150º-N170º and a minor set at N0º-20º. The mafic dykes (gabbro to fine-grained dolerite and trachybasalt) suffered a low-grade metamorphism and hydrothermal alteration. They are attributed to tholeiitic and alkaline affinities due to the trace elements analysis (Mortaji, 1989; Ikenne *et al*., 1997; Gasquet *et al*., 2004). The dacitic dykes have been dated, giving an age of 600+5 Ma (U-Pb), the pegmaticic dykes and porphyritic

microgranites have an age of 1760+3 Ma (Pb evaporation on zircon) and 1755+25 Ma (Kr-Ar on muscovite and EMP on monazite) respectively (Gasquet *et al*., 2004). Some rhyodacitic dykes are found in the inlier crosscutting the schists and granites (Gasquet *et al*., 2004). Quarz veins are grouped in sets, one is older and parallel to the regional foliation and a younger related to the Pan-African shear zones. Quartz veins related to the Variscan event crosscut all the series. The two first groups are linked with mineralization (Fe, Cu, Au and Pb) (Zouhair *et al*., 1991).

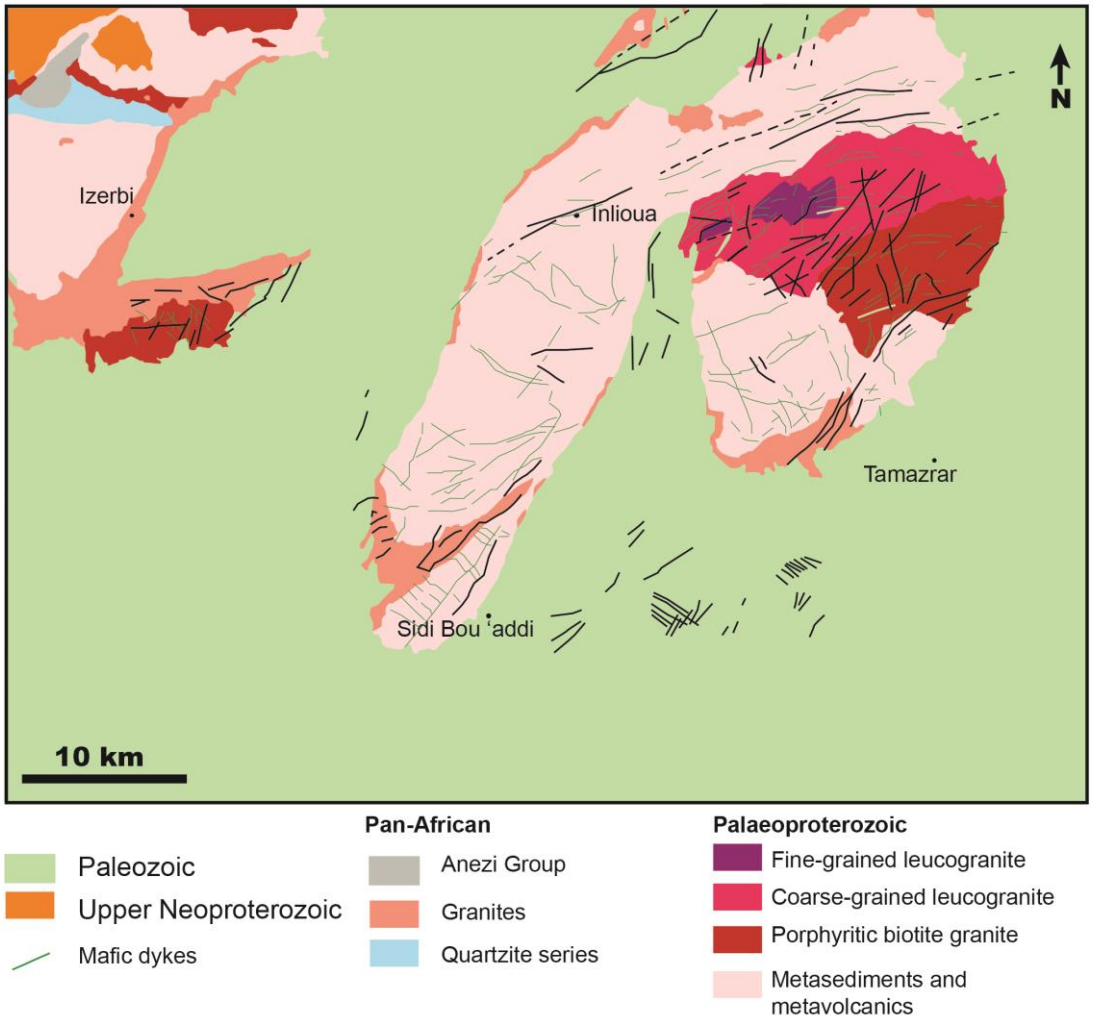

Fig. 3. 49. Geological map from the Tagragra d'Akka inlier (modified from Gasquet *et al*., 2004).

The composition and mineralogy of the calc-alkaline suite is related to I-type granites. The isotopic analysis and REE suggest partial melting of the crust or metasomatism in the mantle as the source of the magmas (Mrini, 1993). The peraluminous suite of granodiorites, granites and leucogranites derived from a continental crustal origin. The age of this magmatism is unkown but an approximation of 1504+39 Ma to 1773+42 Ma for leucogranites was made (Lama *et al*., 1993). This is not a true crystallization age, it is related to a later hydrothermal event.

3.4.2.2.3. Kerdous

The Kerdous inlier is located in the south west of Morocco, south to the Anti-Atlas Major Fault and at ~50 km south-east of Agadir. It has a surface of 4500 km^2. It represents the inlier with the biggest extension of all the studied in this work (Fig. 3.45; 3. 46c and 3. 50).

Some research performed in the inlier suggest that only one Precambrian orogenic event affect the area, the Pan-African one (Nachit *et al*., 1996). Later studies suggested the two orogenies hypothesis based on the comparison of U-Pb geochronology in Kerdous with others inliers (Malek *et al*., 1998).

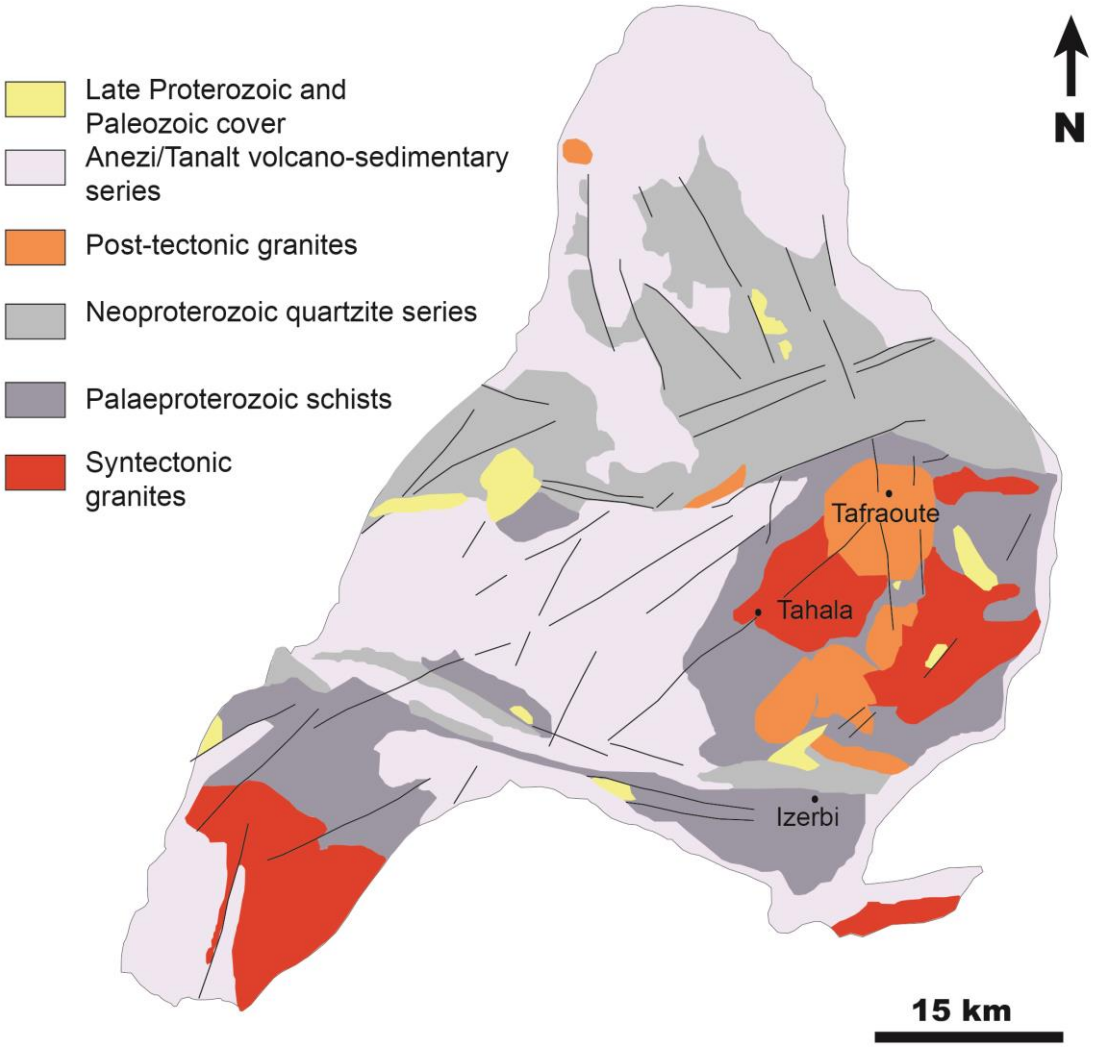

Fig. 3. 50. Geological map from the Kerdous inlier (modied from Barbey *et al*., 2004).

The basement rocks are mainly metapsamites with a low-grade metamorphism and slightly deformed (Kerdous schists) (Thomas *et al*., 2002). The deformation produced WNW-ESE folds with a weak cleavage originated by the D_1 granites

intruded in the basement, producing a contact metamorphism aureole. The Azguemerzi granite shows a magmatic deformation produced by the Eburnean Orogeny (Ennih *et al*., 2001). Covering the basement is found the Quartzite series, that correspond to the younger rocks of the Pan-African orogeny (Hassenforder *et al*., 1987), although some quartzite layers seems to belong to the older Kerdous Schist group (Nachit *et al*., 1996). The quartzites also display a low-grade metamorphism and deformation. These rocks are intruded by sills and dykes of gabbroic affinity with an age of 788+22 Ma (Rb-Sr, Clauer, 1976). The different deformation phases let distinguish between the syntectonic and post-tectonic intrusions. It is found that the regional schistosity is deformed by a subsequent foliation that increases in intensity towards the granitic intrusion (Barbey *et al*., 2004). The emplacement of the plutons then is attributed the the phase D1 of regional deformation (Barbey *et al*., 2004). The Jebel Ouiharen laccolith and the Tasserhirt migmatites show a parallel disposition to the regional foliation (Barney *et al*., 2004). Syntectonic granites dated (Rb-Sr) display Palaeoproterozoic ages and post-tectonic granitoids are dated as Pan-African (Charlot *et al*., 1982).

In the inlier there are dolerite dykes with a NW-SE to N-S orientation with several meters of length and a width up to ~1.5 meters. They are related to other mafic intrusions without any sign of magmatic deformation (El Aouli *et al*., 2010). These characteristics are shared by the dykes and mafic bodies in the Igherm and Ifni inliers as well. The intrusions took place into the Palaeoproterozoic basement composed by schist-greywackes, granites and limestones and quartzites (previous to the Upper Cryogenian conglomerates) (El Aouli *et al*., 2010). The limestones show a contact metamorphism aureole in greenschist facies anf the quartzites have fine grain margins (Choubert and Faure-Mauret, 1973). All these basement and Cryogenian formations, together with the mafic dykes show the effect of a regional NE-SW squistosity due to the Pan-African deformation phase (El Aouli *et al*., 2010). The dykes intrude the mafic bodies and older dykes with tholeiitic affinities, these dykes do not crosscut the Lower Cryogenian quartzites (El Aouli *et al*., 2001a; El Aouli, 2004) The calc-alkaline mafic rocks are not common in the Anti-Atlas, only in the western part we can find this type of dolerite dykes (e.g. in Tagragra de Tata inlier) (Ikenne *et al*., 1995 and El Aouli *et al*., 2010). Although they are well described in the western inliers (Kerdous and Tagragra d'Akka inliers). The tectonic setting for the intrusion of this type of orogenic mafic magmatism is supposed to be an extensional area with melting related to decompression of the sub-continental mantle (enriched by a previous subduction) (El Aouli *et al*., 2010). According to El Aouli *et al*. (2010), the tholeiitic, transitional and alkaline rocks are the result of the extension during the Cryogenian (720-635 Ma), right before the beginning of the melting in the lithospheric mantle with production of calc-alkaline magmas.

3.4.2.3. Summary of dyke intrusions

In orther to sum up the different Precambrian dyke generations described in the Anti-Atlas, we enumerate the following:

i) Palaeoproterozoic tholeiitic dykes in Tagragra de Tata with an age of 2040+6 Ma (SHRIMP U-Pb, Walsh *et al*., 2002). Other analysis gave older ages for the same intrusions ~2.07-2.15 Ga, probably linked with an older magmatic event (Rhyacian) coeval with the metatuffs found in Tagragra de Tata (Walsh *et al*., 2002). No Archaean inherit zircons have been found in the intrusions (Gasquet *et al*., 2004).

ii) Microgranitic dykes and pegmatites with an age of 1760+3 Ma (Upper Palaeoproterozoic, Statherian) in Kerdous (Pb-Pb, Gasquet *et al*., 2004). These intrusions are related to the mafic dykes found in Tagragra d'Akka.

iii) Mafic dykes (tholeiitic and alkaline) with Cryogenian age, this dykes are attributed to a back-arc rifting in the Central Anti-Atlas (Clauer *et al*., 1982). Although U-Pb dating has obtained an age of 761+2 Ma (Samson *et al*., 2004).

iv) Mafic dykes in Bas Drâa inlier dated as 575+4 Ma (U-Pb, Aït Malek *et al*., 1998) and dacitic dykes in Tagragra d'Akka with an age of 600+5 Ma (U-Pb, Gasquet *et al*., 2004). The Upper Neoproterozoic dacite dykes are coeval with the granodiorite intrusion in Kerdous, previous to the Neoproterozoic volcanism (Aït Malek *et al*., 1998).

v) A final hydrothermal phase during the Variscan event, 301+7 Ma. This is related to the Au-quartz deposits and dacitic dykes.

The latest results provided for the age of dyke intrusions in several Anti-Atlas inliers (Kouyate *et al*., 2012) are mainly in the Zenaga inlier: 2040+2 ma, 1656+9 Ma, ~1650 Ma and ~885 Ma U-Pb ages. This results support three supercontinents assemblage for the WAC. The oldest dykes (2040 Ma) and granites from the Eburnean, are possibly linked to the breakup of WAC from nearby cratons. The 1650 Ma dykes is similar in age to another magmatic pulse found in Baltica, which in the SAMBA reconstruction both terrains are located closely. The final ages obtained between 890-850 Ma are found in other areas of east Africa and these intrusions could mark the beginning of the Rodinia breakup.

3.4.3. Methodology and results

We tried to perform a classical structural analysis characterization for the different selected areas where the dykes were more visible (and accessible). Among the methods used, there are classical cartography, dyke wall measurement, foliation measurement and photo stich, for later digital analysis. Desert outcrops are very difficult to study in aerial images if the linear features are not outstanding, since the desert patina cover all the types of rocks and layered rocks or schists can be misidentified as mafic dykes.

3.4.3.1. Dyke trends and segmentation structures

Zenaga

This *boutonnière* had been already studied by the group in previous field campaings (Carreras *et al*., 2008; Castaño, 2010). The work done was a continuation of previous field works in order to progress the dyke characterization and the deformation processes (Fig. 3. 51).

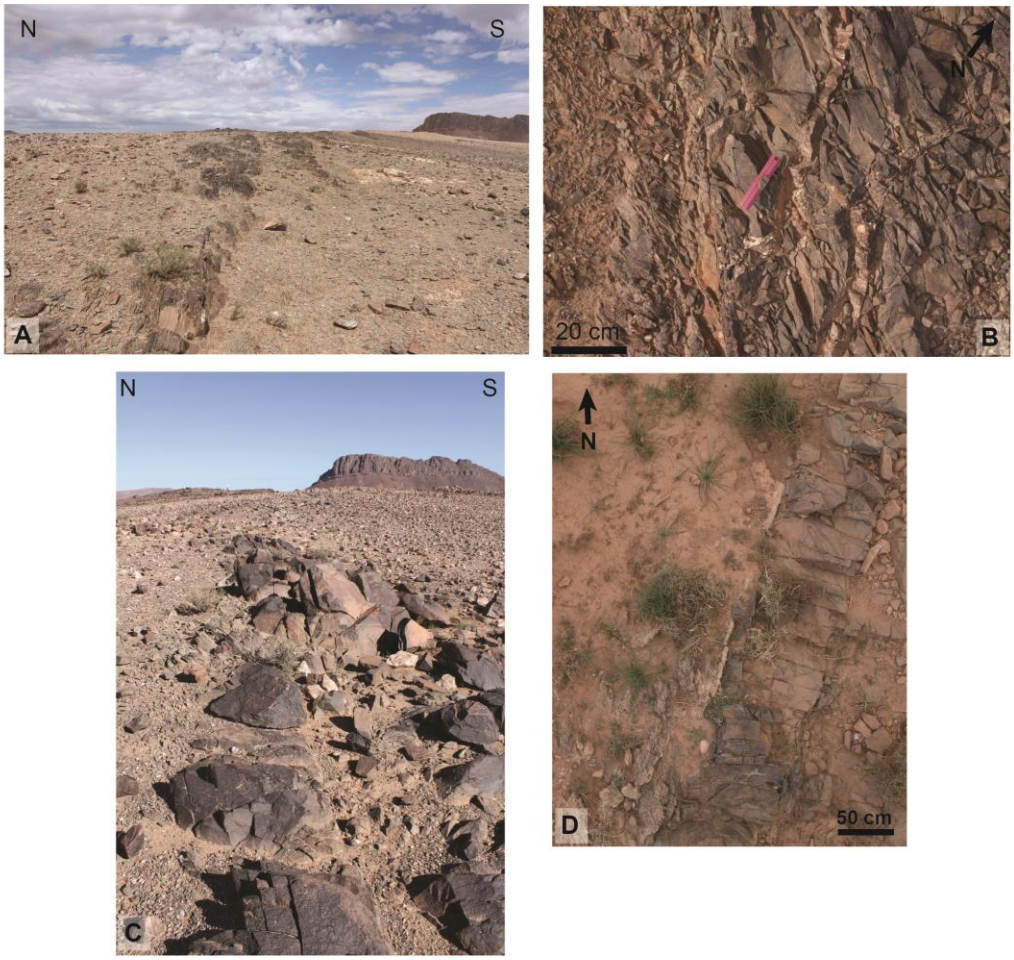

Fig. 3. 51. Images from dyke examples in the Zenaga inlier. A) and C) View of the dykes in the outcrops, B) and D) Examples from sub-horizontal plane of dyke segments.

The rose diagram (Fig. 3. 54a) constructed with the data of dyke walls measured from aerial images (Bing) gives a wide range of dyke intrusion. The main set is oriented at ~N65º with others secondary sets at ~N130º, ~N90º and ~N40º. It is significant the stepping structures observed in these aerial images, the segmentation occur in short segments, propably separated due to shear zones/faults (Fig. 3. 58).

Tagragra d'Akka

The outcrop area in this *boutonnière* was not studied before by the MIET group. We found very good dykes affected by shear zones with quartz veins as

indicator of the deformation (Fig. 3. 52). The difficulty was to do a good cartography due to the large extension of the dykes, with thickness of meters and longitude of thousands meters.

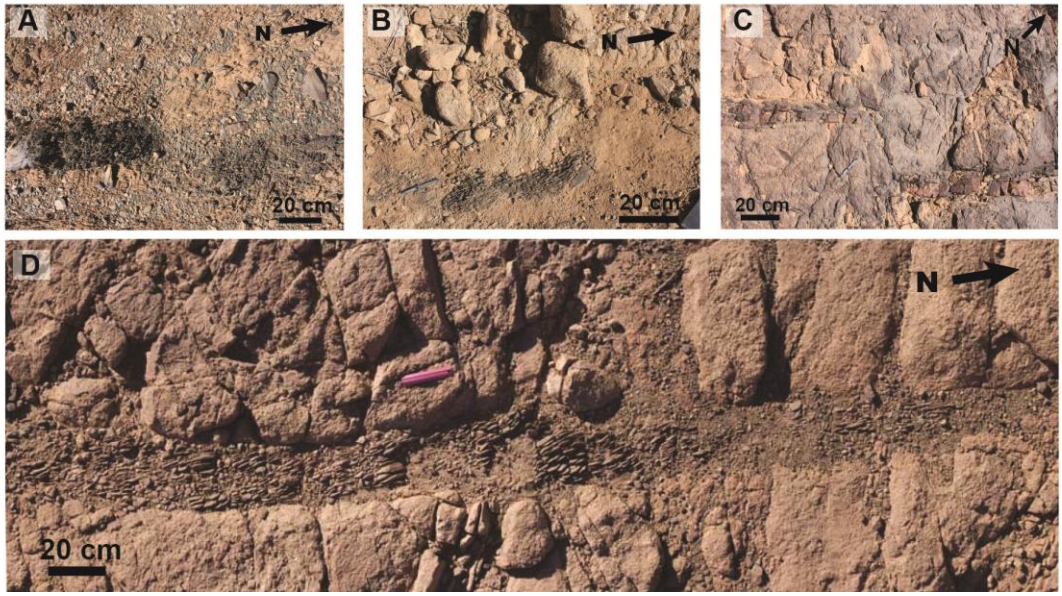

Fig. 3. 52. Images from dykes examples in the Tagragra d'Akka inlier. Photographs taken on sub-horizontal outcrops. Notice in images A), B) and D) a foliation is present inside the dykes. C) Dyke offset in a discontinuous right stepped segment.

The analysis of aerial images from Google, give us the structure of the dykes and the shear zones (Fig. 3. 58). We can even define some kind of foliation structures due to the desert patinas that overprint the more resistant rocks (Fig. 3. 52) .

The rose diagram of the dyke trends measured digitally gives us two main set directions (Fig. 3. 54b), the first one at ~N65º, which is the more frequent, and another set at ~N10º. There is a secondary set at ~N90º, probably related to steps and changes in orientation due to the fracture network in the host rock.

Kerdous

This area was previously studied by other members of the research group (Carreras *et al*., 2008; Castaño, 2010), so there was a better understanding of the zone. We did a digital measurement of the dykes using aerial photographs (®Bing). The results are displayed in the rose diagram (Fig. 3. 54c) with a main set of dykes at ~N120º. In this area, dykes show a continuous and homogeneous outcropping.

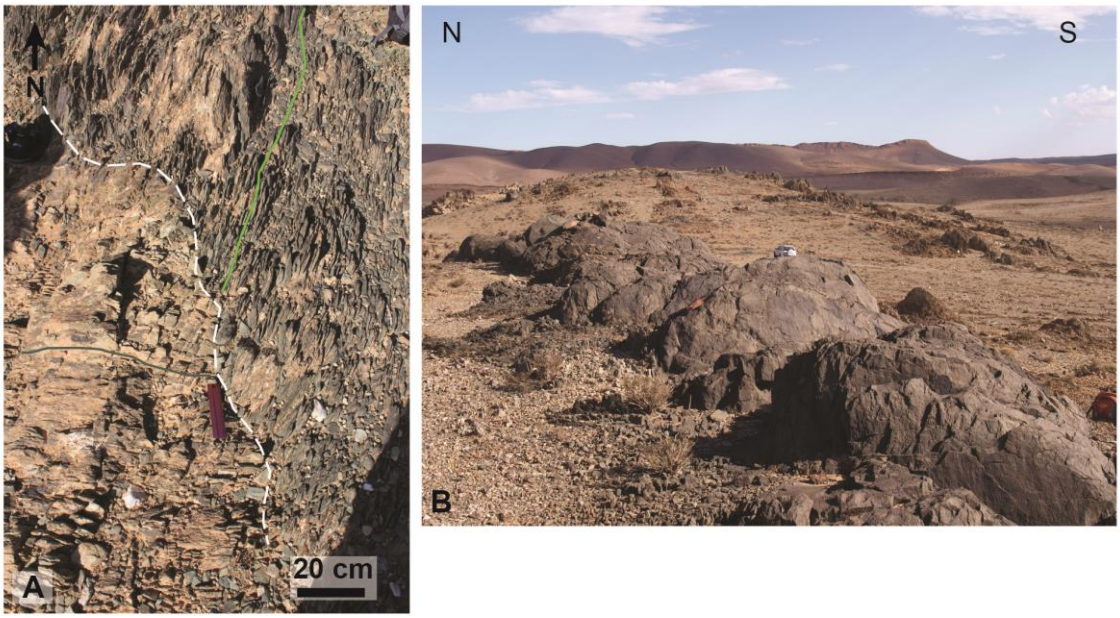

Fig. 3. 53. Images from dykes examples in the Kerdous inlier. A) Oblique view of the surface of a strongly foliated dyke. B) Outcrop view of a massive dyke.

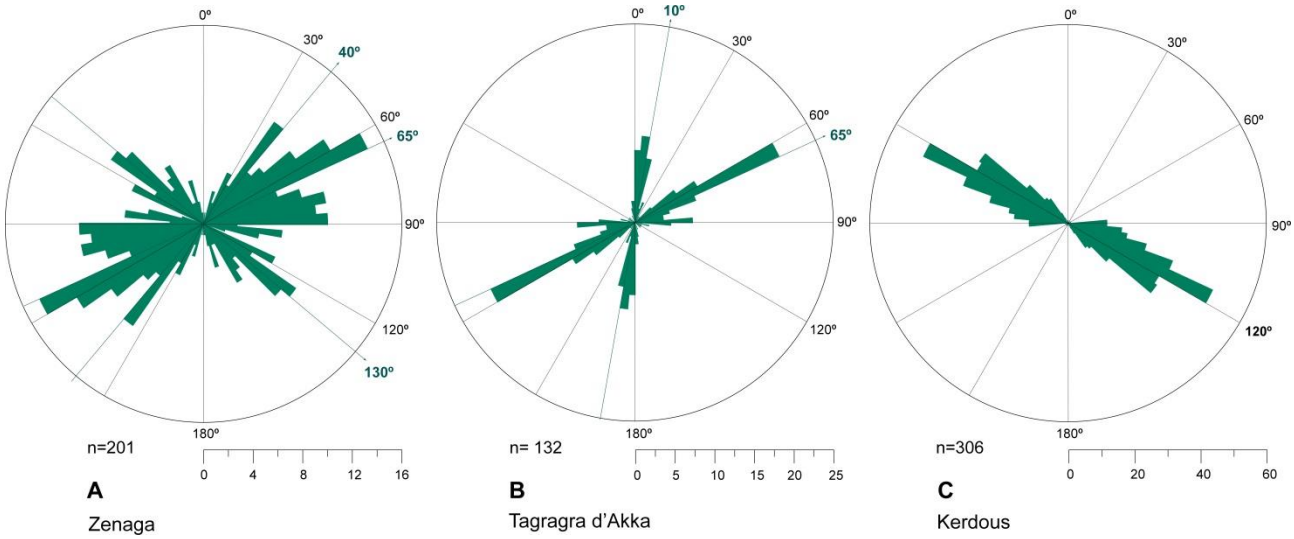

Fig. 3. 54. Rose diagrams of dyke trends measured from the aerial orthophotograph. A) Zenaga measurements, B) Tagragra d'Akka measurements and C) Kerdous measurements.

In the aerial images we can even observe coalescence structures between two dykes, since the scale of the dykes is quite large. We can recognize two non-overlapping segments leave a raft of host rock between them, with bended tips (Fig. 3. 58).

If we look in detail the rose diagrams for the dykes orientation (Fig. 3. 54), there is no coincident trend in the four inliers diagrams. The only two diagrams where some dyke sets match are the Tagragra de Tata and Kerdous diagrams, in which the ~N120º-N125º trend coincide. Among the western Anti-Atlas inliers

there are not any more similarities. The Tagraga d'Akka inlier do not show any set that matches with the rest of their neighbor inliers. However, in the Zenaga inlier (Central Anti-Atlas) there is a wide range of orientations, including ~N120º, which could be related to the same tectonic setting as in the western inliers or not.

3.4.3.2. Deformation features description.

In spite of the lack of data measurement, we could do a small pre-analysis of the deformation patterns in the three outcrops we could access.

We constructed a diagram of poles of Sp inside the dykes (Fig. 3. 55). However, the results were not conclusive because they were not enough to be analysed statistically. Nevertheless, the poles of the different areas do not show any coincident trend and they are oriented in all the directions. Only the data from Kerdous (Fig. 3. 55) shows a higher concentration in the SW quadrant of the stereogram plot.

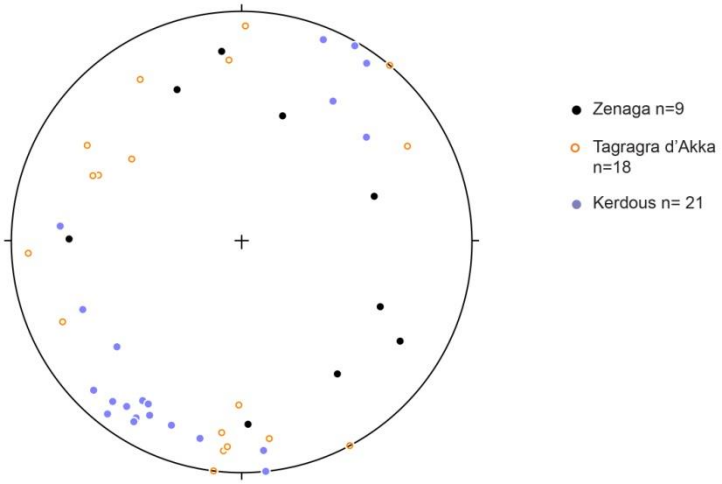

Fig. 3. 55. Equal area, lower hemisphere stereoplot of poles to Sp from fabric measured in dykes interiors in the inliers.

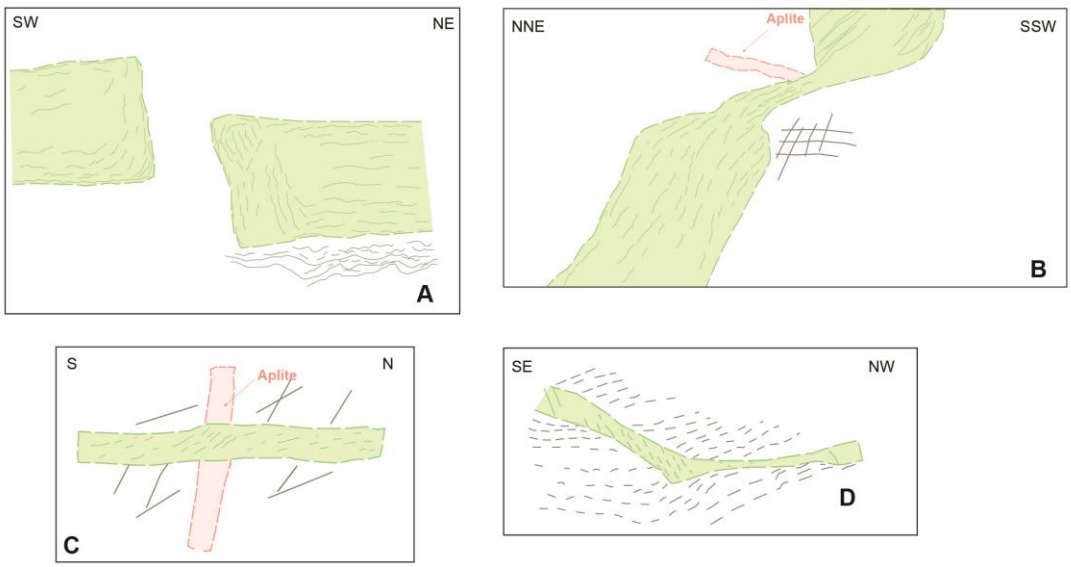

Fig. 3. 56. Sketches of field outcrops in sub-horizontal plane. A) Two dyke segments where we can see the foliation inside in the dyke and outside in the host rock (granite), very similar in orientation, in Tagragra d'Akka inlier. B) Left stepped dyke where we can see foliation inside the dyke and several joint sets oriented perpendicularly, in Tagragra d'Akka inlier. C) Dyke crosscutting an aplite vein (show apparent dilation normal to the dyke walls). It also present a fabric inside the dyke and joint systems in the host rock, in Tagragra d'Akka inlier. D) Dyke segment where we can see an oblique foliation inside the dyke with a different orientation than the foliation in the host rock (schist) in Kerdous inlier.

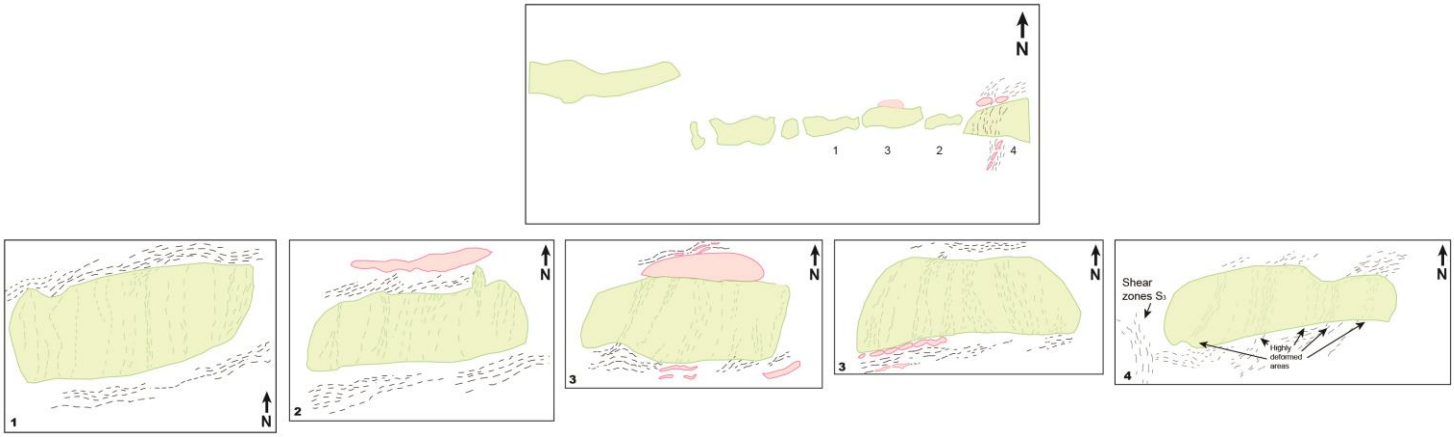

Fig. 3. 57. Sketch of a long dyke segment. From left to right (1-5). We can observe an almost normal to the dyke walls fabric very oblique to the host rock foliation. Inside the dykes there are zones highly deformed.

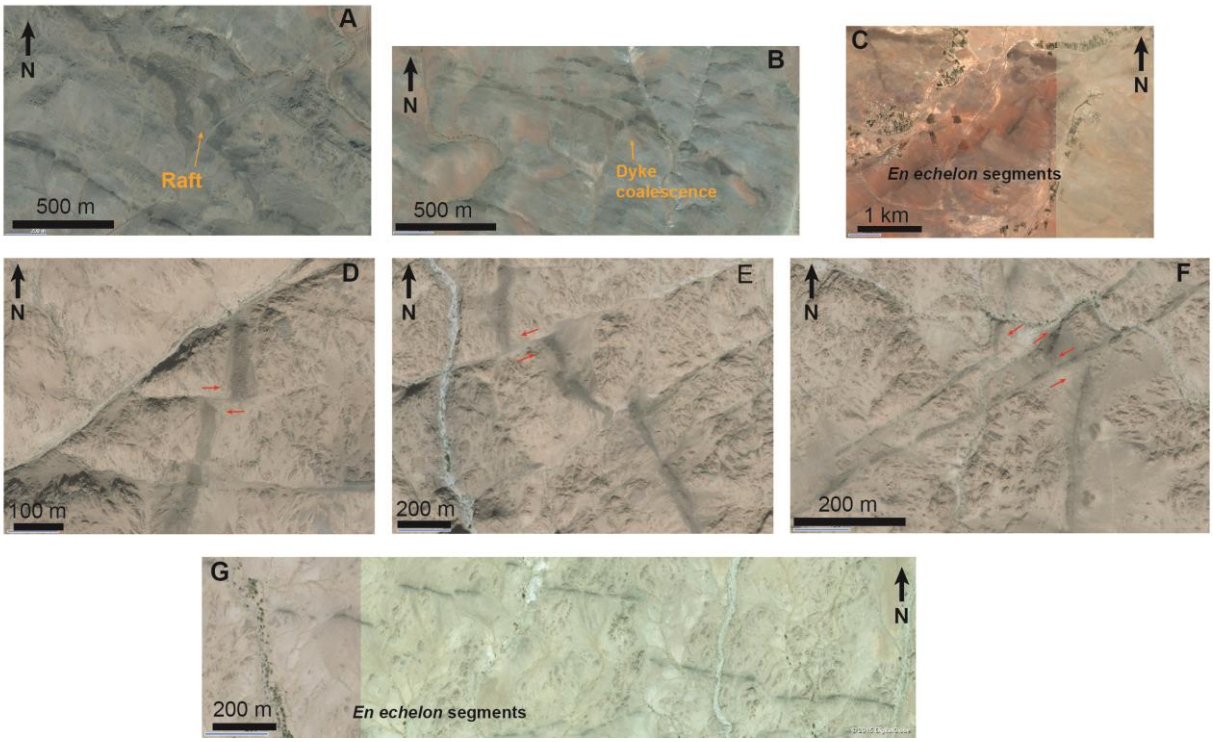

Fig. 3. 58. Aerial images from shear structures present in the dykes. A) Raft of host rock between two bended tips of dykes in Kerdous inlier. B) Left stepped dyke which probably corresponds to a coalescence structure in Kerdous inlier. C) En echelon segments of dykes in Zenaga inlier. D), E) and F) Dyke segments separated by several shear zones in Tagragra d'Akka inlier. G) En echelon segments of dykes in Tagragra d'Akka inlier.

Analyzing the outcrops we can distinguish the foliation of the host rock and the fabric inside the dykes (Fig. 3. 51; 3. 52; 3. 53). This was a major interest factor previous to the beginning of the study, the understanding of the foliation deflection or the foliation origin inside the magmatic bodies. In the sketches made from the outcrop analysis (Fig. 3. 56 and 3. 57) it is significant the difference in orientation between the fabric inside dykes and the foliation in the schists. In some dykes, the internal fabric has a perpendicular orientation in relation to the host rock foliation (Fig. 3. 57). The origin of the dyke foliation can be related to the cooling of the magma. In other cases, the internal foliation is slightly/highly oblique to the external fabric (Fig. 3. 56).

3.4.3.3. Thin section description.

Zenaga

706-Z1a
The thin section is from a mafic dyke (Fig. 3. 59a to c). The sample has a very fine grain with a quartz-feldespatic matrix and altered and replaced phenocrysts. No preferent orientation is noticeable, just a few refilled fractures. The mineral assemblage is: plagioclase, chlorite (in pyroxene or olivine pseudomorphs), muscovite, quartz, Fe oxides, talk and calcite.

706-Z1b
This sample has the same texture and structure as the previous (Fig. 3. 59d). It is very altered to sericite. The mineral assemblage is: plagioclase, quartz, chlorite, Fe oxides and dark ores, muscovite, calcite and talk.

706-Z2
This sample is from the border of a mafic dyke, in the less deformed area (Fig. 3. 59e to g). The thin section has a very fine grain size with an altered matrix. Pyroxene phenocysts and metallic ores show an orientation. The phenocrysts are elongated and all the sample present a pervasive alteration. There are several fractures not filled with secondary mineral. Only in the margins there is some alteration material. The mineral assemblage is: Dark ores, Fe oxides, chlorite, pyroxene, phlogopite, alteration minerals.

706-Z3a
In this case, the thin section belongs to the center of the same dyke as in the previous sample (Fig. 3. 59h to j). It has the same structure as in the other rock. The phenocrysts show a preferent orientation and the fractures are not refilled with secondary minerals. The mineral assemblage: plagioclase and feldspar are totally altered, muscovite and chlorite.

706-Z3b
The sample is from the same rock as the previous one (Fig. 3. 59k to m). The thin section has a very fine grain and the matrix is altered (plagioclase-sericite). The quartz phenocrysts show ondulant extinction and they are oriented. The

fractures are oriented as the phenocrysts and they are filled with secondary minerals. The alteration is to chlorite and calcite. There are also present Fe oxides. The mineral assemblage: Quartz, chlorite, plagioclase, calcite and Fe oxides.

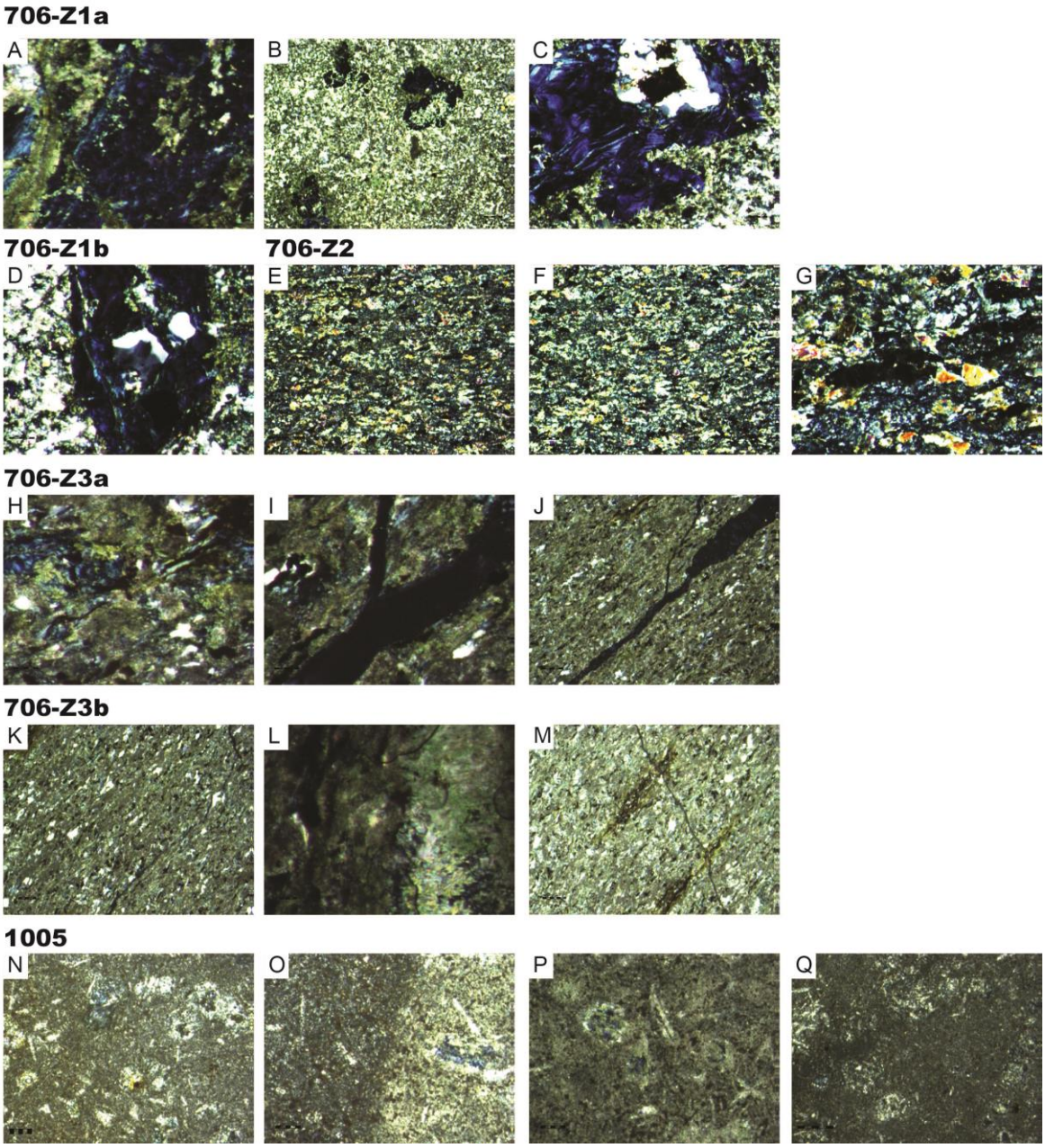

Fig. 3.59. Thin sections from the Zenaga inlier.

1005

This sample belongs to a mafic dyke with a very fine grain size. It has phenocrysts and planar minerals that show orientation. There is a xenolith in the sample with a pale colour. The matrix is vitreous and it has a lot of opaque minerals. The tecture can be named as —hyaline". The mineral assemblage is: opaque minerals, Fe oxides, plagioclase and alteration minerals (Fig. 3. 59n to q) .

Tagragra d'Akka

A-1a
This sample is from a mafic dyke (Fig. 3. 60a and b). The rock is totally altered. It presents some orientation in the plagioclases. There are a lot of fractures, some of them are refilled with secondary minerals and others are not. The mineral assemblage: plagioclases totally altered to sericite, quartz, metallic ores.

A-1b
The thin section is from the same rock as the previous one (Fig. 3. 60c to e). It is totally altered (saussuritization) and it has a lot of opaque minerals. It present also a lot of fractures filled with alteration minerals. Preferent orientation is observed in the phenocrysts. The mineral assemblage is: quartz, plagioclase, Fe oxides, opaque ores, calcite, K-feldespar.

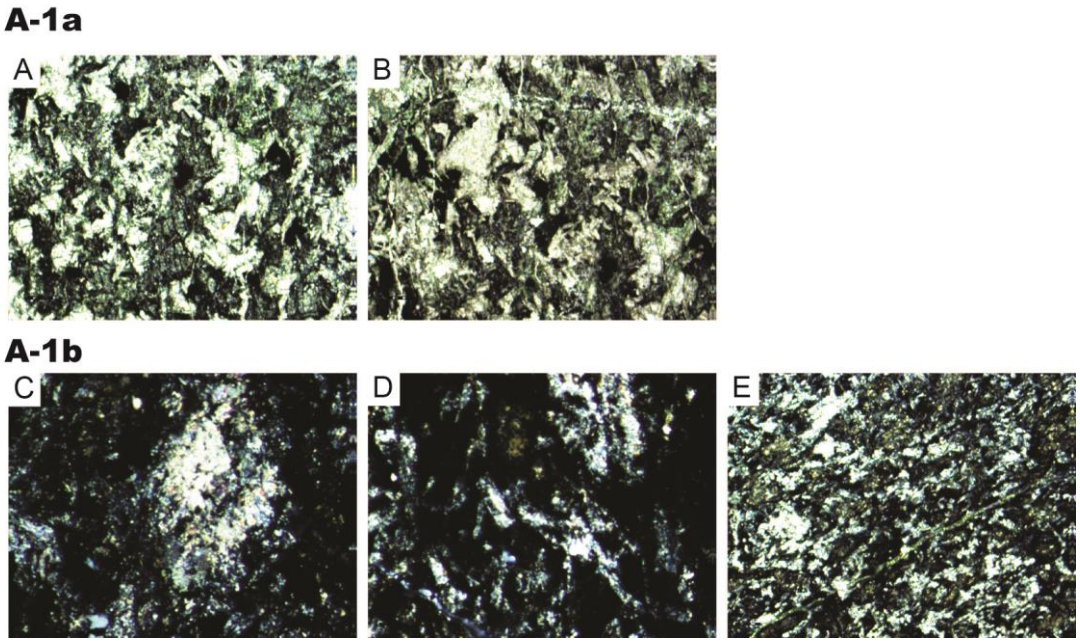

Fig. 3. 60. Thin sections from the Tagragra d'Akka inlier.

Kerdous

714-1
This thin section belongs to a dyke with few joints in its interior (Fig. 3. 61a to c). It present fractures that crosscut phenoscrysts and are refilled by new minerals. The matrix has very fine grain and the phenocrysts have planar shape. The mineral assemblage: opaque minerals, clinopyroxene, plagioclase, chlorite, quartz and carbonates.

716-1a
This thin section is from a more fractured dyke (Fig. 3. 61d). All the fractures are refilled by secondary minerals. The grain size is fine and there are planar minerals and opaque minerals preferentially oriented. The sample is very

altered to chlorite. The mineral assemblage: Plagioclase, chlorite, calcite, quartz, opaque minerals.

716-1b

The thin section belongs to the same dyke as the previous one (Fig. 3. 61e to g). It has a very fine grain size, with big plagioclase phenocrysts. There are also K-feldspar and a lot of opaque ores, but without any preferred orientation. The rock is much fractured and refilled with secondary minerals (carbonates) and seritization alteration. The mineral assemblage is: opaque ores, plagioclase, K-feldspar, quartz, calcite and Fe oxides.

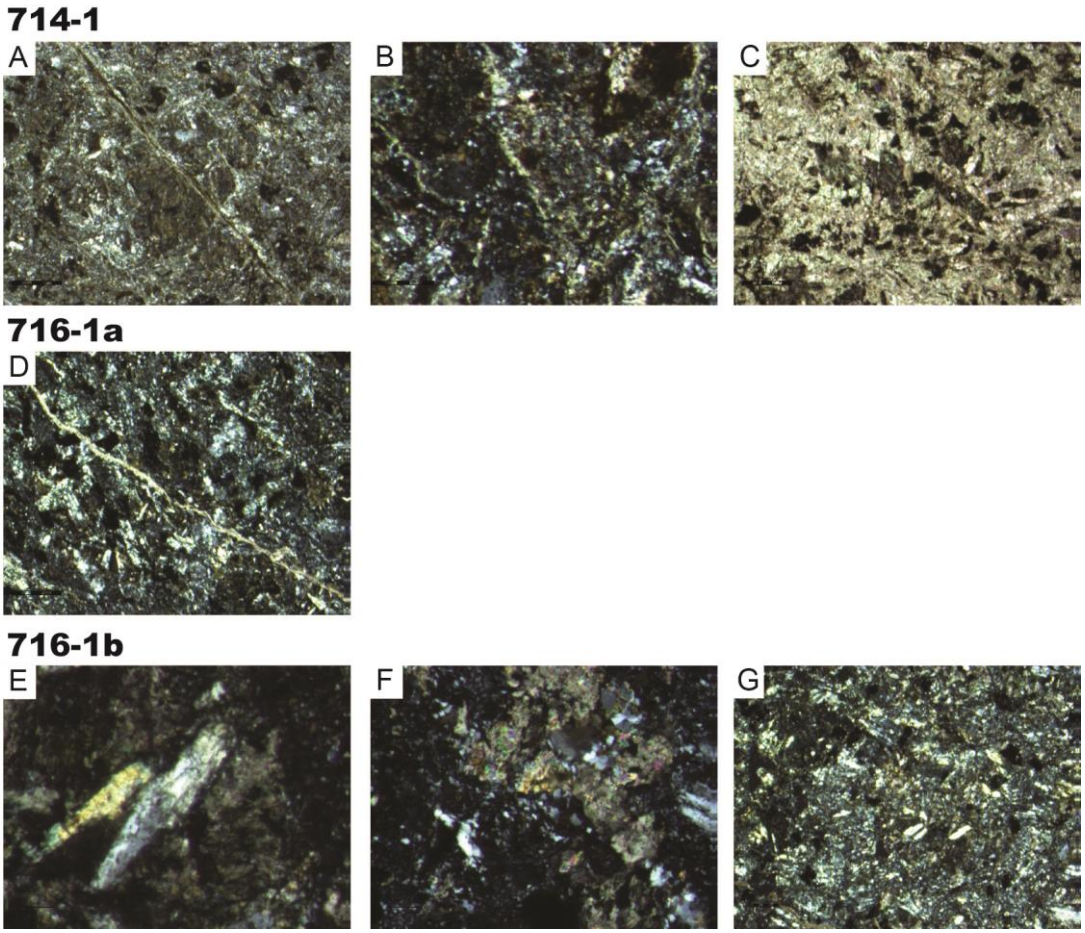

Fig. 3. 61. Thin sections from the Kerdous inlier.

3.4.4. Discussion

We described the dyke trends in the three *boutonnières* trying to find any kind of connection between structures. Comparing between rose diagrams (Fig. 3. 54), we find out no relation between inliers. The three cases show approximate main dyke trend sets between ~N10º and ~N135º. However, in Zenaga and Tagragra d'Akka, the dyke disposition is more irregular; mostly in Zenaga where we can define up to three main dyke sets (one is ~N130º, close to the Kerdous principal

sets). Also in Tagragra d'Akka the dyke trends show a very different disposition from its closest inlier neighbor, Kerdous, being both in the western part of the Anti-Atlas. Therefore, there is no conclusive result that could link the inliers under the same tectonic regime since the dyke dispositions are not coincident. Probably related to different local stress regimes.

Segmentation structures are not much noticeable at outcrop scale, although in the aerial images (Fig. 3. 58) we can observe a wide range of features. Steps in long segments and big scale coalescence structures (Fig. 3. 58b) are present, as well as, overlapping segments of dykes. The majority of the dykes show a continuous disposition with thickness up to tens of meters. Moreover, offsets produced by shear zones can be distinguished from these aerial images.

The microstructure description shown in the thin sections give us a clear note of the deformation processes underwent in the dyke masses. All the thin sections from the three inliers surveyed have a high degree of secondary alteration (secondary minerals and fractures refilled with alteration minerals) due to the desertic conditions and the marked fabric that act as alteration paths (Fig. 3. 59; 3. 60 and 3. 61). There is grain size reduction in some of the samples (706-72 from Zenaga; 716-1a and 716-1b from Kerdous Fig. 3. 61g) from mafic dyke borders, together with oriented minerals (phenocrystals) and a weak foliation fabric in dyke centers (706-Z3a in Zenaga Fig. 3. 59h to j). Other samples show a preferent orientation in the plagioclases (A-1a and A-1b from Tagragra d'Akka Fig. 3. 60). If the thin sections had been oriented, then a good fabric value would have been obtained for the inliers. Even a comparison between them would have been possible if the zones had a similar S orientation.

The presence of high quantity of ore minerals and Fe oxides is a good indicator for a probable future AMS study. This technique would help with the intrusion path characterization and magmatic flux.

The foliation grade observed in the dyke interiors varies depending on the outcrop analysed. Some dykes show a parallel to slightly oblique fabric to the previous regional foliation found in the host rock (Fig. 3. 56). However, in other areas, the dykes show no foliation evidences or a perpendicular fabric to the dyke wall, probably produced by the cooling of the magma (Fig. 3. 51d). Moreover, in this dykes we can find localised bands where there is a higher grade of foliation (Fig. 3. 57).

As described by Carreras *et al*. (2006), the oblique to sub-parallel fabric in the dykes is similarly oriented to the E-W Pan-African deformation phase foliation that affects the host rock (granitic or metamorphic). In the cases where no (or weak) foliation is described in the dykes, the host rock present a weak fabric related to the Eburnean deformation (Hafid *et al*., 2001, Carreras *et al*., 2006). Nevertheless, in areas where there is present Pan-African deformation, some dykes do not display any fabric. The same situation occurs in areas without Pan-African deformation evidences, so the development of deformation features could be also related to the dyke disposition inside this deformation bands (shear zones). This is also applicable to *composite dykes*, some parts show internal deformation while others are less or non-deformed. Consequently, the

intrusion should have occurred in different pulses (Carreras *et al*., 2006). Another important factor that controls the fabric development is the competence contrast between the intrusion and the host rock. For the case of the intrusion of this mafic magma into a granitic or a schistose host rock, the mafic fluid was supposed to be still melted to have a lower competence than the granitoids or the schists where dykes intruded, so they can suffered deformation. This hypothesis was supported by the analog models made by Carreras *et al*. (2006) compared with real examples dykes from Zenaga and Kerdous inliers. In the models, the deformation is organized in shear zones surrounding the analog material for the dyke (melted chocolate coverture) as seen in many examples in the field (Fig. 3. 58.). These evidences match with other research made in the Tagragra de Tata inlier (Walsh *et al*., 2002). Therefore, the deformation processes occurred during the dyke intrusion, that it is interpreted to have occurred during the Pan-African event.

Dykes would have intruded through previous fractures located in the granitic and metamorphic basement only driven by the tectonic forces in a transpressive context.

More work should be done in order to better constrain the dyke swarms in the inliers. Due to the huge size of the outcrops and the main features, aerial images would be of good help. Also the application of other techniques, for example, in detail geochronology analysis of the intrusions and their host rock with new and more reliable techniques as in previous works. The combination of several geological areas would determine the nature of this dyke swarms.

Previous to this study, Carreras *et al*. (2006) made a first approach to the foliation characterization in the dykes and in their host rocks, mainly in the Kerdous and Zenaga inliers. During the Pan-African event, the coetaneous dykes developed a subvertical fabric and a dipping lineation. There were also evidences of shear zones. Therefore, dykes intruded under a compressive to transpresive regime. However previously, the dyke intrusions were classified as rifting related during the Pan-African orogeny (Hafid *et al*., 2001, Thomas *et al*., 2002, Gasquet *et al*., 2005). Carreras *et al*. (2006) linked the dyke swarm with the break up of the northern margin of the WAC during the Saghro collisional event. Moreover, the cross disposition of the dyke segments correlate with a compressional fracture pattern. Walsh *et al*. (2002) also supports the hypothesis of a collisional setting for the dyke emplacement, during the Pan-African phase.
The description made by Carreras *et al*. (2006) of the dykes shows a different grade of deformation patterns. The dykes found closed to Pan-African deformation bands show an intense fabric and are oriented sub-parallel to the regional E-W Pan-African foliation. In the cases where the Eburnean deformation is preserved, dykes show less foliation and show a linear disposition (Hafid *et al*., 2001). Therefore, the dykes can be defined between Post-Eburnean and Pan-African (Hafid *et al*., 2001; Thomas *et al*., 2002; Gasquet *et al*., 2005). Also the ages obtained match with this theory, 740-800 Ma (Clauer, 1976; Leblanc y Lancelot, 1980; Cahen *et al*., 1984), for the contact metamorphism. However, Carreras *et al*. (2006) described a more complex explanation for the dyke intrusion setting (for Zenaga and Kerdous inliers): i) there are dykes with deformation features and others that do not show any kind

of fabric, although they are located in areas where there is a Pan-African deformation. ii) In areas where the Pan-African deformation is not noticeable, the dykes also present a different degree of fabric development. They tend to not show any deformation but in some particular cases, the fabric is located in the dyke margins or even in the centers. iii) There are *composite dykes* with some areas deformed and not others. This could be related to a different intrusion pulse with different deformation conditions. Moreover, the competence

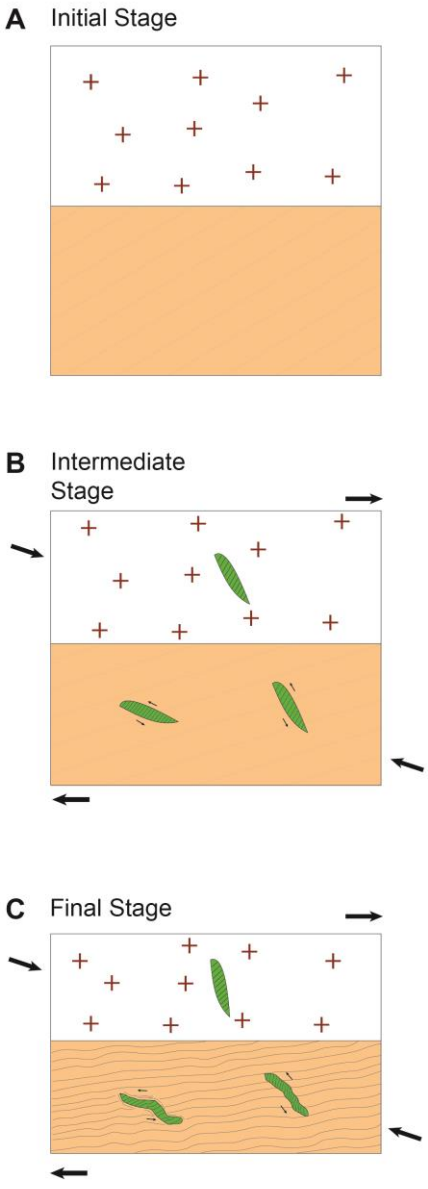

Fig. 3. 62. Proposed model for dyke intrusion and deformation stages for dykes in the Kerdous inlier. A) Initial stage, only a weak Eburnean foliation is present in the schistose material (lower part of the block). B) Intermediate state where dykes intrude in both lithologies with different orientation. An incipient fabric develops in the dyke interiors. C) Final stage, as seen in the field, here the deformation continues and foliation inside dykes as a different angle than in the host rock. This angle depends on the rock rheology.

contrast between materials during the intrusion is a more reasonable explanation for this case, since the temperature of the magma fluids should have been higher than the host rock during the fabric development. In the analog modelling experiment performed by the MIET group (Carreras *et al.*,

2006) to analyse deformation of dyke-like bodies embedded in layered rocks, shear zones tend to localise in the limits of the dykes intrusions. They support Walsh *et al*. (2002) interpretation of a syn-tectonic intrusion during the Pan-African event.

3.4.5. Conclusions.

The evidences support a dyke intrusion during the main Pan-African deformation phase. This period is characterized by the formation of shear zones in some areas (e.g. Zenaga inlier), the cross disposition of the dyke sets and, also, a subvertical foliation in the host rock and in some of the intrusion bodies. Linking the evidences, Carreras *et al*. (2006) proposed a compressive to transpressive intrusional setting. Early work attributed this dykes as classic indicators of rifting processes in the WAC dunring the Pan-African event (Hafid *et al*., 2001; Thomas *et al*., 2002; Gasquet *et al*., 2005). However, later work (as in Carreras *et al*., 2006, Walsh *et al*., 2002) and this present research linked this dyke swarm intrusion with the break up of the northern margin of the WAC during the collision of the Saghro magmatic arc (Pan-African). This collisional context is similar to the Independence Dyke Swarm studied in the previous section of this volume and to a large mafic dyke swarm in Groenland (Hanmer *et al*., 1997).

The the mineral assemblage in the thin section and evidences of seritization suggest a deformation process that evolves from high temperature to low temperature. This alteration process probably occurred during the deformation stage (green schists facies and lower). This mechanism would made the dykes even more incompetent so the strain was localized in the dyke over the host rock. The type of host rock was also another factor in the competence contrast. The competence contrast between the schist host rock and the mafic material is lower than the value for the granitoid/mafic rock system. Then, the schists are more likely to be deformed during the shear process and shear zones are nucleated in the schists and in the host rock/dyke interface.

In this case, foliation refraction found in the field is not indicative of refraction as classically understood. However, this type of apparent refraction is produced by several stages of deformation. The schist was deformed by the first Pan-African phase, during which *en echelon* fractures were produced amd mafic magma intruded in this preferential orientations. Then, strain started to localized in dykes and a fabric with an oblique angle from the host rock was developed. The deformation process continue so it results a dispare angle in the host rock and in the dyke which imply the same relation as in a refraction process.

In conclusion, we can affirm that clearly there was a small competence contrast during the intrusion of the dykes that lead to the nucleation of deformation structures inside the mafic bodies. They intruded during a transpressional period in the collisional event occurred in the Pan-African orogeny. Because of the differences in deformation features present in the dykes we can propose an extended period of intrusion pulses with changes in the tectonic stresses within shear zones that produced this type of dyke arrangement.

CHAPTER 4

ANALOGUE MODELLING

4.1. MODELS OF DYKE EMPLACEMENT INTO PREVIOUSLY FRACTURED BASEMENT.

4.1.1. Introduction

These experiments were the first approach we performed with analog modelling in order to understand the emplacement/deformation events related to dyke intrusion into a lithologically homogeneous host rock with pre-existing fractures. From the beginning of the research, the aim of our work has been to describe the mechanism related to syntectonic magmatic intrusion of mafic magma. For this purpose, two experiments were designed, both consisting of a pre-fractured plasticine block (analog of the the host rock) that can be intruded by molten chocolate (analog of magma).

The execution of the analog model was chosen as an approach to reproduce conditions of magmatic bodies intruding into host rock. In this case, we tried to simulate the situation observed in Aiguablava (Catalan Coastal Ranges). In there, we find a dyke swarm intruded into a pre-existing joint network characterized by the presence of five distinct joint sets (Martínez-Poza *et al*., 2014). From these five joint sets, only three are exploited by the intruding magma. Therefore, the aim of this experiment is trying to identify the cause of intrusion into particular orientations and not in others. The starting premise is the influence of the relative orientation of pre-existing fractures with regard to the principal stress/strain axes.

In many natural settings, mafic dykes as the ones intruded in Aiguablava, behaves as an incompetent material compared to the granitic rocks, so they can develop an internal fabric during and after emplacement (Gayer *et al*.,1978; Talbot and Sokoutis, 1995).

This approach to modelling magma intrusion into pre-existing fractures represents one of the few works dealing with this topic (Ferre *et al*., 2012; Le Corvec *et al*., 2013). Broader analog modelling of melt emplacement during deformation has been further explored (e.g. Grujic and Mancktelow, 1998; Román-Berdiel, 1999; Galland *et al*., 2003; Druguet and Carreras, 2006; Castaño, 2010; and own work developed in the context of this thesis: Martinez-Poza and Druguet, 2015). The majority of the past research has been centered on fracture development and the propagation paths of dykes (Spence *et al*., 1987; Lister and Kerr, 1991; Maccaferri *et al*., 2010).

4.1.2. Experimental setting

This was the first approach to this kind of experiments in the MIET lab, so the two first setting were attempts to understand the behavior of fractures and melted fluids. We used the deformation apparatus BCN-stage (at the Universidad Autónoma de Barcelona). In previous works some experiments have been based on deformation analysis around molten masses (Druguet and

Carreras, 2006; Bons *et al*., 2008; Druguet and Castaño, 2010; Castaño, 2010), but nothing similar to this new approximation.

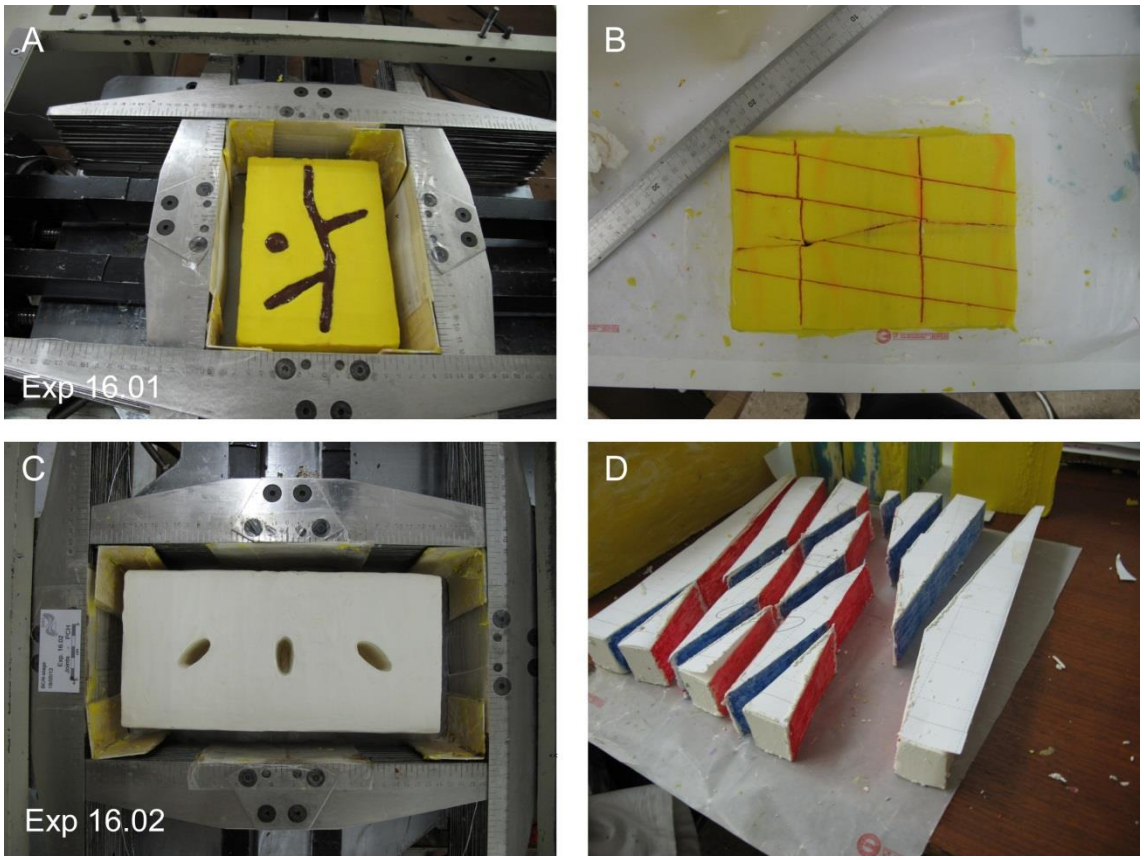

Fig. 4.1. A) and B) preparation of the model 16.01; C) and D) preparation of the model 16.02.

The two models have approximately the same dimensions and deformation parameters. The analog materials used are also the same in both experiments, for the experiment 16.01 we used a yellow plasticine (Fig. 4.1. A) and B)) and white plasticine for the experiment 16.02 (Fig. 4.1. C) and D)). Although both plasticines (OcluPlast S.A. with an effective viscosity ~10^7 Pa·s) supposedly have the same viscosity value, the white one behaves more rigid than the yellow one, so that we change the material in the second experiment. The plasticine reproduces the brittle-ductile host rock where there is a set/several sets of pre-existing fractures. The molten couverture chocolate simulates the mafic material (Nestlé, S.A., with viscosity ranging from <100 Pa·s and <107 Pa·s at the experimental temperatures of 30-26 ºC). The apparatus has pure shear conditions and the strain rate was set at a rate of $2.5x10^{-5}$ and 25ºC of room temperature. Later, the temperature was increased to keep the chocolate in molten conditions. The deformation conditions were set in the apparatus at a strain rate of $2.5x10^{-5}s^{-1}$, with a pure shear movement. This conditions were constant for both experiments. The experiments had a duration between 3 to 5 hours aprox., which suppose a shortening along the Z axis of around ~30%.

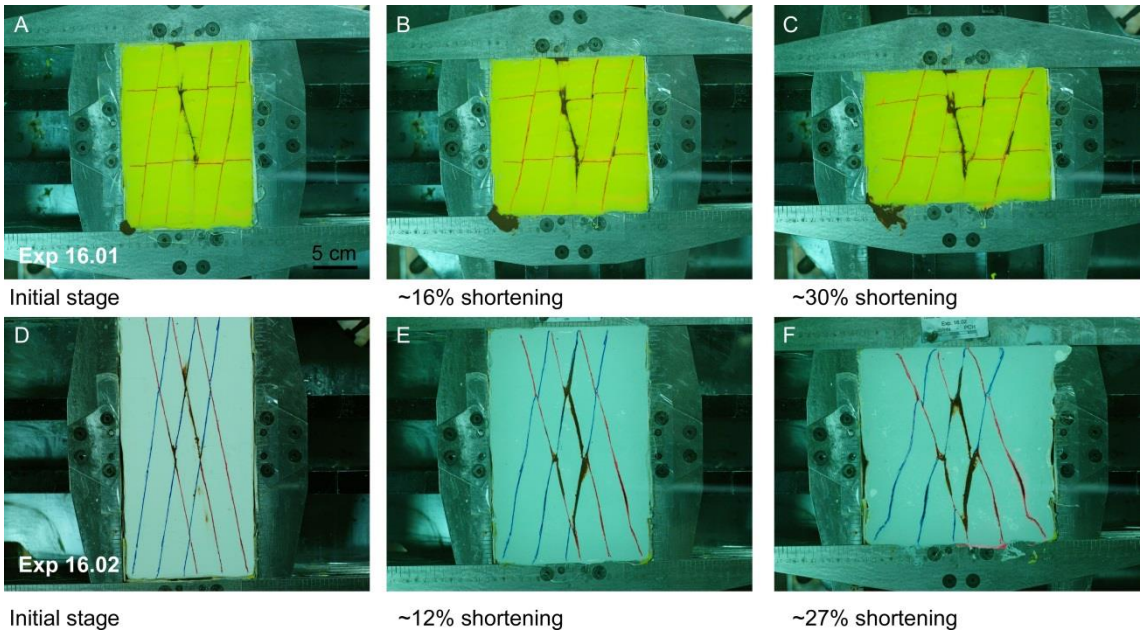

Fig. 4.2. A), B) and C) experiment 16.01 setting. D), E) and F) experiment 16.02 setting.

4.1.2.1. Experiment 16.01

We set up the experiment in the deformation apparatus BCN-stage, with the conditions previously explained. We built a plasticine basal block or unit of 20x15x6 cm in which we dug irregular shaped hollows (Fig. 4.1. A) and B)), an elongated dyke like structures with two apophisys and a pod like structure in the middle part of the basal block. In another block of plasticine (top block), 20x15x4 cm, we cut two fracture sets. One set at 10º from the Z axis (shortening axis) and 3 cm spacing between fractures and in the other set the fractures are oriented at 90º from the Z axis and 6 cm spacing (Fig. 4.1. B)). The last fracture produced in the block, was an irregular crack in the center of the model. This fracture follows the same orientation as the dyke like structure in the basal block. Later we refilled the holes in the bottom block with the melted couverture chocolate (~34ºC), placed the fractured block on top and sealed the top-bottom contact with plasticine to give it more consistency. The total time of the experiment was 3h and 50 minutes. This time represent a bulk shortening of ~30% of the model along the Z axis (Fig. 4. 2. A), B) and C)).

4.1.2.2. Experiment 16.02

This second experiment has the same dimensions for the upper (4 cm) and lower (6 cm) units, but it is longer along Z axis, 30x15x10 cm in total. We used the same analog materials and deformation conditions as in the first one. However, it has several changes with respect to the experiment 16.01. The first one is in the basal block of the experiment. We dug three ellipsoid-like hollows in three different orientations. The first one has its long axis at ~140º from the Z axis of the stage, the second hollow is at 90º from the axis and the third one is at ~40º from the axis. The plasticine upper block of the model was also pre-fractured, although we modified the fracture sets orientation. One fracture set is

oriented at 170º to Z axis (red lines) and 3 cm spacing (Fig. 4. 1. D)). The other is at 10º (blue lines) and also has 3 cm of spacing between fractures (Fig. 4. 1. D)). We filled up the ellipsoid holes with the melted couverture chocolate and placed the top block over it (Fig. 4.1. C)) and we sealed the contact between both parts, following the procedure of the previous model. The experiment was running during 4h and 24 minutes. This time supposes a bulk shortening of ~27% of the model (Fig. 4. 2. D), E) and F)).

4.1.3. Model analysis

A photograph of the upper part of the model was automatically taken every 10 minutes. This helped us to record the deformation that was taking place during the progress of the experiment (Fig. 4. 2.). On the model upper surface, we marked the fracture sets to be used as markers of the deformation during the experiment (Figs. 4.1 and 4. 2.). We could see how the linear fractures where bending due to the shortening process (Fig. 4. 3.), the slip between fractures that creates small shear zones (Fig. 4. 3. A), B) and D)) and also, the thickening of the intrusion through the cracks. In the experiment 16.01, we chose an image from the half time of the experiment, which correspond to a ~16% of shortening, and the final result of the experiment, which was a ~30% of shortening (Fig. 4. 2. A) and B)). In the case of the experiment 16.02, we selected the same time periods for the images, but due to the measurement differences, the half time image was for a shortening of ~12% and the final result was a bulk shortening of ~27% (Fig. 4. 2. C) and D)).

Additionally, after the experiment was finished, the model block was cut in several sections in depth. The resultant slabs were scans individually, so we could observe the vertical domain and the evolution in depth of the original structures after the deformation process (Figs. 4. 4a and 4b).

4.1.4. Results

In general, the results from both analyses show that effectively an intrusion through the pre-existing fractures occurred, as well as, a preferential intrusion in some orientations over others.

The final remarks from both experiments are:

In the Experiment 16.01, as a result of the deformation process, we can observe the change in shape of the fractures, the intrusion of the chocolate into the intersection points and a prevalence of chocolate injection and propagation through the fracture which is parallel to the initial dyke orientations and also

along the fracture oriented at 10º to the shortening axis Z (Fig. 4. 3. A) and B)). It is noticeable that chocolate did not flow along fractures normal to Z axis.

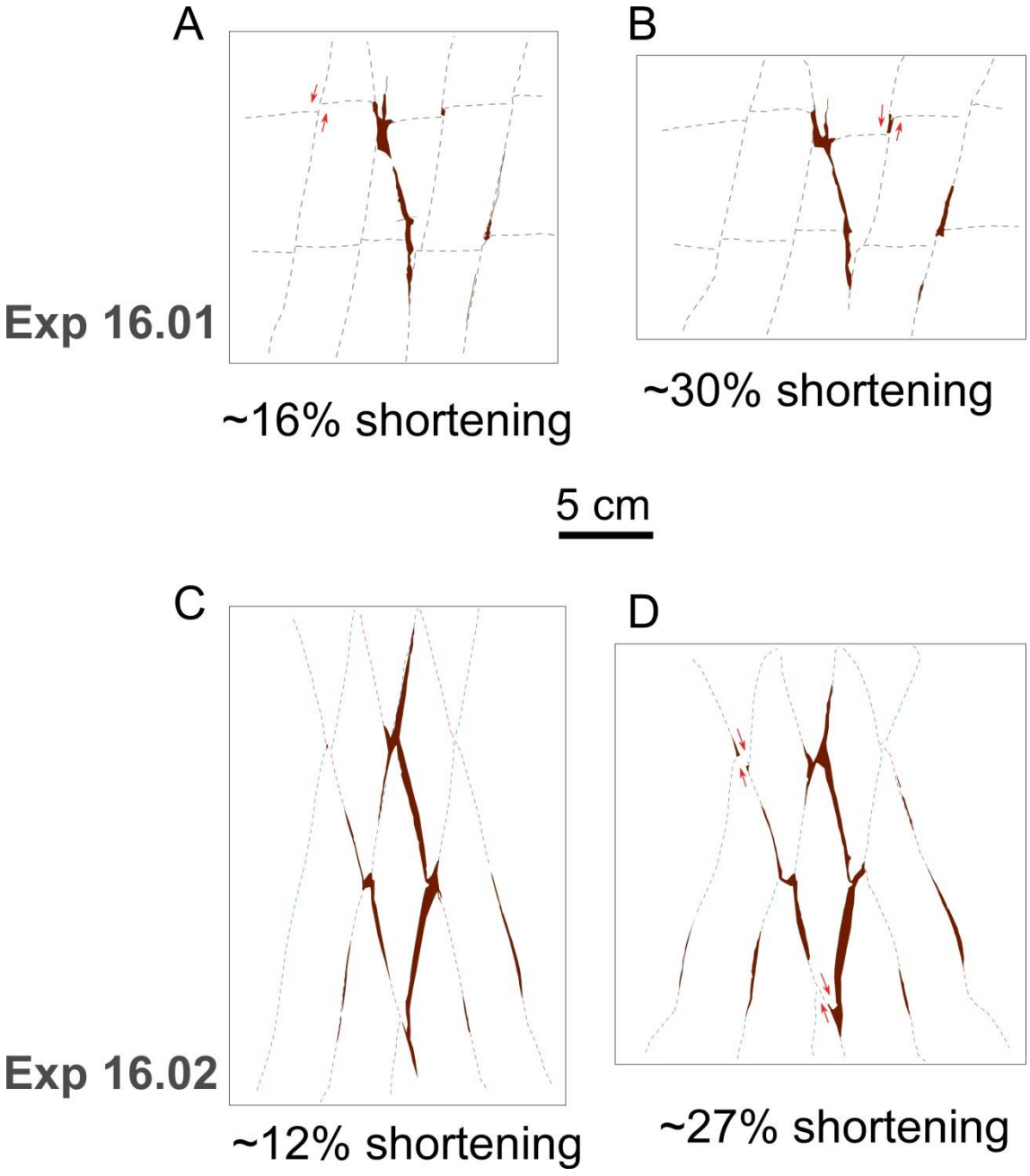

Fig. 4.3. A) and B) deformation analysis of experiment 16.01 D) and E) deformation analysis of experiment 16.02.

In the vertical sections, we can see the propagation of the chocolate through the fractures up to the top of the model (Fig. 4. 4a). Likewise, the final shape of the structures that contain the molten chocolate are indicative of the forces that have affected the model (Fig 4. 4a. D)). We can see how the structures perpendicular to Z axis had suffered compression, up to closing their volume, e.g., the apophysis (Fig. 4. 4a. D)). While the structures oblique or parallel to Z

axis, increase their volume in this direction, e.g. the elongate dyke (Fig. 4. 4a. D).

In the Experiment 16.02 the last stage of deformation gives as a result the bending of the fractures and the injection of the melted chocolate through them, mostly in the center and upper part of the model (Fig. 4. 4b). In this case, the intrusion occurred in both joint sets and not only along one set as in the previous experiment. This situation is similar to the zigzagging dyke intrusion patterns where the intrusion occurs along two different joint sets (Fig 4. 5) or even it can be produced by a single joint set. There is also a thickening of the dykes with the intrusion of more chocolate from the ~12% shortening situation to the final phase of the model.

The scans of the vertical slabs of the model show a coincident behavior as in experiment 16.01. In this case, as both basal hollows had ellipsoid shape and they are located oblique to the Z axis, the final form is very similar to the pod like structure in experiment 16.01; this is, an hourglass figure oblique to Z axis (Figs. 4. 4a. E) and 4. 4b. F)), due to the extension in X axis and compression in Z axis.

4.1.5. Discussion and conclusions

This preliminary work helped us to know the improvements for later analysis in the same topic (Martinez-Poza and Druguet, 2015).

Firstly, the experiment would have required longer time running in order to obtain better quality results since the deformation features could develop largely.

Temperature conditions are not approximate to the real situation. Moreover, the chocolate cooled down fast enough to act as a rigid body at the end of the experiment. In the following experiments, we tried to keep the chocolate molten as long as possible.

There were noticeable differences in the plasticine properties in both experiments. The yellow plasticine from the first model (Exp 16.01) showed more fluidity than the white plasticine from the second model (Exp 16.02). This evidence helped us to choose the white plasticine over the yellow one, since the white plasticine could act as a better analog material to simulate a brittle granitic host rock (Martinez-Poza and Druguet, 2015).

Boundary conditions and plasticine flow affected the model, as seen in the images (Fig. 4. 2) where the plasticine flowed on the stage corners. In addition, the effects of magmatic pressure were not able to explore because of the the lack of fluid (chocolate) pressure.

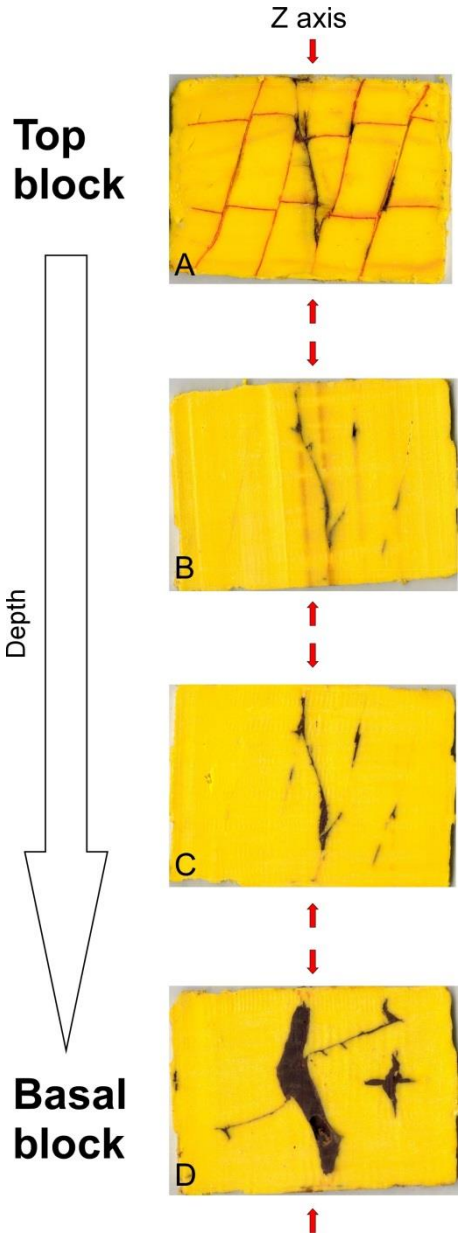

Fig. 4.4a. Horizontal scanned sections of the model 16.01.

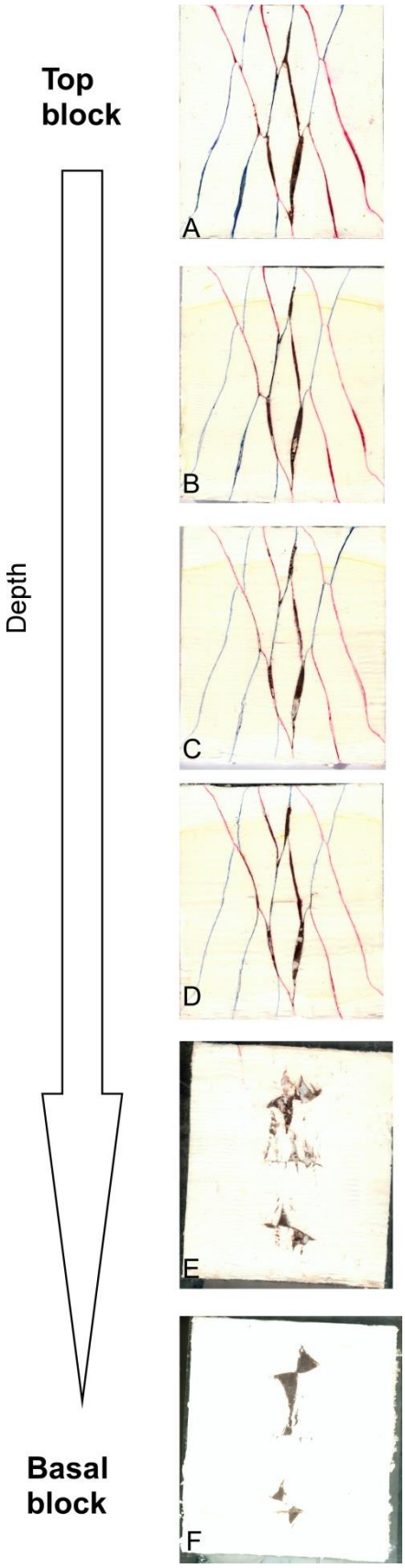

Fig. 4.4b. Horizontal scanned sections of the model 16.02.

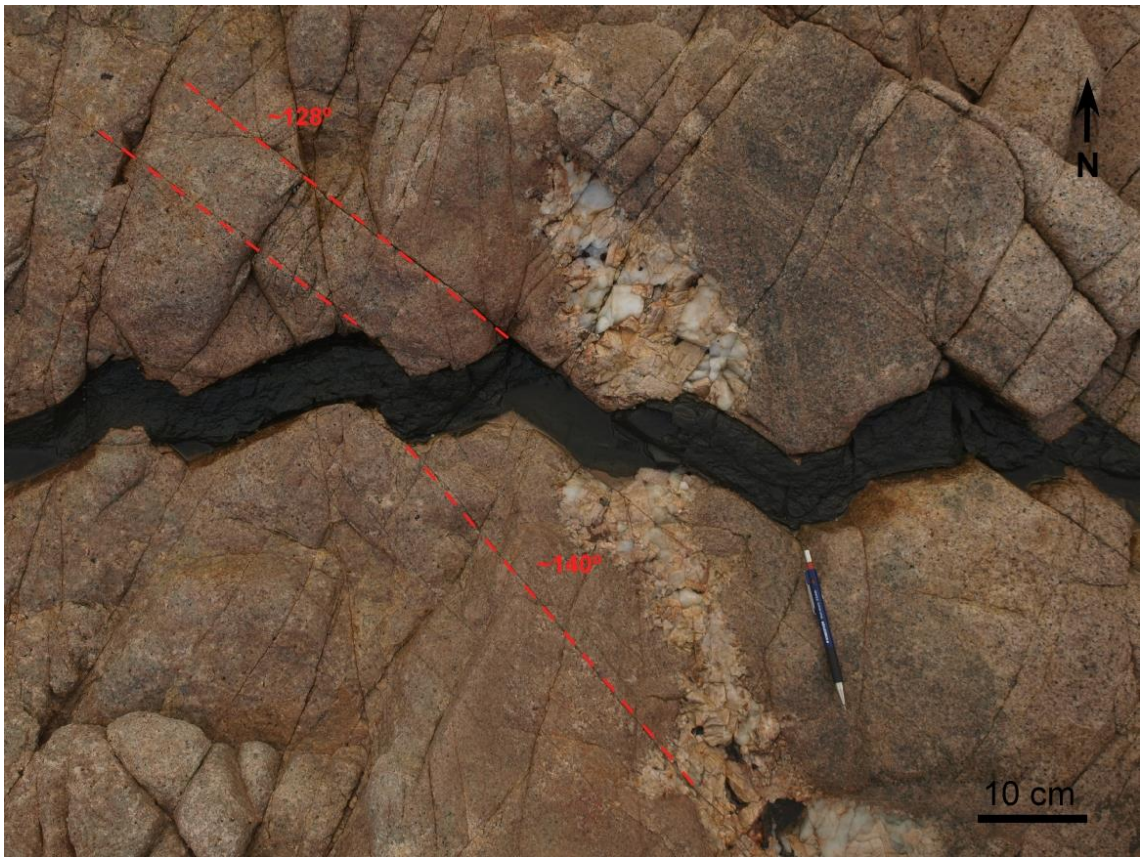

Fig.4.5. Example of zigzagged dyke in Aiguablava dyke swarm.

More experiments with different joint sets orientation would be interesting to be carried out. Series of several analysis would help to discriminate which orientations are more likely to be intruded by fluids/magma than other. Although, these values can be obtain numerically, analog modelling would provide the resulting structures observed in nature.

In conclusion, this first approach to analog modelling of dykes intruding into pre-existing structures shows us a connection between joint orientation and dyke injection. The results are consistent with previous hypothesis. Depending on the orientation of fractures with respect to the stress/strain axes, dykes will be able or not to intrude along pre-existing fractures. In the absence of magma overpressure (such in these experiments), dykes can only intrude into fractures that are able to open, that is, fractures at <45º to the instantaneous shortening axis Z (or σ_1).

In the 16.01 experiment we see an intrusion along the central fracture and the 10º oriented fractures. No chocolate intrudes along the 90º fractures. However, in the 16.02 model, the chocolate intrude likewise in both, symmetrically arranged fracture sets and recreate the shape of zig-zag dykes that we have observed in the field (Fig. 4. 5).

4.2. MODELS OF DUCTILE DEFORMATION OF PARTIALLY MOLTEN DYKES IN ISOTROPIC HOST ROCKS. ANALYSIS OF DYKE SHAPES AND FABRICS.

4.2.1. Introduction

Syntectonic magmatic dykes are important geological structures because they carry information on many aspects of magmatic and tectonic processes. They are present at all crustal levels and scales and under different tectonic regimes, and are useful to recognize the interaction between deformation processes and emplacement of magmas (Petford *et al*., 2000).

At mid- to lower crustal domains where ductile conditions prevail, hydrofracturing produces an episodic embrittlement of the wall rocks, and dykes intrude at dilation sites (Davidson *et al*., 1994; Brown and Solar, 1998). Until full crystallization, brittle and ductile processes can operate simultaneously in the dyke-wall rock system. After dyke emplacement, the system recovers the original overall ductile behavior, and veins or dykes and their host rocks deform depending on their relative competences. It is interesting to note that at these latest stages of solid-state ductile behavior, mafic dykes may keep an incompetent behavior compared to the host rocks, developing a characteristic internal foliation (Gayer *et al*., 1978; Talbot and Sokoutis, 1995). To date, little attention has been paid to these complex magmatic-tectonic interactions in

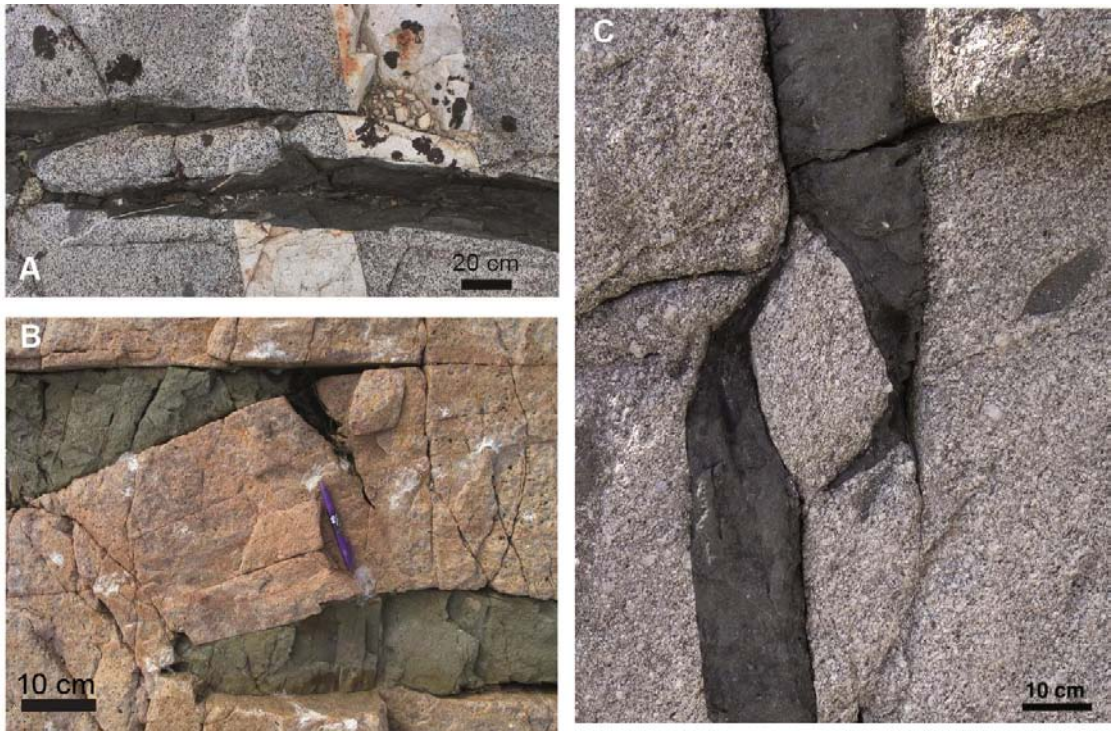

Fig. 4. 6. Examples of "en echelon"mafic dykes.A) Independence Dyke Swarm (California, USA). Notice the effects of superimposed ductile strain (foliations and shearing). B) Aiguablava dyke swarm (Costa Brava, Girona). C) SE Sardinia dyke swarm (Italy).

terms of modelling (e.g., Grujic and Mancktelow, 1998; Galland *et al*., 2003; Druguet and Carreras, 2006), compared to the more abundant literature on fracture and dyke propagation along elastic media (e.g., Spence *et al*., 1987; Lister and Kerr, 1991; Maccaferri *et al*., 2010).

Here we present some preliminary results of analogue modelling experiments on the deformation of syntectonic —enechelon" or stepped dykes, which represent a particular but very common geometry in nature (e.g., Ehlers and Ehlers, 1977; Nicholson and Pollard, 1985; Martínez-Poza *et al*., 2014; Fig. 4. 6). We analyze the deformation processes occurred during the variable time period when dykes are not fully crystallized and thus are less competent than the ductile host rock.

4.2.2. Experimental setting

Two experiments were performed using the deformation apparatus BCN-stage (Univ.Autònoma de Barcelona). Several previous works have experimentally studied the deformation around molten bodies in the same deformation Stage (Druguet and Carreras, 2006; Bons *et al*., 2008; Druguet and Castaño, 2010).

The two models differ in the initial arrangement of the dyke system, within the shortening strain field in Exp. 16.03 (Figs. 4.7A), B) and C)) and extensional strain

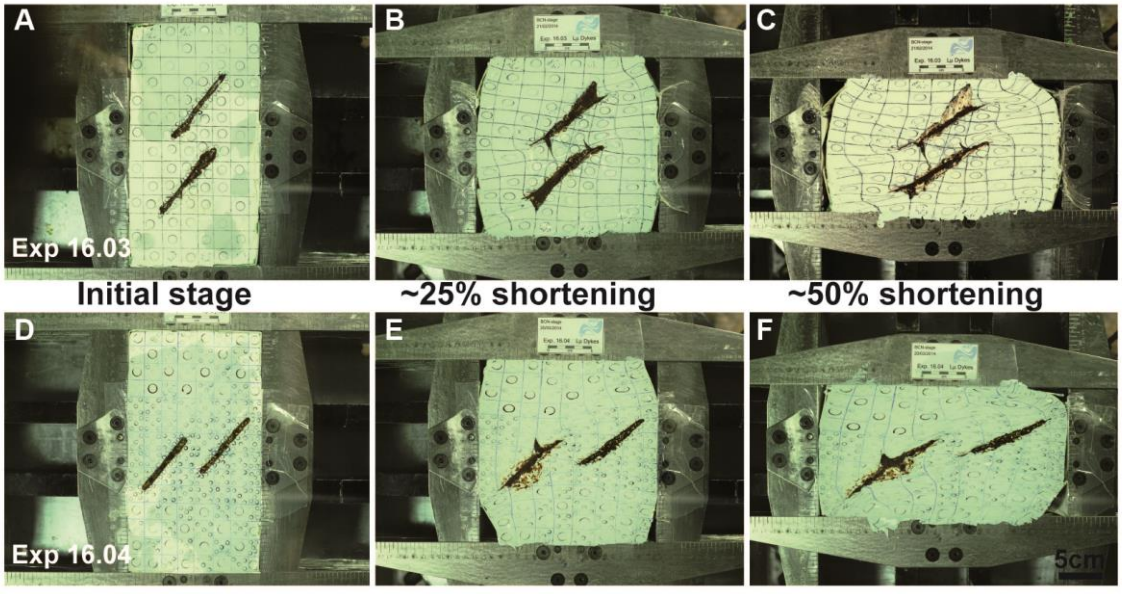

Fig. 4. 7. A), B) and C) experiment 16.03 setting. D), E) and F) experiment 16.04 setting.

field in Exp. 16.04 (Figs. 4. 7 D), E) and F)). All the other geometric and deformation parameters remained constant in both models. The analogue materials used for the experiments are white plasticine (from Oclu-Plast S.A., with an effective viscosity ~10^7 Pa·s.), simulating the brittle-ductile host rock,

and partially molten couverture chocolate (Nestlé, S.A., with viscosity ranging from <100 Pa·s. and $<10^7$ Pa·s. at the experimental temperatures of 30-26 ºC) as analogue for the melted dykes. These are the same materials previously used in the experimental works by Druguet and Carreras (2006) and Druguet and Castaño (2010). Pairs of overlapping stepped elongated cavities displayed at 40º to the shortening Z axis of the BCNStage were filled with chocolate molten at 35-40 ºC.As the dyke system arrangement vary from one to the other experiment, the resulting spacing between the chocolate filled dykes and the sides of the deformation cell are different in the two experiments (Figs. 4. 7 A) and D)).

Deformation conditions were those of pure shear at a fixed strain rate of 2.5x 10^{-5} s^{-1}, with an initial room temperature of 25 ºC. The duration of the experiments was around 7:00-7:30 hours, which represents almost a 50%bulk shortening along Z axis. During the experiments the temperature was eventually raised to maintain the viscosity of chocolate lower than that of the plasticine matrix.

4.2.3. Model analysis

Photographs of the upper surface of the models were taken with 10 min. interval, allowing us to record the deformation sequence of each model. Two main analyses of the different deformation steps were made after conducting the experiments.

The first approach was a contour analysis of strain intensity, by measuring the axial ratio RXZ (X=long axis and Z=short axis of ellipses that resulted from deforming the circles drawn in the upper surface at the onset of the experiments, Fig. 4. 8. A) and D)).Although graphite pencil shavings had been disseminated on top of the chocolate dykes, these were not useful to analyze strain within dykes, since graphite markers tended to clump together. The strain contours were made for a ~25% bulk shortening stage (Figs. 4. 8 G) and I)) and for the final stage of ~50% bulk shortening (Fig. 4. 8. H) and J)).

A second analysis consisted of drawing continuous X axis traces by extrapolating the long axes of the elliptic markers in the plasticine. This was also performed for the ~25% and ~50% bulk shortening stages (Fig. 4. 9. K), L), M) and N)), allowing us to achieve how deformation was accommodated in the matrix around the deforming dykes. Finally, stretch and rotation of dykes and growth and development of new fractures in the plasticine were directly analyzed from the photographs of the upper surfaces.

Appart from this, we cut the experimental block in slices of some cms width. Each slab was scanned in the laboratory, so we can see the dyke intrusions in depth. The resultant images would help us to see the evolution of the pre-exisitant structures, in vertical sections, after the deformation process (Fig. 4. 10a and 10b).

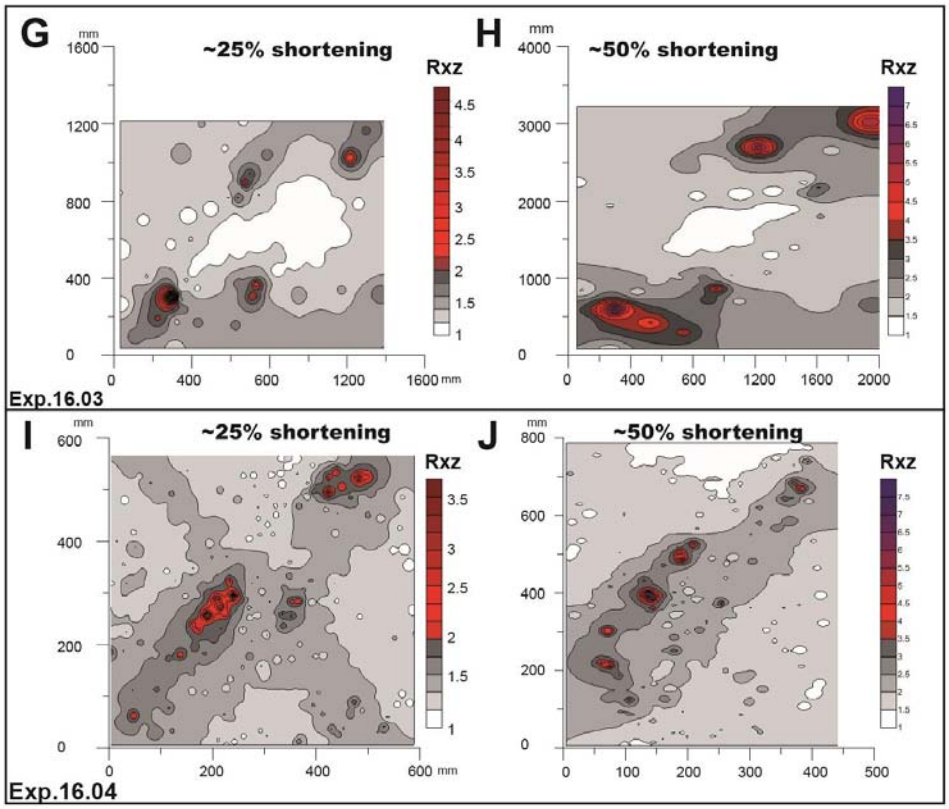

Fig. 4. 8. G), H), I) and J) contour analysis of Rxz for both experiments at ~25% and ~50% shortening.

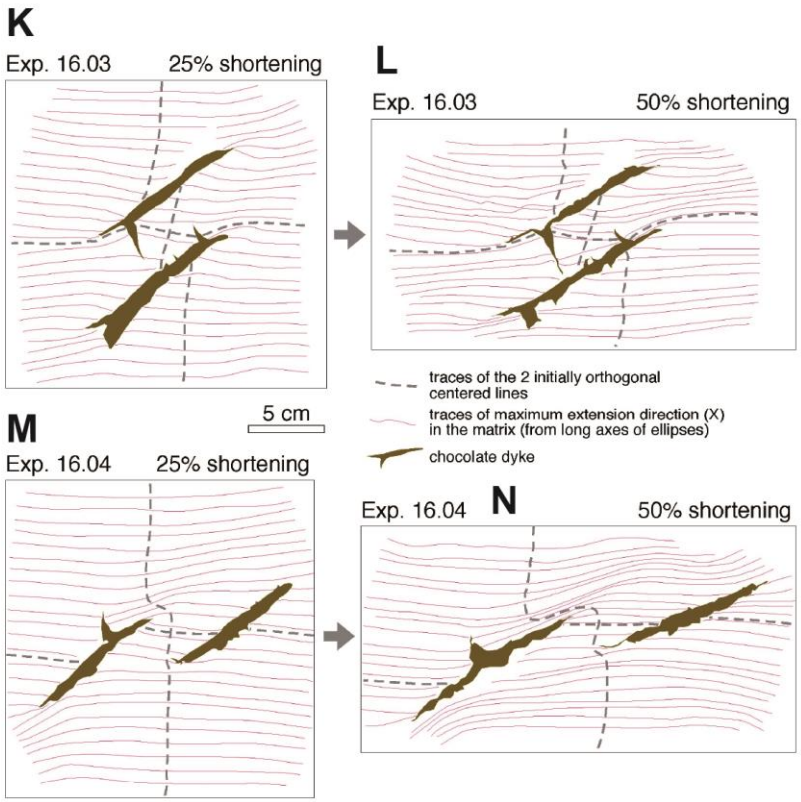

Fig. 4. 9. K), L), M) and N) X traces analysis for both experiments at ~25% and ~50% shortening.

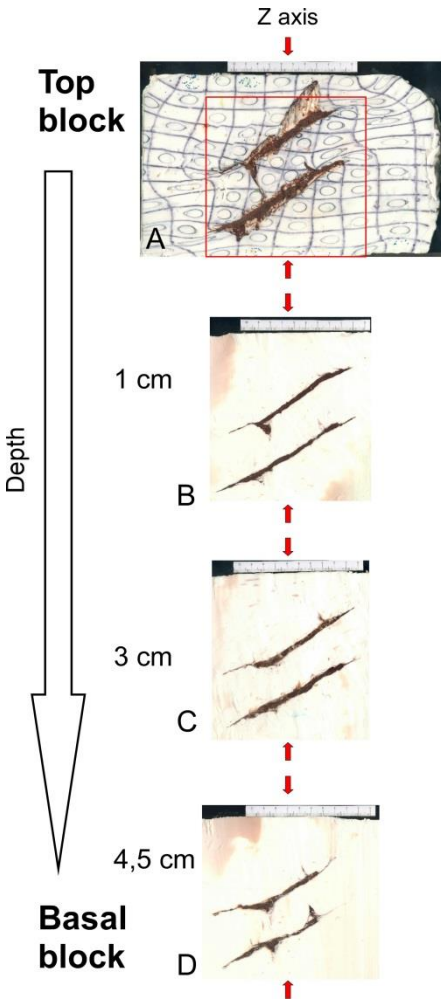

Fig. 4. 10a. Horizontal scanned sections of the model 16.03.

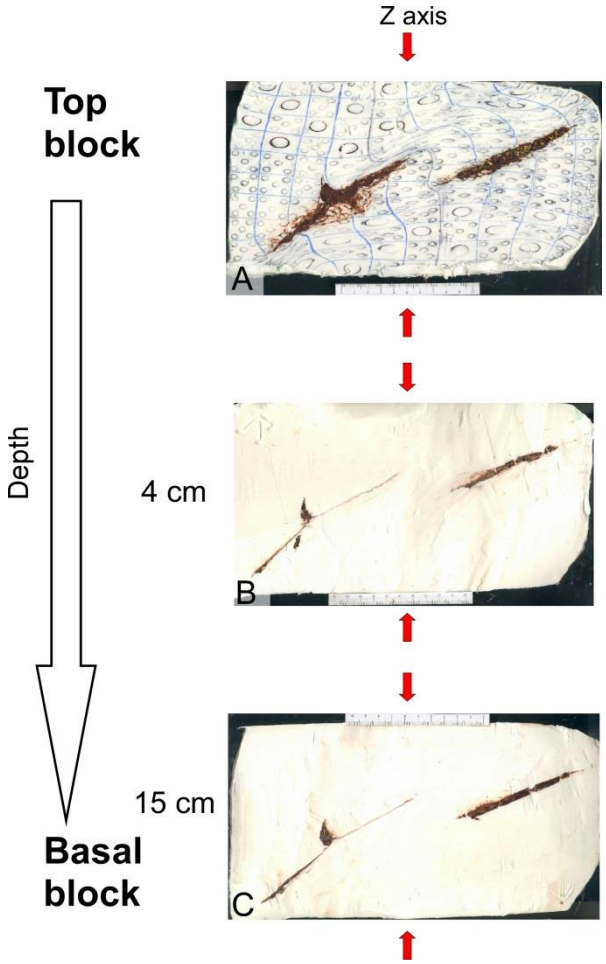

Fig. 4. 10b. Horizontal scanned sections of the model 16.04.

4.2.4. Results

The performed analyses show the highly heterogeneous distribution of strain around the deforming dykes in both experiments 16.03 and 16.04 (Fig. 4. 8). This occurs because of the strong competence contrast between the melted chocolate, which made little resistance to deformation, and the brittle-ductile plasticine matrix.

Dykes stretch and rotate at a higher rate than the matrix, leaving a strain shadow in the central part between the two dykes, which is almost free of strain in Exp. 16.03. On the contrary, strain is mostly concentrated at the tips of the dykes and, in the case of Exp. 16.04, also along the outer dyke margins, where the most prominent ductile shear zones develop. Values of RXZ > 7 are recorded in these higher strain zones.

Thus, deformation is localized around dykes, whose longitudinal stretching and clockwise rotation is accommodated by the matrix in the form of ductile

deflections and sinistral shear zones. This feature is very common in dykes-host rock systems deformed under ductile conditions in mid to lower crustal domains (Fig. 4. 6. B)). The strain shadow between the two dykes in Exp. 16.03 suffers rigid body rotation synthetic to rotation of the dykes (see the traces of the 2 initially orthogonal lines in Fig. 4. 9. K, L), whereas in Exp. 16.04, the central part is relatively more deformed, developing into a lozenge-shaped body surrounded by the shear zones. These significant differences in the structural evolution of the two models are due to the variation in the initial arrangement of the dyke system (within the shortening or the extensional strain field).

Moreover, initial arrangement of the dike system is also the main reason for differences in the evolution of the dyke-fractures themselves. The initial arrangement of dyke system in Exp. 16.03 (displaying a shortening strain field arrangement) leads to a drastic increase in dyke overlapping with progressive deformation, generating a local stress state favorable to the development of new fractures in the plasticine. These fractures are perpendicular to the dykes long axes and progressively propagate and become filled with the partially molten chocolate. One of these horn-like structures almost connects the two dykes with the other, forming a bridge in the central, overlapping area, a feature that resembles many natural structures in dykes (see e.g. Fig. 4. 6). On the contrary, in the Exp. 16.04 (displaying an extensional strain field arrangement), dyke stretching led to a mutual separation between the dykes, and to the disappearance of the former dyke overlapping feature. The only new fracture opened in the model is in the outer part of the dyke, so no connection between the two dykes was possible.

If we look in detail Figs. 4. 10a and 4. 10b, we can observe the final result of the dyke bodies after the deformation process. In both cases, the different slabs show a very similar shape in depth of the dyke bodies (Fig 4. 10a. D) and 4. 10b. C)). This always depends on the original orientation of the dyke with respect the principal stress axis. However, there is not a remarkable change of shape in depth; they preserve the form in the vertical section.

4.2.5. Conclusions

This work allowed us to find the connection between a structure commonly found in syntectonic dykes and the process and variables responsible for its presence in the nature.

Despite some limitation of the experimental modelling, such as the boundary conditions effect and the absence of fluid/magma (chocolate in the experiments) pressure, information is gained on the main controls on the development of deformed stepped dykes. Deformation is localized at the dyke tips and margins, with development of deflections and zones of high strain (shear zones). This ductile behavior can be simultaneous to brittle deformation associated to the presence of a molten phase. The patterns of both ductile and brittle structures depend on the initial arrangement of the stepped dykes with regard to the imposed boundary conditions.

CHAPTER 5

DISCUSSION AND CONCLUSIONS

This chapter will discuss the main implications of the different sections of this thesis. As a result of the study of four case studies in different geological context, we can try to discern the similarities and differences between each area. This process can help us to find intrusion and deformation models for different settings, validated by the experimental models carried out in the analogue modelling laboratory. In what follows, a discussion of the main findings is presented.

5.1. DYKE FEATURES

In this section, the main dyke features found in the outcrops will be described. The studied dykes were emplaced into brittle or into brittle-ductile conditions. Thus some important remarks can be made. We are going to distinguish between the brittle and ductile structures produced in dykes.

5.1.1. Brittle structures

In brittle settings we can divide our observations in external and internal aspects, that is, structures developed in the interior of the dykes and at the boundary or contact zone between the dyke and the host rock. These brittle features are usually formed during the injection and emplacement event, so they are intrusive structures.

Dykes are tabular structures with planar walls. They are however usually segmented into offset separated sections or sections with different orientations (Fig. 5.1. E, F, G and H). Segmentation structures are many times defined by *en echelon* arrays, which are inherent to the propagation process (Delaney and Pollard, 1981). Other segmentation structures are controlled by the litho-mechanical properties of the host rocks or by interactions between the far field stress conditions and magma pressure (Olson and Pollard, 1989; Pollard and Aydin, 1984; Baer, 1991; Hoek, 1991; Weinberger et al., 2000; Gudmundsson, 2002; Druguet et al., 2012).

Usually dyke segments can be differentiated into continuous and discontinuous sections (Fig. 5. 1.). Among the discontinuous offsets we can see long segments arranged in right or left stepping offsets (Fig. 5. 1. E, F and G) with overlapping or no overlapping configurations (Fig. 5. 1.) This type of segmented-stepped morphologies leaves a bridge of host rock between the dyke tips (raft) (Fig. 5. 1. C and D). In these spaces, a perturbation of the stress field is produced by the interaction between tips (Pollard and Aydin, 1984; Rogers and Bird, 1987; Hoek, 1991, Ramsay and Lisle, 2000 and Tentler and Amcoff, 2010). Horns in dyke tips are the result of coalescence between two dyke tips; they are produced by bending of the dyke tips in this perturbation (e.g. of formation of the structure in analogue modelling, in Chapter 4). Dyke tips can also propagate in secondary joints or produce new fractures, so they create horn structures (Fig. 5. 1. B and C).

The continuous dykes may form of various mechanisms. One probable way is by merging and coalescence of two dyke segments (Fig. 5. 1. D). This can be originated by intrusion in secondary fractures or creating new ones (hydrofracture) (Nicholson and Pollard, 1985). When two overlapping segments

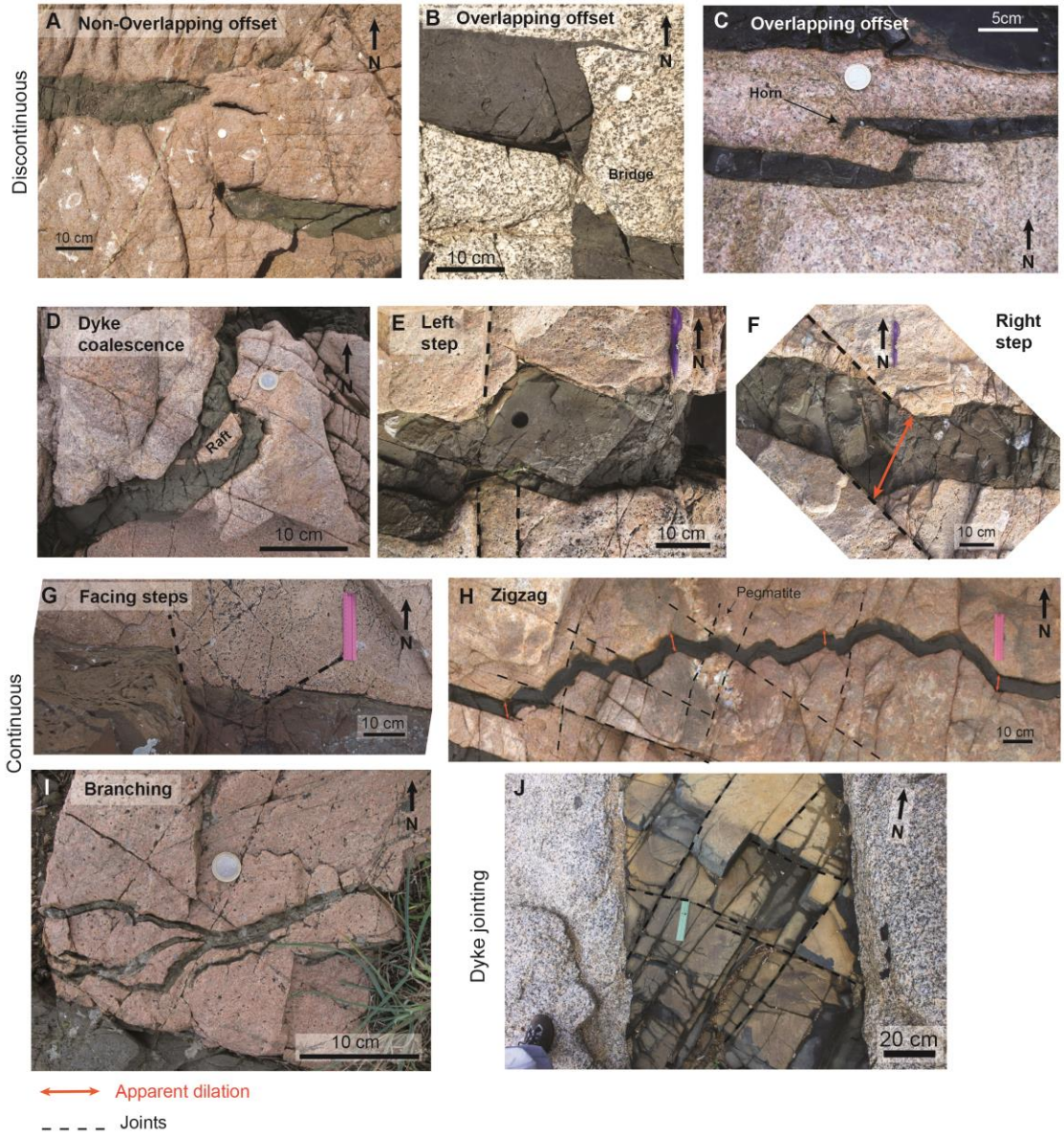

Fig. 5. 1. Summary of brittle structures found in the dyke swarms. A, B and C are discontinuous segmentation. A) Non-overlapping offset in Aiguablava dyke swarm. B) Overlapping offset, almost colliding, with secondary tips in SE Sardinia dyke swarm. C) Overlapping offset with horn structures and a bridge of host rock between segments in Aiguablava dyke swarm. D to I are continuous segmentation. D) Coalescence of two segments with a raft of host rock in Aiguablava dyke swarm. E) Left step found in Aiguablava dyke swarm. F) Right step found in Aiguablava dyke swarm. G) Facing steps in Aiguablava dyke swarm. H) Zigzag structure observed in a dyke from Aiguablava dyke swarm. I) Branching structure found in a dyke tip in Aiguablava dyke swarm. J) Dyke jointing in SE Sardinia dyke swarm.

collide, usually they leave a raft of host rock in between the segments. In the case of non-overlapping segments, dykes are linked through a connector new segment but dyke tips continue its path for a short distance. Parallel segments of dykes can be connected by new apophyses that result at high angle, leaving rhomb-shaped host rock between them. One more mechanism to produce

continuous dyke segments is the injection through secondary joints which produce stepped and zigzag patterns (Fig. 5. 1. E, F, G and H). These features can be seen also in sub-vertical sections due to the presence of sub-horizontal joint systems. The steps and zigzags matching offsets can be used to calculate apparent dilation directions (Fig. 5. 1. F and H).

Other secondary structures observed are branching (Fig. 5. 1. I) and local damage zones of dyke tips.

In many dykes there is a pervasive jointing inside the dykes (Aiguablava and Sardinia), probably produced by magma cooling. This jointing is normally oblique to the dyke walls or networks of several joint sets. E.g. in Sardinia, some dykes present internal joint sets that do not match with the joint sets in the host rock (Fig. 5. 1. J).

5.1.2. Brittle-ductile and ductile structures

Brittle-ductile or ductile structures inside the dykes can be generated during the intrusive phase (e.g. magmatic foliations and lineations) or due to later deformation under brittle-ductile conditions. Most of the examples from the study cases fall on the second type. In these cases, the primary emplacement-related structures can be partly modified or even transposed as a result of post-emplacement brittle-ductile deformation.

For instance, we can see how dyke tips, apophyses or horn structures are bended (Fig. 5. 2. A and B).

Internal fabrics can be noticeable in dykes as foliation, e.g. in the Anti-Atlas dykes, where they can be parallel or oblique to the dyke walls (Fig. 5. 2. F, G and H). The presence of intense internal foliations in dykes is usually indicative of the incompetent behaviour of dykes with respect to their host rocks during ductile deformation (Talbot and Sokoutis, 1995). In Kerdous, the majority of dykes show well developed internal fabrics (foliation and spaced cleavage). Then, it can be confirmed the fact that when there are incompetent dykes in comparison to their host rock, deformation localizes in the dyke masses. Also in some dykes, we can find a mineral lineation (hornblendes) as in the IDS dykes, where we can observe shear zones in dyke margins which develop a mylonitic foliation. This can be a local process produced by magma-wall rock interaction (Carl and Glazner, 2002). Shear zones parallel to the dyke walls are observed. Some dykes even display a sigmoidal foliation which describes the shearing sense. In thin section we can see these parts with grain size reduction and fishes of minerals, indicative of shearing processes (Fig. 5. 2. D and F). In some areas, the final disposition of the dyke swarms can be very complicated if they crosscut heterogeneous media and refraction occurs due to deformation or when deformation overlap previous structures.

There is a great variety of structural setting of dykes; these include the geometry of the bulk swarm, the individual shapes and internal structures of the dykes and the structural relations with the host rock.

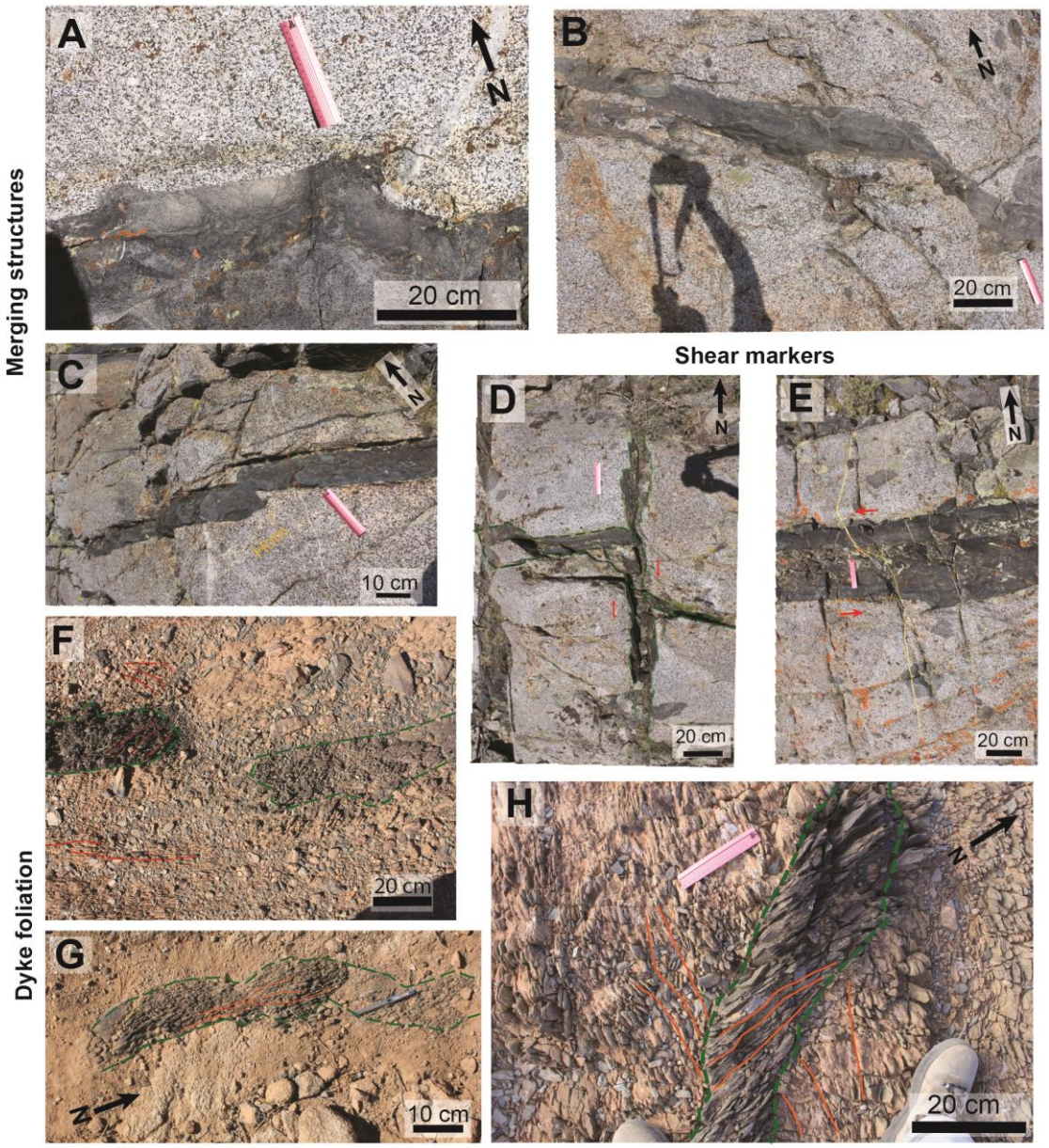

Fig. 5. 2. Summary of brittle-ductile structures found in the dyke swarms. A, B and C are merging structures of two segments or dyke tip-host rock. A) Deformed dyke tip found in IDS. B) Merging structures between two segments in IDS. C) Merging structures of two segments, with secondary tips, in IDS. D and E are shear markers. D) Dyke displaced in a dextral shear zone along a later dyke in IDS. E) Aplite intruded and displaced dextrally along a IDS dyke. F, G and H are fabric relations between dykes and host rock. F) Foliation inside the dyke and in the schist host rock described in Tagragra d'Akka inlier. G) Foliation inside the dyke and no foliated granite host rock observed in Tagragra d'Akka inlier. H) Apparent foliation refraction observed in the host rock and in the dyke in Kerdous inlier.

There are three main factors controlling the final internal and external structures of dykes: (i) stress field and kinematic setting, (ii) mechanical properties of magmas and rocks (dykes and host rock) and (iii) structural level of emplacement and subsequent deformations (tectonic history).

5.2. EFFECTS OF REGIONAL STRESS FIELDS AND ASSOCIATED TECTONIC REGIMES ON DYKES AND DYKE SWARM PATTERNS

Syntectonic dykes can be very useful in paleostress and geodynamic analyses in upper-mid crustal settings and in strain and kinematic analysis of ductily deformed domains. This is because, among other factors, the regional stress field (orientation and relative magnitudes of principal stress axes) and the tectonic regime play an important role on dyke intrusion patterns and subsequent deformation. Purely tectonic controls on dyke and dyke swarm features have been evaluated on the basis of differences found between dyke swarms from the study cases emplaced under two different geotectonic contexts: one is an anorogenic extensional setting with the development of sub-parallel dyke intrusions (Aiguablava and Sardinia study cases); the other is orogenic transpressional/transtesional to strike-slip setting, where two dyke sets intrude with mutual crosscutting relations (Anti-Atlas and IDS).

Generally, the global attitude of a dyke swarm reflects the geotectonic regime at the time of emplacement and subsequent events than can modify the intrusion patterns.

The regional stress state controls the general trend of intrusion of the dykes depending on the differential stress. In the middle-upper crust, this regional stress fields are low, so the orientation could be more variable and local heterogeneities, like fracture systems, can variate the intrusional pattern. The majority of the analysed dykes are included in the hydrofracture range between extension and conjugate fractures.

In crustal-scale extensional settings σ_1 is vertical while σ_2 and σ_3 are horizontal. In consequence, the swarms consist on vertical and parallel dykes as the examples of Aiguablava and Sardinia. However, this pattern can be altered depending on relative magnitudes of the principal stress axes and magma pressure, as observed in Aiguablava and Sardinia study cases.

From the observed characteristics of the dykes in the Anti-Atlas case, it can be inferred that this syn-tectonic dykes in transpressive contexts show sub-vertical dispositions and sub-horizontal opening directions (close to normal to σ_1 which is also sub-horizontal). They can form conjugate systems with hybrid orientations. The fabric in the host rock is also vertically disposed, while stretching lineation varies from sub-horizontal to sub-vertical (Castaño, 2010). Dispersion in the stretching reflects a change in the maximum extrusion during transpression, compatible with the low differential stresses from the middle to low crust. On the other hand often progressive, polyphase or superposed deformation determines de final shape of the dykes. In the IDS case, dykes are intruded in *en echelon* arrays of fractures (Glazner et al., 1999) related to the a sinistral shearing process in a transtensional setting.

5.3. EFFECTS OF MECHANICAL PROPERTIES OF MAGMAS AND ROCKS

This work evidenced the important role of rheology of the dyke/host rock system. Host rock can be homogeneous or heterogeneous but homogeneous rocks can contain mechanical anisotropies (e.g. foliations) or discontinuities (e.g.joints). It follows from this study that the relative rheology values between host rock and dyke plays an important role in cases were sin- and post emplacement deformations are involved.

The study areas include rather homogeneous host rocks. Mainly we can find granitoids except for the Anti-Atlas zone, in the Kerdous and Zenaga inliers where we can find dyke intrusions into schistose materials. However, in spite of the lithological host rock homogeneity, pervasive sets of joints are present in the granitoid host rocks. Some of them presumably were produced before the dyke injection. Therefore, the joint families perform an important role in the intrusion localization of the mafic magmas. These joint networks suppose an important structural control for the 3-D dyke configuration, although the final configuration is also determined by the regional stress field and geotectonic regime.

From the rheological point of view, the granitic host rock act as a more competent material while the mafic bodies behave as incompetent bodies that concentrates the deformation. The competence contrast is higher between the dykes-granitoids than between dykes-schists.

Incompetent dykes are key tools for tectonic analysis of deformation and kinematics in shear zones at the mid-lower crust. The typical structure that we can find in the studied dykes is internal foliation (Talbot, 1999). In the Kerdous case (Anti-Atlas) the extreme and abnormal refraction of foliation (Fig. 5.2.H) at the host schist and basic dyke interface, cannot be explained in terms of mechanical refraction and thus the methodology for cleavage refraction proposed by Treagus (1983, 1988, 1999) and Sengupta (1997) is not applicable. Our case indicates a foliation deflection in the dykes that does not match with strain refraction due to competence contrast, but to a differential deformation record in time during progressive deformation. This is, dykes intruded into pre-foliated host rock (schists). Progressive deformation generates a foliation in the host rock (S_2) prior to the intrusion of the dykes, while dykes intruded syn-tectonically during the deformation process and only record part of this as internal oblique fabric. Then, S_2 foliation would develop in dyke interiors with an orientation determined by the regional stresses and independently of the dyke orientation. Another important remark of this area is the fact that dyke structures evidence low competence contrast between the mafic dyke and the schistose host rock. This lead to the localization of the deformation in the dykes but the scarcity of boudinage or other structures (e.g. cuspate margins) arising from high competence contrast.

In shallow crustal levels, dykes do not localize ductile deformation. Also in the Aiguablava and Sardinia case studies, no superimposed deformations have been recognized. Same thing occurs in the IDS dykes intruded in upper levels of the crust (mainly southern outcrops), no deformation is recorded unlike in the

dykes intruded in deeper levels (dykes in this study). Therefore, dyke swarm pattern depends essentially on the interaction of the stress field, magmatic pressure, preexisting joints and fractures generated during dilatation and dyke propagation. Some of the dyke orientations match with the orientation of the main joint sets. Segmentation structures observed in the dykes are probably originates by the different fracture orientation. Usually we find a higher degree of segmentation in subhorizontal sections than in the subvertical ones. This fact is supported by the stress analysis, since σ_1 axis was located sub-vertically, related to an extensional regime.

In the experiments that reproduce the conditions of emplacement into a pre-fractured host rock we can observe a certain intrusion of the analog fluid through the pre-existing fractures. The fluid intruded into the favourable fractures to the stress axis (those at <45º to the shortening axis). Even though there was no fluid pressure, the simulation was very close to the ones found in the nature where the fluid presure is very low ($P_m < \sigma_2$).

In the other hand, the experiment of deformation of partially molten bodies gives as conclusions a localization of the deformation around dyke tips and margins, together with areas of high strain (shear zones). We observed an arrangement of the structures depending the disposition of the analogue bodies.

5.4. STRUCTURAL LEVEL OF EMPLACEMENT AND SUBSEQUENT DEFORMATIONS: TECTONIC HISTORY

Rheology of host rocks varies significantly with depth (i.e. depending on the increase of confining pressure and temperature). Thus, in crystalline rocks located in shallow structural levels, pre-existing or newly formed fractures may open, while host rocks do no suffer strain. In deeper crustal levels, fracturing and ductile strain proceeds simultaneously or in a pulsatory mode. Rheological contrasts (viscosity contrasts) decreases under increasing P and T. Thus, in upper crustal levels dykes tend to occupy extensional (opening) fractures (pre-existing or newly formed) leaving the host rock unaffected.

.

However, remarkable fractures appear in damage zones at the tips of dykes (Fig. 3. 20, Chapter 3; Fig. 5. 1i, of this Chapter). In these situations, if deformation proceeds during emplacement, deformation tends to localize at the dykes interior or margins (Figs. 3. 28; 3. 31; 3. 36; 3. 60, Chapter 3). Some of the studied areas, basically, Aiguablava dyke swarm and SE Sardinia dyke swarm, show no deformation processes later to the intrusion event. The emplacement of these mafic injections occurs under brittle conditions in the upper/middle crust , which implies a short intrusions time. This means that these zones have remained undeformed for thousands of years, so they develop a cratonic behaviour. We do not take into account the possible exhumation brittle events that they could have suffered, since they only produce superficial effects.

However, in the other settings (e.g. Independence Dyke swarm and Anti-Atlas, dykes), dykes has suffered later deformation processes. Likewise, we do not take into account either the brittle episodes due to exhumation.

In mid-crustal levels where dyke emplacement is associated to crustal shortening (compressional, transpresssional or wrench), host rock and dykes tend to deform. Arising structures depend on the original orientation (Ramsay, 1967) and on the viscosity contrast in the host rocks but also in the viscosity contrasts between host and dyke. As we have seen in the analogue modelling, the evolution of the structures all through the initial increment of strain until the end of the deformation has enabled to compare obtained structures with the ones found in the nature. Experiment on deformation of partially molten bodies gives as conclusions a localization of the deformation around dyke tips and margins but also domains of high strain (shear zones) in the dyke interior. Progressive deformation during dyke emplacement of some dyke swarms presumably occured when the mafic intrusions were still molten. Gradual cooling induces an increment and/or reversal of viscosity contrast due to the properties change of the dyke. However, often the channeling of fluids during cooling causes the alteration of the dykes, which remain softer than the host rock during the whole deformation episode.

More complicated to describe are settings generated by tectonic superposition of unrelated geological events or phases. In these situations, shallow emplaced dykes (orogenic or anorogenic) can subsequently deform in mid-crustal levels. As well as, exhumed deeply emplaced dykes can be deformed under low P-T conditions. All this variables (intrinsic and extrinsic) cause a wide spectrum of structural features.

Some of the studied areas, basically, Aiguablava dyke swarm and SE Sardinia dyke swarm, show no deformation processes later to the intrusion event. This means that these zones have remained undeformed for thousands/millions of years, so they develop a cratonic behaviour. We do not take into account the possible exhumation brittle events that they could have suffered, since they only produce superficial effects.

However, in the other two areas, Independence Dyke swarm and Anti-Atlas, dykes have suffered later deformation processes. We do not take into account either the brittle episodes due to exhumation, erosion or glaciation. The only processes described will be related to the effects of deformation in dykes.

As we have seen in the analogue modelling, the evolution of the structures from the first moment of intrusion up to the end of the deformation events can display an array of features that we can compare with the ones found in the nature.

The complex geometry present in a deformed magmatic body is the key of the beginning of this study. The observed structures can be caused by a later deformation process but also by the emplacement process in itself. There is a confirmed relation between the emplacement and deformation structures developed in the dyke systems and the general evolution of the tectonic setting.

Therefore, we could guess a particular context with the knowledge of the emplacement features related to the dykes.

5.4.1. Aiguablava and Sardinia: discussion on emplacement in anorogenic conditions and evolution concerning plate-tectonics history

The case studies of Aiguablava and Sardinia correspond to a shallow anorogenic extensional setting with little impact of tectonic features produced during later events. On the contrary, Independence and Anti-Atlas dyke swarms correspond to more complex setting involving syn- to post emplacement deformation produced in mid-crustal tectonic levels.

The principal reasons for establishing this correlation between the Aiguablava lamprophyre dyke swarm and the SE Sardinia dyke swarm is their apparent similar characteristics. Both dyke swarms share their tectonic origin as parts of the Variscan belt in close locations (spatially and temporarily). Moreover they share a very similar magmatic activity during the Middle Permian. In both areas, methods used for characterize dyke swarms were the same, thus quantitative results are able to be compared. On the contrary, spatial orientation of structures as dykes, joints, axes orientations and other features cannot be compared since each area has suffered different rotation phases in the past. Aside from this limitation, the rest of the calculated parameters result to be very similar in both dyke intrusion settings.

Both dyke swarms intruded into a pre-existing network of fractures. In each case we can assume a dyke pattern coincident with the direction of the main joint sets. Joints form a network of several main sets with sub-vertical disposition, although there are sub-horizontal joints responsible of the outcrop surfaces. The main joint system was possibly developed during cooling and decompression.

In SE Sardinia, there is a smaller orientation range of dykes able to dilate, then this is caused by a smaller driving pressure (R‘). In Sardinia, magmatic pressure is lower than the intermediate stress (σ_2), whereas in Aiguablava the magmatic pressure equals σ_2. On the contrary, slightly different stress ratios (Φ) correlate with slightly larger σ_2-σ_3 differential stress in SE Sardinia. As a result, the SE Sardinia dyke swarm would have been a more tectonic driven intrusion than Aiguablava, as supported by the presence of previous fractures, reactivated faults and dyke thickness and regional extension (more than double from the Aiguablava values). The regional tectonic setting for both dyke swarms is extensional, although main stress orientation varies from one area to the other.

In relation to the Variscan basement where the two dyke swarms intruded, both areas experienced a complex tectonic history since the Pangea disposition (Late Paleozoic) to present times. The main implications for compare both dyke swarms are the different block rotations suffered by the two dyke systems. In Sardinia, the Variscan basement has suffered at least two main post- Permian episodes of major changes. Initially, the rotation of the Corso-Sardinian block

occurred together with the Iberian realm with respect to the stable Eurasian plate in the Cretaceous. Later, the Corso-Sardinian block rotated relative to the Western European plate in the Neogene. The estimated value for the anti-clockwise rotation of the Corso-Sardo block ranges between 30º to 50º with respect to the stable Western European plate.

Table 5.1. describes the comparable parameters between Aiguablava and SE Sardinia dyke swarms:

	Aiguablava (Catalan Coastal Ranges)	**SE Sardinia** (Corso-Sardinian block)
Dyke lithology/ Geochemistry	Lamprophyres: spessartites (calc-alkaline) bostonites (alkaline)	Dolerites, phorphyritic dolerites and minor lamprophyres (calc-alkaline and minor tholeiitic)
Dyke Age	Upper Permian (253 ± 5 Ma)	Upper Permian (259 ± 3 Ma)
Host rock	Pervasively jointed leucogranites and minor granodiorites	Moderately jointed granitoids (mainly granodiorites)
Mean dyke Orientation	N110º sub-vertical	N150º sub-vertical
Mean net dilation direction	019/02	246/02
Maximum dyke thickness	5 m	13 m
Mean regional extension (%)	12%	29%
Degree of dyke segmentation	high-intermediate	intermediate
Degree of dyke interaction	mid-low	low
Principal stress axes	σ_3: 021/05 sub-horizontal σ_2: 291/05 sub-horizontal σ_1: 154/83 sub-vertical	σ_3: 244/05 sub-horizontal σ_2: 335/13 sub-horizontal σ_1: 135/77 sub-vertical
Stress ratio	φ= 0.29 close-to-prolate stress ellipsoid (σ1>>>σ2>σ3)	φ=0.33 close-to-prolate stress ellipsoid (σ1>>σ2>σ3)
Driving pressure (magma pressure, Pm)	R′= 0.27 (Pm=σ_2)	R‘= 0.13 (Pm<σ_2)
Degree of dyke reactivation of pre-existing fractures	intermediate	intermediate
Regional tectonic setting	NNE-SSW-directed crustal extension	ENE-WSW-directed crustal extension

Table 5. 1. Comparative list of the main features for the Aiguablava (Catalan Coastal Ranges) and SE Sardinia mafic dyke swarms (summarized from Martínez-Poza *et al*., 2014 and this work).

5.4.2. Anti-Atlas and Independence dyke swarms: discussion on emplacement and deformation localization in orogenic conditions.

This two dyke swarms share characteristics of depth of emplacement and syn to post-tectonic deformation. Nevertheless, each study case occurred in different time periods and separated tectonic settings, so the same type of comparison as in the previous section cannot be made with this two dyke swarms.

The mean trend for the Independence dyke swarm (IDS) is between ~N140º and ~N155º (Moore and Hopson, 1961; Chen and Moore, 1979 and James, 1989). Our observations give an orientation of ~N95º. This rotation was proposed previously, although with a lower value (Glazner et al., 1999). Maybe it could be related to a later deformation phase during the Cretaceous (Moore and Sisson, 1987) or later block faulting in this specific area.

The typology of dykes follows the same characteristics as in the other swarms, but some distinctions can be made. In the IDS case, four different dyke intrusions can be disthinghised, 1) a pre-IDS set of mafic dykes; 2) Composite dykes (IDS) as aggregates of several *dikelets*; 3) IDS mafic dykes main phase and 4) felsic plus xenolith composite. In resume, dyke families suppose an ensemble of different magma pulses and variation in stress regime in a short time.

The more valid hypothesis for the IDS dyke intrusion supposes a transtensional/transpressional setting, related to subduction, and a magma injection into a pre-fractured host rock (Glazner et al., 1999). We tried to characterized the joint network as in the other cases, but it was not possible to analyse since it is a very fractured area. Maybe due to the glacial polish, erosion and exhumation consequences. Dyke segmentation is well observed in the field (IDS). Nearly all of them present a linear disposition and sub-vertical dipping. There is also presence of dyke offsets, jogs and steps. Horns structures are also described in merging-like structures. We found out the range of dyke thickness between ~0.4 to 1 m (up to 3.3 m the thickest). Other important feature in the IDS is the mylonitic fabric present in the outcrops, both outside and inside dykes and aplites and locallized in dyke margins. Dykes and aplites show displacement related to sinistral shear zones. Normally, the deformation is accomodated in the margin of the dykes as shear zones, this is due to a weaker behaviour of the dyke. This shear event probably occurred later to the dyke injection.

The dilation value obtained for the IDS is not correct because it is not perpendicular to the mean orientation of the dykes. This variation in the dilation result can be related to a displacement in the dyke opening markers, probably due to a deformation phase. This opening could have been N-S (Glazner et al., 1999) which would have been oblique to the dyke walls. Other option is a perpendicular opening and a later displacement because of a shear event. The 3-D stress analysis show a rotation of the principal axes possibly due to a deformation phase. The setting of the intrusion propose a WNW oriented σ_3 with a NNE σ_1. The transtension/transpression is accomodated in the mylonitic

zones. The 3-D analysis of the dyke walls determined the stress axes as follows, the principal axis (σ_1) has a N181/77 orientation; the intermediate axis (σ_2) is sub-horizontal, N286/4 and the minimum stress axis (σ_3) is N017/13. The value of σ_3 compared with the apparent dilation direction do not match (~N140E/9), thus a probable rotation of the dilation markers occurred during deformation. The stress ratio (Φ) and the driving pressure ratio (R‘) values for the IDS case, if we assume the analysis as valid, the fluid pressure is lower to σ_2 and we obtain a prolate ellipsoid for the axis configuration. The IDS intrusion then would have been controlled by the tectonic regime of the area rather than by the magmatic pressure.

Regarding dyke composition, the IDS dykes analysed show a mafic affinity with abundance of intermediate dykes. Previous studies pointed out the more silicic character of the IDS dyke swarm than other similar large swarms (Hopson, 1988), maybe induced by the different tectonic regime. The petrographic description made of the IDS samples illustrate the results of the deformation process in the dykes. Many indicators of shear events can be described: grain size reduction, quartz grains with ondulant extintion, oriented minerals or amphibole porphyroclasts. Most of these elements are found in dyke margins, where the shear deformation is located. All of this was developped at low to medium grade conditions, as seen in the mineral assemblage.

The age of the IDS is constrained after numerous age analysis, they range between 147 to 190 Ma (Early Jurassic). The host rock age (Tinemaha granodiorite) is assumed to be ~165 Ma, so a coeval intrusion is emplied for the two systems.

Finally, the emplacement model for the IDS would imply two different phases, an intrusive one and a second phase, very close in time, where a deformation process occurred. Even the deformation could be a syn-intrusion phase, since all the evidences support a melted mafic material during the sinistral shearing process. The general framework for the IDS intrusion should have been a shear zone related to the deformation partitioning in the continental arc. In an area intruded by plutons and affected by thermal weakening, which is consistent with a sinistral subduction in the Cordilleran orogeny (Oldow et al., 1984).

In the Anti-Atlas, each inlier has a particular mean orientation for the sub-vertical dykes. The western inliers show disparity between them (Tagragra d‘Akka and Kerdous) and with the eastern inlier (Zenaga). Thus, there is no a particular trend in the dyke orientations for the Anti-Atlas inliers. This could be related to the big extension and the probable change in local stress regimes between them. The segmentation structures observed in the dykes are coincident with the analyses of other dyke swarms. In this cases, it is very difficult to make a characterization at outcrop scale, due to the large size of the intrusions. However, using aerial images (©Bing) a good analysis of the features can be made. Usually these dykes tend to be very linear, in some areas there are steps and overlapping segments. Composite dykes are also found. Other outstanding features are dyke offsets produced by shear zones, also observable from aerial images (Fig. 3. 56). Dyke thickness range from 10s centimeters to more than 10s meters. Foliation is very significative in dyke

interiors, as well as in some areas of the host rock (in the schists). A great quantity of dykes show an oblique to sub-parallel foliation to the dyke walls. It is also oblique to the foliation present in the basement rocks. This fabric is concentrated in bands in some of the dykes, as areas of higher deformation (Fig. 3. 55). Nevertheles, other outcorps do not show any fabric in the dykes. In some parts, the foliation in the dykes is probably produced by the cooling of the magma and marked by the later erosion. But in others, the fabric is the result of a deformation phase during the Pan-African orogeny, the time when the dyke swarms intruded. Some composite dykes present dikelets more deformed than others. Therefore, the intrusion should have been in pulses, as well as the deformation processes, since some areas are more affected than others. A very important factor for the control of the deformation is the competence contrast between materials. Here, dykes tended to localize deformation while they were still melted. The mafic magma act as a less competent material compared to the host rock (schist or granitoid). Evidences of shear zones are noticeable in the field and in aerial images (as already explained in Chapter 3) with displacements of several meters. The thin section description from the Anti-Atlas samples display signs of deformation processes. Moreover, they are pervasively altered, all the samples show secondary minerals. Linear fabric and grain size reduction is visible in the minerals.

The paleostress analysis has not been possible to carry out in the Anti-Atlas case. A significative amount of data is needed so more field work would be necessary to complete this part of the investigation.

The Anti-Atlas zones can be resumed in dykes intruded into a basement with signs of Eburnean deformation (foliation) during the Pan-African orogeny. The cross disposition of the dyke sets in the inliers can relate the intrusion with a compresional regime, very close to a transpressive setting (NW-SE oriented) with a dextral movement.

5.5. CONCLUDING REMARKS

Mafic dykes exist in different geotectonic regimes and crustal levels (low to high confining pressure and temperature). Dyke swarms patterns (at different scales, from km- to outcrop-scale) furnish evidences about paleostress and crustal kinematics during the emplacement event.

Structures arisen from subsequent deformations (progressive or superimposed) of dykes allow characterizing the tectonic events as well as the rheology of the host rock-dyke system.

From simple to more complex patterns distinction: in simplest cases (extensional regime), it is important the interplay between tectonic stresses and magma pressure. Swarms of sub-parallel dykes correspond to extensional fractures normal to σ_3. However, heterogeneities in the host rock produce local effects (e.g. joints and joint networks), because magma exploits this previous

anisotropies. This is the case of Aiguablava and Sardinia; in Aiguablava, a pre-existing joint network supposes a large role in the dyke intrusion orientation, however in Sardinia a lesser degree of control is exerted by the joint systems. The result is that the parallel pattern supposed in an extensional swarm is modified to a segmented configuration. Consequently, the degree of segmentation depends on the favorable orientation of the fractures to the intrusion direction and the amount of secondary joint sets available to be intruded by the magma material. These types of relations have been tested experimentally within the analogue modelling series of previously fractured basements.

More complex dyke swarms in this study comprises those intruded into higher confining pressure settings. The intrusion occurred in a tectonic framework with lower differential stresses than in an extensional setting. Although the mechanism of dyke intrusions is the same (hydrofracturing), more complex patterns result: *en echelon* dykes are more common, conjugate sets of hybrid dykes or cross disposition dykes. Moreover, if deformation continues after dyke emplacement, strain localization processes around dykes give rise to shear zones, foliated dykes, etc. This situation has been reproduced experimentally within the analogue modelling series of ductile deformation of partially molten material as analogue of dykes in isotropic host rocks.

Particular complexities can be found in each of the dyke swarms related to this regime. In the Anti-Atlas case, lithology (schists vs. granitoids) of host rocks implies a different competence contrast, which produces particular fabric variations. As seen in the lower angle between the foliation in the host rock and inside dykes. Likewise, it exists a higher localization of the deformation in the dykes when the host rock is granitic material due to the competence contrast. The transpressive setting produce a cross organization of the dykes and the development of shear zones. In the case of the Independence dyke swarm, the complexity is related to the multiple dyking pulses observed. Described as *dikelets* that forms thicker dykes or as various dyke sets with crosscutting relations between them. Age estimation supposes a coeval intrusion of the different dyke families, also coincident with the range age of the host rock intrusion. Apart from this, a deformation process occurred shortly after the intrusion that added an important modification to the initial dyke structure and arrangement.

Future work in this topic should be conducted in the way of a better three-dimensional understanding of the tectonics of dyke swarms, combining analogue and numerical modelling. New technologies can be used, as drones, to help with the low attitude mapping in areas of difficult access. Also more work in geochronology would be helpful for constraining sequences of intrusion and time relations between magmatism and deformation events.

References

Abràmoff, M.D., Magalhâes, P.J., Ram, S.J., 2004. Image processing with ImageJ. Biophoton. Int. 11, 36–42.

Affaton, P., Rahaman, M. A., Trompette, R. and Sougy, J. 1991. The Dahomeyide Orogen: tectonothermal evolution and relationships with the Volta basin. In: Dallmeyer, R. D. and Lecorché , J. P. (eds) The West African Orogens and Circum-Atlantic Correlatives. Springer, Berlin, 107–122.

Airoldi, G., Muirhead, J.D., White, J.D.L., Rowland, J., 2011. Emplacement of magma at shallow depth: insights from field relationships at Allan Hills, south Victoria Land, East Antarctica. Antarct. Sci. 23, 281–296.

Aït Malek, H., Gasquet, D., Bertrand, J-M. and Leterrier, J. 1998. Géochronologie U–Pb sur zircon de granitoïdes éburnéens et panafricains dans les boutonnières d'Igherm, du Kerdous et du Bas Drâa (Anti-Atlas occidental, Maroc), C. R. Acad. Sci. Paris, Ser. IIa 327 819–826.

Albertz, M., Paterson, S.R., Okaya, D. 2005. Fast strain rates during pluton emplacement: magmatically folded leucocratic dikes in aureoles of the Mount Stuart Batholith, Washington and the Tuolumne Intrusive Suite, California, Geological Society of America Bulletin 117, 450-465.

Allmendinger, R.W., 2002, Stereonet, v. 6.3 X for Windows: http://www.geo.cornell.edu/geology/faculty/RWA/programs/.

Alvarez, W. 1972. Rotation of the Corsica-Sardinia microplate. Nature Physics Science, 235: 103-105.

Alvarez, W., S. Franks, and A. Nairn. 1973. Palaeomagnetism of Plio- Pleistocene basalts from northwest Sardinia, Nature, 243, 10–11.

Anderson, E. M., The dynamics of sheet intrusion, Proc. R. Soc. Edinburgh, 58, 242 – 251, 1938.

Anderson, E.M., 1951. The Dynamics of Faulting and Dyke Formation with Applications to Great Britain. Oliver and Boyd, Edinburgh 206p.

André, A.-S., Sausse, J., Lespinasse, M., 2001. New approach for the quantification of paleostress magnitudes: application to the Soultz vein system (Rhine graben, France). Tectonophysics 336, 215–231.

Angelier, J., 1984. Tectonic analysis of fault slip data sets. J. Geophys. Res. 89, 5835–5848.

Arthaud F. and Matte P. 1966. Contribution à l'étude de tectoniques superposées dans la chaine hercynienne: étude microtectonique des séries metamorphiques du Massif des Maures (Var.). Comptes Rendus de l'Académie des Sciences de Paris, 262: 436-439.

Arthaud F. and Matte P.H., 1975. Les décrochments tardihercyniens du sud-ouest de l'Europe. Géométrie et essai de reconstruction des conditions de déformation. Tectonophysics, 25, 131-171.

Arthaud F. and Matte P.H., 1977a. Synthèse provisoire sur l'evolution tectonique et les raccords entre les segments hercyniens situés autour du bassin nord-Baléare (Sud de la France, Espagne, bloc corso-sarde). Coll. Int. CNRS (Rennes), 243, 497-513.

Arthaud F. and Matte P.H., 1977b. Late Paleozoic strike slip faulting in southern Europe and northern Africa: Results of a lateral shear-zone between the Appalachians and the Urals. Geol. Soc. Am. Bull., 88, 1305- 1320.

Atzori, P. and Traversa, G. 1986. Post-granitic permotryassic dyke magmatism in eastern Sardinia (Sarrabus p.p., Barbagia, Mandrolisai, Goceano, Baronie and Gallura). *Period. Mineral.*, 55, 203- 231.

Atzori, P., Cirrincione R., Del Moro A. and Mazzoleni P. 2000. Petrogenesis of late Hercynian calc-alkaline dykes of mid-eastern Sardinia: petrographical and geochemical data constraining hybridization process. European Journal of Mineralogy, 12, 1261-1282.

Aubele, K., V. Bachtadse, G. Muttoni, A. Ronchi, and M. Durand. 2012. A Paleomagnetic study of Permian and Triassic rocks from the Toulon-Cuers basin, SE France: Evidence for intra-Pangea block rotations in the Permian, Tectonics, 3, TC3015, doi:10.1029/2011TC003026.

Aubele, K., Bachtadse, V., Muttoni, G. and Ronchi, A. 2014. Paleomagnetic data from Late Paleozoic dykes of Sardinia: Evidence for block rotations and implications for the intra-Pangea megashear system. Geochem. Geophys. Geosyst., 15, 1684–1697, doi:10.1002/2014GC005325.

Babiker, M., Gudmundsson, A., 2004. Geometry, structure and emplacement of mafic dykes in the Red Sea Hills, Sudan. J. Afr. Earth Sci. 38, 279–292.

Badia, D. and Fuchs, Y. 1989. Le volcanisme du Massif central méridional. In: Chateauneuf, J.-J. and Farjanel, G. (eds) Synthèse Géologique des Bassins Permiens Français. Mémoires du Bureau de Recherches Géologiques et Minières, 128, 219–224.

Baer, G., 1991. Mechanisms of dike propagation in layered rocks and in massive, porous sedimentary rocks. J. Geophys. Res. 96, 11,911–11,929.

Baer, G., Beyth, M., 1990. A mechanism of dyke segmentation in fractured host rock. In: Parker, A.J., Rickwood, P.C., Tucker, D.H. (Eds.), Mafic Dykes and Emplacement Mechanisms. A.A. Balkema, Rotterdam, pp. 3–11.

Baer, G., Beyth, M., Reches, Z., 1994. Dikes emplaced into fractured basement, Timna Igneous Complex, Israel. J. Geophys. Res. 99, 24039–24051.

Barbey, P., Oberli, F., Burg, J.-P., Nachit, H., Pons, J. and Meier, M. 2004. The Palaeoproterozoic in western Anti-Atlas (Morocco): a clarification. Journal of African Earth Sciences 39, 239–245

Basson, I., Viola, G., 2003. Structural overview of selected Group II kimberlite dyke arrays in South Africa: implications for kimberlite emplacement mechanisms. S. Afr. J. Geol. 106, 375–394.

Bateman, P. C. 1964. Geological map of Big Pine 15‘ quadrangle, California. U.S. Geological Survey Map.

Bateman, P.C., and Moore, J.G. 1965. Geologic map of the Mount Goddard quadrangle, Fresno and Inyo Counties, California: U.S. Geological Survey Map GQ-429, 1:62,500.

Bateman, P.C., and Clark, L.D. 1974. Stratigraphic and structural setting of the Sierra Nevada batholith: Pacific Geology, v. 8, p. 79-89.

Bateman, P.C., 1992. Plutonism in the central part of the Sierra Nevada batholith: U.S. Geological Survey Professional Paper 1483, 186 p.

Beach, A. 1980. Numerical models of hydraulic fracturing and the interpretation of syntectonic veins. Journal of Structural Geology 2, 425–438.

Belayneh, M., Cosgrove, J.W. 2010. Hybrid veins from the southern margin of the Bristol Channel Basin, UK. Journal of Structural Geology 32, 192–201.

Belfoul, M.A., Faik, F. and Hassenforder, B. 2002. Evidence of a tangential tectonic event prior to the major folding in the Variscan belt of the western Anti-Atlas, Morocco, J. Afr. Earth Sci. 32 (4) 723–739.

Benek, R., Kramer, W., Mccann, T., Scheck, M., Negendank, J. F. W., Korich, D., Huebscher, H. D. and Bayer, U . 1996. Permo- Carboniferous magmatism of the Northeast German Basin. Tectonophysics, 266, 379–404.

Benn, K., Odonne, F., de Saint-Blanquat, M. 1998. Pluton emplacement during transpression in brittle crust: new views from analog experiments. Geology 26, 1079–1082.

Benziane, F., Yazidi, A., 1992. Corrélations des formations du Proterozoïque supérieur. Notes et Memoires du Service Géologique du Maroc 366, 147–157.

Benziane, F., Yazidi, A., Walsh, G.J., Armstrong, T.R., Kouhen, M.A., Yazidi, M., Khamlichi, M.A., Aleinikoff, J.A., Carte géologique au 1/50 000 feuille Afouzar. Notes et Mémoires du Service Géologique du Maroc 422, Feuille NH-29-XI-3-c, in press.

Best, M.G. 2003. Igneous and Metamorphic Petrology. 2nd ed. Oxford Blackwell Science. 729 pp.

Bing maps. 2013. Microsoft Corporation.

Black, R., Caby, R., Moussine-Pouchkine, A., Bertrand, J. M. L., Boullier, A. M., Fabre, J. and Lesquer, A. 1979. Evidence for Precambrian plate tectonics in West Africa. Nature, 278, 223–227.

Black, R., Latouche, L., Liégeois, J. P., Caby, R. and Bertrand, J. M. 1994. Pan-African displaced terranes in the Tuareg shield (central Sahara). Geology, 22, 641–644.

Black, R. and Liégeois, J. P. 1993. Cratons, mobile belts, alkaline rocks and continental lithospheric mantle: the Pan-African testimony. Journal of the Geological Society, London, 150, 89–98.

Black, LP, Kamo S, Allen CM,. 2004. Improved 206Pb/238U microprobe geochronology by the monitoring of a trace-element-related matrix effect; SHRIMP, ID-TIMS, ELA-ICP-MS and oxygen isotope documentation for a series of zircon standards. Chemical Geology 205: 115–140.

Blatt, H., Tracy R.J., Owens, B.E. 2006. Petrology, W. H. Freeman and Company, New York (2006) p. 530.

Blès, J., D. Bonijoly, and C. C. Y. Gros. 1989. Successive post-Variscan stress fields in the French Massif Central and its borders (Western European plate): Comparison with geodynamic data, Tectonophysics, 169, 79–111.

Bons, P.D., Becker, J.K., Elburg, M.A., Urtson, K. 2009. Granite formation: stepwise accumulation or connected networks? Transactions of the Royal Society of Edinburgh 100, 105-115.

Bons, P.D., Druguet, E., Castaño, L.M. and Elburg, M.A. 2008. Finding what is now not there anymore: recognizing missing fluid and magma volumes. Geology 36, 851-854.

Bons, P.D., Dougherty-Page, J., Elburg, M.A., 2001. Stepwise accumulation and ascent of magmas. J. Metamorph. Geol. 19, 627–633.

Bons, P. D., Druguet, E., Castaño, L. M., and Elburg, M. A. 2008. Finding what is not there anymore: recognizing missing fluid and magma volumes, Geology, 36, 851–854.

Bouchez, J.L., Hutton, D.H.W., Stephens, W.E. (Eds) 1997. Granite: From Segregation of Melt to Emplacement Fabrics. Kluwer, Dordrecht.

Boudda, A., Choubert, G., and Faure-Muret, A. 1979. Essai de stratigraphie de la couverture sédimentaire de l'Anti-Atlas : Adoudounien– Cambrien inférieur, Notes Mém. Serv. géol. Maroc 271, 96.

Boulin, J., Bouabdelli, M. and El-Houicha, M. 1998. Évolution paléogéographique et géodynamique de la chaîne Paléozoïque du moyen Maroc : un essai de modélisation, C. R. Acad. Sci. Paris, Ser. II 306, 1501–1506.

Bouougri, E. H. and Saquaque, A. 2004. Lithostratigraphic framework and correlation of the Neoproterozoic northern West African craton passive margin sequence (Siroua, Zenaga, Bouazzer-Elgraara inliers, Central Anti-Atlas, Morocco): an integrated approach. Journal of African Earth Sciences, 39, 227–238.

Bowring, S.A., Grotzinger, J.P., Isachsen, C.E., Knoll, A.H., Pelechaty, S.M. and Kolosov, P., 1993. Calibrating rates of Early Cambrian evolution. Science 261, 1293–1298.

Bralia A,m Ghezzo C., Guasparri G. Sabatini G. 1982. *Aspetti genetici del batolite ercinico sardo*. «Rend. Soc. Miner. Petr.», 38, 701-764 (1982).

Breitkreuz, C., Cortesogno, L. and Gaggero, L. 2001. Crystal-rich mass flow deposits related to the eruption of a sublacustrine silicic cryptodome (Early Permian Collio Basin, Italian Alps). Journal of Volcanology and Geothermal Research, 114, 373–390.

Breitkreuz, C. and Kennedy, A. 1999. Magmatic flare-up at the Carboniferous–Permian boundary in the NE German Basin revealed by SHRIMP zircon ages. Tectonophysics, 302, 307–326.

Brisbin W. C. 1986. Mechanics of pegmatite intrusion. American Mineralogist 71, 644-651.

Brotzu, P., Ferrini, V., Masi, U. 1983. Stable isotope geochemistry of Hercynian granitoid rocks from the Sarrabus Massif (southeastern Sardinia Italy). Isot. Geosc., 1, 77-90.

Brotzu P., Callegari E. and Secchi F. 1993. *The search for the parental magma of the high-K calcalkaline rock-serie in the southrenmost Sardinia Batholith*. «Per. Mineral.», 62, 253-280.

Brotzu P. and Morbidelli L., 1974. Lineamenti petrografici e geostrutturali di un settore del Sarrabus meridionale (Sardegna sud-orientale). Atti Acc. Naz. Licei Serie VIII, XII (I).

Brown, M. 1994. The generation, segregation, ascent and emplacement of granite magma: the migmatite-to-crustally-derived granite connection in thickened orogens. Earth Science Reviews 36, 83–130.

Brown, M. 2008. Granites, migmatites and residual granulites: relationships and processes. En: Working with migmatites (eds E. W. Sawyer & M. Brown). Short Course Series, no. 38, 97–144. Québec, Canada: Mineralogical Association of Canada.

Brown, M., 2010. The spatial and temporal patterning of the deep crust and implications for the process of melt extraction. Philos. Trans. R. Soc. A Math. Phys. Eng. Sci. 368, 11–51.

Brown, M., Solar, G.S. 1998. Granite ascent and emplacement during contractional deformation convergent orogens. Journal of Structural Geology 20, 1365-1393.

Brown, M., Solar, G.S., 1999. The mechanism of ascent and emplacement of granite magma during transpression: a syntectonic granite paradigm. Tectonophysics, 312, 1–33.

Bruguier, O., Becq-Giraudon, J. F., Bosch, D. and Lancelot, J. R. 1998. Late Viséan hidden basins in the internal zones of the Variscan belt: U–Pb zircon evidence from the French Massif Central. Geology, 26, 627–630.

Bryan, S.E. and Ernst, R.E., 2008. Revised definition of large igneous provinces (LIPs). Earth Science Reviews 86, 175–202.

Buggisch, W. and Fluegel, E. 1988. The Precambrian/Cambrian boundary in the Anti-Atlas (Morocco); discussion and new results, in: V.H. Jacobshagen (Ed.), The Atlas System of Morocco; Studies on its Geodynamic Evolution, Springer-Verlag, Berlin– Heidelberg–New York, pp. 81–90.

Buggisch, W. and Siegert, R. 1988. Paleogeography and facies of the „grès terminaux"; uppermost Lower Cambrian, Anti-Atlas, Morocco, in: V.H. Jacobshagen (Ed.), The Atlas System of Morocco; Studies on its Geodynamic Evolution, Springer-Verlag, Berlin– Heidelberg–New York, pp. 107–121.

Buraglini, N., Traversa, G., 2000. Petrology andmineral chemistry of late-Hercynian dykes from NW Corsica (France). Period. Mineral. 69, 269–310.
Bussell, M.A., 1989. A simple method for the determination of the dilation direction of intrusive sheets. J. Struct. Geol. 11, 679–687.

Burkhard, M., Caritg, S., Helg, U., Robert-Chaurre, C. and Soulaimani, A. 2006. Tectonics of the Anti-Atlas of Morocco. Comptes Rendus Geoscience, 338, 11–24.

Bussell, M.A., 1989. A simple method for the determination of the dilation direction of intrusive sheets. J. Struct. Geol. 11, 679–687.

Cadman, A., Tarney, J., Park, R.G., 1990. Intrusion and crystallization features in Proterozoic dyke swarms. In: Parker, A.J., Rickwood, P.C., Tucker, D.H. (Eds.), Mafic Dykes and Emplacement Mechanisms. A.A. Balkema, Rotterdam, pp. 13–14.

Cahen, L., Snelling, N.J., Delhal, J., Vail, J.R., Bonhomme, M., Ledent, D., 1984. The Geochronology and Evolution of Africa. Oxford University Press, Oxford, pp. 512.

Caritg, S., Burkhard, M., Ducommun, R., Helg, U., Kopp, L. and Sue, C. 2004. Fold interference patterns in the Late Palaeozoic Anti-Atlas belt of Morocco. Terra Nova, 16, 27–37.

Caritg, S. 1993. Géologie structurale dans l'Anti-Atlas occidental du Maroc. Implications tectoniques sur les relations entre domes de socle et couverture plissée en front de chaîne de montagne, PhD thesis, University of Neuchâtel.

Carl, B.S., Bartley, J.M., and Glazner, A.F. 1995. Structural geology of Independence Dikes, eastern Sierra Nevada, Calif.: Geological Society of America Abstracts with Programs, v. 27, p. 9.

Carl, B.S., Bartley, J.M., and Glazner, A.F. 1996. Mechanical model for synintrusive Nevadan deformation in the eastern Sierra: EOS (Transactions, American Geophysical Union), v. 77, p. F641.

Carl, B.S., Glazner, A.F., and Bartley, J.M. 1997. Composite Independence dikes: Geological Society of America Abstracts with Programs, v. 29, p. 391.

Carl, B.S., Glazner, A.F., Bartley, J.M., Dinter, D.A., Coleman, D.S., 1998. Independence dikes and ma®c rocks of the eastern Sierra. In: Behl, R. (Ed.), Geological Society of America Cordilleran Section 1998 Field Guidebook. California State University at Long Beach, Long Beach, California, pp. 4.1±4.26.

Carl, B.S., 2000, Structure, Intrusion, and Tectonic Origin of the Independence Dike Swarm, Eastern California [Ph.D. thesis]: Chapel Hill, University of North Carolina, 269 p.

Carl, B.S., and Glazner, A.F. 2002. Extent and significance of the Independence dike swarm, in Glazner, A.F., Walker, J.D., and Bartley, J.M., eds., Geologic evolution of the Mojave Desert and southwestern Basin and Range: Geological Society of America Memoir 195, p. 117–130.

Carmignani, L., R. Carosi, L. Disperati, A. Funedda, G. Musumeci, S. Pasci, and P. Pertusati. 1992. Tertiary transpressional tectonics in NE Sardinia, Italy, in Contributions to the Geology of Italy With Special Regard to the Paleozoic Basements, edited by L. Carmignani and F. Sassi, pp. 45–62, Int. Geol. Correl. Prog., Paris.

Carreras, J., Druguet, E., 2014. Framing the tectonic regime of the NE-Iberian Variscan segment. In: Schulmann, K., Martínez Catalán, J.R., Lardeaux, J.M., Janoušek, V., Oggiano, G. (Eds.), Geological Society, London, Special Publications 405, pp. 249–264.

Carreras, J., Gimeno, D., 2000. Geozona 354: Eixam de dics a Aiguablava i Aigua-Xelida: Generalitat de Catalunya. http://www20.gencat.cat/portal/site/
mediambient/menuitem.8f64ca3109a92b904e9cac3bb0c0e1a0?vgnextoid=118c1a22693d7210
VgnVCM1000008d0c1e0aRCRD (accessed February 2014).

Carreras, J., Ortuño F. 1990. Fundamento geométrico y cinemático de la modelización teórica y experimental de deformaciones no-coaxiales. Acta Geológica Hispánica 25, 237-259.

Castaño, L. M. 2010. Emplazamiento y deformación de venas y diques magmáticos en cinturones tectonometamórficos: Análisis a partir de estudios de campo y modelización analógica. Tesis doctoral, UAB, p. 262.

Castro, A. 1985. The Central Extremadura batholith: geotectonic implications (European Hercynian Belt)-An outline. Tectonophysics, 120, 57-68.

Cassinis G., Cortesogno L., Gaggero L., Ronchi A., Sarria E., Serri R. and Calzia P., 2003. Reconstruction of igneous, tectonic and sedimentary events in the latest Carboniferous- Early Permian Seui Basin (Sardinia, Italy), and evolutionary model. Boll. Soc. Geol. It., Vol. Spec., 2: 99-117.

Cassinis, G., Durand, M., and Ronchi, A. 2003. Permian-Triassic continental sequences of Northwest Sardinia and South Provence: stratigraphic correlations and palaeogeographical implications. Bull. Soc. Geol. It., 2, 119-129.

Cassinis, G., C. Perotti, and A. Ronchi. 2011. Permian continental basins in the Southern Alps (Italy) and peri-Mediterranean correlations, Int. J. Earth Sci., doi:10.1007/s00531-011-0642-6, in press.

Cembrano, J., Lara, L. 2009. The link between volcanism and tectonics in the southern volcanic zone of the Chilean Andes: A review, Tectonophysics, 471, 96-113.

Chang Z, Vervoort JD, McClelland WC, and Knaack C. 2006. U–Pb dating of zircon by LA-ICP-MS. Geochemistry, Geophysics, Geosystems 7: Q05009.

Charlot, R., 1976. The Precambrian of the Anti-Atlas (Morocco): a geochronological synthesis. Precambrian Research 3, 273–299.

Charlot, R., 1982. Caractérisation des évé éburnéens et panafricains dans l'Anti-Atlas marocain: approt de la méthode géochronologique Rb–Sr. Notes et Mémoires du Service Géologique du Maroc 313, 106.

Chen, Y., Henry, B., Faure, M., Becq-Giraudon, J.-F., Talbot, J.-Y., Daly, L. and Goff, M. L. 2006. New Early Permian paleomagnetic results from the Brive basin (French Massif Central) and their implications for Late Variscan tectonics, Int. J. Earth Sci., 95, 306–317.

Chen, J.H., and Moore, J.G. 1979. Late Jurassic Independence dike swarm in eastern California: Geology, v. 7, p. 129-133.

Chen, J.H., and Moore, J.G. 1982. Uranium-lead isotopic ages from the Sierra Nevada batholith, California: Journal of Geophysical Research, v. 87, p. 4761-4784.

Choubert, G., Faure-Muret, A., 1970. Les corrélations du Précambrien: Anti-Atlas occidental et central. Notes et Mémoires du Service Géologique du Maroc 229, 259.

Choubert, G. and Faure-Muret, A. 1971. Anti-Atlas (Maroc), in: Tectonic de l'Afrique, in: UNESCO Earth Sci. Series, 1971, pp. 163–175.

Choubert, G., Faure-Muret, A., Hassenforder, B., Jeannette, D., 1974. Nouvelle interpretation du Precambrian ancient de l'Anti-Atlas. Maroc. C. R. Acad. Sci. Paris 278 (17), 2095–2098.

Choubert, G., Faure-Muret, A., 1983. Carte gé du Maroc 1:100 000, Igherm. Notes et Mémoires du Service Géologique du Maroc 309, Feuille NH-29-XVI-2.

Choubert, G., 1963. Histoire géologique du Précambrien de l'Anti-Atlas. Notes et Mémoires du Service Géologique du Maroc, Tome 1, 162, 352 pp. Rabat.

Christiansen, P.P., Pollard, D.D., 1997. Nucleation, growth and structural development of mylonitic shear zones in granitic rocks. Journal of Structural Geology 19, 1159e1172.

Clauer, N., Caby, R., Jeannette, D., Trompete, R., 1982. Geochronology of sedimentary and metasedimentary rocks of the West African craton. Precamb. Res. 18, 53–71.

Clauer, N., 1976. Géochimie isotopique du strontium des milieux sédimentaires. Application à la géochronologie de la couverture du craton ouest africain, Sciences Géologiques, Mémoires, 45. Strasbourg, 256 p.

Clemens, J.D., Mawer, C.K., 1992. Granitic magma transport by fracture propagation. Tectonophysics, 204, 339–360.

Clemens, J.D., Petford, N. 1999. Granitic melt viscosity and silicic magma dynamics in contrasting tectonic setting. J. Geol. Soc. London 156, 1057–1060.

Cloos, H. 1923. Einführung in die tektonische Behandlung magmatischer Erscheinungen. Teil 1: Das Riesengebirge in Schlesien. Gebrüder Bornträger, Berlin, 194 pp.

Cocherie A., Rossi P., Fanning C.M. and Guerrot C., 2005. Comparative use of TIMS and SHRIMP for U-Pb zircon dating of A-type granites and mafic tholeiitic layered compexes and dikes from the Corsican Batholith (France). Lithos, 82: 185-219.

Cohen, C.R., 1980. Plate tectonic model for the Oligo-Miocene evolution of the western Mediterranean. Tectonophysics, 68, 283–311.

Cohen, C. 1981. Plate tectonic model for the Oligo-Miocene evolution of the western Mediterranean, Tectonophysics, 68, 283–311.

Coleman, D.S., Bartley, J.M., Glazner, A.F., and Carl, B.S. 1994. Late Cretaceous dikes in the Independence swarm, Calif.: EOS (Transactions, American Geophysical Union), v. 75, p. 686.

Coleman, D.S., Glazner, A.F., Miller, J.S., Bradford, K.J., Frost, T.P., Joye, J.L., and Bachl, C.A. 1995. Exposure of a Late Cretaceous layered mafic-felsic magma system in the central Sierra Nevada batholith, California: Contributions to Mineralogy and Petrology, v. 120, p. 129–136.

Coleman, D.S., and Glazner, A.F. 1997. The Sierra crest magmatic event: rapid formation of juvenile crust during the Late Cretaceous in California: International Geology Review, v. 39, p. 768–787.

Coleman, D.S., Carl, B.S., Glazner, A.F., and Bartley, J.M. 2000. Cretaceous dikes within the Jurassic Independence dike swarm in eastern California: Geological Society of America Bulletin, v. 112, p. 504-511.

Coleman, D.S., Bartley, J.M, Glazner, A.F., and Law, R.D. 2005. Incremental assembly and emplacement of Mesozoic plutons in the Sierra Nevada and White and Inyo Ranges, Geological Society of America Field Forum Field Trip Guide (Rethinking the Assembly and Evolution of Plutons: Field Tests and Perspectives, 7–14 October 2005), 59 p., doi:10.1130/2005.MCBFYT.FFG.

Compston,W., Williams, I.S., Kirschvink, J.L., Zhang, Z.,Ma, G., 1992. Zircon U/Pb ages for the early Cambrian timescale. Journal of the Geological Society of London 149, 171–184.

Correa-Gomes, L.C.C., de Souza, M.N., Correa, D.R.; Silva, I.R., Falcáo, A.C.S., Cobucci, M.L.P., Jshioka. K.T., Espineira, A.R., Moraes, J.W.O. 1991. Mafic dykes: Relationships among geometry, internal fractures and fissural tectonic patterns. Bol. IGUSP, Pub. Esp., 10: 1-8.

Corti, G., Moratti, G., Sani, F. 2005. Relations between surface faulting and granite intrusions in analogue models of strike-slip deformation. Journal of Structural Geology 27, 1547-1562.

Cortesogno, L., Cassinis, G., Dallagiovanna, G., Gaggero, L., Oggiano, G., Ronchi, A., Seno, S. and Vanossi, M. 1998. The Variscan post-collisional volcanism in Late Carboniferous–Permian sequences of Ligurian Alps, Southern Alps and Sardinia (Italy). Lithos, 45, 305–328.

Cottle JM, Horstwood MSA, and Parrish RR. 2009a. A new approach to single shot laser ablation analysis and its application to in situ Pb/U geochronology. Journal of Analytical Atomic Spectrometry 24: 1355–1363.

Coward, M. P. 1995. Structural and tectonic setting of the Permo-Triassic basins of NW Europe. In: BOLDY, S. (ed.) Permian and Triassic Rifting in Europe. Geological Society, London, Special Publications, 91, 7–39.

Coward, M.P. and Ries, A.C. 2003. Tectonic development of North African basins, in: T. Arthur, S. MacGregor Duncan, N.R. Cameron (Eds.), Petroleum Geology of Africa; New Themes and Developing Technologies, Geological Society, London, pp. 61–83.

Currie, K.L., Ferguson, J., 1970. The mechanism of intrusion of lamprophyre dykes indicated by —ffsetting" of dikes. Tectonophysics, 9, 525–535.

Davidson, C., Schmid, S.M., Hollister, L.S. 1994. Role of melt during deformation in the deep crust. Terra Nova, 6, 133-142.

Davis, M.J., Farber, D.L., Wooden, J.L., and Anderson, J.L. 1994. Conflicting tectonics? Contraction and extension at middle and upper crustal levels along the Cordilleran Late Jurassic arc, southeastern California: Geology, v. 22, p. 247-250.

Debon, F., Zimmermann, J.L., 1993. Mafic dykes from some plutons of the Western Pyrenean Axial Zone (France, Spain): markers of the transition from Late-Hercynian to early Alpine events. Schweiz. Mineral. Petrogr. Mitt. 73, 421–433.

De Beer, C.H., Chevallier, L.P., De Kock, G.S., Gresse, P.G., Thomas, R.J., 2000. Mémoire explicatif de la carte géologique du Maroc au 1/50 000 feuille Sirwa. Notes et Mémoires du Service Géologique du Maroc 395, 87.

de Jong, K., M. Manzoni, T. Stavenga, F. van Dijk, R. van der Voo, and J. Zijderveld (1973), Palaeomagnetic evidence for rotation of Sardinia during early Miocene, Nature, 243, 281–283.

De Kock, G.S., De Beer, C.H., Chevallier, L.P., Dresse, P.G., Thomas, R.J., 2000. Carte géologique au 1/50 000 feuille Taghdout. Notes et Mémoires du Service Géologique du Maroc 396.

Deckart, K., Bertrand, H. and Liégeois, J. P. 2005. Geochemistry and Sr, Nd, Pb isotopic composition of the Central Atlantic Magmatic Province (CAMP) in Guyana and Guinea. Lithos, 82, 282–314.

Delaney, P.T., Pollard, D.D., 1981. Deformation of host rocks and flow of magma during growth of minette dikes and breccia-bearing intrusions near Ship Rock, New Mexico. U. S. Geol. Surv. Prof. Pap. 1202 (61 pp.).

Delaney, P.T., Pollard, D.D., Zioney, J.I., McKee, E.H., 1986. Field relations between dikes and joints: emplacement processes and paleostress analysis. J. Geophys. Res. 91, 4920–4938.

Deroin, J. P., and B. Bonin (2003), Late Variscan tectonomagmatic activity in Western Europe and surrounding areas: The mid-Permian Episode, Bol. Soc. Geol. It., 2, 169–184.

De Saint Blanquat, M., Tikoff, B., Teyssier, C., Vigneresse, J.L. 1998. Transpressional kinematics and magmatic arcs. In: Holdsworth, R.E., Strachan, R.A., Dewey, J.F. (Eds.), Continental Transpressional and Transtensional Tectonics. Geol. Soc. Spec. Publ., vol. 135, pp. 327–340.

Destombes, J. 1976. The Ordovician of the Moroccan Anti-Atlas, in: M.G. Bassett (Ed.), The Ordovician System, Univ. Wales Press and Natl. Mus. Wales, 1976, pp. 411–413.

Destombes, J., Hollard, H. and Willefert, S. 1985. Lower Paleozoic rocks of Morocco, in: C.H. Holland (Ed.), Lower Palaeozoic of North-Western and West-Central Africa, Trinity Coll., Dep. Geol., Dublin, Ireland, pp. 91–336.

Dieni, I., F. Massari, and J. Médus. 2008. Age, depositional environment, and stratigraphic value of the Cuccuru ‘e Flores conglomerate: Insight into the Palaeogene to Early Miocene geodynamic evolution of Sardinia, Bull. Soc. Geol. Fr., 179, 51–72, 2008.
Dingwell, D.B. 1995. Viscosity and anelasticity of melts. En: T. Ahrens (ed.) Mineral Physics and Crystallography, A Handbook of Physical Constants, AGU Reference Shelf 2, 209-217.

Dinter, D.A., Carl, B.S., Bartley, J.M., and Glazner, A.F. 1996a. AMS evidence for sinistral shear during emplacement of the Independence dike swarm, California: Geological Society of America Abstracts with Programs, v. 28, p. 247.

Dinter, D.A., Whitmarsh, R., Bartley, J.M., and Carl, B.S. 1996b. AMS character of Late Jurassic (?) Independence dikes near China Lake, California: EOS (Transactions, American Geophysical Union), v. 77, p. F641.

Di Pisa A., Del Moro A., Macera P., Oggiano G. and Squadrone A. 1988. *Studio geochimico e radiometrico, con il metodo Rb/Sr, dei graniti perallimuniferi sintettonici di Tarra Padedda (Sardegna settentrionale).* S.I.M.P. notizie, 7,67.

D‘Lemos, R. S., Inglis, J. D. and Samson, S. D. 2006. A newly discovered orogenic event in Morocco: Neoproterozoic ages for supposed Eburnean basement of the Bou Azzer inlier, Anti-Atlas mountains. Precambrian Research, 147, 65–76.

Doblas, M., Lopez-Ruiz, J., Cebria, J.M., Youbi, N., Degroote, E., 2002. Mantle insulation beneath the West African Craton during the Precambrian-Cambrian transition. Geology 30, 839–842.

Doblas,M., Ubanell, A.G., 1991. Los sistemas filonianos tardihercínicos del centro peninsular como resultado de una deformación progresiva dentro de una zona de cizalla transcurrente dextral de escala megacontinental. 16, Cadernos Laboratorio Xeolóxico de Laxe pp. 169–177.

Donzeau, M., 1974. Les déformations hercyniennes dans le Paléozoïque des Monts d'Ougarta. C. R. Acad. Sci. Paris 278D, 417–420.

Dornsiepen, U. F., Manutsoglu, E. and Mertmann, D. 2001. Permian– Triassic palaeogeography of the external Hellenides. Palaeogeography, Palaeoclimatology, Palaeoecology, 172, 327–338.

Douglas, R.W. 1963. Rheology of inorganic glasses. Proceedings of the International Congress on Rheology, Vol. 1, 3-27.

Druguet, E. and Carreras, J. 2006. Analogue modelling of syntectonic leucosomes in migmatitic schists. Journal of Structural Geology 28, 1734-1747.

Druguet, E. and Castaño L.M. 2010. Analysis of syntectonic magmatic veins at the mesoscale. Journal Geological Society of India 75, 60-73

Druguet, E., Castaño, L.M., Czeck, D.M., Hudleston, P.J., Carreras, J., 2012. The tectonicsignificance of dikes of irregular fold-like shape. Geology 40, 579–582. http://dx.doi.org/10.1130/G32960.

Druguet, E., Czeck, D.M., Carreras, J., Castaño, L.M., 2008. Emplacement and deformation features of syntectonic leucocratic veins from the Rainy Lake zone (Western Superior Province, Canada). Precambrian Res. 163, 384–400.

Druguet, E., Hutton, D.H.W. 1998. Syntectonic anatexis and magmatism in a mid-crustal transpressional shear zone: an example from the Hercynian rocks of the eastern Pyrenees. Journal of Structural Geology 20, 905-916.

Druguet, E., Passchier, C.W., Pennacchioni, G., Carreras, J., 2013. Geoethical education: a critical issue for geoconservation. Episodes 36, 11–18.
Emerman, S.H., Marrett, R. 1990. Why dykes? Geology 18, 231–233.

Du, Y., Aydin, A. 1991. Interaction of multiple cracks and formation of échelon crack arrays. Int. J. Num. Analyt. Meth. Geomech. 15, 205–218.

Duchesne, J.C., Liégeois, J.-P., Bolle, O., Vander Auwera, J., Bruguier, O., Matukov, D., Sergeev, S.A., 2013. The fast evolution of a crustal hot zone at the end of a transpressional regime : the Saint-Tropez peninsula granites and related dykes (Maures Massif, SE France). Lithos, 162-163, 195-220.

Ducrot, J., Lancelot, J.R., 1977. Problème de la limite Précambrian–Cambrien: etude radiochronolgie par la méthode U–Pb sur zircons du volcan du Jbel Boho (Anti-Atlas marocain). Can. J. Earth Sci. 14, 2771–2777.

Dunne, G.C., and Walker, J.D., 1993, Age of Jurassic volcanism and tectonism, southern Owens Valley region, east-central California: Geological Society of America Bulletin, v. 105, p. 1223-1230.

Dunne, G.C., Walker, J.D., Stern, S.M., and Linn, J.K. 1994. New U-Pb age constraints on Late Jurassic magmatism and contractile deformation in east-central California: Geological Society of America Abstracts with Programs, v. 26, p. A386.

Edel, J.-B. 2000. Hypothèse d'une ample rotation horaire tardi-varisque du bloc Maures-Estérel-Corse-Sardaigne, Geol. Fr., 1, 3–19.

Edel, J. B., R. Montigny, and R. Thuizat. 1981. Late Paleozoic rotations of Corsica and Sardinia: New evidence from paleomagnetic and K/Ar studies, Tectonophysics, 79, 201–223.

Edelman, S.H. 1991. Relationships between kinematics of arc-continent collision and kinematics of thrust faults, folds, shear zones, and foliations in the Nevadan orogen, northern Sierra Nevada, California: Tectonophysics, v. 191, p. 223-236.

Ehlers, C. and Ehlers, M. 1977. Shearing and multiple intrusion in the diabases of Aland archipelago, SW Finland. Geological Survey of Finland, Bulletin 289, 31 pp.

El Aouli, E.H., Gasquet, D. and Ikenne, M. (2001). Le magmatisme basique de la boutonnière d'Igherm (AntiAtlas occidental, Maroc) : un jalon des distensions néoprotérozoïques de la bordure nord du craton ouestafricain. Bull. Soc. Géol. France. 172 (3) : pp 309317.

El Aouli, E.H. (2004). Les roches mafiques du Cryogénien (PII inférieur) de l'AntiAtlas occidental (Igherm) et central (IguerdaTalfast et Agadir Melloul): Pétrologie, Géochimie et implications géodynamiques. Thèse Doctorat d'état, Université Ibn Zohr, Agadir, Maroc, pp 257.

El Aouli, E., Ikenne, M. and Amaouain.H. 2010. Petrographic and geochemical characterization of cryogenian mafic dykes of the IguerdaTaïfast inlier (Central AntiAtlas, (Morocco). INTERNATIONAL JOURNAL OF GEOMATICS AND GEOSCIENCES Volume 1, No 3.

Emmer, B., V. Bachtadse, G. Muttoni, A. Ronchi, and D. V. Kent. 2005. Paleomagnetism of Late Paleozoic dyke swarms from Sardinia, Eos Trans. AGU, 86(52), Fall Meet. Suppl., Abstract GP11A-0015.

Engebretson, D.C., Cox, A., and Gordon, R.G. 1985. Relative motions between oceanic and continental plates in the Pacific basin: Geological Society of America Special Paper 206, 59 p.

Ennih, N. and Liégeois, J.-P. 2001. The Moroccan Anti-Atlas; the West African craton passive margin with limited Pan-African activity; implications for the northern limit of the craton, Precambr. Res. 112 (3–4) 289–302.

Ennih, N., Liégeois, J.P., 2008. The Boundaries of the West African Craton, with Special Reference to the Basement of the Moroccan Metacratonic Anti-Atlas Belt: Geological Society, London, Special Publications, 297, pp. 1–17.

Enrique, P., 1990. The Hercynian intrusive rocks of the Catalonian Coastal Ranges (NE Spain). Acta Geol. Hisp. 25, 39–64.

Enrique, P., 2009. Las espesartitas, camptonitas y bostonitas del complejo intrusivo de Aiguablava (Cadenas Costeras Catalanas): cartografía y composición. Geogaceta 47, 125–128.

Enrique, P., Butjosa, L., Esteve, S., 2012. Estudio cartográfico de los diques compuestos y multi-intrusivos de lamprófidos del sector oriental del plutón de Aiguablava (Cadenas Costeras Catalanas, NE España). Geotemas 13, 153.

Ernst, W.G. 1997. Metamorphism of mafic dikes from the central White-Inyo Range, eastern California: Contributions to Mineralogy and Petrology, v. 128, p. 30-44.

Ernst R.E., Baragar W.R.A. 1992. Evidence from magnetic fabric for the flow pattern of magma in the Mackenzie giant radiating dyke swarm. Nature 356, 511–513.

Ernst, R.E., Buchan, K.L., Palmer, H.C., 1995. Giant dyke swarms: Characteristics, distribution and geotectonic implications. In: Baer, G., Heimann, A. (Eds.), Physics and chemistry of dykes. Balkema, Rotterdam, pp. 3-21.

Ernst R.E., Grosfils E.B., Mege D. 2001. Giant dyke swarms on Earth, Venus, and Mars. Ann. Rev. Earth Planet. Sci. 29, 489–534.

Ernst, R.E. and Bleeker,W., 2010. Large Igneous Provinces (LIPs), giant dyke swarms, and mantle plumes: significance for breakup events within Canada (and selected adjacent regions) from 2.5 Ga to present. Canadian Journal of Earth Sciences 47, 695–739.

Ernst, R.E., Buchan, K.L., Palmer, H.C., 1995. Giant dyke swarms: characteristics, distribution and geotectonic implications. In: Baer, G., Heimann, A. (Eds.), Physics and Chemistry of Dykes. Balkema, Rotterdam, pp. 3–21.

Ernst, R.E., Head, J.W., Parfitt, E., Grosfils, E.,Wilson, L., 1995. Giant radiating dyke swarms on earth and venus. Earth-Sci. Rev. 39, 1–58.

Escher, A., Jack, S., Watterson, J. 1976. Tectonics of the North Atlantic Proterozoic dyke swarm. Philosophical Transactions of the Royal Society of London, Series A: Mathematical and Physical Sciences 280, 529–539.

Esteve, S., Enrique, P., Galán, G., 2014. The camptonites in the multiple intrusion of Platja Fonda (Girona, NE Spain): mechanisms of intrusion and geochemistry. J. Geosci. 59, 23–40.

Faccenna, C., F. Speranza, F. D'Ajello Caracciolo, M. Mattei, and G. Oggiano. 2002. Extensional tectonics on Sardinia (Italy): Insights into the arc–back-arc transitional regime, Tectonophysics, 356, 213–232.

Fackler-Adams, B.N., Busby, C.J., and Mattinson, J.M. 1997. Jurassic magmatism and sedimentation in the Palen Mountains, southeastern California: implications for regional tectonic controls on the Mesozoic continental arc: Geological Society of America Bulletin, v. 109, p. 1464-1484.

Fahrig, W.F. 1987. The tectonic setting of continental mafic dyke swarms: failed arm and early passive margin. In: Halls, H.C., and Fahrig, W.F. (eds.) Mafic Dyke Swarms. Geological Association of Canada Special Paper 34, p. 331-348.

Faure-Muret, A., 1992. Carte géologique du Maroc 1/ 100 000, Agadir Melloul. Notes et Mémoires du Service Géologique du Maroc 359, Feuille NH-29-XVII-1.

Feinberg, H., Aifa, T., Pozzi, J.-P., Khattach, D. and Boulin, J. 1990. Courbes de dérive apparente des pôles magnétiques de l'Afrique et de la Meseta marocaine pendant le Paléozoique, C. R. Acad. Sci. Paris, Ser. II 310, 913–918.

Feng R, Machado N, and Ludden J. 1993. Lead geochronology of zircon by LaserProbe-inductively coupled plasma mass spectrometry (LP-ICPMS). Geochimica et Cosmochimica Acta 57: 3479–3486.

Fernández, C., Castro, A. 1999. Brittle behaviour of granitic magma: the example of Puente del Congosto, Iberian Massif, Spain. En: Castro, A., Fernández, C. y Vigneresse, J.L. (eds.): Understanding Granites: Integrating New and Classical Techniques. Geological Society, London, Special Publications 168, 191-206.

Ferrandini, J., J. Gattacceca, M. Ferrandini, A. Deino, and M. Janin. 2003. Chronostratigraphie et paléomagnétisme des dépôts Oglio-Miocènes de Corse: Implications géodynamiques pour l'ouverture du bassin liguroprovençal, Bull. Soc. Geol. Fr., 174, 357–371.

Ferre, E., Galland, O., Montanari, D., Kalakay, T.J. 2012. Granite magma migration and emplacement along thrusts. International Journal of Earth Sciences 101, 1673- 1688.

Ferrés, M., 1998. Géochronologie, pétrogenèse et évolution géochimique des intrusions granitiques alcalines des Chaînes côtières Catalanes dans le cadre du magmatisme hercynien de la Méditerranée nord-occidentale. Ph.D. thesis, Université de Genève.

Fialko, Y., Rubin, A., 1999. Thermal and mechanical aspects of magma emplacements in giant dike swarms. J. Geophys. Res. 104, 23033–23049.

Fitch, T.J., 1972. Plate convergence, transcurrent faults, and internal deformation adjacent to southeast Asia and the western Pacific. Journal of Geophysical Research 77, 4432-4460.

Francis, E. H. 1978. The Midland Valley rift, seen in connection with the Late Paleozoic European Rift system. In: Ramberg, I. B. and Neumann, E. R. (eds) Tectonics and Geophysics of Continental Rifts. NATO Advanced Study Institute, Series C, Mathematics & Physical Sciences, 37, 133–148.

Frost, B.R., Barnes, C.G., Collins, W.J., Arculus, R.J., Ellis, D.J., Frost, C.D. 2001. A geochemical classification for granitic rocks. Journal of Petrology 42, 2033–2048.

Frost, T.P., and Mahood, G.A. 1987. Field, chemical, and physical constraints on mafic-felsic magma interaction in the Lamarck Granodiorite, Sierra Nevada, California: Geological Society of America Bulletin, v. 99, p. 272–291, doi: 10.1130/0016-7606(1987)99<272: FCAPCO>2.0.CO;2.

Fryer BJ, Jackson SE, and Longerich HP. 1993. The application of laser ablation microprobe-inductively coupled plasma-mass spectrometry (LAM-ICP-MS) to in situ U–Pb geochronology. Chemical Geology 109: 1–8.

Furlong, K.P., Hanson, R.B., and Bowers, J.R. 1991, Modeling thermal regimes. En: Contact Metamorphism (D.M. Kerrick, ed.). Reviews in Mineralogy 26, 437–505.

Gaggero, L., Oggiano, G., Buzzi, L., Slejko, F., Cortesogno, L., 2007. Post-Variscan mafic dikes fromthe late orogenic collapse to the Tethyan rift: evidence fromSardinia. Ofioliti 32, 15–37.

Galland, O., de Bremond d'Ars, J., Cobbold, P.R., and Hallot, E. 2003. Physical models of magmatic intrusion during thrusting. Terra Nova 15, 405-409.

Gasquet, D., Chèvremont, P., Baudin, T., Chalot-Prat, F., Guerrot, C., Cocherie, A., Roger, J., Hassenforder, B., Cheilletz, A., 2004. Polycyclic magmatism in the Tagragra and Kerdous-Tafeltast inliers (Western Anti-Atlas, Morocco). Journal of African Earth Sciences 39, 267–275.

Gasquet, D., Levresse, G., Cheilletz, A., Azizi-Samir, M.R., Mouttaqi, A., 2005. Contribution to a geodynamic reconstruction of the Anti-Atlas (Morocco) during Pan-African times with the emphasis on inversion tectonics and metallogenic activity at the Precambrian–Cambrian transition. Precambrian Research 140, 157–182.

Gast, R. 1988. Rifting im Rotliegenden Niedersachsens. Die Geowissenschaften, 6, 115–122.

Gattacceca, J., Deino, A., Rizzo, R., Jones, D.S., Henry, B., Beaudoin, B. and Vadeboin, F. 2007. Miocene rotation of Sardinia: New paleomagnetic and geochronological constraints and geodynamic implications. Earth and Planetary Science Letters, 258 (3-4): 359-377.

Gayer, R.A., Powell, D.B. and Stephen, R. 1978. Deformation against metadolerite dykes in the Caledonides of Finnmark, Norway. Tectonophysics, 46, 99-115.

Gehrels, GE, Valencia VA, and Ruiz J. 2008. Enhanced precision, accuracy, efficiency, and spatial resolution of U–Pb ages by laser ablation-multicollector-inductively coupled plasma-mass spectrometry. Geochemistry, Geophysics, Geosystems 9: Q03017.

Geyer, G., Landing, E. and Heldmaier, W. 1995. Faunas and depositional environments of the Cambrian of the Moroccan Atlas region, in: G. Geyer, E. Landing (Eds.), MOROCCO'95 – The Lower– Middle Cambrian Standard of Western Gondwana, Beringeria, Special Issue 2, University of Würzburg, Germany, pp. 47–119.

Ghezzo A. and Di Vincenzo. 1996. *Evidence of two different components in a hercynian peraluminous cordierite-bearing granite: the San Basilio intrusiopn (central Sardinia, Italy).* «Journ. Petrol.», 37, 1175-1206.

Ghezzo, C. and Orsini, J.B. 1982. Lineamenti strutturalie composizionali del batolite ercinico Sardo-Corso in Sardegna. *in* «Guida alla Geologia del Paleozoico Sardo, Guide Geologiche

Regionali». Carmigniani L., Cocozza T., Ghezzo C., Pertusati P.C. and Ricci C.A. eds. *Mem. Soc. Geol. It.*, 151-156.

Gil-Imaz, A., Lago-San José,M., Galé, C., Pueyo-Anchuela, O., Ubide, T., Tierz, P., Oliva-Urcia, B., 2012. The Permian mafic dyke swarm of the Panticosa pluton (Pyrenean Axial Zone, Spain): simultaneous emplacement with the late-Variscan extension. J. Struct. Geol. 42, 171–183.

Gimeno, D., 2002. Estructura ymecanismos intrusivos de los lamprófidos de Sa Planassa—Punta d'Es Mut (Costa Brava, Cordillera Litoral Catalana): su interés didáctico. 11, Treballs del Museu de Geologia de Barcelona pp. 105–133.

Glazner, A.F., Bartley, J.M., Carl, B.S., 1999. Oblique opening and noncoaxial emplacement of the independence dike swarm, California. J. Struct. Geol. 21, 1275–1283.

Glazner, A.F., Bartley, J.M., and Walker, J.D. 1989. Magnitude and significance of Miocene crustal extension in the central Mojave Desert, California: Geology, v. 17, p. 50-54.

Glazner, A.F., Walker, J.D., Bartley, J.M., Fletcher, J.M., Martin, M.W., Schermer, E.R., Boettcher, S.S., Miller, J.S., Fillmore, R.P., and Linn, J.K. 1994. Reconstruction of the Mojave block, *in* McGill, S.F., and Ross, T.M., compilers, Geological Investigations of an active margin: Geological Society of America Cordilleran Section Fieldtrip Guidebook, v. 27, p. 3-30.

Glazner, A.F., Carl, B.S., Coleman, D.S., Miller, J.S., and Bartley, J.M. 2008. Chemical variability and composite nature of dikes from the Jurassic Independence dike swarm, eastern California, *in* Wright, J.E., and Shervais, J.W., eds., Ophiolites, arcs, and batholiths: A tribute to Cliff Hopson: Geological Society of America Special.

Gómez-Rivas, E. 2008. Localización de deformación en medios dúctiles y anisótropos: estudio de campo, experimental y numérico. Tesis doctoral, Univ. Autónoma de Barcelona, 247 pp.

Gong, Z., C. Langereis, and T. Mullender. 2008. The rotation of Iberia during the Aptian and the opening of the Bay of Biscay, Earth Planet. Sci. Lett., 273, 80–93.

Grujic, D. and Mancktelow, N.S. 1998. Melt-bearing shear zones: analogue experiments and comparison with examples from southern Madagascar. Journal of Structural Geology 20, 673-680.

Guasparri G., Riccobono F. and Sabatini G. 1984. *Leucogranites of Sardinian batholith: petrological aspects and their relevance to metallogenesis*. «Per. Mineral.», 53, 17-52.

Gudmundsson, A., 2002. Emplacement and arrest of sheets and dykes in central volcanoes. J. Volcanol. Geotherm. Res. 116, 279–298. http://dx.doi.org/10.1016/S0377-0273(02)00226-3.

Gudmundsson, A., Fjeldskaar, I., Brenner, S.L., 2002. Propagation pathways and fluid transport in jointed and layered rocks in geothermal fields. J. Volcanol. Geotherm. Res. 116, 257–278.

Guillong M and Heinrich CA (2007) Sensitivity enhancement in laser ablation ICP-MS using small amounts of hydrogen in the carrier gas. Journal of Analytical Atomic Spectrometry 22: 1488–1494.

Guillong M, Horn I, and Günther D (2003) A comparison of 266 nm, 213 nm and 193 nm produced from a single solid state Nd:YAG laser for laser ablation ICP-MS. Journal of Analytical Atomic Spectrometry 18: 1224–1230.

Guineberteau, B., Bouchez, J L. and Vigneresse, J.L. 1987. The Mortagne granite pluton (France) emplaced by pullapart along a shear zone; structural and gravimetric arguments and regional im- plication. Geological Society of America Bulletin 99, 763-770.

Günther D, Frischknecht R, Heinrich CA, and Kahlert H-J. 1997. Capabilities of an argon fluoride 193 nm excimer laser for laser ablation inductively coupled plasma mass spectometry microanalysis of geological materials. Journal of Analytical Atomic Spectrometry 12: 939–944.

Günther D and Heinrich CA. 1999a. Comparison of the ablation behaviour of 266 nm Nd:YAG and 193 nm ArF excimer lasers for LA-ICP-MS analysis. Journal of Analytical Atomic Spectrometry 14: 1369–1374.

Günther D and Heinrich CA. 1999b. Enhanced sensitivity in laser ablation-ICP mass spectrometry using helium–argon mixtures as aerosol carrier. Journal of Analytical Atomic Spectrometry 14: 1363–1368.

Guiraud, R., Doumnang Mbaigane, J.C., Carretier, S. and Dominguez, S., 2000. Evidence for a 6000km length NW–SE-striking lineament in northern Africa: the Tibesti lineament. J. Geol. Soc., London 157, 897–900.

Guiraud, R., Bosworth, W., Thierry, J. and Delplanque, A. 2005. Phanerozoic geological evolution of Northern and Central Africa: an overview. Journal of African Earth Sciences, 43, 83–143.

Haddoum, H., Guiraud, R. and Moussine-Pouchkine, A. 2001. Hercynian compressional deformations of the Ahnet–Mouydir Basin, Algerian Saharan Platform: far-field stress effects of the Late Palaeozoic orogeny, Terra Nova 13 (3) 220–226.

Hafid, A., Sagon, J.P., Julivert, M., Arboleya, M.L., Saquaque, A., El Boukhari, A., Saidi, A., Soler, J.M.F., 2001. Le magmatisme basique filonien néoprotérozoïque de la boutonnière de Zenaga, Anti-Atlas central, Maroc: pétrologie, géochimie et signification géodynamique. Journal of African Earth Sciences 32, 707–721.

Hafid, A., 1999. Magmatisme basique filonien neoproterozoTque (Precambrien II inferieur) dans l'Anti-Atlas central et occidental. Mineralogie, geochimie, petrogenese et implication geodynamique. These Doctorat Etat Sciences, Universite Cadi Ayyad, Faculte des Sciences Marrakech, Maroc, 222p.

Hall, A. 1996. Igneous Petrology. Longman Group Ltd., 2nd ed., Essex UK, 551 p.

Halls, H.C., 1982. The importance and potential of mafic dyke swarms in studies of geodynamic processes. Geosci. Can. 9, 145–154.

Hallot, E., Davy, P., Bremond d'Ars, J., Martin, B., Van Damme, H. 1996. Non-Newtonian effects during injection in partially crystallised magmas. J. Volcanol. Geotherm. Res. 71, 31–44.

Handy, M.R., Streit, J.E. 1999. Mechanics and mechanisms of magmatic underplating: Inferences from mafi c veins in deep crustal mylonite: Earth and Planetary Science Letters, 165, 271–286.

Hanmer, S., Mengel, F, Connelly, J. y van Gool, J. 1997. Significance of crustal-scale shear zones and synkinematic mafic dykes in the Nagssugtoqidian orogen, SW Greenland: a re-examination. Journal of Structural Geology, 19, 59-75.

Hanmer, S., Passchier, C.W., 1991. Shear-sense indicators: a review. Geol. Surv. Can. Pap. 90–17, 72.

Hanski, E., Mertanen, S., Rämö, T., Vuollo, J. (Eds.), 2006. Dyke Swarms — Time Markers of Crustal Evolution. Taylor & Francis, London.

Hanson, R.B., Glazner, A.F. 1995. Thermal requirements for extensional emplacement of granitoids. Geology 23, 213-216.

Harper, G.D., Saleeby, J.S., and Heizler, M. 1994. Formation and emplacement of the Josephine ophiolite and the Nevadan Orogeny in the Klamath Mountains, California-Oregon: U/Pb zircon and $^{40}Ar/^{39}Ar$ geochronology: Journal of Geophysical Research, v. 99, p. 4293-4321.

Harris, N.B., Pearce, J.A., Tindle, A.G. 1986. Geochemical characteristics of collision-zone magmatism. En: Coward M.P., Ries A.C. (Eds.): Collision tectonics, Geol. Soc. Spec. Publ. 19, 67–81.

Hassenforder, B. 1987. La tectonique panafricaine et varisque de l'Anti-Atlas dans le massif du Kerdous (Maroc), PhD thesis, University of Strasbourg, France.

Hassenforder, B., Roger, J., Baudin, T., Chalot-Prat, F., Gasquet, D., Berrahma, A., Chèvremont, P., Marquer, D., Razin, P., Benlakhdim, A., 2001. Carte géologique au 1/50 000 feuille Sidi Bou'Addi. Notes et Mémoires du Service Géologique du Maroc 414

Hefferan, K.P., Admou, H., Karson, J.A. and Saquaque, A. 2000. Anti- Atlas (Morocco) role in Neoproterozoic western Gondwana reconstruction, Precambr. Res. 103 (1–2) 89–96.

Hefferan, K.P., Admou, H., Hilal, R., Karson, J.A., Saquaque, A., Juteau, T., Bohn, M.M., Samson, S.D. and Kornprobst, J.M. 2002. Proterozoic blueschist-bearing melange in the Anti-Atlas Mountains, Morocco, Precambr. Res. 118 (3–4) 179–194.

Helbing, H., W. Frisch, P. D. Bons, and J. Kuhlemann. 2006. Tension gash-like back-arc basin opening and its control on subduction rollback inferred from Tertiary faulting in Sardinia, Tectonics, 25, TC4008, doi:10.1029/2005TC001904.

Helg, U., Burkhard, M., Caritg, S. and Robert-Charrue, C. 2004. Folding and inversion tectonics in the Anti-Atlas of Morocco, Tectonics 23, 17, TC 4006.

Hergenroder, R. 2006. Hydrodynamic sputtering as a possible source for fractionation in LA-ICP-MS. Journal of Analytical Atomic Spectrometry 21: 517–524.

Hernando, S., Schott, J., Thuizat, T. and Montgny, R. 1980. Age des andesites des sediments interstratifies de la region d'Atienza (Espagne): étude stratigraphique, géochronologique et paléomagnetique. Sciences Géologiques Bulletin, 32, 119–128.

Hirata T and Nesbitt RW (1995) U–Pb isotope geochronology of zircon: Evaluation of the laser probe-inductively coupled plasma mass spectrometry technique. Geochimica et Cosmochimica Acta 59: 2491–2500.

Hoek, J.D., 1991. A classification of dyke-fracture geometry with examples from Precambrian dyke swarms in the Vestfold Hills, Antarctica. Geol. Rundsch. 80, 233–248.

Hogan, J.P., Price, J.D., Gilbert, M.C. 1998. Magma traps and driving pressure: consequences for pluton shape and emplacement in an extensional regime. Journal of Structural Geology 20, 1155–1168.

Hollard, H. 1981. Tableaux de corrélations du Silurien et du Dévonien de l'Anti-Atlas, Notes Serv. géol. Maroc, 42.

Hooper, A., Ófeigsson, B., Sigmundsson, F., Lund, B., Einarsson, P., Geirsson, H., Sturkell, E., 2011. Increased capture of magma in the crust promoted by ice-cap retreat in Iceland. Nat. Geosci. 4, 783–786.

Hopson, C.A. 1988. Independence dike swarm: origin and tectonic significance: EOS (Transactions, American Geophysical Union), v. 69, p. 1479.

Horn, I and Günther, D. 2003. The influence of ablation carrier gasses Ar, He and Ne on the particle size distribution and transport efficiencies of laser ablation-induced aerosols: Implications for LA-ICP-MS. Applied Surface Science 207: 144–157.

Horstwood, MSA.2008. Data reduction strategies, uncertainty assessment and resolution of LA-(MC-)ICP-MS isotope data. In: Sylvester PJ (ed.) Laser Ablation ICP-MS in the Earth Sciences: Current Practices and Outstanding Issues. Mineralogical Association of Canada Short Course Series, vol. 40, pp. 283–303. Quebec: Mineralogical Association of Canada.

Hou, G., 2012. Mechanism for three types of mafic dyke swarms. Geosci. Front. 3, 217–223.

Howard, K.A., and Hopson, R.F. 1997. Vertical axis rotations in the Mojave; evidence from the Independence dike swarm: Comment: Geology, v. 25, p. 1051-1052.

Hutton, D.H.W. 1982. A tectonic model for the emplacement of the main Donegal granite. J. Geol. Soc. Lond. 139, 615–631.

Hutton, D.H.W., 1988. Granite emplacement mechanisms and tectonic controls: inferences from deformational studies. Trans. R. Soc. Edinb. Earth Sci. 79, 245–255.

Hutton, D.H.W., Reavy, R.J. 1992. Strike-slip tectonics and granite petrogénesis. Tectonics, 11, 960-967.

Ikenne, M., Mortaji, A., Gasquet, D., Stussi, J.M., 1997. Les filons basiques des boutonnieres du Bas-Drla et de la Tagragra d'Akka: temoins des distensions neoproterozoiques de l'Anti-Atlas occidental (Maroc). Journal African Earth Sciences 25, 209-223.

Ingersoll, R.V., and Schweickert, R.A. 1986. A plate-tectonic model for Late Jurassic ophiolite genesis, Nevadan Orogeny and forearc initiation, northern California: Tectonics, v. 5, p. 901-912.

Inglis, J. D., Maclean, J. S., Samson, S. D., D'Lemos, R. S., Admou, H. & and Hefferan, K. 2004. A precise U–Pb zircon age for the Bleïda granodiorite, Anti-Atlas, Morocco: implications for the timing of deformation and terrane assembly in the eastern Anti-Atlas. Journal of African Earth Sciences, 39, 277–283.

Ingram, G. M. and Hutton, D. H. W. 1994. The great Tonalite Sill: Emplacement into a contractional shear zone and implications for Late Cretaceous to early Eocene tectonics in southeastern Alaska and British Columbia. Geological Society of America Bulletin 106, 715-728.

Isozaki, Y. 2009. Illawarra reversal: The fingerprint of a superplume that triggered Pangean breakup and the end-Guadalupian (Permian) mass extinction, Gondwana Res., 15, 421–432.

Jaeger, J.C. 1957. The temperature in the neighborhood of a cooling intrusive sheet. American Journal of Science 255, 306-18.

Jaeger, J.C. 1968. Cooling and solidification of igneous rocks. En: Hess, H.H., Poldervaart, A. (eds), Basalts, the Poldervaart Treatise on Rocks of Basaltic Composition Vol. 2, Wiley, New York. 503–536.

James, E.W. 1989. Southern extension of the Independence dike swarm of eastern California: Geology, v. 17, p. 587-590.

Jarrard, R.D., 1986. Terrane motion by strike-slip faulting of forearc slivers. Geology 14, 780-783.

Jeannette, D. and Piqué, A., 1981. Le Maroc hercynien: plateforme disloque´e de craton ouest-africain. C. R. Acad. Sci. Paris 293, 79–82.

Jolly, R.J.H., Sanderson, D.J., 1995. Variation in the form and distribution of dykes in the Mull swarm, Scotland. J. Struct. Geol. 17, 1543–1557.

Jolly, R.J.H., Sanderson, D.J., 1997. A Mohr circle construction for the opening of a preexisting fracture. J. Struct. Geol. 19, 887–892.

Karish, C.R., Miller, E.R., and Sutter, J.F. 1987. Mesozoic tectonic and magmatic history of the central Mojave desert: Arizona Geological Digest, v. 18, p. 15-32.

Kirby, S., and Kronenberg, A.K. 1987. Rheology of the lithosphere: selected topics: Reviews of Geophysics, v. 25, p. 1219-1244.

Kirscher, U., Aubele, K., Muttoni, G., Ronchi, A. and Bachtadse V. 2011. Paleomagnetism of Jurassic carbonate rocks from Sardinia: No indication of post-Jurassic internal block rotations. Journal of Geophysical Research, Vol. 116, B12107, doi:10.1029/2011JB008422.

Knight, M.D., and Walker, G.P.L. 1988. Magma flow directions in dikes of the Koolau Complex, Oahu, determined from magnetic fabric studies: Journal of Geophysical Research, v. 93, p. 4301-4319.

Kosler J and Sylvester PJ. 2003. Present trends and the future of zircon in geochronology: Laser ablation ICPMS. In: Hanchar JM and Hoskin PWO (eds.) Zircon. Reviews in Mineralogy and Geochemistry, vol. 53, pp. 243–275. Washington, DC: Mineralogical Society of America.

Kosler, J, Wiedenbeck M, Wirth R, Hovorka J, Sylvester P, and Mikova J. 2005. Chemical and phase composition of particles produced by laser ablation of silicate glass and zircon—Implications for elemental fractionation during ICP-MS analysis. Journal of Analytical Atomic Spectrometry 20: 402–409.

Kouyaté, D., Söderlund, U., Youbi, N., Ernst, R., Hafid, A. and Ikenne, M. 2012. U–Pb baddeleyite and zircon ages of 2040 Ma, 1650 Ma and 885 Ma on dolerites in the West African Craton (Anti-Atlas inliers): Possible links to break-up of Precambrian supercontinents. Lithos, doi:10.1016/j.lithos.2012.04.028.

Kushiro, I. 1980. Viscosity, density, and structure of silicate melts at high pressures, and their petrologic applications. En R.B. Hargraves (Ed.): Physics of Magmatic Processes, 93- 120. Princeton University Press, Princeton, New Jersey.

Lago, M., Arranz, E., Pocoví, A., Galé, C., Gil-Imaz, A., 2004. Permian magmatism and basin dynamics in the southern Pyrenees: a record of the transition from late Variscan transtension to early Alpine extension. In: Wilson, M., Neumann, E.-R., Davies, G.R., Timmerman, M.J., Heeremans, M., Larsen, B.T. (Eds.), Permo-Carboniferous Magmatism and Rifting in Europe. Geol. Soc. Lond. Spec. Publ., 223, pp. 439–464 (London).

Lago, M. and Pocovi, A. 1984. Le vulcanisme calc-alcaline d'âge Stéphanien–Permien dans la Chaîne Iberique (Est de l'Espagne). Supplement, Bulletin de Mineralogie, 110, 42–44.

Lahren, M.M., Schweickert, R.A., Mattinson, J.M., and Walker, J.D. 1990. Evidence of uppermost Proterozoic to Lower Cambrian miogeoclinal rocks and the Mojave-Snow Lake fault: Snow Lake pendant, central Sierra Nevada, California: Tectonics, v. 9, p. 1585-1608.

Lama, C., Zimmermann, J.L., Mortaji, A., Macaudiere, J., Stussi, J.M., 1993. Age K–Ar proterozoique moyen des leucogranites a deux micas de la Tagragra d'Akka (Anti Atlas occidental, Maroc). Comptes Rendus de l'Academie des Sciences de Paris 317, 1601–1607.

Landing, E., Bowring, S.A., Davidek, K.L., Westrop, S.R., Geyer, G., Heldmaier, W., 1998. Duration of the Early Cambrian: U–Pb ages of volcanic ashes from Avalon and Gondwana. Can. J. Earth Sci. 35, 329–338.

Lasheras, E., Lago, M., Garcia Belles, J., and Arranz E. 1999. Petrologia de diques doleriticos y basaltos, Permico superior en el Macizo de Cinco Villas (Pirineo Navarro). Geogaceta, 25, 115-118.

Latham, A.J., Riding, R., 1990. Fossil evidence for the location of the Precambrian–Cambrian boundary in Morocco. Nature 344, 752–754.

Latypov, R.M., Mitrofanov, F.P., Alapieti, T.T., and Halkoaho, T.A., Petrology of the Lower Layered Horizon of the Western Pansky Tundra Intrusion, Kola Peninsula, *Petrologiya,* 1999a, vol. 7, no. 5, pp. 509–538.

Le Bas, M.J., Streckeisen, A.L., 1991. The IUGS systematics of igneous rocks. J. Geol. Soc. Lond. 148, 825–833.

Leblanc, M. and Lancelot, J.R. 1980. Interprétation géodynamique du domaine pan-africain (Précambrien terminal) de l'Anti-Atlas (Maroc) à partir de données géologiques et géochronologiques, Can. J. Earth Sci. 17 (1) 142–155.

Leblanc, M., 1975. Ophiolites précambriennes et gîtes arséniés de cobalt: Bou Azzer, Maroc. Université des sciences et techniques du Languedoc, Centre géologique et géophysique, Montpellier, France.

Leblanc, M. 1981. The late Proterozoic ophiolites of bou Azzer (Morocco): evidence for Pan-African plate tectonics. In: Kroner, A. (Ed.), Precambrian Plate Tectonics. Elsevier, Amsterdam, pp. 435–451.

Le Corvec, N., Menand, T., Lindsay, J. 2013. Interaction of ascending magma with pre-existing crustal fractures in monogenetic basaltic volcanism: an experimental approach. Journal of Geophysical Research 118, 968–984.

Lefort, J.P. and Agarwal, B.N.P. 1999. Of what is the centre of the Ibero-Armorican arc composed? Tectonophysics, 302, 71–81.

Le Gall, B., Tshoso, G., Dyment, J., Kampunzu, A.B., Jourdan, F., Féraud, G., Bertrand, H., Aubourg, C., Vétel,W., 2005. The Okavango giant mafic dyke swarm (NE Botswana): its structural significance within the Karoo Large Igneous Province. J. Struct. Geol. 27, 2234–2255.

Liégeois, J. P., Benhallou, A., Azzouni-Sekkal, A., Yahiaoui, R. and Bonin, B. 2005. The Hoggar swell and volcanism: reactivation of the Precambrian Tuareg shield during Alpine convergence and West African Cenozoic volcanism. In: Foulger, G. R., Natland, J. H., Presnall, D. C. and Anderson, D. L. (eds) Plates, Plumes and Paradigms. Geological Society of America, Special Paper, 388, 379–400.

Lister, J.R., Kerr, R.C., 1991. Fluid-mechanical models of crack propagation and their application to magma transport in dykes. J. Geophys. Res. 96, 10049–10077.

López-Gómez, J., Arche, A., Pérez-López, A., 2002. Permian and Triassic. In: Gibbons, W., Moreno, T. (Eds.), The Geology of Spain. The Geological Society, London, pp. 185–212.

Losantos, M., Montaner, J., Solà, J., Mató, E., Sampsó, J., Picart, J., Calvet, F., Enrique, P., Ferrés, M., Solé, J., 2000. Mapa Geològic de Catalunya 1:25.000, Palafrugell 335-1-1 (79–25), ICC (Servei Geològic de Catalunya), Barcelona.

Maaløe, S. 1987. The generation and shape of feeder dykes from mantle sources. Contributions to Mineralogy and Petrology 96, 47-55.

Maccaferri F., Bonafede M. and Rivalta E. 2010. A numerical model of dyke propagation in layered elastic media. Geophysical Journal International 180, 1107-1123.

Mahan, Kevin H. , Bartley, John M., Coleman, Drew S., Glazner, Allen F. and Carl, Brian S. 2003. Sheeted intrusion of the synkinematic McDoogle pluton, Sierra Nevada, California Geological Society of America Bulletin; 115, no. 12;1570-1582.

Manzoni, M. 1975. Paleomagnetic data from tertiary volcanics of the Campidano and associated grabens, Sardinia, Earth Planet. Sci. Lett., 27, 275–282.

Mardia, K.V., 1972. Statistics of Directional Data. Academic Press, New York.

Malusa, M. G., Polino, R., Feroni, A. C., Ellero, A., Ottria, G., Baidder, L. and Musumeci, G. 2007. Post-Variscan tectonics in eastern Anti-Atlas (Morocco). Terra Nova, 19, 481–489.

Margaritz, M.,Kirschvink, J.L., Latham,A.J., Zhuravlev, A.Y.,Rozanov,A.Y.,1991. Precambrian/ Cambrian boundary problem: carbon isotope correlations for Vendian and Tommotian time between Siberia and Morocco. Geology 19, 847–850.

Marsh, B.D. 1982. On the mechanics of igneous diapirism, stoping and zone melting. American Journal of Science 282, 808-855.

Martí, J. 1996. Genesis of crystal-rich volcaniclastic facies in the Permian red beds of the Central Pyrenees (NE Spain). Sedimentary Geology, 106, 1–19.

Martí, J. and Barrachina, A. 1987. Las ignimbritas de Castellar de N'Hug, Pirineo Catalan. Acta Geologica Hispanica, 21–22, 561–568.

Martin, M.W., Glazner, A.F., Walker, J.D., and Schermer, E.R. 1993. Evidence for right-lateral transfer faulting accommodating en echelon Miocene extension, Mojave Desert, California: Geology, v. 21, p. 355-358.

Martínez-Poza, A. I. and Druguet, E. 2015. Brittle and ductile deformation around partially melted stepped dykes: insights from analogue modelling. Geogaceta, vol. 57.

Martínez-Poza, A.I., Druguet, E., Castaño, L.M., Carreras, J., 2012. The Aiguablava dyke swarm from a structural point of view. Geotemas 13, 153.

Martinez-Poza, A.I., Druguet, E., Castaño, L.M. and Carreras, J. 2014. Dyke intrusion into a pre-existing joint network: The Aiguablava lamprophyre dyke swarm (Catalan Coastal Ranges). Tectonophysics, 630, 75-90.

Martinez-Poza, A.I., Glazner, A.F. and Bartley, John M. 2013. 3D analysis of a multiple dike intrusion and later deformation, Independence Dike Swarm, California. Geological Society of America *Abstracts with Programs*, Vol. 45, No. 7, p. 612.

Marx, J., Huebscher, H. D., Hoth, K., Korich, D. and Kramer, W. 1995. Vulkanostratigraphie und Geochemie der Eruptivkomplexe. In: Plein, E. (ed.) Norddeutsches Rotliegendbecken. Rotliegend- Monographies, Tiel II, Courier Forschungs-Institut, Senckenberg, 183, 54–83.

Marzoli, A., Renne, P. R., Piccirillo, E. M., Ernesto, M., Bellieni, G. and De Min, A. 1999. Extensive 200-million-year-old continental flood basalts of the Central Atlantic Magmatic Province, Science, 284, 616–618.

Matte, P. 2001. The Variscan collage and orogeny (480-290 Ma) and the tectonic definition of the Armorica microplate: a review. *Terra Nova*, 13 (2): 122-128.

Mauldon, M., Dunneb, W.M., Rohrbaugh Jr., M.B., 2001. Circular scanlines and circular windows: new tools for characterizing the geometry of fracture traces. J. Struct. Geol. 23, 247–258.

May, S.R., Beck, M.E., Jr., and Butler, R.F. 1986. North American apparent polar wander, plate motion, and left-oblique convergence: Late Jurassic-Early Cretaceous orogenic consequences: Tectonics, v. 8, p. 443-451.

May, S.R., and Butler, R.F. 1989. North American Jurassic apparent polar wander: implications for plate motion, paleogeography, and Cordilleran tectonics: Journal of Geophysical Research, v. 91, p. 11519-11544.

Mazzarini, F., Isola, I., 2007. Hydraulic connection and fluid overpressure in upper crustal rocks: evidence from the geometry and spatial distribution of veins at Botrona quarry, southern Tuscany, Italy. J. Struct. Geol. 29, 1386–1399.

Mazzarini, F., Musumeci, G., Cruden, A.R., 2011. Vein development during folding in the upper brittle crust: the case of tourmaline-rich veins of eastern Elba Island, northern Tyrrhenian Sea, Italy. J. Struct. Geol. 33, 1509–1522.

McBirney, A.R., Murase, T. 1984. Rheological properties of magmas. Ann. Rev. Earth Planet. Sci. 12, 337-357.

McCaffrey, R., 1992. Oblique plate convergence, slip vectors, and forearc deformation. Journal of Geophysical Research 97, 8905-8915.

Mccann, T. 1996. The North Celtic Sea Reflector—a possible Caledonian basement structure, offshore southern Ireland. Tectonophysics, 266, 361–377.

Mccann, T., Pascal, C., Timmerman, M.J., Krzywiec, P., López-Gómez, J., Wetzel, A., Krawczyk, M., Rieke, H. and Lamarche, J. 2006 Post-Variscan (end Carboniferous–Early Permian) basin evolution in Western and Central Europe from Gee, D. G. and Stephenson, R. A. (eds). European Lithosphere Dynamics.
Geological Society, London, Memoirs, 32, 355–388. 0435-4052/06.

McClay, K.R. 1976. The rheology of plasticine. Tectonophysics, 33, T7-T15.

Macdonald, G. A., and Katsura, T. 1964. Chemical composition of Hawaiian lavas: Journal of Petrology, v. 5, p. 82-133.

McKeagney, C.J., Boulter, C.A., Jolly, R.J.H., Foster, R.P., 2004. 3-D Mohr circle analysis of vein opening, Indarama lode-gold deposit, Zimbabwe: implications for exploration. J. Struct. Geol. 26, 1275–1291.

McKenzie, D. P., and J. A. Jackson. 1983. The relationship between strain rates, crustal thickening, paleomagnetism, finite strain, and fault movement within a deforming zone, Earth Planet. Sci. Lett., 65, 182–202.

McManus, S.G., and Clemens-Knott, D. 1997. Geochemical and oxygen isotope constraints on the petrogenesis of the Independence dike swarm, San Bernardino Co., California, *in* Girty, G.H., Hanson, R.E., and Cooper, J.D. (eds.), Geology of the western Cordillera: perspectives from undergraduate research: Pacific Section Society of Economic Paleontologists and Mineralogists, v. 82, p. 91-102.

Means,W.D., Hobbs, B.E., Lister, G.S., Williams, P.F. 1980. Vorticity and non coaxiality in progressive deformation. Journal of Structural Geology 2, 371–378.

Mehnert, K.R. 1968. Migmatites and the Origin of Granitic Rocks. Elsevier, Amsterdam.

Mériaux, C., Jaupart, C. 1998. Dike propagation through an elastic plate. Journal of Geophysical Research 103, 18295-18314.

Michard, A., Yazidi, A., Benziane, F., Hollard, H. and Willefert, S. 1982. Foreland thrusts and olistostromes on the pre-Sahara margin of the Variscan Orogen, Morocco, Geology 10 (5) 253–256.

Michard, A., 1976. Elements de ge´ologie marocaine. Notes et Mémoires du Service Géologique du Maroc 252.

Mifdal, A., Peucat, J.J., Charlot, R., 1982. NDS 250, Precambrian– Cambrian, U–Pb/zircon, Morocco. In: Odin, G.S. (Ed.), Numerical Dating in Stratigraphy, Part II. Wiley, Chichester, United Kingdom, pp. 941–943.

Mitchell, R.H., 1994. The lamprophyre facies. Mineral. Petrol. 51, 137–146.

Mitra, G. and Mount, V.S. 1998. Foreland basement involved structures, AAPG Bull. 82 (1), 70–109.

Mondal, T.K., Mamtani, M.A., 2013. 3-D Mohr circle construction using vein orientation data from Gadag (southern India) — implications to recognize fluid pressure fluctuation. J. Struct. Geol. 56, 45–56.

Montigny, R., J. Edel, and R. Thuizat. 1981. Oligo-Miocene rotation of Sardinia: K-Ar ages and paleomagnetic data of Tertiary volcanics, Earth Planet. Sci. Lett., 54, 261–271.

Moore, J.G. 1963. Geology of the Mt. Pinchot quadrangle, southern Sierra Nevada, California: U.S. Geological Survey Bulletin 1138, 152 p.

Moore, J.G., and Hopson, C.A. 1961. The Independence dike swarm in eastern California: American Journal of Science, v. 259, p. 241-259.

Mortaji, A., 1989. La boutonniere precambrienne de la Tagragra d'Akka (Anti-Atlas occidental; Maroc): Petrologie et geochimie des granitoides, filons basiques et metamorphismes associees. Unpublished These 3eme cycle. Universite de Nancy I, France, 211 p.

Moser, E., V. Bachtadse, D. Kent, G. Muttoni, and A. Ronchi. 2005. Paleomagnetism of Permian sediments and volcanic rocks from Sardinia, Eos Trans. AGU, 86(52), Fall Meet. Suppl., Abstract GP11A-0014.

Muller W, Shelley M, Miller P, and Broude S. 2009. Initial performance metrics of a new custom-designed ArF excimer LA-ICPMS system coupled to a two-volume laser-ablation cell. Journal of Analytical Atomic Spectrometry 24: 209–214.

Murase, T., McBirney, A.R. 1973. Properties of some common igneous rocks and their melts at high temperatures. Geological Society of America Bulletin, 84, 3563-3592.

Muttoni, G., D. V. Kent, E. Garzanti, P. Brack, N. Abrahamsen, and M. Gaetani. 2003. Early Permian Pangea B to Late Permian Pangea A, Earth Planet. Sci. Lett., 215, 379–394.

Nakamura, K. 1977. Volcanoes as possible indicators of tectonic stress orientation — principle and proposal. Journal of Volcanology and Geothermal Research 2, 1–16.

Nachit, H., Barbey, P., Pons, J., Burg, J.P., 1996. L'Eburne´en existe-t-il dans l'Anti-Atlas occidental marocain? L'exemple du massif du Kerdous. C.R. Acad. Sci. Paris 322 (Série IIa), 677–683.

Naidoo, D.D., Bloomer, S.H., Saquaque, A., Hefferan, K., 199 1. Geochemistry and significance of metavolcanic rocks from the Bou-Azzer El grdara ophiolite (Morocco). Precambrian Research 53, 79-97.

Neff, T.R., 1973. Emplacement of a Dike Swarm in the Buffalo Mountain Pluton, Nevada. Geol. Soc. Am. Bull. 84, 3689–3696.

Nelson, C.A. 1966a. Geologic map of the Blanco Mountain quadrangle, Inyo and Mono Counties, California: U.S. Geological Survey Geologic Quadrangle Map GQ-529, scale 1:62,500.

Nelson, C.A. 1966b. Geologic map of the Waucoba Mountain quadrangle, Inyo County, California: U.S. Geological Survey Geologic Quadrangle Map GQ-528, scale 1:62,500.

Nicholson, R., Pollard, D.D., 1985. Dilation and linkage of echelon cracks. J. Struct. Geol. 7, 583–590.

Nicoletti M., Ardanese L.R. and Colasanti S. 1982. *La granodiorite di Capo Carbonara (Sardegna-Italia). Età K/Ar di fasi minerali in paragenesi*. «Rend. Soc. It. Mineral. Petrol. », 38, 765-769.

O‘ Connor, E.A., 2010. Geology of the Draa, Kerdous, and Boumalne Districts, Anti-Atlas, Morocco. Technical Report IR/10/072. British Geological Survey, Keyworth, Nottingham, England, pp. 310.

Ode, H., 1957. Mechanical analysis of the dike pattern of the Spanish Peaks area, Colorado. Geol. Soc. Am. Bull. 68, 567–576.

Oldow, J.S., AveÂ Lallemant, H.G., Schmidt, W.J., 1984. Kinematics of plate convergence deduced from Mesozoic structures in the western Cordillera. Tectonics 3, 201±227.

Olivet, J.-L. 1996. La cinématique de la plaque ibérique, Bull. Cent. Rech. Explor. Prod. Elf Aquitaine, 20, 131–195.

Olson, J., Pollard, D.D., 1989. Inferring paleostresses from natural fracture patterns: a new method. Geology 17, 345–348.

Orejana, D., Villaseca, C., Billstrom, K., Paterson, B.A., 2008. Petrogenesis of Permian alkaline lamprophyres and diabases from the Spanish Central System and their geodynamic context within western Europe. Contrib. Mineral. Petrol. 156, 477–500.

Page, B.M., and Engebretson, D.C. 1984. Correlation between the geologic record and computed plate motions for central California: Tectonics, v. 3, p. 133-155.

Paquet, F., Dauteuil, O., Hallot, E., Moreau, F., 2007. Tectonics and magma dynamics coupling in a dyke swarm of Iceland. J. Struct. Geol. 29, 1477–1493.
Passchier, C.W., 2007. Photograph of the month. J. Struct. Geol. 29, 1871.

Parker, A.J., Rickwood, P.C., Tucker, D.H. (Eds.), 1990. Mafic Dykes and Emplacement Mechanisms. A.A. Balkema, Rotterdam.

Paschier, C.W. and Trouw, R. J. A, 2005. Microtectonics. Ed. Springer p.366.

Paterson, S.R., Fowler, T.K. 1993. Re-examining pluton emplacement processes. Journal of Structural Geology 15, 191-206.

Paterson, S.R., Tobisch, O.T. 1992. Rates of processes in magmatic arcs: Implications for the timing and nature of pluton emplacement and wall rock deformation: Journal of Structural Geology 14, 291–300.

Paterson, S.R., Vernon, R.H., Tobisch, O.T. 1989. A review of criteria for the identification of magmatic and tectonic foliations in granitoids. Journal of Structural Geology 11, 349-363.

Paton, C., Hellstrom, J., Paul, B., Woodhead, J., and Hergt, J. 2011. Iolite: freeware for the visualization and processing of mass spectrometer data. Journal of Analytical Atomic Spectrometry, 26, 2508-2518.

Paton, C., Woodhead, JD, Hellstrom JC, Hergt, JM, Greig A, and Maas R. 2010. Improved laser ablation U–Pb zircon geochronology through robust downhole fractionation correction. Geochemistry, Geophysics, Geosystems 11: Q0AA06.

Peacock, D.C.P., Sanderson, D.J. 1992. Effects of layering and anisotropy on fault geometry. Journal of the Geological Society 149, 793-802

Pearce, J.A. 1996. Sources and settings of granitic rocks. Episodes 19, 120 125.

Pennacchioni, G., Mancktelow, N.S., 2007. Nucleation and initial growth of a shear zone network within compositionally and structurally heterogeneous granitoides under amphibolite facies conditions. Journal of Structural Geology 29,1757e1780. http://dx.doi.org/10.1016/j.jsg.2007.06.002.

Pennacchioni, G. and Zucchi, E. 2013. High temperature fracturing and ductile deformation during cooling of a pluton: The Lake Edison granodiorite (Sierra Nevada batholith, California). Journal of Structural Geology 50, 54-81.

Pereira, M.F., Castro, A., Chichorro, M., Fernández, C., Díaz-Alvarado, J., Martí, J., Rodríguez, C., 2014. Chronological link between deep-seated processes in magma chambers and eruptions: Permo-Carboniferous magmatism in the core of Pangaea (Southern Pyrenees). Gondwana Res. 25, 290–308.

Petford, N., Cruden, A., McCaffrey, K., Vigneresse, J-L. 2000. Granite magma formation, transport and emplacement in the Earth's crust, Nature 408, 669-673.

Perini, G., Cebria, J.M., Lopez-Ruiz, M., Doblas, M., 2004. Carboniferous-Permian mafic magmatismin the Variscan Belt of Spain and France: implications for mantle sources. In:Wilson,M., Neumann, E.-R., Davies, G.R., Timmerman,M.J., Heeremans, M., Larsen, B.T. (Eds.), Permo-Carboniferous Magmatism and Rifting in Europe. Geol. Soc. Lond. Spec. Publ., 223, pp. 415–438 (London).

Petrus, JA and Kamber, BS. 2012. Vizual Age: A novel approach to laser ablation ICP-MS U–Pb geochronology data reduction. Geostandards and Geoanalytical Research 36: 247–270.

Pfiffner, O.A. and Ramsay, J.G. 1982. Constraints on geological strain rates: arguments from finite strain states of naturally deformed rocks. Journal of Geophysical Research, 87, 311–321.

Philpotts, A.R., Asher, P.M., 1994. Magmatic flow-direction indicators in a giant diabase feeder dike, Connecticut. Geology 22, 363±366.

Piqué, A., Bouabdelli, M., Soulaimani, A. Youbi, N. and Iliani, M.1999. Upper Neoproterozoic PIII conglomerates in the Anti-Atlas, southern Morocco; Pan-African molasses, or indicators of Upper Proterozoic rifting?, C. R. Acad. Sci. Paris, Ser. IIa 328 (6) 409–414.

Pirinu M.N., 1991. Le sieniti del Sarrabus meridionale. Tesi di Dottorado, Università di Napoli.

Pisonero J, Fliegel D, and Gu¨nther D. 2006. High efficiency aerosol dispersion cell for laser ablation-ICP-MS. Journal of Analytical Atomic Spectrometry 21. 922–931.

Pitcher, W.S. 1979. The Nature, ascent and emplacement of granitic magmas. J. Geol. Soc. of London 136, 627-662.

Platten, I.M., 2000. Incremental dilation of magma filled fractures: evidence from dykes on the Isle of Skye, Scotland. J. Struct. Geol. 22, 1153–1164.

Pollard, D.D., 1973. Derivation and evaluation of a mechanical model for sheet intrusions. Tectonophysics,19, 233–269.

Pollard, D.D., 1987. Elementary fracturemechanics applied to the structural interpretation of dykes. In: Halls, H.C., Fahrig, W.H. (Eds.), Mafic Dyke Swarms. Geol. Assoc. Can. Spec. Pap., 34, pp. 5–24.

Pollard, D., Aydin, A., 1984. Propagation and linkage of oceanic ridge segments. J. Geophys. Res. 89, 10017–10028.

Pollard, D., Aydin, A., 1988. Progress in understanding jointing over the past century. Geol. Soc. Am. Bull. 100, 1181–1204.

Pollard, D. D., Fink, J. H., and Delaney, P. T. 1984. Igneous dikes at Long Valley, CA; emplacement mechanisms and associated geologic structures. In Proceedings of Workshop XIX (pp. 130-146).

Powell, R.E., Whittington, C.L., Grauch, V.J.S., and McColly, R.A., 1984, Mineral resources potential of the Eagle Mountains wilderness study area (CDCA-334), Riverside County, California: U.S. Geological Survey Open File Report 84–631, 25 p.

Ramsay, J.G. 1981. Emplacement mechanics of the Chindamora Batholith, Zimbabwe. Journal of Structural Geology, 3, 93.

Ramsay, J.G. 1989. Emplacement kinematics of a granite diapir: The Chindamora batholith, Zimbabwe. Journal of Structural Geology 11, 191-209.

Ramsay, J.G., Lisle, R., 2000. The techniques of modern structural geology. Volume 3: applications of continuum mechanics in structural geology. Academic Press, London.

Ranalli, G. 1995. Rheology of the Earth, 2nd ed., Chapman & Hall, London.

Riley, T.R., Leat, P.T., Curtis, M.L., Millar, L.L., Fazel, A., 2005. Early-Middle Jurassic dolerite dykes from western DronningMaud Land (Antarctica): identifying mantle sources in the Karoo large igneous province. J. Petrol. 46, 1489–1524.

Rinehart, C.D., and Ross, D.C. 1964. Geology and mineral deposits of the Mount Morrison quadrangle, Sierra Nevada, California: U.S. Geological Survey Professional Paper 385, 106 p.

Rivalta, E., Böttinger, M., Dahm, T., 2005. Buoyancy-driven fracture ascent: experiments in layered gelatine. J. Volcanol. Geotherm. Res. 144, 273–285.

Rivalta, E., Taisne, B., Bunger, A. P., Katz, R. F. 2015. A review of mechanical models of dike propagation: Schools of thought, results and future directions. Tectonophysics, 638, 1–42.

Rivers, T., Corrigan D. 2000. Convergent margin on southeastern Laurentia during the Mesoproterozoic: tectonic implications, Can. Journal of Earth Sciences 37, 359–383.

Robardet, M. 2003. The Armorica „microplate": fact or fiction? Critical review of the concept and contradictory palaeobiogeographical data. Palaeogeography, Palaeoclimatology, Palaeoecology, 195: 125-148.

Rogers, R.D., Bird, D.K., 1987. Fracture propagation associated with dike emplacement at the Skaergaard intrusion, East Greenland. J. Struct. Geol. 9, 71–86.

Roger, J., Gasquet, D., Baudin, T., Chalot-Prat, F., Hassenforder, B., Marquer D., Chèvremont, P., Berrahma, A., Destombes, J., Razin, P. and Benlakhdim, A., 2001. Carte géologique au 1/50 000 feuille Tamazrar. Notes et Mémoires du Service Géologique du Maroc 415.

Rodgers, J. 1987. Lines of basement uplifts within cratons marginal to orogenic belts, Am. J. Sci. 287, 661–692.

Rollet, N., Déverchère, J., Beslier, M.-O., Guennoc, P., Réhault, J.-P., Sosson, M., and Truffert, C. 2002. Back arc extension, tectonic inheritance and volcanism in the Ligurian Sea, Western Mediterranean: Tectonics, v. 21, p. 10.1029/2001TC900027.

Román-Berdiel, T., 1999. Geometry of granite emplacement in the upper crust: contributions of analogue modelling. In: Castro, A., Fernandez, C., Vigneresse, J.L. (Eds.), Understanding Granites: Integrating New and Classical Techniques: Geological Society, London, Special Publication, vol. 168, pp. 7794.

Román-Berdiel, T., Aranguren, A., Cuevas, J., Tubía, J.M., Gapais, D., Brun, J.P. 2000. Experiments on granite intrusions in transtension. En: J.L. Vigneresse, Y. Mart and B. Vendeville (Eds.): Salt, Shale and Igneous Diapirs in and Around Europe. Geological Society, London, Special Publications 174, 21 42.

Román-Berdiel, T., Gapais, D., Brun, J.P. 1997. Granite intrusion along strike-slip zones in experiment and nature. American Journal of Science 297, 651–678.

Ron, H., and Nur, A. 1996. Vertical axis rotation in the Mojave: evidence from the Independence dike swarm: Geology, v. 24, p. 973-976.

Ron, H., and Nur, A. 1997. Vertical axis rotations in the Mojave; evidence from the Independence dike swarm; Reply to comment: Geology, v. 25, p. 1052.

Ronca S., 1996. Petrologia del magmatismo filoniano tardo-ercinico del Sarrabus (Sardegna sud-orientale). Tesi di Dottorato, Universita degli Studi di Perugia.

Ronca S. and Traversa G., 1996. LateHercynian dyke magmatism of Sarrabus (SE Sardinia). Per. Mineral. , 65, 35-70.

Ronca, S., del Moro, A., Traversa, G., 1999. Geochronology, Sr–Nd isotope geochemistry and petrology of late-Hercynian dyke magmatism from Sarrabus (SE Sardinia). Period. Mineral. 68, 231–260.

Ronchi, A., Broutin, J., Diez, J. B., Freytet, B., Galtier, J., and Lethiers, F. (1998). New palaeontological discoveries in some Early Permian sequences of Sardinia. Biostratigraphic and palaeogeographic implications. C. R. Acad. Sci. Paris, 327, 713-719.

Rosenbaum, G., G. Lister, and C. Duboz. 2002. Relative motions of Africa Iberia, and Europe during Alpine orogeny, Tectonophysics, 359, 117–129.

Rubin, A., 1993a. Dikes vs. diapirs in viscoelastic rocks. Earth Planet. Sci. Lett. 19, 641–659.

Rubin, A.M., 1995. Propagation of magma-filled cracks. Annu. Rev. Earth Planet. Sci. 23, 287–336.

Ryan, M.P., Blevins, J.Y.K. 1987. The viscosity of synthetic and natural silicate melts and glasses at high temperatures and at 1 bar (105Pa) pressure and at higher pressures, U.S. Geol. Surv. Bull., 17864, 563 pp.

Saleeby, J.B., Kistler, R.W., Longiaru, S., Moore, J.G., and Nokleberg, W.J. 1990. Middle Cretaceous silicic metavolcanic rocks in the Kings Canyon area, central Sierra Nevada, California, in Anderson, J.L., ed., The nature and origin of Cordilleran magmatism: Boulder, Colorado, Geological Society of America Memoir 174, p. 251–270.

San Miguel Arribas, A., 1952. Observations pétrologiques sur les roches lamprophyriques de la Costa Brava Catalanne (Bagur). Comptes Rendus XIXth International Geological Congress, Algiers, pp. 77–79.

Samson, S. D., Inglis, J. D., D'Lemos, R. S., Admou, H., Blichert-Toft, J. and Hefferan, K. 2004. Geochronological, geochemical, and Nd-Hf isotopic constraints on the origin of Neoproterozoic

plagiogranites in the Tasriwine ophiolite, Anti-Atlas orogen, Morocco. Precambrian Research, 135, 133–147.

San Miguel de la Cámara, M., 1936. Estudio de las rocas eruptivas de España.
Memorias de la Academia de Ciencias de Madrid. Serie Ciencias Naturales, Tomo 6 (660 pp.).

Santana, V., Vegas, N., Pinotti, L., Tubía, J.M., 2006. Fábrica magnética de diques doleríticos del Plutón de Panticosa (Zona Axial, Pirineos). Geogaceta 39, 19–22.

Saquaque, A., Admou, H., Karson, J.A., Hefferan, K. and Reuber, I. 1989. Precambrian accretionary tectonics in the Bou Azzer-El Grara region, Anti-Atlas, Morocco, Geology 17, 1107–1110.

Sato, K., Yamaji, A., Tonai, S., 2013. Parametric and non-parametric statistical approaches to the determination of paleostress from dilatant fractures: application to an Early Miocene dike swarm in central Japan. Tectonophysics, 588, 69–81.

Scaillet, B., Holtz, F., Pichavant, M. 1998. Phase equilibrium constraints on the viscosity of silicic magmas I: Volcanic plutonic comparison. Journal of Geophysical Research 103, 27257–27266.

Scarrow, J.H., Molina, J.F., Bea, F., Montero, P., Vaughan, A.P.M., 2011. Lamprophyre dikes as tectonic markers of late orogenic transtension timing and kinematics: a case study from the Central Iberian Zone. Tectonics 30, TC4007.

Schaltegger, U. and Brack, P. 1999. Short-lived events of extension and volcanism in the Lower Permian of the Southern Alps (Northern Italy, Southern Switzerland). Journal of Conference Abstracts, 4, 296–297.

Schenk, P.E. 1971. Southeastern Atlantic Canada, Northwestern Africa, and Continental Drift, Can. J. Earth Sci. 8, 1218–1251.

Schermer, E.R., and Busby, C.J. 1994. Jurassic magmatism in the central Mojave Desert: Implications for arc paleogeography and preservation of continental volcanic sequences: Geological Society of America Bulletin, v. 106, p. 767-790.

Schermer, E.R. 1993. Mesozoic structural evolution of the west-central Mojave Desert, *in* Dunne, G. and McDougall, K.A. (eds.), Mesozoic paleogeography of the western United States II: Pacific Section, Society of Economic Paleontologists and Mineralogists, p. 307-322.

Schlische, R.W. 2003. Relative timing of CAMP, rifting, continental breakup, and basin inversion; tectonic significance. En: Hames, W E; McHone, J Gregory; Renne, Paul R; Ruppel, C., eds., The Central Atlantic Magmatic Province; insights from fragments of Pangea. Geophysical Monograph, vol.136, pp.33-59.

Schoene, B. 2013. U-Th-Pb Geochronology, In Holland, H.D. and Turekian, K.K., *Treatise on Geochemistry 2nd edition, vol. 4,* p 341-378. Oxford: Elsevier.

Schweickert, R.A., and Lahren, M.M. 1990. Speculative reconstruction of the Mojave-Snow Lake fault: Implications for Paleozoic and Mesozoic orogenesis in the western United States: Tectonics, v. 9, p. 1609-1629.

Secchi F., Brotzu P. and Callegari E. 1991. The Arburése igneous body (SW Sardinia, Italy) An example of dominant igneous fractionation leading to peraluminous cordierite-bearing leucogranites as residual melts-. «Chem. Geol.», 92, 213-249.

Secchi, F., Lorrai, M. 2001. Some geological and environmental aspects of the Sàrrabus-Gerrei Region (SE Sardinia, Italy). Rendiconti Seminario Facoltà Scienze Università Cagliari Supplemento Vol. 71 Fasc. 2, 187-208.

Sederholm, J.J. 1907. Om granit och gneis, deras uppkomst, upp tradande och utbred ning inom urberget I Fennoskandia. Bulletin de la Commission Géologique de Finlande 23, 110 pp.

Sengupta, S. 1997. Contrasting fabrics in deformed dykes and host rocks: natural examples and a implified model. In: Sengupta, S. (Ed.), Evolution of Geological Structures in Micro- to Macro-scales. Chapman and Hall, London, pp. 293–318.

Sibson, R.H., Robert, F., Poulson, K.H., 1988. High-angle reverse faults, fluid-pressure cycling, and mesothermal gold–quartz deposits. Geology 16, 551–555.

Sisson, T.W., Grove, T.L., and Coleman, D.S., 1996, Hornblende gabbro sill complex at Onion Valley, California, and a mixing origin for the Sierra Nevada batholith: Contributions to Mineralogy and Petrology, v. 126, p. 81–108, doi: 10.1007/s004100050237.

Sleep, N.H. 1988. Tapping of melt by veins and dykes. Journal of Geophysical Research 93, 10,255-10,272.

Smith, A.G. 1999. Gondwana: its shape, size and position from Cambrian to Triassic times, J. Afr. Earth Sci. 28 (1) 71–97.

Smith, G.I. 1962. Large left-lateral displacement on Garlock fault, California, as measured from offset dike swarm: American Association of Petroleum Geologists Bulletin, v. 46, p. 85-104.

Smith, J.V., 1996. Geometry and kinematics of convergent conjugate vein array systems. Journal of Structural Geology 18, 1291–1300.

Solé, J., Pi, T., Enrique, P., 2003. New geochronological data on the Late Cretaceous alkaline magmatism of the northeast Iberian Peninsula. Cretac. Res. 24, 135–140.

Sorensen, S.S., Dunne, G.C., Hanson, R.B., Barton, M.D., Becker, J., Tobisch, O.T., and Fiske, R.S., 1998, From Jurassic shores to Cretaceous plutons: Geochemical evidence for paleoalteration environments of metavolcanic rocks, eastern California: Geological Society of America, v. 110, p. 326–343, doi: 10.1130/0016-7606(1998)110<0326:FJSTCP>2.3.CO;2.

Soulaimani, A. 1998. Dynamique et interactions Socle/Couverture dans l'Anti-Atlas occidental (Maroc) : Rifting fini-protérozoïque et orogenèse hercynienne.
Soulaimani, A., Le Corre, C. and Farazdaq, R. 1997. Deformation hercynienne et relation socle/couverture dans le domaine du Bas-Draa (Anti-Atlas occidental, Maroc), J. Afr. Earth Sci. 24 (3) 271–284.

Soulaimani, A., Piqué, A. and Bouabdelli, M. 2001. La série du PII–PIII de l'Anti-Atlas occidental (Sud marocain): un olistostrome à la base de la couverture post-panafricaine (PIII) du Protérozoïque supérieur, Earth Planet. Sci. Lett. 332, 121–127.

Soulaimani, A., Bouabdelli, M. and Piqué, A. 2003. L'extension continentale au Néo-Protérozoïque supérieur–Cambrien inférieur dans l'Anti-Atlas (Maroc), Bull. Soc. géol. France 174 (1) 83–92.

Soulaimani, A., Bertrand, H., El Janati, M., Chaham, K.R., Laville, E., Piqué, A., Amrhar, M. and Charroud, M. 2004. A restatement of the Mesozoic Atlasic rifting (Morocco). Journal of African Earth Sciences, 38, 145–153.

Speight, J. M. and Mitchell, J. G. 1979. The Permo-Carboniferous dyke-swarm of northern Argyll and its bearing on dextral displacement on the Great Glen Fault. Journal of the Geological Society, London, 136, 3–11.

Spence, D.A., Turcotte, D.L., 1985. Magma-driven propagation of cracks. J. Geophys. Res. 90, 575–580.

Spence, D.A., Turcotte, D.L. 1990. Buoyancy-driven magma fracture: a mechanism for ascent through the lithosphere and the emplacement of diamonds. Journal of Geophysical Research B95, 5133–5139.

Spence, D., Sharp, P. and Turcotte, D. 1987. Buoyancy-driven crack propagation: a mechanism for magma migration. Journal of Fluid Mechanics 174, 135–153.

Spera, F.J., Borgia, A., Strimple, J. 1988. Rheology of melts and magmatic suspensions 1. Design and calibration of concentric cylinder viscometer with application to rhyolite magma. Journal of Geophysical Research 93, 10,273– 10,294.

Speranza, F., Villa, J.M., Sagnotti, L., Florindo, D., Cosentino, P., Cipollari, P., Mattei, M., 2002. Age of the Corsica–Sardinia rotation and Liguro–Provençal Basin spreading: new paleomagnetic and Ar/Ar evidence. Tectonophysics, 347, 231–251.

Srivastava, R.K. (Ed.), 2011. Dyke Swarms: Keys for Geodynamic Interpretation. Springer-Verlag, Berlin, Heidelberg.

Stampfli, G.M. 1993. Le Briançonnais, terrain exotique dans les Alpes? Eclogae geologicae Helvetiae. 86(1), 1-45.

Stampfli, G.M. and Borel, G.D. 2002. A plate tectonic model for the Paleozoic and Mesozoic constrained by dynamic plate boundaries and restored synthetic oceanic isochrons, Earth Planet. Sci. Lett. 196 (1–2) 17–33.

Stephens, K.A., Schermer, E.R., and Walker, J.D. 1993. Mesozoic intra-arc tectonics in the Northeast Mojave Desert, California: Geological Society of America Abstracts with Programs, v. 25, p. 150.

Stern, T.W., Bateman, P.C., Morgan, B.A., Newell, M.F., and Peck, D.L. 1981. Isotopic U-Pb ages of zircons from the granitoids of the central Sierra Nevada: U.S. Geological Survey Professional Paper, v. 1071, p. 17.

Stone, D. 2002. Morphology of the Casper Mountain uplift and related subsidiary structures, central Wyoming: Implications for Laramide kinematics, dynamics, and crustal inheritance, AAPG Bull. 86 (8) 1417–1440.

Sumita, I., Ota, Y., 2011. Experiments on buoyancy-driven crack around the brittle–ductile transition. Earth Planet. Sci. Lett. 304, 337–346.

Sun, S.S., McDonough, W.F., 1989. Chemical and isotopic systematics of oceanic basalts: implications for the mantle composition and processes. In: Saunders, A.D., Norry, M.J. lEds.), Magmatism in the Ocean Basins. Geolgical Society London Publication 42, 313-345.

Sylvester, A.G. 1988. Strike-slip faults: Geological Society of America Bulletin, v. 100, p. 1669-1703.

Sylvester, PJ. 2008. LA-(MC)-ICP-MS trends in 2006 and 2007 with particular emphasis on measurement uncertainties. Geostandards and Geoanalytical Research 32: 469–488.

Takada, A. 1994. Accumulation of magma in space and time by crack interaction. En: Ryan, M.P. (Ed.): Magmatic Systems, pp. 241–257. Academic Press, San Diego.

Talbot, C.J. and Sokoutis, D. 1995. Strain ellipsoids from incompetent dykes: Application to volume loss during mylonitization in the Singö gneiss zone, central Sweden. Journal of Structural Geology 17, 927-948.

Taylor, G.K., Randall, D.E., 2000. Structural analysis of dyke emplacement directions as an aid to palaeomagnetic studies: an example from northern Chile. Geophys. J. Int. 141, 252–258.

Tentler, T., Amcoff, O., 2010. Interaction of microfractures: the mechanism of network building. Tectonophysics, 485, 215–230.

Thomas, R.J., Chevallier, L.P., Gresse, P.G., Harmer, R.E., Eglington, B.M., Armstrong, R.A., De Beer, C.H., Martini, J.E.J., De Kock, G.S., Macey, P.H. and
Ingram, B.A. 2002. Precambrian evolution of the Sirwa Window, Anti-Atlas Orogen, Morocco, Precambr. Res. 118, 1–57.

Thomas, R. J., Fekkak, A., Ennih, N., Errami, E., Loughlin, S.C., Gresse, P.G., Chevallier, L.P., Liégeois, J.-P. 2004. A new lithostratigraphic framework for the Anti-Atlas Orogen, Morocco. Journal of African Earth Sciences, 39, 217–226.

Tikoff, B., Teyssier, C. 1992, Crustal-scale, en-echelon —P-shear" tensional bridges; A possible solution to the batholithic room problema. Geology 20, 927–930.

Tobisch, O.T., Paterson, S.R., Longiaru, S., and Bhattacharya, T. 1987. Extent of the Nevadan Orogeny, central Sierra Nevada, California: Geology, v. 15, p. 132-135.

Toda, S., Stein, R., 2002. Evidence from the AD 2000 Izu islands earthquake swarm that stressing rate governs seismicity. Nature 419, 58–61.
Tokarski, A.K., 1990. Dyke swarms as stress indicators: two constraints. In: Parker, A.J., Rickwood, P.C., Tucker, D.H. (Eds.), Mafic Dykes and Emplacement Mechanisms. A. A. Balkema, Rotterdam, pp. 101–104.

Tommasini S. Poli G. 1992. Petrology of the late-Carboniferous Punta Falcone gabbroic complex, northern Sardinia, Italy. Contrib. Mineral. Petrol., 110, 16-32.

Traversa G., Ronca S., Del Moro A., Pasquali C., Buraglini N. and Barabino G., 2003. Late to post-hercynian dike activity in the Sardinia-Corsica Domain: A transition from orogenic calc-alkaline to anorogenic alkaline magmatism. Boll. Soc. Geol. It., Vol. Spec., 2: 131.152.

Traversa G. and Vaccaro C. 1992. REE distribution in the late hercynian dykes from Sardinia. IGCP n.276, Newsletter, Vol. 5, Siena 1992, 215-226.

Treagus, S.H. 1983. A theory of finite strain variation through contrasting layers, and its bearing on cleavage refraction. Journal of Structural Geology 5, 351-368.

Treagus, S.H. 1988. Strain refraction in layered systems. Journal of Structural Geology 10, 517-527.

Treagus, S.H. 1999. Are viscosity ratios measureable from cleavage refraction? Journal of Structural Geology 21, 895–901.

Tryggvason, E., 1984. Widening of the Krafla fissure swarm during the 1975–1981 volcano-tectonic episode. Bull. Volcanol. 47, 47–69.

Tryggvason, E., 1986. Multiple magma reservoirs in a rift zone volcano: ground deformation and magma transport during the September 1984 eruption of Krafla, Iceland. J. Volcanol. Geotherm. Res. 28, 1–44.

Turcotte, D.L. 1987. Physics of magma segregation processes, Magmatic processes: physiochemical principles. Geochemical Society, Special Publication 1, 69–74.

Turcotte, D.L., Schubert, G. 1982. Geodynamics: Applications of Continuum Physics to Geological Problems. Wiley, New York, 450 pp.

Ubide, T., 2013. The Cretaceous Alkaline Magmatismin Northeast Iberia: Igneous Processes and Geodynamic Implications. Ph.D. thesis , Universidad de Zaragoza.

Ubide, T., Galé, C., Arranz, E., Lago, M., 2008. Composition of the Aiguablava Camptonite Sill (Costa Brava Batholith). Macla 9, 249–250.

Ubide, T., Lago,M., Arranz, E., Galé, C., Larrea, P., 2010. The lamprophyric sub-vertical dyke swarm from Aiguablava (Catalonian Coastal Ranges): petrology and composition. Geogaceta 49, 83–86.

Umili, G., Ferrero, A., Einstein, H.H., 2013. A new method for automatic discontinuity traces sampling on rock mass 3D model. Comput. Geosci. 51, 182–192.

Vaccaro C. 1990. Magmatismo filoniano Carbonifero-Permiano della Sardegna: consederazioni geologiche, petrologiche e geocronologiche. Tesi di Dottorato, Consorzio Università di Napoli-Catania.

Vaccaro C., Atzori P., Del Moro A., Oddone M., Traversa G. and Villa I., 1991. Geochronology and Sr Isotope geochemistry of late-hercynian dykes from Sardinia. Schweitz. Mineral. Petrogr. Mitt., 71, 221-230.

Valentine, G.A., Krogh, K.E.C., 2006. Emplacement of shallow dikes and sills beneath a small basaltic volcanic center – The role of pre-existing structure (Paiute Ridge, southern Nevada, USA). EPSL 246, 217–230.

van Achterbergh, E, Ryan CG, Jackson SE, and Griffin WL. 2001. Data reduction software for LA-ICPMS: Appendix. In: Sylvester PJ (ed.) Laser Ablation ICP–MS in the Earth Sciences: Current Practices and Outstanding Issues, Mineralogical Association of Canada Short Course Series, vol. 29, pp. 239–243. Ottawa: Mineralogical Association of Canada.

Vanderhaeghe, O., 1999. Pervasivemelt migration from migmatites to leucogranite in the Shuswap metamorphic core complex, Canada: control of regional deformation. Tectonophysics, 312, 35–55.

Vanderhaeghe, O. 2001. Melt segregation, pervasive melt migration and magma mobility: the structural record from pores to orogens. Physics and Chemistry of the Earth 26, 213-223.

Van der Voo, R. 1969. Paleomagnetic evidence for the rotation of the Iberian peninsula, Tectonophysics, 7, 5–56.

Verati, C., Bertrand, H. and Feraud, G. 2005. The farthest record of the Central Atlantic Magmatic Province into West Africa craton: Precise 40Ar/39Ar dating and geochemistry of Taoudenni basin intrusives (northern Mali). Earth and Planetary Science Letters, 235, 391–407.

Vétel, W., Cartwright, J., 2010. Emplacement mechanics of sandstone intrusions: insights from the Panoche Giant Injection Complex, California. Basin Res. 22, 783–807.

Vicat, J.P., Léger, J.M., Nsifa, E., Piguet, P., Nzenti, J.P., Tchaméni, R. and Pouclet, A., 1996. Distinction, au sein du craton congolais du Sud-Ouest du Cameroun, de deux épisodes doléritiques initiant les cycles orogeniques éburnéen (Paléoprotérozoique) et panafricain (Néoprotérozoïque). C. R. Acad. Sci. 323 (7), 575–582.

Vigliotti, L., W. Alvarez, and M. O. McWilliams. 1990. No relative rotation detected between Corsica and Sardinia, Earth Planet. Sci. Lett., 98, 313–318.
Villasimius page geological map (DEM 5m). Geografia della Sardegna. Sardegna Geoportale (http://www.sardegnageoportale.it/). Region della Sardegna.

Vigneresse, J.L., Barbey, P., Cuney, M. 1996. Rheological transitions during partial melting and crystallisation with application to felsic magma segregation and transfer. Journal of Petrology. 6, 1579 - 1600.

Vigneresse, J.L., Clemens, J.D. 2000. Granitic magma ascent and emplacement: neither diapirism nor neutral buoyancy. Geological Society, London, Special Publications 174, 1-19.

Vigneresse, J.L., Tikoff, B. 1999. Strain partitioning during partial melting and crystallizing felsic magmas. Tectonophysics, 312, 117–132.

Villasimius page geological map (DEM 5m). Geografia della Sardegna. Sardegna Geoportale (http://www.sardegnageoportale.it/). Region della Sardegna.

Walker, J.D., Martin, M.W., Bartley, J.M., and Coleman, D.S. 1990b. Timing and kinematics of deformation in the Cronese Hills, California, and implications for Mesozoic structure of the south-western Cordillera: Geology, v. 18, p. 554-557.

Walker, J.D., Martin, M.W., Bartley, J.M., and Glazner, A.F. 1990c. Middle to Late Jurassic deformation belt through the Mojave Desert, California: Geological Society of America Abstracts with Programs, v. 22, p. 91.

Walker, J.D., and Martin, M.W. 1991. Style and timing of middle to Late Jurassic deformation in the Mojave Desert and eastern California: Geological Society of America Abstracts with Programs, v. 23, p. 249.

Walsh, G.J., Aleinikoff, J.N., Benziane, F., Yazidi, A. and Armstrong, T.R. 2002. U–Pb zircon geochronology of the Paleoproterozoic Tagragra de Tata inlier and its Neoproterozoic cover, western Anti-Atlas, Morocco, Precambr. Res. 117, 1–20.

Watanabe, T., Masuyama, T., Nagaoka, K., Tahara, T. 2002. Analog experiments on magma-filled cracks: Competition between external stresses and internal pressure. Earth, Planets and Space, 54, 1247-1261.

Weinberger, R., Lyakhovsky, V., Baer, G., Agnon, A., 2000. Damage zones around en echelon dike segments in porous sandstone. J. Geophys. Res. 105, 3115–3133.

Weinberg, R.F., Mark, G. 2008. Magma migration, folding and disaggregation of migmatites in the Karakoram Shear Zone, Ladakh, NW India. Geological Society of America Bulletin 120, 994–1009.

Wendt, J. 1985. Disintegration of the continental margin of northwestern Gondwana; Late Devonian of the eastern Anti-Atlas (Morocco), Geology 13 (11) 815–818.

Westphal, M., C. Bardon, A. Bossert, and R. Hamzeh. 1973. A computer fit for Corsica and Sardinia against Southern France, Earth Planet. Sci. Lett., 18, 137–140.

Westphal, M., J. Orsini, and P. Vellutini. 1976. Le microcontinent corso-sarde, sa position initiale: Donnees paléomagnétiques et raccords géologiques, Tectonophysics, 30, 141–157.

Wheeler, J., 1987. The determination of true shear senses from the detection of passive markers in shear zones. Journal of the Geological Society of London 144, 73±77.

Whitmarsh, R.S. 1996. A geologic map of the Coso Range, with supplemental U-Pb geochronology and Ar-Ar thermochronology: Geological Society of America Abstracts with Programs, v. 28, p. 124.

Whitmarsh, R.S. 2000. Structural development of the Coso Range and adjacent areas of east-central California: unpublished Ph.D. dissertation, University of Kansas, Lawrence.

Wiebe, R.A., and Collins, W.J. 1998. Depositional features and stratigraphic sections in granitic plutons: Implications for the emplacement and crystallization of granitic magma: Journal of Structural Geology, v. 20, p. 1273–1289, doi: 10.1016/S0191-8141(98)00059-5.

Wickham, S.M. 1987. The segregation and emplacement of granitic magmas. Journal of the Geological Society, London 144, 281-297.

Wolf, M.B., and Saleeby, J.B. 1995. Late Jurassic dike swarms in the southwestern Sierra Nevada foothills terrane, California: implications for the Nevadan Orogeny and North American plate motion, *in* Miller, D.M., and Busby, C. (eds.), Jurassic magmatism and tectonics of the North America Cordillera: Geological Society of America Special Paper 299, p. 203-288.

Woolley, A.R., Bergman, S.C., Edgar, A.D., Le Bas, M.J., Mitchell, R.H., Rock, N.M.S., Scott Smith, B.H., 1996. Classification of lamprophyres, lamproites, kimberlites, and the kalsilitic, melilitic, and leucitic rocks. Can. Mineral. 34, 175–186.

Wright, T., Ebinger, C., Biggs, J., Ayele, A., Yirgu, G., 2006. Magma-maintained rift segmentation at continental rupture in the 2005 Afar dyking episode. Nature 442, 291–294.

Yamaji, A., Sato, K., 2011. Clustering of fracture orientations using a mixed Bingham distribution and its application to paleostress analysis from dike or vein orientations. J. Struct. Geol. 33, 1148–1157.

Yamaji, A., Sato, K., Tonai, S., 2010. Stochasticmodeling for the stress inversion of vein orientations: paleostress analysis of Pliocene epithermal veins in southwestern Kyushu, Japan. J. Struct. Geol. 32, 1137–1146.

Yazidi, A., Benziane, F., Walsh, G.J., Armstrong, T.R., Kouhen, M.A., Yazidi, M., Khamlichi, M.A., Carte géologique au 1/50 000 feuille Zawyat Si Nisser. Notes et Mémoires du Service Ge´ologique du Maroc 423, Feuille NH-29-X-4-d, in press.

Yazidi, A., 1976. Les formations sédimentaires et volcaniques de la boutonnière d'Ifni, Maroc. Thèse, Université de Grenoble. France.

Yoshinobu, A.S. Okaya, D.A. Paterson, S.R. 1998. Modeling the thermal evolution of fault-controlled magma emplacement models: implications for the solidification of granitoid plutons, Journal of Structural Geology 20, 1205–1218.

Zulauf, J., Zulauf, G. 2004. Rheology of plasticine used as rock analogue: the impact of temperature, composition and strain. Journal of Structural Geology 26, 725–737.

Zattin, M., F. Massari, and J. Médus. 2008. Thermochronological evidence for Mesozoic-Tertiary tectonic evolution in the eastern Sardinia, Terra Nova, 20, 469–474, 2008.

Ziegler, P. A. 1990. Geological Atlas of Western and Central Europe, 2nd edn. Shell International Petroleum (distributed by Geological Society, London).

Ziegler, P.A., 1993. Late Palaeozoic-Early Mesozoic Plate reorganization: evolution and demise of the Variscan fold belt. In: von Raumer, J.F., Neubauer, F. _Eds.., Pre-Mesozoic Geology in the Alps. Springer-Verlag, pp. 171–201.

Ziegler P.A., Cloetingh S., Guiraud R. and Stampfli G.M., 2001. Peritethyan platforms: constraints on dynamics of rifting and basin inversion. In: P.A. Ziegler, W. Cavazza and A.H.F. Robertson (Eds.), Peritethyan rift/wrench basins and passive margins, Mem. Mus. Nat. Hist. Nat. Paris, 186:9-49.

Ziegler, P., and P. Dëzes. 2006. Crustal evolution of Western and Central Europe, Geol. Soc. Spec. Publ., 32, 43–56.

Ziegler, P.A., Stampfli, G.M., 2001. Late Paleozoic Early Mesozoic plate boundary reorganisation: collapse of the Variscan orogen and opening of Neotethys. In: Cassinis, R. (Ed.), The Continental Permian of the Southern Alps and Sardinia (Italy) Regional Reports and General Correlations: Annali Museo Civico Science Naturali, Brescia. 25, pp. 17–34.

Zijderveld, J. D., K. A. De Jong, and R. Van der Voo. 1970. Rotation of Sardinia: Palaeomagnetic evidence from Permian rocks, Nature, 226, 993–994.

Ziv, A., Rubin, A.M., Agnon, A., 2000. Stability of dike intrusion along pre-existing fractures. J. Geophys. Res. 105, 5947–5961.

Zouhair, M., Marignac, C., Macaudie`re, J., Boiron, M.C., 1991. Gold deposition in the gold-bearing quartz veins of the Tagragra d_Akka (Western Anti-Atlas, Morocco): P–T–X conditions and place in the evolution of metamorphic fluids. In: Pagel, Leroy (Eds.), Source, Transport and Deposition of Metals. Balkema, Rotterdam, pp. 723–726.

Appendix

Appendix 1. Table 1. LOI data

Sample	Cruciable (gr)	Undried mass+cruciable (gr)	Undried mass (gr)	Dried mass + cruciable (gr)	Dried mass (gr)	Ignited mass+cruciable (gr)	Ignited mass (gr)	LOI (%)
SH-1	4,545	7,915	3,369	7,905	3,360	7,862	3,316	1,286
PC-1	4,092	7,190	3,098	7,719	3,626	7,699	3,607	0,543
PC-2b	4,634	8,288	3,654	8,269	3,635	8,204	3,570	1,777
PC-3b	4,545	8,024	3,479	8,089	3,544	7,956	3,411	3,745
OV-1a	4,513	7,681	3,168	7,640	3,127	7,582	3,070	1,826
OV-1b	5,130	8,565	3,435	8,553	3,423	8,516	3,386	1,081
OV-3	5,189	8,375	3,185	8,367	3,178	8,352	3,163	0,478
OV-4a	4,634	8,667	4,033	8,659	4,025	8,637	4,003	0,539
OV-4b	4,252	8,457	4,206	8,448	4,197	8,428	4,176	0,493
CC-1	4,314	8,341	4,027	8,329	4,015	8,235	3,921	2,341
BPN1-a	4,579	8,214	3,634	8,203	3,624	8,183	3,604	0,571
BPN1-12a	4,788	8,294	3,507	8,285	3,498	8,263	3,475	0,638
BPN1-12b	5,159	8,512	3,353	8,505	3,346	8,492	3,333	0,392
BPN1-13a	5,130	8,913	3,783	8,904	3,774	8,883	3,753	0,562
BPN1-13b	4,634	8,491	3,857	8,478	3,844	8,440	3,806	0,976
BPN1-14a	5,249	9,033	3,784	9,017	3,768	8,986	3,738	0,804
BPN1-14b	4,314	8,091	3,777	8,079	3,765	8,036	3,722	1,139
BPN1-25	4,631	8,285	3,655	8,274	3,644	8,250	3,620	0,661
BPN2-2a	4,512	7,466	2,954	7,455	2,943	7,442	2,929	0,455
BPN2-2b	4,095	7,405	3,311	7,398	3,304	7,373	3,278	0,784

BPN2-7a	4,233	7,846	3,614	7,839	3,606	7,818	3,585	0,593
BPN2-7b	4,579	8,803	4,224	8,789	4,210	8,745	4,165	1,052
BPN2-9a	4,606	7,869	3,264	7,862	3,256	7,836	3,230	0,786
BPN2-9b	5,035	8,272	3,237	8,262	3,227	8,238	3,203	0,722
BPN2-16c	4,634	7,864	3,231	7,852	3,218	7,826	3,193	0,802
BPN2-19b	4,095	8,323	4,228	8,311	4,217	8,285	4,191	0,619
BPN2-24a	5,354	9,605	4,251	9,595	4,242	9,569	4,215	0,622
BPN2-24b	4,308	8,814	4,506	8,805	4,496	8,771	4,462	0,758
BP2N2-10b	5,160	8,855	3,695	8,841	3,681	8,822	3,662	0,516
BN2N2-15a	4,252	7,718	3,466	7,710	3,458	7,694	3,442	0,474
BN2N2-15b	5,190	8,056	2,867	8,050	2,861	8,026	2,837	0,825
BN2N2-15c	4,252	7,688	3,436	7,680	3,428	7,665	3,413	0,443
BP2N2-16b	4,517	8,052	3,535	8,039	3,523	8,016	3,499	0,659
BP2N2-16z	4,512	7,903	3,391	7,891	3,379	7,864	3,351	0,820
BP2N2-18b	4,606	7,777	3,171	7,766	3,160	7,745	3,139	0,639
BP2N2-18c	4,431	7,565	3,134	7,555	3,124	7,526	3,095	0,912
14-BP-01	4,243	8,052	3,809	8,040	3,797	8,000	3,757	1,056
14-BP-02	5,208	8,695	3,487	8,686	3,479	8,656	3,448	0,883
14-BP-03	4,644	9,084	4,439	9,071	4,427	9,046	4,402	0,567
14-BP-04	4,842	8,966	4,124	8,952	4,110	8,910	4,068	1,024

Appendix 1. Table 2. XRF+LOI data

Sample	Na2O	MgO	Al2O3	SiO2	P2O5	K2O	CaO	TiO2	MnO	Fe2O3	Total %	LOI
SH-1	3,184	4,292	19,213	52,799	0,232	0,323	8,628	1,085	0,193	10,599	100,548	1,285
PC-1	3,676	2,008	15,682	67,813	0,106	2,736	4,166	0,432	0,076	3,759	100,454	0,543
PC-2b	2,691	6,275	18,638	49,751	0,327	0,853	10,452	0,976	0,177	9,969	100,109	1,777
PC-3b	3,315	4,393	18,039	52,379	0,298	1,449	7,838	1,216	0,18	10,892	99,999	3,744
OV-1a	3,742	4,884	19,164	49,972	0,759	3,754	5,584	1,625	0,196	10,212	99,892	1,826
OV-1b	2,818	6,250	17,269	50,126	0,262	1,828	10,272	0,922	0,25	10,130	100,127	1,080
OV-3	3,698	0,870	16,889	65,257	0,134	5,376	2,984	0,597	0,079	4,293	100,177	0,478
OV-4a	3,675	3,841	19,610	53,053	0,265	1,585	8,043	0,855	0,141	9,012	100,080	0,539
OV-4b	3,588	3,982	19,137	53,381	0,272	1,327	8,238	0,890	0,153	9,352	100,320	0,493
CC-1	2,965	4,731	17,318	55,070	0,594	2,953	5,609	1,119	0,173	9,054	99,586	2,341
BPN2-2a	3,502	5,627	17,044	51,884	0,381	1,407	9,907	0,892	0,151	9,130	99,925	0,455
BPN2-2b	2,651	7,319	15,738	51,806	0,247	1,607	10,180	0,855	0,167	9,849	100,419	0,784
BPN1-a	3,428	4,315	15,578	60,025	0,192	2,214	7,089	0,673	0,132	6,450	100,096	0,571
BPN2-7a	3,482	6,616	16,017	51,390	0,277	0,777	10,424	0,788	0,18	10,660	100,611	0,593
BPN2-7b	2,715	6,602	16,314	50,989	0,265	1,875	10,450	0,790	0,17	10,181	100,351	1,052
BPN2-9a	2,927	8,073	16,021	51,678	0,169	1,304	9,806	0,651	0,157	8,641	99,427	0,786
BPN2-9b	1,752	10,571	15,174	50,083	0,148	1,347	11,163	0,588	0,161	8,824	99,811	0,722
BP2N2-10b	2,836	6,789	15,715	51,332	0,239	1,050	11,600	0,828	0,167	9,761	100,317	0,516
BPN1-12a	3,929	1,293	17,048	65,338	0,22	2,996	4,018	0,422	0,083	4,263	99,610	0,740
BPN1-12b	3,778	3,389	17,753	55,250	0,356	2,024	7,345	0,947	0,183	8,712	99,737	0,391
BPN1-12c	4,779	3,204	17,946	56,337	0,367	1,393	6,559	0,931	0,146	8,782	100,444	0,637
BPN1-13a	4,098	5,641	17,291	52,227	0,383	0,828	9,973	0,909	0,145	8,984	100,479	0,561
BPN1-13b	2,853	7,237	15,400	51,164	0,335	1,623	10,120	0,854	0,164	9,739	99,489	0,975
BPN1-14a	3,497	5,824	17,792	50,817	0,287	0,998	10,186	0,959	0,164	9,486	100,010	0,804

BPN1-14b	2,952	7,122	17,326	49,984	0,27	1,178	10,582	0,945	0,167	9,433	99,959	1,139
BN2N2-15a	4,247	1,848	17,465	61,800	0,426	2,542	50,370	0,516	0,1	5,813	145,127	0,474
BN2N2-15b	4,087	0,870	16,156	68,195	0,157	3,501	27,290	0,278	0,107	2,780	123,421	0,825
BN2N2-15c	1,798	7,284	11,936	48,810	1,32	2,363	11,095	2,134	0,394	12,226	99,360	0,443
BP2N2-16b	2,634	7,294	15,084	53,666	0,268	2,092	9,572	0,702	0,162	9,126	100,600	0,658
BPN2-16c	2,899	7,136	16,504	47,997	0,738	2,366	9,166	1,803	0,168	11,217	99,994	0,801
BP2N2-16z	2,878	7,009	16,309	48,062	0,724	2,743	8,766	1,780	0,189	11,441	99,901	0,819
BP2N2-18b	2,569	6,228	15,849	53,256	0,264	2,214	9,814	0,825	0,152	9,508	100,679	0,639
BP2N2-18c	2,599	8,090	15,865	49,950	0,295	1,505	10,271	1,012	0,185	10,591	100,363	0,912
BPN2-19b	3,373	3,243	16,593	61,178	0,207	2,694	5,473	0,614	0,153	6,393	99,921	0,618
BPN2-24a	3,829	5,305	17,426	52,070	0,389	1,388	9,511	0,923	0,139	9,211	100,191	0,622
BPN2-24b	3,113	6,609	16,223	51,701	0,35	1,653	9,710	0,874	0,158	9,680	100,071	0,758
BPN1-25	4,103	3,253	17,851	56,418	0,37	2,499	6,083	0,930	0,116	8,655	100,278	0,661
14-BP-01	3,549	3,501	16,886	61,001	0,219	2,671	5,649	0,658	0,108	6,596	100,838	1,056
14-BP-02	1,993	10,014	15,809	50,304	0,158	1,504	10,639	0,636	0,177	9,259	100,493	0,883
14-BP-03	4,173	3,474	20,103	50,98	0,484	2,606	7,401	1,075	0,127	10,195	100,618	0,567
14-BP-04	3,268	6,244	16,887	48,818	0,748	2,781	8,566	1,852	0,172	11,108	100,444	1,024

Appendix 1.

Table 3. Zircon U-Pb data

Sample	U ppm	$^{207}Pb/^{235}U$	2s	$^{206}Pb/^{238}U$	2s	rho	Final Age
Z Line 2-1	117	0,180	0,007432	0,03	0,000616	0,71442	166
Z Line 2-2	123	0,183	0,005721	0,03	0,00068	0,55925	168
Z Line 2-3	261	0,219	0,01184	0,03	0,000661	0,72468	167
Z Line 2-4	355	0,177	0,004581	0,03	0,000636	0,7005	167
Z Line 2-5	377	0,176	0,004259	0,03	0,000631	0,68021	167
Z Line 2-6	627	0,180	0,004224	0,03	0,000589	0,64731	167
Z Line 2-7	296	0,203	0,004661	0,03	0,000655	0,45377	190
Z Line 2-8	334	0,198	0,005085	0,03	0,00066	0,68546	185
Z Line 2-9	335	0,190	0,004907	0,03	0,00067	0,67308	175
Z Line 2-10	1331	0,178	0,004295	0,03	0,000585	0,86297	162
Z Line 2-11	1545	0,170	0,003893	0,02	0,000537	0,86526	155
Z Line 2-12	811	0,186	0,004654	0,03	0,000609	0,8617	172
Z Line 2-13	276	0,195	0,004679	0,03	0,000626	0,64429	179
Z Line 2-14	158	0,197	0,005139	0,03	0,000629	0,38509	181
Z Line 2-15	293	0,192	0,005133	0,03	0,000661	0,76073	180
Z Line 2-16	463	0,190	0,004598	0,03	0,000604	0,63472	176
Z Line 2-17	552	0,187	0,004495	0,03	0,000621	0,84009	173
Z Line 2-18	527	0,192	0,00519	0,03	0,000737	0,90613	175
Z Line 2-19	634	0,190	0,00478	0,03	0,0007	0,88047	176
Z Line 2-20	384	0,186	0,004781	0,03	0,000605	0,60614	169
Z Line 2-21	709	0,190	0,004972	0,03	0,000624	0,76514	172
Z Line 2-22	599	0,189	0,004644	0,03	0,000613	0,88134	175
Z Line 2-23	626	0,183	0,004496	0,03	0,000625	0,87807	171
Z Line 2-24	726	0,189	0,004524	0,03	0,000621	0,82204	175
Z Line 2-25	168	0,201	0,006108	0,03	0,000657	0,58959	186
Z Line 2-26	201	0,201	0,00514	0,03	0,000643	0,70976	185
Z Line 2-27	304	0,205	0,005143	0,03	0,000685	0,62176	187
Z Line 2-28	187	0,202	0,005902	0,03	0,000686	0,62099	185
Z Line 2-29	800	0,189	0,00495	0,03	0,000663	0,90303	175
Z Line 2-30	159	0,189	0,005948	0,03	0,000628	0,46766	175
Z Line 2-31	188	0,194	0,005287	0,03	0,000638	0,39923	177
Z Line 2-32	502	0,188	0,004753	0,03	0,000609	0,70846	175
Z Line 2-33	699	0,181	0,004519	0,03	0,00062	0,9024	169
Z Line 2-34	486	0,227	0,008852	0,03	0,000606	0,7826	168
Z Line 2-35	813	0,205	0,005132	0,03	0,00063	0,69809	176
Z Line 2-36	1377	0,202	0,005274	0,03	0,000647	0,68654	175
Z Line 2-37	229	0,188	0,005201	0,03	0,000661	0,71894	172
Z Line 2-38	219	0,182	0,004781	0,03	0,000576	0,73959	168
Z Line 2-39	146	0,192	0,004871	0,03	0,000604	0,55378	174

Z Line 2-40	596	0,181	0,004347	0,03	0,000576	0,84325	168
Z Line 1-1	102	0,161	0,006461	0,02	0,00061	0,61862	155
Z Line 1-2	97	0,171	0,006138	0,02	0,000592	0,49083	155
Z Line 1-3	47	0,180	0,018356	0,02	0,000647	0,087887	151
Z Line 1-4	138	0,162	0,004995	0,02	0,000546	0,40656	149
Z Line 1-5	146	0,156	0,004759	0,02	0,000585	0,60746	147
Z Line 1-6	1370	0,181	0,005695	0,03	0,00092	0,93541	160
Z Line 1-7	219	0,199	0,005786	0,03	0,000578	0,53222	169
Z Line 1-8	95	0,195	0,012618	0,02	0,000626	0,5723	153
Z Line 1-9	202	0,162	0,004698	0,02	0,000544	0,66203	150
Z Line 1-10	121	0,167	0,005057	0,02	0,000532	0,49507	153
Z Line 1-11	298	0,162	0,004218	0,02	0,000581	0,69051	152
Z Line 1-12	166	0,163	0,005008	0,02	0,00056	0,38449	151
Z Line 1-13	316	0,163	0,003938	0,02	0,00054	0,63371	152
Z Line 1-14	185	0,160	0,004601	0,02	0,000548	0,68394	152
Z Line 1-15	152	0,164	0,004192	0,02	0,000539	0,39859	150
Z Line 1-16	355	0,212	0,021424	0,02	0,000617	0,57455	152
Z Line 1-17	135	0,165	0,004809	0,02	0,000572	0,43629	151
Z Line 1-18	125	0,178	0,007231	0,02	0,000572	0,18729	153
Z Line 1-19	99	0,163	0,005477	0,02	0,000567	0,57222	151
Z Line 1-20	233	0,163	0,004363	0,02	0,00061	0,81817	152
Z Line 1-21	230	0,164	0,004793	0,02	0,000533	0,45599	153
Z Line 1-22	255	0,163	0,004048	0,02	0,00053	0,66028	151
Z Line 1-23	281	0,164	0,004253	0,02	0,000567	0,63857	149
Z Line 1-24	195	0,162	0,005144	0,02	0,000561	0,47733	151
Z Line 1-25	144	0,180	0,006743	0,02	0,000541	0,44906	155
Z Line 1-26	134	0,167	0,004765	0,02	0,000593	0,34004	155
Z Line 1-27	315	0,188	0,012575	0,02	0,000733	0,5976	158
Z Line 1-28	161	0,165	0,004665	0,02	0,000555	0,5899	154
Z Line 1-29	251	0,161	0,004474	0,02	0,000623	0,82762	150
Z Line 1-30	175	0,164	0,005323	0,02	0,000613	0,55193	151
Z Line 1-31	312	0,164	0,004381	0,02	0,000553	0,50442	152
Z Line 1-32	207	0,160	0,005125	0,02	0,000591	0,67636	149
Z Line 1-33	255	0,162	0,004627	0,02	0,00056	0,56496	153
Z Line 1-34	177	0,167	0,004837	0,02	0,000576	0,60492	153
Z Line 1-35	184	0,160	0,004591	0,02	0,000566	0,57469	151
Z Line 1-36	95	0,160	0,005847	0,02	0,000554	0,47237	149
Z Line 1-37	317	0,160	0,004313	0,02	0,000525	0,83139	149
Z Line 1-38	211	0,170	0,005167	0,02	0,000599	0,74291	155
Z Line 4-1	307	0,184	0,006619	0,03	0,000863	0,84565	173
Z Line 4-2	1600	0,178	0,005285	0,02	0,000707	0,90508	159
Z Line 4-3	445	0,180	0,006323	0,03	0,000851	0,9322	167
Z Line 4-4	394	0,179	0,005908	0,03	0,000755	0,89612	164
Z Line 4-5	347	0,182	0,005639	0,03	0,000762	0,88176	168
Z2 Line 2-1	1207	0,190	0,004966	0,03	0,000572	0,66417	167
Z2 Line 2-2	1486	0,174	0,003866	0,03	0,000558	0,88899	162

Z2 Line 2-3	176	0,173	0,004926	0,03	0,000558	0,53274	165
Z2 Line 2-4	271	0,184	0,004681	0,03	0,000614	0,64449	171
Z2 Line 2-5	327	0,192	0,005191	0,03	0,000667	0,79985	176
Z2 trpl Line-1	829	0,337	0,007341	0,05	0,00101	0,78717	295
Z2 trpl Line-2	3430	0,234	0,008008	0,03	0,001322	0,4955	176